Ministero dell'Istruzione, dell'Università e della Ricerca

UNIVERSITÀ DEGLI STUDI DI SALERNO

DIPARTIMENTO DI INGEGNERIA CIVILE

Dottorato di Ricerca in Ingegneria delle Strutture e del Recupero Edilizio ed Urbano

X Ciclo N.S. (2008-2011)

SHEAR STRENGTHENING OF MASONRY WALLS BY FRP LAMINATES: EXPERIMENTAL INVESTIGATION AND NUMERICAL ANALYSIS

Carmen Sguazzo

Il Tutor
Prof. Ing. Ciro Faella

Il Co-Tutor
Dott. Ing. Enzo Martinelli

Il Coordinatore
Prof.Ing. Ciro Faella

Alla mia famiglia.

(...) Ma, si dirà, e la scienza? La scienza è fede?! Sì. Per avere potenza sul mondo, la scienza ha rinunciato da tempo ad essere «verità», nel senso attribuito a questa parola dalla tradizione filosofica. La scienza è divenuta sapere ipotetico. Sa di non essere sapere assoluto («verità», appunto) - e in questo senso non è fede ma dubbio -; tuttavia per aver potenza sul mondo deve aver fede nella propria capacità di trasformarlo; ed è all' interno di questa fede che essa elabora, risolve o conferma i propri dubbi. (...)

Emanuele Severino

Ringraziamenti

Vorrei esprimere la mia gratitudine a coloro i quali son stati guida scientifica e sostegno morale durante questi anni, ormai trascorsi, di dottorato.

Sinceri ringraziamenti vanno al Prof. Ciro Faella, tutor della presente tesi, che confidando nelle mie capacità, ha seguito l'intera attività di dottorato offrendomi la possibilità di confronto scientifico ed al suo esempio quotidiano di imparzialità e moderazione.

Ringrazio il Dott. Enzo Martinelli, co-tutor della presente tesi, che ne ha delineato i contenuti, dandomi la possibilità di un confronto scientifico profondamente costruttivo durante l' intero sviluppo degli stessi. Ed alla sua paziente rilettura dell' intero lavoro.

Al Prof. Paulo B. Lourenço vanno i miei più vivi ringraziamenti, per avermi dato la possibilità di trascorrere un periodo di ricerca presso il Dipartimento di Ingegneria Civile dell' Universidade do Minho, seguendone attentamente gli sviluppi e concedendomi la possibilità di usufruire degli strumenti informatici sino alle ultime fasi della tesi; per avermi reso pienamente partecipe delle attività del gruppo di studenti di dottorato.

Profondi ringraziamenti vanno al Prof. Daniel V. Oliveira, per aver seguito costantemente ed attentamente la parte analitica del presente lavoro ed all'ottimismo ed alla grinta inculcatemi durante l'intero periodo di ricerca.

Ringrazio il Dott. Giancarlo Marcari, che ho avuto il piacere di conoscere di persona presso UMinho, per l'amicizia dimostratami sin dai primissimi giorni. Un sincero ringraziamento per aver seguito le varie fasi del lavoro, per avermi fornito il materiale bibliografico e per il flusso continuo di idee scambiate durante i meeting settimanali.

Ai colleghi di dottorato vanno i ringraziamenti per le ore di corso, di studio e di laboratorio trascorse insieme; a coloro i quali son diventati sinceri amici sento di rivolgere il mio affettuoso pensiero: grazie dei sorrisi che mi hanno accolto i primi giorni, dei "don't worry!" e dei "controlliamo insieme", dei "consigli spassionati", degli "inviti a pranzo alle 14.45", delle telefonate, del navigatore con l'accento abruzzese; dei momenti trascorsi

in sala dottorandi, dei numerosissimi caffè offerti, dei messaggi trovati e lasciati in bacheca ed un grazie per la "scrivania fraterna" cedutami all'occorrenza. Grazie delle – ahimé poche- giornate trascorse all'aperto, delle lunghe chiacchierate, dei momenti conviviali e delle piacevolissime ore di viaggio trascorse insieme.

Ai miei colleghi e soprattutto alle mie amiche-colleghe di UMinho va il mio più profondo ed affettuoso ringraziamento per le ore trascorse all'università e per le escursioni fatte insieme: la vostra amicizia ha arricchito di indimenticabili ricordi i dieci mesi trascorsi a Guimarães, quasi annullando la nostalgia di casa. Un ringraziamento particolare, infine, va al mio amico e collega di ufficio ed alla nostra sintonia di vedute.

Ed ancora grazie...

ai miei amici, vicini e lontani, per tutte le volte in cui, più o meno inconsapevolmente, hanno rallegrato i miei giorni ed al loro forte sostegno durante il tempo trascorso all'estero.

Al mio parroco don Matteo Mottola, primo ad incoraggiarmi nella fase di studio che ha preceduto il dottorato: mi manca oggi non potergli raccontare la gioia di averlo concluso.

Ai miei cugini ed ai miei zii, che con il loro entusiasmo hanno seguito ogni passo di questo lungo percorso.

Ai miei nonni, che mi hanno insegnato come vivere le emozioni che accompagnano ogni momento della vita ed alla loro assoluta fiducia in me ed in quel che intraprendo.

A mio fratello ed alla sua incredibile arte di sdrammatizzare e di strapparmi il sorriso anche nei momenti difficili ed al nostro baricentro del "non far niente", che mi accoglie al termine di lunghe giornate per quelle chiacchierate che fanno bene al cuore.

A mia madre e mio padre che mi hanno insegnato l'ottimismo e la fiducia da riporre nei sacrifici ed inculcato il senso del dovere per ogni impresa che si intraprende; al loro amore ed al loro sostegno.

Al mio fidanzato, per avermi trasmesso costantemente fiducia nel lavoro; alla sua inesauribile capacità di ascoltarmi, di incoraggiarmi e di farmi ridere, ai suoi consigli... al suo amore incondizionato.

SUMMARY

FOREWORD

The present Doctoral Thesis reports a detailed study on the contribution of FRP composites to the shear strength of masonry walls under in-plane seismic actions.

The work is organised in seven chapters, which will be briefly described in the following.

In the first chapter an introduction on the typical damages of masonry due to in-plane seismic actions is presented. Strengthening techniques, both traditional and innovative, against in-plane damage of masonry walls are also described.

In chapter 2 code provisions and analytical models on the shear strength of masonry walls externally strengthened by FRP composites are introduced.

Chapter 3 reports the complete description of the wide database of experimental results collected by the author of the present thesis: diagonal compression and shear-compression tests belonging to several laboratory test campaigns on unstrengthened and strengthened masonry walls are presented.

The assessment of the analytical models is finally reported through the comparison between experimental results, collected within the database, and theoretical results, derived from the models application.

In chapter 4 micro and macro modelling approaches of masonry are described.

In chapter 5 the mathematical and physical characterisation of the developed model for masonry walls strengthened by FRP composite is presented within the framework of the finite element method.

Chapter 6 presents the assessment of the developed finite element model. The chapter describes the validation of the proposed numerical model for unreinforced masonry and the implementation and validation of plane interfaces in the strengthened model, within the elastic range.

Chapter 7 includes the parametric assessment of both unstrengthened and FRP strengthened models; the discussion of the results of nonlinear analyses performed on the model with different types of composite strengthening and the conclusions are finally reported.

Symbols

In the present thesis the adopted symbols are inspired to CNR DT 200/2004 (2009) Guidelines and to Eurocode 6 (1998). Symbols derive from the criterion shown in the following.

Notations

A	cross section area
E	Young's modulus of elasticity
G	shear modulus
N	axial force
V	shear capacity
d	effective length
l	length
f	strength
h	height
t	thickness
Γ	fracture energy
δ	displacement
ε	strain
γ	partial factor
μ	friction
ν	Poisson's ratio
ρ	density
σ	vertical stress
τ	tangential stress

Uppercase/Lowercase

$(.)_a$	value of quantity (.) for the adhesive
$(.)_b$	value of quantity (.) for the single brick
$(.)_{eff}$	effective value of quantity (.)
$(.)_f$	value of quantity (.) for the fiber-reinforced composite
$(.)_{fib}$	value of quantity (.) for the fiber

$(.)_m$ value of quantity (.) for masonry
$(.)_{ma}$ value of quantity (.) for the matrix
$(.)_g$ value of quantity (.) for the grout
$(.)_r$ value of quantity (.) for the generic reinforcement
$(.)_R$ value of quantity (.) as resistance
$(.)_u$ ultimate value of quantity (.)
$(.)^{exp}$ experimental value of quantity (.)
$(.)^h$ value of quantity (.) in the horizontal direction(.)
$(.)^{nr}$ value of quantity (.) for the not reinforced specimens
$(.)^r$ value of quantity (.) for the reinforced specimens
$(.)^{th}$ theoretical value of quantity (.)
$(.)_0$ value of quantity (.) in absence of vertical load
$(.)_{.,d}$ design value of quantity (.).
$(.)_{.,db}$ value of quantity (.) in conditions of debonding
$(.)_{.,k}$ characteristic value of quantity (.)
$(.)_{.,m}$ average value of quantity (.)

Recurrent Symbols

A_f area of FRP reinforcement
E_{fib} Young's modulus of elasticity of fiber itself
V_R shear strength of masonry
$V_{R\,m}$ masonry contribution to the shear capacity
$V_{R\,f}$ FRP contribution to the shear capacity
d effective length of the section
f_b compressive strength of a brick
f_f tensile strength of FRP reinforcement
f_m compressive strength of masonry
f_{mt} tensile strength of masonry
f_v shear strength of masonry
f_{v0} shear strength of masonry in absence of vertical load
l length of the masonry section
l_f length of FRP reinforcement
h height of the masonry section
p center to center spacing

t	thickness of the masonry section
t_f	thickness of the FRP composite reinforcement
$\varepsilon_{fib,\,u}$	ultimate strain of the fiber
$\varepsilon_{fib,\,eff}$	effective strain of the fiber
σ_0	average axial stress
ρ_f	horizontal ratio of FRP reinforcement computed on the masonry wall section
ρ_{fib}	fiber density

CHAPTER 1

1. Introduction

1.1 Earthquakes and damage

Masonry constructions are often damaged by seismic events of significant intensity.

In the scientific literature, several post earthquake damage data and evaluation vulnerability methods are available. Their study is relevant to define suitable structural models able to prevent the effective behaviour of the constructions (Decanini, 2009a; Decanini, 2009b).

An example of a very extensive collection of observational data from post-earthquake surveys is the CATDAT database. The global CATDAT (Daniell, 2011) damaging earthquakes and secondary effects (tsunami, fire, landslides, liquefaction and fault rupture) database was developed to validate, remove discrepancies and expand global databases, giving the possibility to better understand the trends in vulnerability, exposure, and possible future impacts of such earthquakes.

Sources of information utilised to present data are more than 17000 and contain about 12200 earthquake induced damages. A considerable number of earthquakes dating from 1900 have been examined and validated before the data entry. The data set of each earthquake includes buildings damages information, seismological information and ranges of social and economic losses.

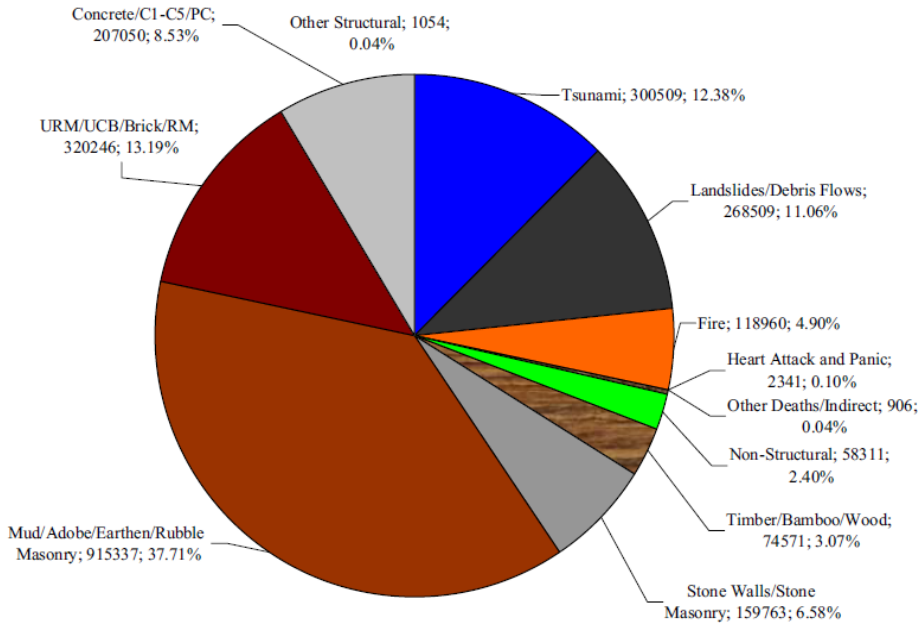

Fig. 1.1: Shaking and Secondary Effect Deaths Worldwide for 1996 fatal earthquakes (Daniell, 2011).

The updated version of the worldwide database (v5.024) for 1996 fatal earthquakes from 1900 to April 2011 and the secondary effects (tsunami, landslides and fire) of 7000 earthquakes are shown in Fig. 1.1.

The earthquake shaking effects cover 57.5 % of casualties due to masonry structures, while concrete and wooden structures cover respectively 8.5 % and 3 % of casualties; finally 28.6% are from secondary effects and 2.4% are non-structural casualties.

The significant collection of building damages in the CATDAT database points out that earthquakes in the 20th and 21st centuries globally caused around 2.1 trillion of dollars in terms of damages (Daniell, 2011).

Particularly, the collection of building damages for historic earthquakes demonstrates the high vulnerability of traditional buildings such as masonry, adobe and badly constructed reinforced concrete structures.

In the following, detailed information about the damages of masonry structures registered after some of the strongest events of the last years are reported and discussed.

1.1.1 World earthquakes damage scenarios

A few important information and data on damages of masonry structures struck by earthquakes occurred in Turkey are discussed below.

Unreinforced masonry, reinforced concrete and hımış (buildings composed of timber frames and braces with some infill materials), are the most common structural systems in Turkey. Historical masonry buildings were present in the oldest parts of the city and in special areas such as religious areas. The other masonry buildings and hımış buildings have been built in relatively poor regions. Reinforced concrete structures are generally employed for modern buildings. In urban areas, 48% were brick masonry or timber framed, 30% of all buildings were reinforced concrete frame type and 22% were adobe or rubble masonry. In rural areas, 82% of the housing stock was made of masonry, while 18% were made of timber-frame or reinforced concrete (Doğangün et al., 2008).

Table 1.1 reports damage assessment results for all types of building (masonry, reinforced concrete, etc.) subjected to the earthquakes in Turkey. Information about behaviour observed on masonry structures during those earthquakes are also reported.

Table 1.1: Turkey earthquakes and damages of buildings (Doğangün et al., 2008).

Earthquake	M_w or M_w	Buildings			Behaviour of masonry structures
		Heavily damaged	Medium damaged	Low damaged	
Doğubeyazıt, 2004	5.0	300	200	500	Since the energy release was relatively small, especially poorly constructed rubble (mud-stone) masonry structures were heavily damaged or collapsed. A great majority of the structures with non-load bearing hollow insulation bricks load-bearing walls suffered medium to heavy damage.
Erzurum, 2004	5.1	-	-	-	
Pülümür, 2003	6.0	21	-	-	
Cankırı, 2000	6.1	1500	-	-	
Dinar, 1995	6.1	4909	-	-	
Ceyhan, 1998	6.2	1388	18612	43646	Many stone masonry minarets were damaged, other masonry buildings generally performed well.
Sultandağı , 2002	6.3	4390	1730	9556	Most of the masonry buildings with less than 3 stories have survived the earthquake with minor damage (Erdik et al, 2002)
Erzincan, 1992	6.3	4157	5453	7867	The 8000 unreinforced masonry buildings, generally performed well with the exception of a complex of 40 two-storey buildings constructed with non-load bearing hollow insulation bricks (Sucuoğlu & Erberik, 1997)
Bingöl, 2003	6.4	3214	3448	6096	Throughout the city the unreinforced masonry structures were heavily damaged (KOERI, 2003)
Duzce, 1999	7.1	1364	493	825	Reinforced concrete structures presented high level of damage. Traditional structures relatively performed well (Gülhan & Güney, 2000)
Kocaeli, 1999	7.4	41266	43618	48008	

During the first four earthquakes (Doğubeyazit, Erzurum, Pülümür and Çankırı Earthquakes), as shown in Table 1.1, generally poorly constructed mud-stone masonry structures collapsed or were heavily damaged while only a few of reinforced concrete structures were slightly damaged. However, mud-stone masonry structures were destroyed due to poor mud mortar and weak anchorage between mud and stone. For the other earthquakes, RC structures were also damaged, causing loss of more human lives.

Hollow clay tiles, used as brick units, have been observed to be the major cause of partial or total collapse of buildings. Mud-stone masonry structures collapsed or were heavily damaged due to the same above reasons. The performance of the unreinforced masonry buildings was not generally so good in such earthquakes.

On December 26th 2003 a devastating earthquake of magnitude M_W 6.5 occurred in Bam city, in the south-eastern region of Iran, causing a large number of collapses and human casualties (Kuwata et al., 2005). Among 25700 buildings in Bam and 7200 buildings in Baravat (residential houses and commerce use houses are included), 92% of them collapsed in Bam and 61% in Baravat, covering 100% of adobe masonry structures, 100% of brick masonry structures without concrete frame, 90% of brick masonry structures with concrete frame, 90% of brick and steel structures. Almost any buildings made of masonry structures collapsed completely during the earthquake as indicated in Fig. 1.2.

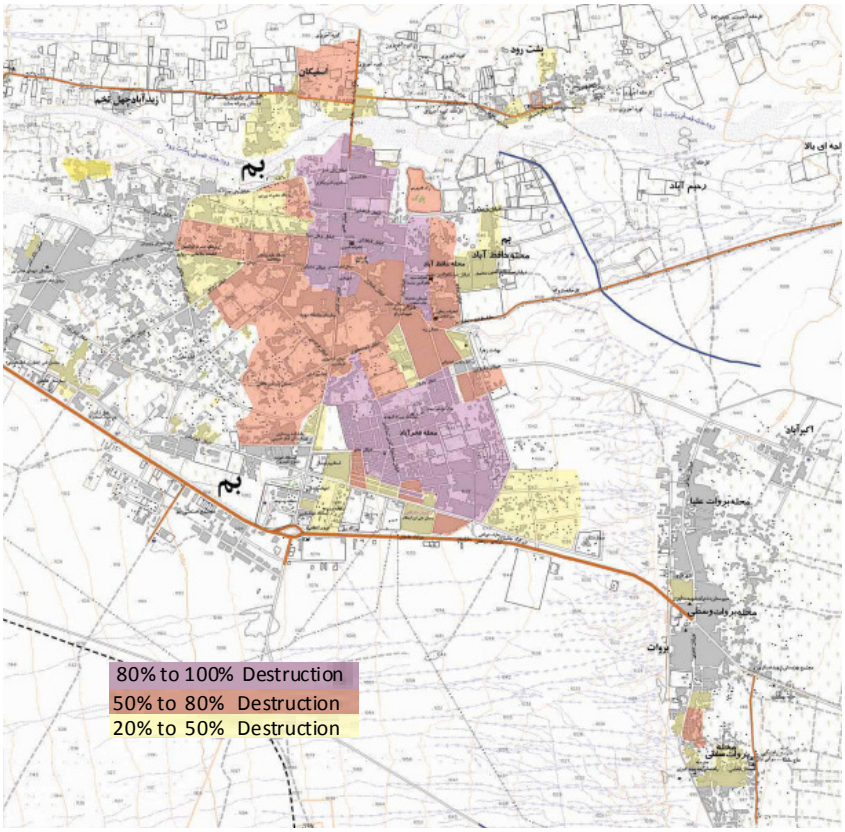

Fig. 1.2: Ratio of completely collapsed buildings (Kuwata et al., 2005).

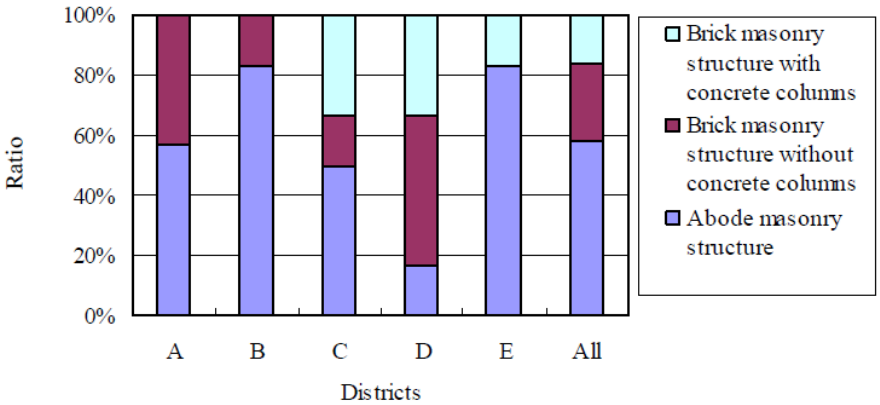

Fig. 1.3: Building structures in questionnaire-surveyed (Kuwata et al., 2005).

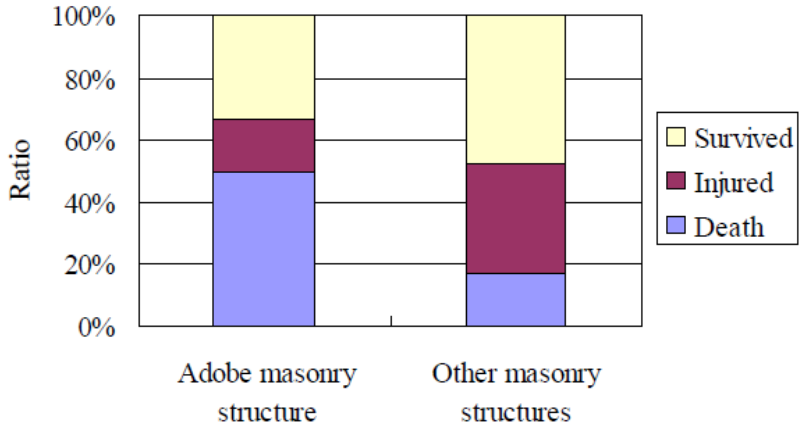

Fig. 1.4: Damage rate for building structures (Kuwata et al., 2005).

Fig. 1.3 shows the distribution within the Bam district of different typologies of structures, derived from the questionnaire for surveyed people while Fig. 1.4 shows that for brick masonry structures the number of injured people was larger than deaths, while the collapse of adobe masonry structures had great influence on the occurrence of deaths.

On October 8th 2005 Kashmir Earthquake was one of the largest earthquakes in Northern Pakistan. It was of magnitude 7.6 on the Richter scale and caused an unprecedented level of damage and destruction in Pakistan Administered Kashmir (PAK) and the North Western Frontier Province (NWFP). It damaged or collapsed more than 0.6 million buildings (Mumtaz et al. 2008).

The performance of buildings (Peiris et al., 2008) has been ranked in terms of four major occupancy categories and performance levels, stated in FEMA 356 (2006).

Table 1.2: Building damage scale (FEMA 2006).

Damage Level	Damage Description	
	Unreinforced Masonry (URM)*	RC Construction
Slight Damage	Diagonal, stair-step hairline cracks on masonry wall surfaces; larger cracks around door and window openings in walls with large proportion of openings; movements of lintels; cracks at the base of parapets	Diagonal (sometimes horizontal) hairline cracks on most infill walls; cracks at frame-infill interfaces.
Moderate Damage	Most wall surfaces exhibit diagonal cracks; some of the walls exhibit larger diagonal cracks; masonry walls may have visible separation from diaphragms; significant cracking of parapets; some masonry may fall from walls or parapets	Most infill wall surfaces exhibit larger diagonal or horizontal cracks; some walls exhibit crushing of brick around beam-column connections. Diagonal shear cracks may be observed in concrete beams or columns.
Extensive Damage	In buildings with relatively large area of wall openings most walls have suffered extensive cracking. Some parapets and gable end walls have fallen. Beams or trusses may have moved relative to their supports.	Most infill walls exhibit large cracks; some bricks may dislodge and fall; some infill walls may bulge out-of-plane; few walls may fall partially or fully; few concrete columns or beams may fail in shear resulting in partial collapse. Structure may exhibit permanent lateral deformation.
Collapse	Structure has collapsed or is in imminent danger of collapse due to in-plane or out-of-plane failure of the walls.	Structure has collapsed or is in imminent danger of collapse due to a combination of total failure of the infill walls and non-ductile failure of the concrete beams and columns.

**URM abbreviation is used to describe all types of unreinforced masonry buildings in this report*

Based on the damage observations, the residential buildings were largely of unreinforced masonry constructions realised by poor quality materials and performed at a collapse prevention or worse level. The commercial (including retail) buildings had a mixed performance: those of masonry performed at a collapse prevention or worse level while the RC constructions performed at an immediate occupancy or life safety level. Government buildings, mostly of concrete block or brick URM, performed at a life safety or collapse prevention performance level. Educational institutions made of concrete block or brick URM performed at a collapse prevention or worse level.

A separate damage scale has been contemporary used to describe the amount of building damage over a spatial region using visual inspections of the satellite images. This damage scale is summarised below:

Extensive (E) – More than 70% of buildings collapsed or heavily damaged.

Moderate (M) – Between 30% and 70% of buildings collapsed or heavily damaged.

Slight (S) – Less than 30% buildings collapsed or heavily damaged.

The above damage scale relies on visual identification of damage to buildings over a certain spatial region. Hence it is a measure of the density of damage as well as the extent of building specific damage that could possibly be identified.

Fig. 1.5 shows a satellite image of Balakot taken after the earthquake (Digital Globe, 2005), which was used to identify key locations of building damage. The city was divided into several zones and each zone was assigned a damage level using the 3-level damage scale for satellite imagery described above based on visual inspection of the satellite image.

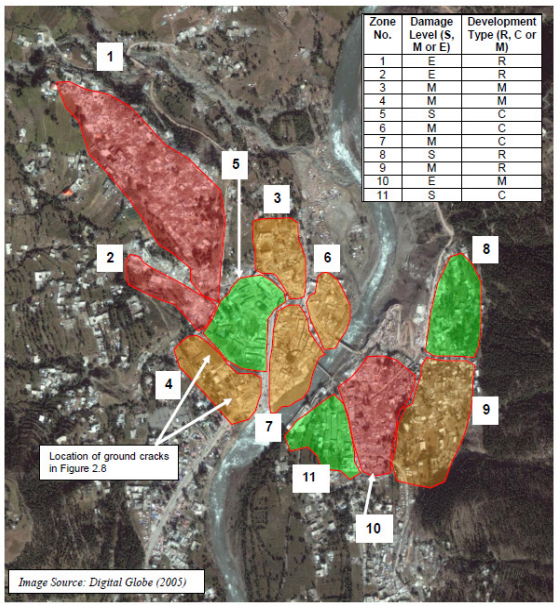

Fig. 1.5: Selected damaged areas in Balakot city (Peiris et al., 2008).

The damage zoning indicates that Balakot largely experienced moderate to extensive damage with some areas experiencing slight damage. The extensive damage occurred in the residential areas of the city, particularly on the hill north-west of the city centre (zone 1) also

shown in Fig. 1.5, where the buildings were mainly concrete block URM with RC slabs as roofs (or floors in the case of 2-storey buildings).

The commercial areas of Balakot city (zone 7 of Fig. 1.5), characterised by RC constructions and a mixture of single and multi-storey buildings experienced moderate damage.

In the afternoon of 12th May 2008, Wenchuanin Sichuan Province of China was struck by an earthquake with a magnitude 8 on the Richter scale (Xiong, 2008). The effects were felt in Beijing, Shanghai and Taipei etc., as far as 1700km away.

A lot of buildings were severely damaged but did not collapse. The building seismic damage data available in the major disaster area were classified according to structural type, construction time and occupancies.

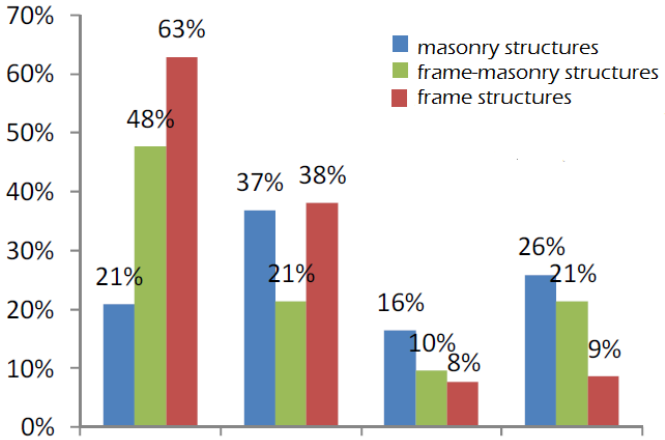

Fig. 1.6: Comparison of seismic damage for masonry structures, frame-masonry structures and frame structures (Lieping, 2008).

Some examples of buildings which were all severely damaged but still standing, saving a lot of people's lives, are shown in Fig. 1.6.

The seismic damage of masonry structures was generally more severe than the damage of RC frames; building structures complying with more recent design codes suffered less damage: buildings in developed regions like cities generally performed better than those in the rural

areas; the seismic damage of public buildings such as schools and factories was generally more severe than that of residential buildings.

More than 40 school buildings completely collapsed and hundreds of buildings irreparably damaged (Xiong, 2008).

Fig. 1.7 reports data of the survey aimed at quantifying collapsed and damaged school buildings which confirms the serious damage status characterizing masonry structures.

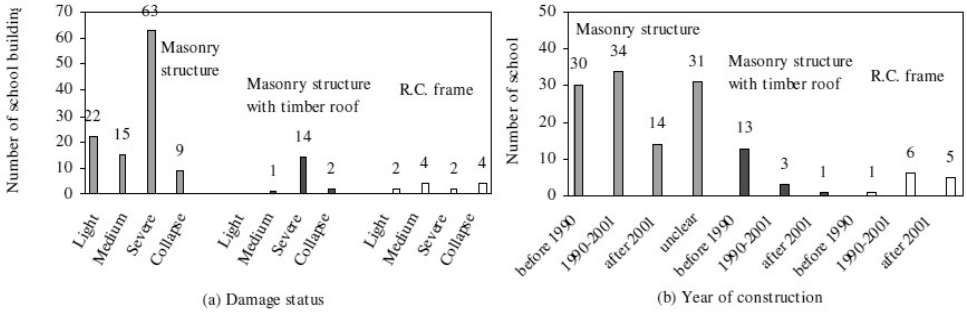

Fig. 1.7: Survey results of damaged school buildings in Wenchuan earthquake (Xiong, 2008).

On February 22nd 2011 a magnitude M_w 6.3 earthquake struck near Christchurch, New Zealand, causing extensive damage to the city.

Table 1.3 and Fig. 1.8 (Kam et al., 2011) present the statistics of the Building Safety Evaluation about the Central Business' Districts buildings, as per 18th March 2011, divided into different construction types.

Table 1.3: Building safety evaluation tagging status for CBD buildings as per 18th March 2011 (Kam et al., 2011).

	Building Safety Evaluation (as per 18th Mar 2011)			
Building Construction	Green	Yellow	Red	Total
Reinforced Concrete	480	300	184	964
Steel	124	34	11	169
Timber	708	241	150	1099
Reinforced Masonry	180	64	45	289
Unreinforced Masonry/Stone	58	122	291	471
Unknown / Not reported	383	101	145	629
Total	1933	862	826	3621

Unreinforced masonry generally performed poorly and a significant number of buildings was damaged. However, only 471 addresses were assessed to be unreinforced masonry, which is somewhat lower than expected. Based on field observation, it was understood that many unreinforced masonry buildings were seriously damaged or collapsed. Besides looking at Fig. 1.8 and following the New Zealand Building Safety Evaluation (Kam et al., 2011), it can be seen as the unreinforced masonry structures have the smallest rate of apparently structural safety, when compared to the others.

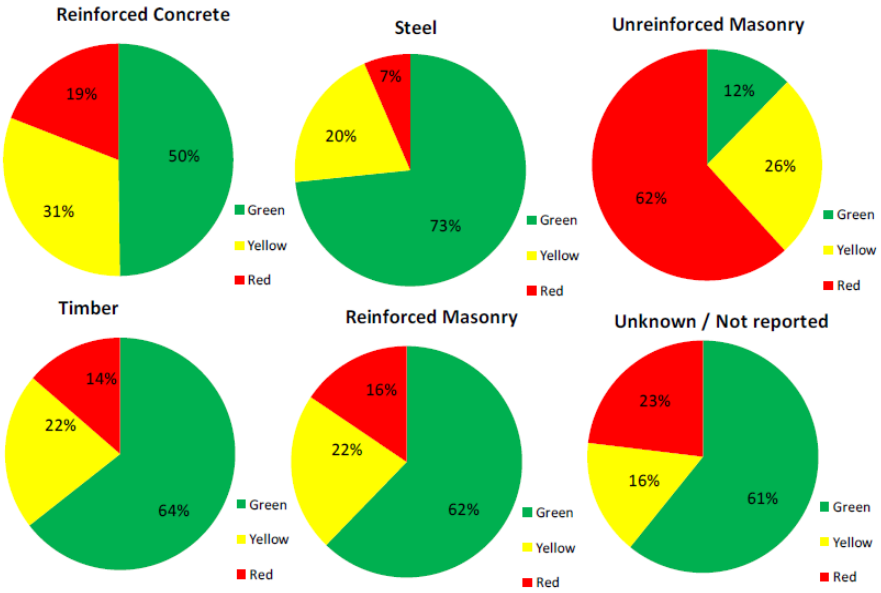

Fig. 1.8: Building safety evaluation tagging status for CBD buildings as per 18th March 2011 (Kam et al., 2011).

1.1.2 Italian earthquakes damage scenarios

Over the past 30 years in Italy, a concerted effort has been made to collect detailed observed damage data (Colombi et al, 2008) registered in the aftermath of earthquakes of significant intensity. The post-earthquake damage surveys from the most important earthquakes that have occurred in Italy are available: Irpinia 1980, Eastern Sicily 1990, Umbria-Marche 1997, Umbria 1998, Pollino 1998 and Molise 2002. Fig. 1.9 shows the map of the mentioned earthquake epicentres and the municipalities which were surveyed following each event while in Table 1.4 the main parameters of the mentioned earthquakes are highlighted.

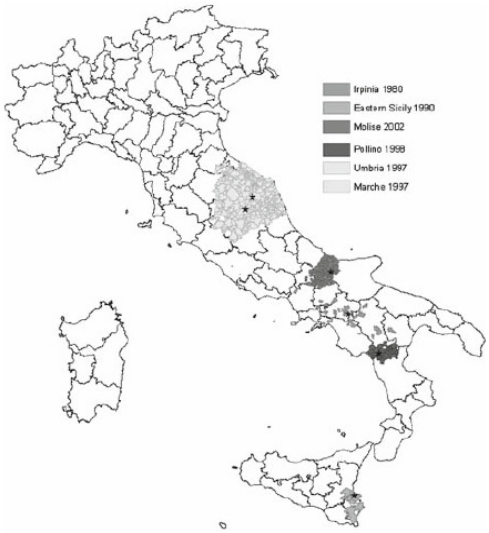

Fig. 1.9: Map illustrating the earthquake epicentres and the surrounding municipalities which were surveyed (Colombi et al, 2008).

Table 1.4: Earthquakes in Italy for which post-earthquake damage surveys are available (Colombi et al, 2008).

Event	Date	Most effected area	Epicentral latitude	Epicentral longitude	Moment magnitude (M_w)
Irpinia 1980	23-Nov-80	Irpinia-Basilicata	40.850	15.280	6.89
Eastern Sicily 1990	13-Dec-90	South eastern Sicily	37.266	15.121	5.68
Umbria-Marche 1997	26-Sept-97	Apennines Umbro-Marchigiano	43.019	12.879	6.05
Umbria 1998	26-Mar-98	Apennines Umbro-Marchigiano	43.252	13.071	5.33
Pollino 1998	09-Sept-98	Apennines Calabro-Lucano	40.038	15.937	5.68
Molise 2002	31-Oct-02	Molise	41.694	14.925	5.78

Gruppo di Lavoro CPTI (2004)

The available data have been organised in terms of damage suffered by the vertical structures. Although the overall damage of buildings cannot be described using simply the damage of the vertical structures, only this description is available.

The damage states which have been used to describe the mentioned events are based on the limit state conditions defined in the Italian seismic design/assessment regulations (Colombi et al, 2008) of that time, OPCM 3274 – 03 (2003): slight damage, significant damage and collapse. The slight damage limit state condition refers to the situation where the building can be used after the earthquake without the need for repair and/or strengthening. Beyond the limit condition of significant damage the building cannot be used after the earthquake without strengthening. Furthermore, this level of damage is such that repairing the buildings is not economically convenient.

The buildings have been classified as masonry, reinforced concrete and buildings with both RC and bearing masonry walls.

Fig. 1.10 presents a summary of the overall damage data which have been reported for each earthquake. It is worth noting that for masonry buildings the levels of damage are much more evenly distributed whereas for reinforced concrete structures, slight damage is the prevailing damage state.

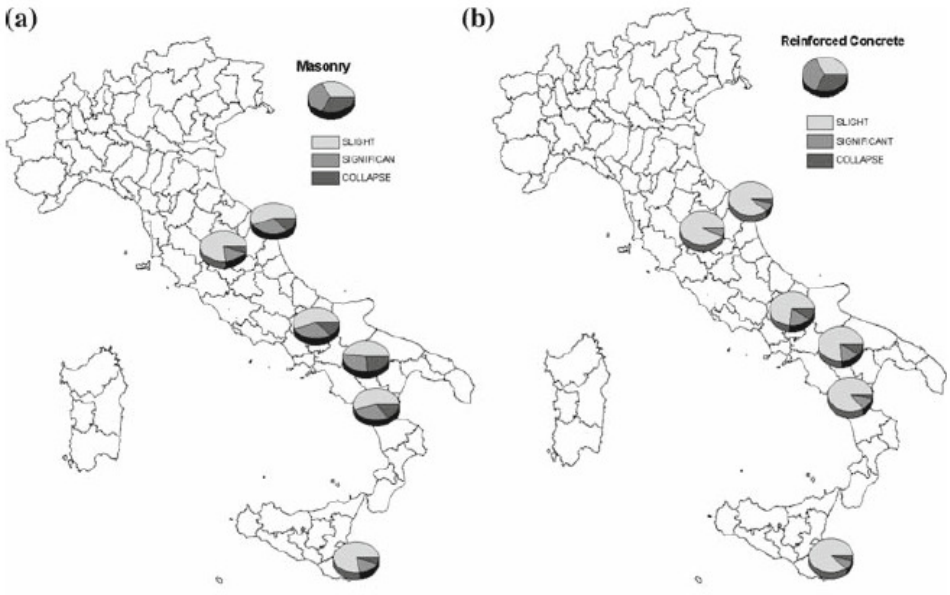

Fig. 1.10: Damage distribution from each earthquake for (a) masonry buildings and (b) reinforced concrete buildings (Colombi et al, 2008).

In presence of seismic actions (Decanini, 2009a; Decanini, 2009b), two mechanisms are generally possible for masonry structures:

- local mechanisms, that essentially concern out of plane actions acting on single masonry walls or portions of the structure: first type collapse mode. Fig. 1.11 – a;
- global mechanisms, that involve the whole structure and concern masonry walls under in plane actions: second type collapse mode. Fig. 1.11 –b.

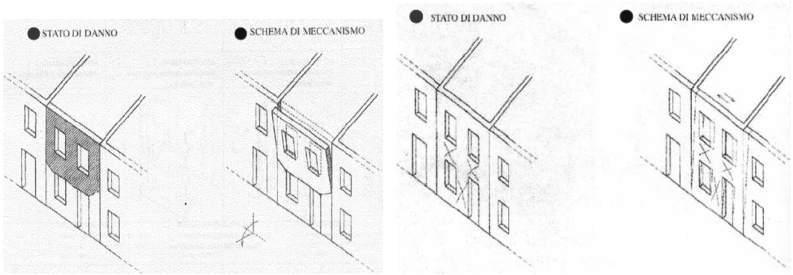

Fig. 1.11: Damage state and corresponding collapse mechanism: a) First type collapse mode; b) second type collapse mode (Decanini, 2009c).

The safety of the structure has to be checked for both types of resistant mechanisms.

The second type of mechanism, described above, and the possibility of strengthening by innovative materials is object of study of the present thesis.

Fig. 1.12 and Fig. 1.13 show one of the most typical damage (Decanini, 2009c) due to in-plane shear action while Fig. 1.14 shows some examples collected during last Italian earthquakes.

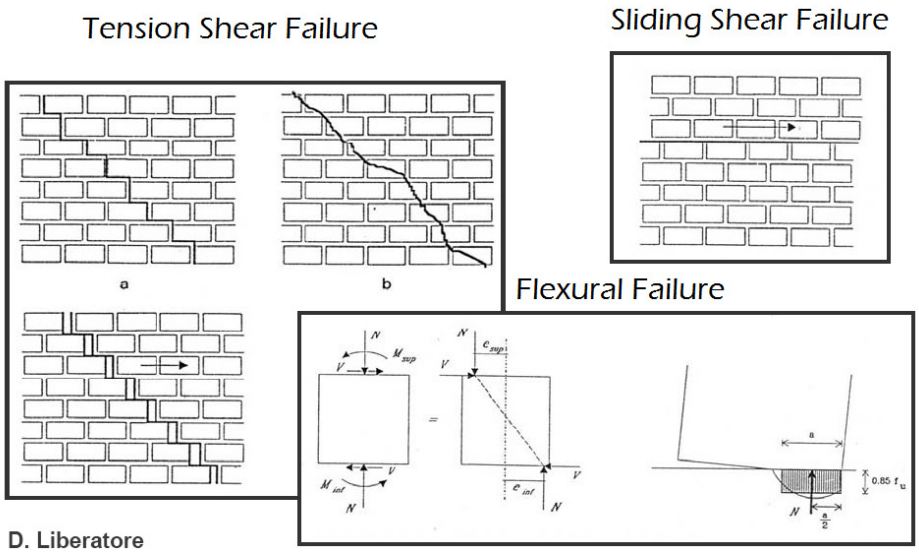

Fig. 1.12: Global mechanisms: in-plane seismic response of unreinforced masonry walls; (Decanini, 2009c).

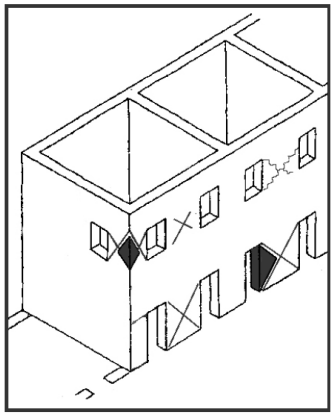

Fig. 1.13: Possible in-plane damages of masonry structures due to shear; (Decanini, 2009c).

Fig. 1.14: In-plane damages of unreinforced masonry walls: a) Irpinia 1980, A.Giuffré; b) - d) Umbria-Marche 1997 L.D. Decanini (Decanini, 2009c).

1.1.3 Final observations on damage of masonry structures.

Some common conclusions can be drawn from the observation of damages on masonry structures, stroke by earthquakes occurred in the last years.

Many masonry buildings subjected to destructive earthquakes were severely damaged or even collapsed due to some unsuitable designs or some mistakes on projects or applications.

Among masonry buildings, especially the historical ones sometimes survived the earthquake with only slightly damaged or even undamaged. In spite of the fact that many new reinforced concrete structures built at the same location have been severely damaged or collapsed. Thus, if masonry buildings are designed to be resistant against earthquake and constructed with good quality materials, they would have survived during the earthquakes. Although the structural type of masonry buildings varies in different earthquake zones, their damage resulting from earthquakes can be commonly classified.

From the observations of the last Turkey's earthquake it has been deduced that many of collapses and damages are attributed to following items: inadequate masonry units, poor mortar, lack of vertical confining elements, irregularities in plane and in vertical direction, inadequate connection of load-bearing walls, insufficient length of load-bearing walls, unconfined gable walls and heavy cantilever elements.

The Kocaeli earthquake points out the fact that reinforced concrete frame system should not be seen as the only alternative for contemporary construction systems, if the masonry buildings can be designed to be earthquake resistant and constructed in order to survive.

As removing of these buildings is not an economic solution, effective seismic strengthening methods must be developed and performed for these buildings.

1.2 Strengthening techniques against in-plane damage of masonry walls

Strengthening techniques of masonry structures can be classified as follows (Circolare del Ministero per i Beni e le Attività Culturali n. 26/2010, 2010):

1. reinforcement aimed at increasing resistance, stiffness, ductility or a combination of them;
2. introduction of new elements, eliminating the local vulnerability of the weakest parts of the structures and improving the global resistance or ductility;
3. introduction of a passive protection through bracing systems and/or base isolating systems;
4. reduction of the structural mass;
5. limitation or variation in the destination of the structure.

This paragraph describes the strengthening techniques for in-plane damages of masonry walls, focusing the attention on the first and second type of interventions and distinguishing between the traditional and the innovative techniques.

The most common traditional techniques for the strengthening of masonry walls, damaged under in-plane actions, are summarized below (EU-India cross cultural program, 2006):

1. injections;
2. reinforced plaster grid;
3. local reconstruction "cuci-scuci technique";
4. external steel reinforcements;
5. artificial diatons.

The use of fiber-reinforced polymer (FRP) materials in structural strengthening is an innovative technique, which, is already of widespread application today. Within the past two decades, FRP systems have been developed for infrastructure applications and used for strengthening and repair of existing structures as an alternative to traditional strengthening methods (Myers, 2011). The use of FRP to retrofit URM wall systems has been proven to be highly effective in improving both the load resistance and the deformability of URM walls subjected to out-of-plane loads and in-plane loads (Myers, 2011). FRP

materials are readily available in several forms such as laminates, sheets, meshes, and bars.

There are several different retrofit methods that can be employed to increase the out-of-plane and in-plane load resistance and improve the behavior of URM wall systems including infill systems.

The two most common retrofit techniques involve externally bonded FRP systems and NSM systems. Both of these techniques have demonstrated promise for upgrading the flexural and shear strengthening of masonry systems. Fig. 1.15 and Fig. 1.16 detail both of these systems.

Fig. 1.15: Externally bonded FRP laminate strengthening for masonry (Myers, 2011).

Fig. 1.16: Near surface mounted (NSM) strengthening for masonry (Myers, 2011).

More recently, new coating technologies such as elastomeric polyurea with and without discrete fibers have also shown great promise for hardening of masonry systems.

In the following both traditional and innovative techniques are described.

1.2.1 Traditional techniques

1.2.1.1 Grout and epoxy injections

Grout injection (ElGawady et al., 2004) is a common strengthening technique, as it does not alter the aesthetic and architectural features of the existing buildings. The main purpose of injections is to restore the original integrity of the wall, filling the voids and cracks present in the masonry Fig. 1.17-a.

Epoxy resin injection, is used for relatively small cracks (less than 2 mm wide) while cement-based grout is considered more appropriate for larger cracks and voids.

Retrofit of walls by cement grouting can be carried out as follows (ElGawady et al., 2004):

- placement of injection ports and sealing of the cracked areas in the basic wall as well as around injection ports;
- washing of cracks and holes with water. Injections of water start from the bottom and go up to the top of the wall, to check which tubes are active;
- injection of grout , with an injection pressure lower than 0.1 MPa, through each port in succession, starting from the lower-most port. After filling all large voids, a second grout mix (cement-based or epoxy) is used for fine cracks.

This technique improves the overall behaviour of the retrofitted URM. Cement-based grout injections can restore the in-plane lateral resistance up to 0.8-1.4 of the unreinforced wall corresponding one (ElGawady et al., 2004), while epoxy injections increase the lateral resistance of about 2-4 times if compared to the unreinforced wall resistance.

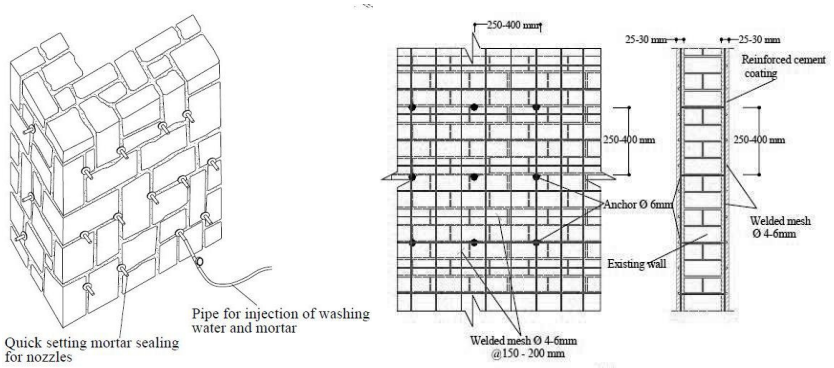

Fig. 1.17: a) Injections (EU-India cross cultural program, 2006) b) Reinforced plaster grid (ElGawady et al., 2004).

1.2.1.2 Reinforced plaster grid

Surface treatment (ElGawady et al., 2004) is a common method, possibly based upon different techniques such as reinforced plaster, ferrocement and shotcrete. This treatment covers the masonry exterior and affects the architectural or historical appearance of the structure.

In case of a reinforced plaster grid, a thin layer of cement plaster applied over high strength steel reinforcement can be used for retrofitting (ElGawady et al., 2004). The steel is generally arranged as a vertical and horizontal mesh but it can be also arranged as diagonal bars. A reinforced plaster can be applied as shown in Fig. 1.17-b.

In diagonal tension test and static cyclic tests, the technique was able to improve the in-plane resistance by a factor of 1.25-3 (ElGawady et al., 2004). The improvement in strength depends on the strengthening layer thickness, the cement mortar strength, the reinforcement quantity and the degree of masonry damage.

1.2.1.3 Local reconstruction: "cuci-scuci technique"

The local reconstruction (EU-India cross cultural program, 2006), also known as "cuci-scuci" technique, consists of a material substitution practised within walls with severe but localized cracks or highly deteriorated parts.

The existing masonry pattern is locally removed where major deterioration has occurred and it is replaced with new masonry closely reproducing the mechanical properties of the original one. It constitutes a historical / traditional technique and was one of the first techniques applied to restoration Fig. 1.18- a.

The main target of the technique is to preserve the mechanical efficiency and regain the continuity in a masonry structure.

It can be considered as a partially reversible intervention which gives the possibility to preserve the structure's appearance.

The relation cost-effect diminishes when the area of intervention becomes larger.

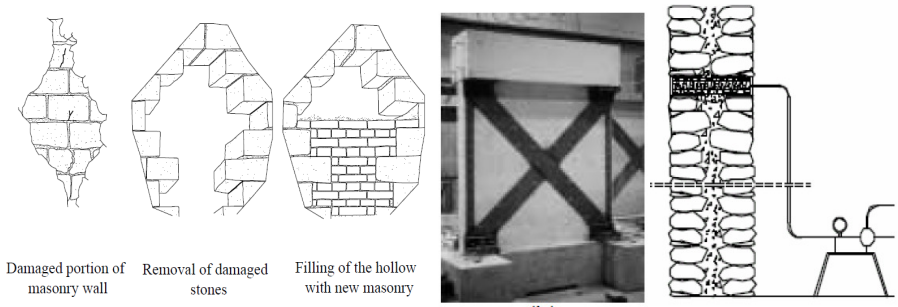

Fig. 1.18: a) Local reconstruction (EU-India cross cultural program, 2006); b) External steel reinforcement (ElGawady et al., 2004); c) Artificial diatons.

1.2.1.4 External steel reinforcement

Steel plates or tubes (EU-India cross cultural program, 2006) can be used as external reinforcements for existing URM buildings. The steel system is attached directly to the existing wall Fig. 1.18- b.

Some experimental tests (EU-India cross cultural program, 2006) using vertical and diagonal steel bracing system demonstrated that this technique can improve the lateral in-plane resistance of the retrofitted wall by a factor of 4.5.

Steel plates are generally used in combination with artificial diatons, whose technique is described below.

1.2.1.5 Artificial diatons

The technique of artificial diatons (EU-India cross cultural program, 2006) is generally applied to multi-leaf masonry walls with inadequate connections between different layers.

Punctual application of artificial diatons to the wall, either with transversal steel bars or with reinforced concrete elements, casts in transversal holes drilled through the whole thickness of the wall Fig. 1.18- c.

The main target of this technique is to avoid the separation between different layers, thus improving the mechanical properties of the wall.

1.2.2 Innovative techniques: FRP

Conventional masonry retrofitting methods (Myers, 2011), which typically involve the use of additional concrete and steel reinforcement, tend to not only add significant mass to a structure, but in many cases the methods result in a reduction of available space for building occupants. In addition to the effects on the building, conventional retrofit methods also tend to be both time consuming and expensive.

The use of modern retrofit systems, which involve the use of fiber reinforced polymers (FRP), are aimed to address and improve upon the negative traits associated with conventional techniques of retrofitting masonry structures.

In the following a brief description of materials, type of fibers, strengthening systems and their mechanical properties are presented.

1.2.2.1 Materials

Continuous fiber-reinforced materials with polymeric matrix (FRP) (CNR-DT-200, 2009) can be considered as composite, heterogeneous, and anisotropic materials with a prevalent linear elastic behaviour up to failure.

Composites for structural strengthening are available in several geometries from laminates used for strengthening of members with

regular surface to bi-directional fabrics easily adaptable to the shape of the member to be strengthened.

Composite materials exhibit the following characteristics:

- they are made of two or more materials (phases) of different nature and "macroscopically" distinguishable;
- at least two phases have physical and mechanical properties quite different from each other, such to provide composite with different properties than those of its constituents.

Fiber-reinforced composites with polymeric matrix (FRP) satisfy both of the above characteristics: they are made of an organic polymeric matrix and fibers. They can be recognized in two categories, regardless of their production technology:

- single-layer: lamina;
- multi-layer: laminates.

Laminates are materials composed of stacked layers (the lamina) whose thickness is usually of some tenths of a millimetre. In the simplest case, fibers are embedded only in the lamina's plane (there are no fibers arranged orthogonally to that plane). The size of laminates is intermediate between those of the fibers and those of engineering structures.

1.2.2.2 Type of fibers

Three types of fibers are commonly used in FRP composites for infrastructure applications (Tumialan et al., 2009): carbon, aramid and glass fibers. In the order listed, these fibers exhibit an ultimate strain ranging from 1 to 4%, with no yielding occurring prior to failure.

In many instances, glass FRP (GFRP) is preferred for strengthening of masonry. The lower elastic modulus of GFRP, as compared to carbon FRP (CFRP), is not as limiting in masonry strengthening applications as it might be in concrete structures because it is more compatible with the low elastic modulus of masonry. In addition, GFRP material costs are substantially less than carbon or aramid materials. Also, experimental data from shear strengthening of masonry walls have shown that use of

CFRP systems do not offer significant improvement in structural performance over similar GFRP systems.

Use of CFRP systems, however, is preferable for applications where masonry elements will be subjected to sustained stresses, such as in retaining walls. CFRP systems are more suitable for these applications since they have better resistance to creep than other fibers. Also, in exterior applications, CFRP is generally a better option because of its superior durability in most environments compared to GFRP.

Aramid is not commonly used in masonry. The material properties for aramid are sensitive to moisture change, which is common in masonry construction.

1.2.2.3 Strengthening systems

FRP systems (CNR-DT-200, 2009) are suitable for external strengthening of structures and can be classified as follows:

- pre-cured systems: manufactured in various shapes by pultrusion or lamination, pre-cured systems are directly bonded to the structural member to be strengthened;
- wet lay-up systems: manufactured with fibers laying in one or more directions as FRP sheets or fabrics and impregnated with resin at the working site to the support;
- prepreg systems: manufactured with unidirectional or multidirectional fiber sheets or fabrics pre-impregnated at the manufacturing plant with partially polymerized resin. They may be bonded to the member to be strengthened with (or without) the use of additional resins.

1.2.2.4 Mechanical properties of FRP strengthening systems

In FRP composites, (CNR-DT-200, 2009) fibers provide both loading carrying capacity and membrane stiffness. In tension the matrix is necessary to ensure sharing of the load among fibers and to protect the fibers themselves from the environment. Most FRP composites are made

of fibers with high strength and stiffness, while their strain at failure is lower than that of the matrix.

Fig. 1.19 shows the stress-strain relationship for an unidirectional FRP material and its constituents: the matrix and the fiber.

The resulting FRP material has lower stiffness than fibers and fails at the same strain, $\varepsilon_{f,max}$, of the fibers themselves. In fact, beyond such ultimate strain, load sharing from fibers to the matrix is prevented.

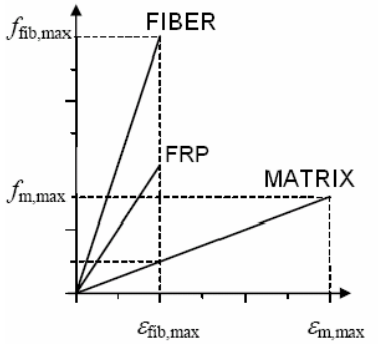

Fig. 1.19: Stress-strain relationship of fibers, matrix and FRP material (CNR-DT-200, 2009).

1.3 Strengthening of masonry structures by FRP composites

The objective of FRP strengthening (CNR-DT-200, 2009) of masonry structures is to increase the capacity of each member as well as the overall capacity of the structure.

FRP materials in the form of laminates, sheets, grids and bars, can be applied on the members by adhesion or by means of mechanical anchorage devices. FRP reinforcement may be applied to the external surfaces of the masonry structure as well as in slots or grooves cut in the masonry itself.

The emerging FRP industry has recognized an opportunity to employ high-strength composites to improve structural capacity or stabilize distress in masonry constructions, especially walls.

FRP (Tumialan et al., 2009) can effectively be used as a flexural or shear strengthening element to upgrade structural capacity, or to restore the original capacity of damaged elements (most commonly walls)

subject to in-plane load. The advantages of FRP composites for masonry retrofitting include lower installation costs, improved corrosion resistance, flexibility of use, and minimum changes in member size (and in some cases appearance) after repair. Disturbance to occupants and loss of usable spaces are also minimal. Furthermore, for earthquake retrofits, seismic mass of the existing structure remains quite unchanged because there is a little addition of weight.

1.3.1 FRP retrofitting techniques

Two FRP techniques are worthy of mention for strengthening masonry structures:

- externally-bonded FRP laminates;
- near-surface-mounted (NSM) FRP bars.

Laminates come in two forms: FRP sheets (fabrics) and pre-cured strips (plates): FRP sheets are typically woven from individual uni-, bi-, or multi-directionally oriented fibers into thin sheets resembling wallpaper without a binding matrix material (Tumialan et al., 2009). FRP sheets are typically applied by manual wet lay-up and are adhered with adhesive onto the prepared surface of the member that is being strengthened.

1.3.1.1 Externally-bonded FRP laminates

Thin glass or (FEMA 308, 1999) carbon fibers woven into a fabric sheet can be applied to the surface of the wall to enhance the stiffness and strength of the wall. The fibers are generally applied to the surface using an epoxy resin binder and can be oriented in one direction or two directions. The composite fibers are used as tension reinforcing for the wall and can therefore increase the in-plane strength of the wall.

The typical repair materials used in this technique are the carbon-fiber or glass-fiber sheets, the epoxy for bonding the sheets to the wall, anchors for attaching composite fiber sheets to substrate and finally surface coatings.

1.3.1.2 Near-surface-mounted (NSM) FRP bars

NSM bars are rectangular or round pultruded elements that contain highstrength fiber embedded in a pre-cured matrix (Tumialan et al., 2009). NSM FRP bars are placed in grooves cut on the masonry surface, typically in joints (if practical), which allows for minimal alteration of appearance. The grooves are partially filled with an epoxy or cement-based paste. The bar is then placed into the groove and lightly pressed to force the paste to flow around the bar.

1.4 Aims and objectives of this work

This Doctoral Thesis addresses the behaviour of masonry walls externally reinforced by FRP laminates under in-plane actions.

Masonry structures represent a significant (Sguazzo et al., 2010) part of the built heritage of southern Europe. In the past, they have been usually realised according to rules of practice or designed against only gravitational loads. Consequently, they are often in need for retrofitting, to improve their seismic performance, possibly meeting the current seismic safety standards. Shear strengthening of masonry walls is actually one of the most common interventions aimed at improving the capacity of the structure against lateral seismic-induced actions. The use of composite materials for this purpose is more and more common.

FRP materials are widely used for strengthening of civil structures, offering a good alternative solution. There are many advantages of using FRPs: lightweight, good mechanical properties, corrosion-resistance and easy application, if compared to the traditional techniques which often present disadvantages like space reduction, heavy mass addition and corrosion.

Particularly masonry (CNR-DT-200, 2009)walls may be strengthened with FRP materials to increase their load carrying capacities or their ductilities for in-plane or out-of-plane loads.

Several analytical models are already available for determining the shear strength of masonry walls externally strengthened by composites (Tomazevic et al., 1993; Triantafillou, 1998). Huge research activities

have been carried out for investigating the in-plane behaviour of externally strengthened masonry walls; the effect of strengthening based on carbon fiber-reinforced polymers (C-FRP) has been investigated (Olivito and Zuccarello, 2005; Micelli and Ombres, 2003; Santa Maria et al., 2004; Alcaino and Santa Maria, 2008; Erol et al., 2004) as well as glass FRP (G-FRP) (Corradi et al., 2002; Marcari et al. 2004; Prota et al., 2005; Aiello et al., 2007; Mahmood et al., 2008) or polyvinyl-alcohol (Valluzzi et al., 2002). Experimental results are also available for masonry walls externally strengthened by carbon-fiber reinforced cement matrix (CFRCM) (Faella et al., 2006; De Nicolo et al., 2004; Marcari et al., 2004) or G-FRCM sheets (Stratford et al., 2002).

However, nowadays no well-established design relationships are yet available and the most recent codes of standards, to predict the shear strength of unreinforced masonry walls (ASTM E 519– 02) and fiber reinforced masonry walls (EC6, 1998; AC125, 2001; CNR - DT 200, 2009), suggest formulations resulting in significant scatter when compared one-another, since each one has been calibrated on few experimental results.

The present thesis, firstly addresses the in-plane behaviour of externally strengthened masonry walls. A wide database of experimental results drawn out by the scientific literature is presented in chapter 3; it collects results deriving from both diagonal compression and shear compression tests. Finally, a comparison between the experimental results, collected within the database, and the theoretical values, deriving from the considered models, will be presented and discussed in the same section.

A strong research effort, possibly supported by refined numerical modelling, is needed as it represents a possible support in this area.

Thus, a refined finite element (FE) model is implemented for simulating the influence of different arrangements and layouts of the FRP reinforcement on the in-plane response of strengthened masonry walls. The model is firstly validated by using experimental results of in plane shear-compression tests carried out on FRP-strengthened tuff-masonry walls and currently available in the scientific literature. Both masonry and FRP strips are modelled according to the "macro-modelling" approach and the bond between FRP and the masonry

substrate is simulated through interface elements. The mechanical parameters of masonry as well as suitable data on bond behaviour of the FRP are derived from available tests. The numerical analyses are carried out by including the nonlinear behaviour of both the masonry elements and FRP-to-masonry interface.

A parametric analysis is presented for understanding the influence of the main geometric and mechanical parameters of both masonry and FRP on the in-plane shear strength and displacement capacity of the strengthened tuff-masonry walls. Finally, the predictions of analytical models currently available either in the scientific literature or in the most recent codes of standards will be compared with the simulation of the numerical analyses with the aim of assessing them and pointing out the possible need for further enhancement of their analytical formulation, which is among the main objectives of future research activities.

.

CHAPTER 2

2. Models

This chapter outlines code provisions and analytical models on the shear strength of masonry walls externally strengthened by FRP composites.

Numerous analytical formulae are available in the scientific literature for evaluating shear strength of masonry walls strengthened by composite materials. They are often empirical in nature, since they have been usually calibrated on the experimental results available in the knowledge of the various researches.

A brief summary of the most well-established models for unstrengthened masonry in shear will be outlined in the next section before of a more in-depth review of the various proposals for determining the shear strength in FRP strengthened walls.

2.1 Reference codes formulations

2.1.1 Shear resistance of unstrengthened masonry walls

Two main failure modes are generally considered for masonry walls under in plane shear actions (Sguazzo et al., 2010).

The first one is characterised by a diagonal crack and the corresponding average shear stress $\tau_{m,m}$ (referred to the nominal transverse section of the wall) can be evaluated as follows (Turnsek and Cacovic, 1970):

$$\tau_{m,m} = \tau_{m,0}\sqrt{1+\frac{\sigma_0}{1.5\tau_{m,0}}} \qquad (2.1)$$

where $\tau_{m,0}$ is the same shear strength evaluated without any axial force, and σ_0 is the average axial stress. Since Eqn. (2.1) is derived by controlling the principal tensile stress, the failure mode described above can be referred as "tension shear".

The second relevant failure mode is characterised by a substantially horizontal crack and the corresponding shear strength f_v (actually, referred at the compressed part of the transverse section) can be evaluated as follows:

$$f_v = f_{v,0} + \mu \cdot \sigma_0 \qquad (2.2)$$

where $f_{v,0}$ is related to the cohesion of masonry and μ is the friction coefficient. Eqn. (2.2) is adopted by both the European (EC6, 1998) and the New Italian Code (NTC 2008), assuming μ=0.40. The corresponding failure mode can be referred as "sliding-shear".

Finally, the shear capacity $V_{R,m}$ of unstrengthened masonry walls can be evaluated by means of Eqn. (2.3) in the case of "tension-shear" failure:

$$V_{Rm} = \tau_{m,m} \cdot l \cdot t \qquad (2.3)$$

where l is the depth of wall horizontal section and t its thickness. On the contrary, the shear capacity of walls failing in "sliding shear" can be defined according to Eqn. (2.4) as follows:

$$V_{Rm} = f_v \cdot l_c \cdot t \qquad (2.4)$$

where l_c is the length of the compressed zone of the transverse section.

2.1.2 Eurocode 6 and Italian Code

Eurocode 6 (1998), in chapter 6.2 defines, the shear resistance of a masonry wall, V_{Rm} as:

$$V_{Rm} = f_v \cdot l_c \cdot t \tag{2.4}$$

The New Italian Code (2008) reminds to proved validated codes, defining the shear strength as in the previous equation (2.4), to verify masonry walls subjected to in plane shear loads.

2.1.3 German Standard (DIN 1053-100)

In the German Standard DIN 1053-100 (Jäger and Schöps, 2008), the value of the shear resistance of masonry V_{Rm} results from:

$$V_{Rm} = \alpha_s \cdot \frac{f_{v,k}}{\gamma_M} \cdot \frac{t}{c} \tag{2.5}$$

where:
$f_{v,k}$ is the characteristic shear strength;
γ_M is the partial safety factor for the material;
α_s is the coefficient of the shear capacity and it can be $\alpha_s = l$ and $\alpha_s = l_c$
t is the thickness of the wall;
c is a factor, considering the shear stress distribution over the cross section and depends on the geometry of the wall as follows:

$$c = 1.0 \quad \text{for } h/l \le 1 \tag{2.6}$$

$$c = 1.5 \quad \text{for } h/l \ge 2$$

where:
h is the height of the wall;

l is the length of the wall.

It can be noted as the German standard includes a factor which considers the distribution of the shear stresses along the wall.

In the German Standard the equations for the shear strength f_v refer to a model by Mann and Müller which, in 1973, enhanced the Coulomb friction criterion (Graubner and Kranzler, 2005).

They developed a failure hypothesis which considers different material properties of units, mortar and joints.

The hypothesis of their study led to the theory that shear stresses exist only in the bed joints.

Consequently only the failure of friction along the bed joints and the tensile failure of the unit are considered.

2.1.3.1 Failure of bed joints due to the friction

In case of failure (Jäger and Schöps, 2008) due to the friction of the bed joint, Mann/Müller criterion gives the following conditional equation (2.7):

$$f_{v,k} = \frac{f_{v,k0} + \mu \cdot \sigma_0}{1 + \mu \cdot \frac{2 \cdot h}{l}} \qquad (2.7)$$

where applying a friction coefficient of $\mu = 0.65$ and a ratio of $h/l = 1/2$, a decreased friction coefficient $\bar{\mu} = 0.4$ and a decreased initial shear strength $f'_{vk,0} = 0.606\ f_{vk,0}$ will result obtaining the equation for verifying shear loading according to DIN 1053-100:

$$f_{v,k} = f'_{v,k0} + \bar{\mu} \cdot \sigma_0 \qquad (2.8)$$

where:

$f'_{vk,0}$ is the decreased initial shear strength depending on the type of mortar;

$\bar{\mu}$ is the decreased friction coefficient which can be used for all types of mortar.

2.1.3.2 Failure of tensile strength of units (ripping of the units)

Mann and Müller (Jäger and Schöps, 2008) also derived the tensile failure of the unit from the first principal stress (tension) in the middle of the unit. There a shear stress factor of 2.3 for the maximal shear stress in the unit was considered. The resulting equation is:

$$f_{v,k} = \frac{f_{bt}}{2.3} \cdot \sqrt{1 + \frac{\sigma_0}{f_{bt}}} \qquad (2.9)$$

where:
σ_0 is the compressive stress at the location of the maximal shear stress;
f_{bt} is the tensile strength of the unit depending on the type of bricks as follows:
$f_{bt} = 0.025\ f_{bk}$ for hollow bricks;
$f_{bt} = 0.033\ f_{bk}$ for perforated bricks and units with grip holes or grip pockets;
$f_{bt} = 0.040\ f_{bk}$ for bricks without grip holes or grip pockets;
f_{bk} is the characteristic value for compressive strength of the unit.

2.1.4 Swiss Code for masonry structures

In 2003 the Swiss Society of Engineers and Architects (SIA) introduced the new masonry code SIA 266 (2003). The basis of this standard are the investigation of Ganz and Thuerlimann (Graubner and Kranzler, 2005) which, in 1958, developed a failure criteria of unreinforced masonry without tensile strength, which was based on the theory of plasticity.

In case of shear with centric normal force (SIA, 2003; Graubner and Kranzler, 2005), the structural safety is verified if the compressive strength is nowhere exceeded, as shown in Fig. 2.1. Inclined compressive stresses up to a value of $f_{\alpha d}$ may be superimposed on the

compressive stresses acting normal to the bed joints up to a value of f_{xd}-f_{ad}.

The uniaxial compressive strength $f_{\alpha d}$ depends on the angle of inclination of the assumed compressive stress field.

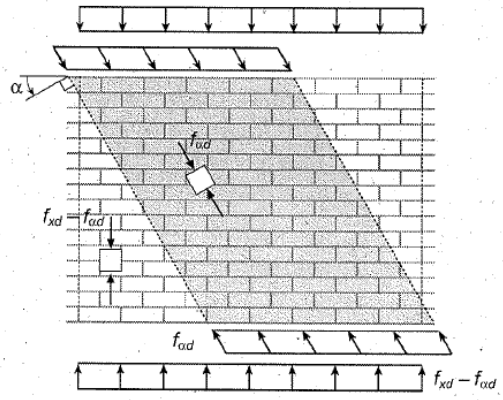

α	$f_{\alpha d}$
0°	f_{xd}
$0 < \alpha \leq \arctan \mu_d$	f_{yd}
$\arctan \mu_d < \alpha < 90°$	0
90°	f_{yd}

Fig. 2.1: Superposition of compressive strress fields and dimensioning value of masonry compressive strength as a function of the inclination of the compressive stresses.

For simple walls the ultimate shear resistance of the wall is defined as:

$$V_{Rm} = k_v \cdot l_l \cdot t_w \cdot f_{yd} \qquad (2.10)$$

where

$$l_l = l_w - \frac{2M_{z1d}}{N_{xd}}$$

l_w is the wall length;
M_{z1d} is the dimensioning value of the bending moment acting at top of wall normal to plane of wall;
N_{xd} is the dimensioning value of N_x;
k_v is the factor defined from the following diagrams:

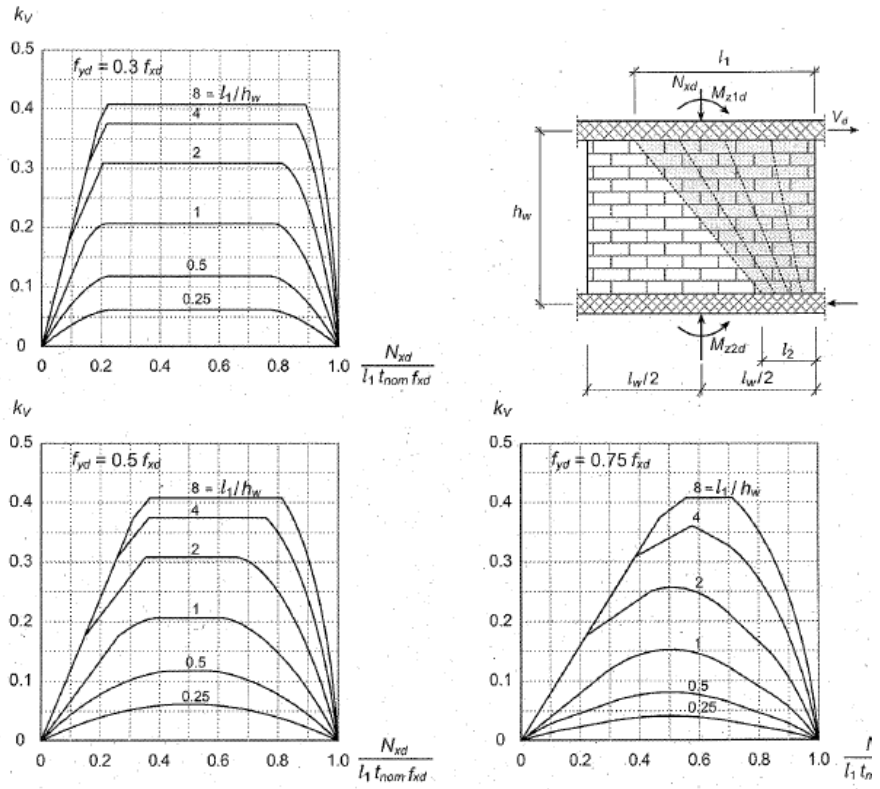

Fig. 2.2: Factors to determine the ultimate resistance under shear (SIA, 2003)

Fig. 2.2 shows the shear capacity for different ratios f_{yd}/f_{xd}. The shear resistance increases significantly with increased values for the masonry compressive strength normal to head joints f_{yd}.

The value of the compressive strength of masonry normal to the bed joints is:

$$f_{xd} = \eta_1 \eta_2 \frac{f_{xk}}{\gamma_M} \qquad (2.11)$$

where:

γ_M =2.0 and f_{xk} is the characteristic value of compressive strength of mortar.

The value of the compressive strength of masonry normal to the head joints is:

$$f_{yd} = \eta_1 \eta_2 \frac{f_{yk}}{\gamma_M} \quad (2.12)$$

where:
γ_M =2.0.

For standard masonry the values of the characteristic value of compressive strength of masonry normal to head joints f_{yk}, shall be assumed as follows, depending on the type of brick:

$$f_{yk} = 0.3 \cdot f_{xk} \quad (2.13)$$

or

$$f_{yk} = 0.5 \cdot f_{xk} \quad (2.14)$$

2.1.5 Australian Standard (AS 3700)

An example of a non-European masonry standard is the Australian Standard (Jäger and Schöps, 2008) which considers the shear capacity of unreinforced masonry walls as:

$$V_{Rm} = V_1 + V_2 \quad (2.15)$$

with:

$$V_1 = \phi \cdot f_v \cdot A \qquad (2.16)$$

$$V_2 = k_v \cdot f_{mj} \cdot A \qquad (2.17)$$

or in short notation:

$$V_{Rm} = \left(\phi \cdot f_v + k_v \cdot f_{mj}\right) \cdot A \qquad (2.18)$$

where:
k_v is the friction coefficient (shear factor), which depends on the type of masonry and varies from 0.12 to 0.3;
f_{vk} is the characteristic shear strength of masonry;
A is the cross-section of the wall;
f_{mj} the minimum compressive stress on the bed joint (not greater than 2 MPa);
ϕ the capacity reduction factor:

$$\phi = \frac{1}{\gamma_M} \qquad (2.19)$$

It can be noted as the Australian Standard (Jäger and Schöps, 2008) provides users with possible reduction factors to evaluate the strength capacity of the masonry wall.

2.2 Shear resistance of FRP strengthened masonry walls

Six proposals for quantifying the term V_{Rf} in equation (2.3) are outlined in the present paragraph (Sguazzo, 2010).

2.2.1 The model by Tomazevic & Al (1993)

Tomazevic model has been originally proposed for masonry walls reinforced with steel bars (Tomazevic at al., 1993; Valluzzi et al., 2002). The masonry contribution V_{Rm} is reduced by an effectiveness factor of 0.90 and the terms V_{Rf} can be expressed as follows (and denoted by $V_{Rf,1}$):

$$V_{Rf,1} = 0.4 \cdot A_f \cdot f_{f,u} \tag{2.20}$$

where A_f is the area of the shear reinforcement and $f_{f,u}$ is the ultimate tensile strength of strengthening. Consequently, the following theoretical expression $V_{R,1}^{th}$ can be introduced for shear strength V_R:

$$V_{R,1}^{th} = 0.9 \cdot t \cdot l \cdot \tau_{m,0} \cdot \sqrt{1 + \frac{\sigma_0}{1.5 \cdot \tau_{m,0}}} + 0.4 \cdot A_f \cdot f_{f,u} \tag{2.21}$$

2.2.2 The Triantafillou (1998) model

The Triantafillou (1998) model introduces the following expression $V_{Rf,2}$ for the term V_{Rf} in Eqn. 2.1, assuming a constant value d=0.8 l for the depth of the section in compression and an effective value $\varepsilon_{fib,eff}$ of the axial strain of fibers at debonding:

$$V_{Rf,2} = 0.9 \cdot d \cdot t \cdot \rho_f \cdot E_{fib} \cdot \varepsilon_{fib,eff} \tag{2.22}$$

where:

ρ_f is the reinforcement ratio of FRP in the horizontal direction;

E_{fib} is the Young Modulus of fibers;

$\varepsilon_{fib,eff}$ is the effective value of axial stress in FRP, defined by the same author considering the experimental results of pull-out tests of FRP strips on concrete blocks:

$$\varepsilon_{fib,eff} = 0.0119 - 0.0205 \cdot \rho_f \cdot E_{fib} + 0.0104 \cdot (\rho_f \cdot E_{fib})^2 \quad (2.23)$$

Finally, the complete expression of the shear strength according to Eqn. 2.1 is:

$$V_{R,2}^{th} = 0.8 \cdot f_v \cdot t \cdot l + 0.9 \cdot t \cdot d \cdot \rho_f \cdot E_{fib} \cdot \varepsilon_{fib,eff} \quad (2.24)$$

2.2.3 EC6 (1998) model

The formula proposed by EC6 (1998) for shear strength of masonry walls internally reinforced by steel bars can be extended to the case of external strengthening with composite materials:

$$V_{Rf,3} = 0.9 \cdot d \cdot t \cdot \rho_f \cdot f_{f,u} \quad (2.25)$$

and the complete expression of the shear strength is:

$$V_{R,3}^{th} = (f_{v0} + 0.4 \cdot \sigma_0) \cdot t \cdot d + 0.9 \cdot d \cdot t \cdot \rho_f \cdot f_{f,u} \quad (2.26)$$

with the above meaning of the symbols.

2.2.4 AC125 (2001) model

An alternative expression $V_{Rf,4}$ of the term V_{Rf} in eq. (2.1) is proposed by AC125 (2001) document:

$$V_{Rf,4} = 0.75 \cdot l \cdot t \cdot \rho_f \cdot f_{f,eff} \tag{2.27}$$

where $f_{f,eff}$ is the effective tensile strength of the composite strengthening defined as follows:

$$f_{f,eff} = \min(0.004 \cdot E_f ; 0.75 \cdot f_{f,u}) \tag{2.28}$$

A tension-shear based term like the one in Eqn. 2.2 is considered in the following application for the masonry contribution to shear strength V_R according to Eqn. 2.1:

$$V_{R,4}^{th} = l \cdot t \cdot \tau_{m,0} \cdot \sqrt{1 + \frac{\sigma_0}{1.5\tau_{m,0}}} + 0.75 \cdot l \cdot t \cdot \rho_f \cdot f_{f,eff} \tag{2.29}$$

2.2.5 CNR-DT 200/2004 guidelines (2009) model

The guidelines CNR - DT 200 (2009) propose the following expression for V_{Rf}:

$$V_{Rf,5} = \frac{0.6 \cdot d \cdot 2 \cdot t_f \cdot b_f \cdot f_f}{p_f} \tag{2.30}$$

where:
t_f is the thickness of FRP laminate;

l_f is the length of FRP reinforcement measured orthogonally to the direction of the fibers;
p_f is the vertical spacing of the strips measured orthogonally to the direction of the fibers;
f_f is the tensile strength of the composite defined as the minimum value between the ultimate strength $f_{f,u}$ and the strength of the composite in condition of debonding $f_{f,db}$. The shear resistance of the masonry reinforced by FRP the CNR - DT 200 (2009) proposes the following expression:

$$V_{R,5}^{th} = \min\left\{\left(f_v \cdot d \cdot t + \frac{0.6 \cdot d \cdot A_f \cdot f_f}{p_f}\right); V_{R,max}\right\} \tag{2.31}$$

where $V_{R,max}$ is the shear resistance corresponding to the failure of the compressed strut of masonry.

If shear strengthening is placed in diagonal configuration, the shear resistance can be evaluated ignoring the contribution of the compressed composite as follows:

$$V_{R,5,diag}^{th} = \frac{\delta}{h}\left(\frac{f_v \cdot x_{min} \cdot t}{0.005} + \frac{h \cdot \cos^3 \alpha}{l} \cdot E_f \cdot A_f\right) \tag{2.32}$$

where:
δ is the relative displacement between the edges of the masonry panel;
h is the height of the panel;

$$\frac{\delta_R}{h} = \min\left(0.005, \frac{f_{f,db} \cdot l}{E_f \cdot h \cdot \cos^2 \alpha}\right) \tag{2.33}$$

$f_{f,db}$ is the debonding strength of FRP reinforcement;
l is the length of the panel;
x_{min} is the distance from extreme compression to neutral axis;
α is the angle of the tight diagonal to the horizontal axis of the panel;
A_f is the area of the diagonal reinforcement in tension.

2.2.6 ACI 440.7R-10 guide (2010) model

In 2010, the American Concrete Institute (ACI) published a new standard ACI 440.7R-10 (2010), which defines the shear resistance of masonry walls with horizontal FRP strengthening.

The shear strength of the FRP-strengthened wall is computed by adding the FRP contribution V_f to the nominal strength of the URM wall:

$$V_{R,6}^{th} = V_{Rm} + V_{Rf} \tag{2.34}$$

V_{Rm} is the existing in-plane strength of the wall, which should be evaluated first. For the shear strength of masonry the ACI 440.7R-10 (2010) takes into account three failure modes which may result from in-plane shear including joint sliding (V_{js}), diagonal tension (V_{dt}) and toe-crushing (V_{tc}). Joint sliding and diagonal tension are shear-controlled failure modes while toe-crushing is a flexural-controlled failure mode.

The nominal shear strength of USM walls should be computed as:

$$V_{Rm} = \min(V_{bjs,} V_{dt}, V_{tc}) \tag{2.35}$$

Unreinforced masonry walls requiring shear strengthening against in-plane loads are those walls whose failure mode is due to either stepped joint sliding or diagonal tension.

The FRP strengthening contribution is:

$$V_{Rf} = v_f l_f \frac{d_v}{p_f} \tag{2.36}$$

l_f is the width of the FRP laminates;
p_f is the center to center spacing between each strip;
d_v is the effective masonry depth for shear calculations given by:

$$d_v = \min(l, h) \tag{2.37}$$

v_f is the force per unit width that the FRP system transfers to the masonry substrate and for surface-mounted FRP systems is calculated as:

$$v_f = n t_f f_{f,eff} \leq 260\ N/mm \tag{2.38}$$

Debonding of the FRP system can occur if the force in the FRP system at the strength limit state cannot be sustained by the masonry substrate. For a typical FRP system that is linear elastic until failure, the level of strain in the FRP system will dictate the level of stress developed in the system. To prevent debonding, a limitation is placed on the strain level developed in the FRP laminate. The maximum strain and corresponding stress that FRP systems can attain before debonding from the masonry substrate are defined as effective strain $\varepsilon_{f,eff}$ and effective stress $f_{f,eff}$.

The effective strain $\varepsilon_{f,eff}$ and effective stress $f_{f,eff}$ to be used for the design of shear in-plane FRP strengthening of masonry walls can be computed respectively as:

$$\varepsilon_{f,eff} = k_v \varepsilon_{f,u}{}^* \leq C_E \varepsilon_{f,u}{}^* \tag{2.39}$$

and

$$f_{f,eff} = E_f \varepsilon_{f,eff} \tag{2.40}$$

where k_v is the bond reduction coefficient for shear-controlled failure modes:

$$k_v = \begin{cases} 0.40 \quad \text{for } \omega_f \le 0.20 \\ 0.64 - 1.2\omega_f \quad \text{for } 0.20 < \omega_f \le 0.45 \\ 0.10 \quad \text{for } \omega_f > 0.45 \end{cases} \tag{2.41}$$

It depends on the FRP reinforcement index ω_f, defined in the following equation:

$$\omega_f = \frac{1}{85}\frac{A_f E_f}{A_n \sqrt{f'_m}} \tag{2.42}$$

For shear-controlled failure modes, the bond reduction coefficient ω_f is again calibrated based on experimental data (ACI 440.7R, 2010). The coefficient for shear-controlled failure modes is equal for both FRP laminates and NSM FRP systems.

CHAPTER 3

3.Experimental Database

3.1 Database composition

A database collecting a set of experimental results (Sguazzo, 2007; Faella et al., 2009; Sguazzo, 2010) of shear tests on unstrengthened masonry (USM) walls and strengthened masonry (SM) walls available in the scientific literature, has been assembled for assessing the capacity models outlined in the previous chapter. It collects 252 tests: 105 tests on USM walls and 147 tests on SM walls, whose geometrical and mechanical properties have a wide range of variation covering various kinds of masonry, fibers quality and texture, composite materials (namely, carbon- or glass-based, but even made out of epoxy as well as cement matrices) and test arrangements.

The considered experimental data have been found in the works by Stratford et al. (2002), Valluzzi et al. (2002), Corradi et al. (2003), Micelli and Ombres (2003), Mera and La Tegola (2004), Marcari et al. (2004), De Nicolo et al. (2004), Erol et al. (2004), Santa Maria et al. (2004), Olivito and Zuccarello (2005); Prota et al. (2005), Lourenço et al. (2005), Faella et al. (2006), Aiello et al. (2007), Marcari et al (2007), Alcaino and Santa Maria (2008), Silva et al. (2008), Mahmood et al (2008).

A quick description of the database structure and content will be drawn out in the following.

The accuracy of the models outlined in the previous chapter will be assessed by means of the experimental results of both USM and SM databases.

3.1.1 Database for unstrengthened masonry

This subsection reports a brief description of the USM database content by means of a classification depending on the nature of masonry specimens and the type of test performed to determinate the shear strength.

The specimens collected in the USM database have been tested either in diagonal compression or in shear compression tests.

Fig. 3.1 deals with tests on USM pointing out that 76 tests have been performed in diagonal compression and 29 in shear compression. Moreover, 56 out of 105 (51% of the total) specimens are made out of natural stones; among those 49 (47% of the total) are bricks and 2 specimen are of natural stones with two rows of solid bricks (Valluzzi et al., 2002).

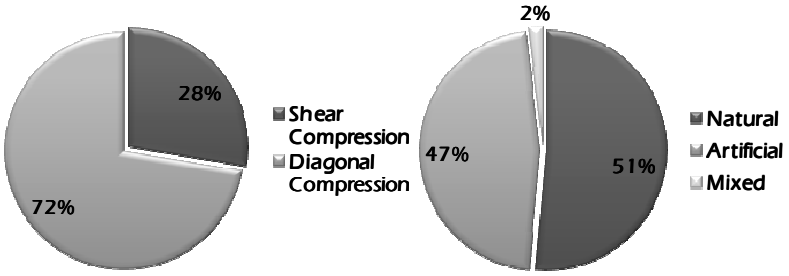

Fig. 3.1: Key properties of the USM experimental database: a) type of performed tests; b) nature of masonry.

3.1.2 Database for strengthened masonry

The description of the SM database is presented, following the same criterion for the classification of the specimens and presenting an additional category on the characteristics of the composite reinforcement applied to the walls.

The SM specimens have been tested either in diagonal compression or in shear compression tests; particularly, 111 tests have been performed in diagonal compression and 57 in shear compression as shown in Fig. 3.2. Moreover, 76 out of 168 (45% of the total) specimens

are made out of natural stones; among those 50 are made by hollow bricks. Fig. 3.3 points out the nature of composite reinforcement assumed by the 147 specimens collected within the database: the specimens are strengthened by FRP strips: Carbon (C-) FRP, Glass (G-) FRP and specimens with polyvinyl alcohol (PVA-) based composites while the remaining ones are reinforced by composite materials with a cement matrix (CFRCM).

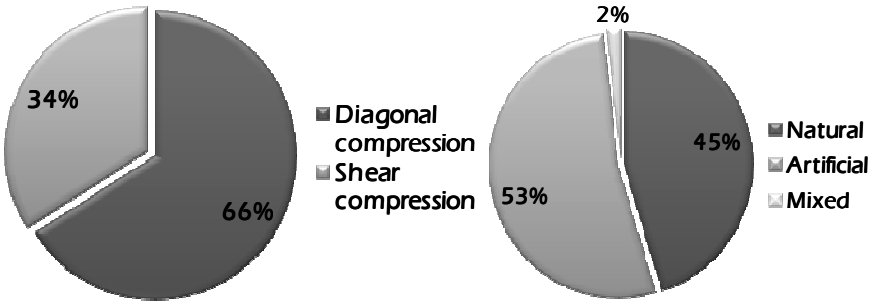

Fig. 3.2: Key properties of the SM experimental database: a) type of performed tests; b) nature of masonry.

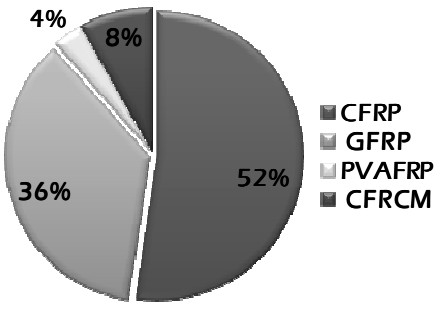

Fig. 3.3: Key properties of the SM experimental database: type of external strengthening

3.2 USM database: data processing

3.2.1 Introduction

The contents of the USM database, previously introduced, have been organized by identifying each experimental data in a context based on Italian (NTC, 2008) and European (EC6, 1998) codes.

The database has been arranged into two sections: a first section containing the experimental results deriving from tests performed on USM walls and a second section containing experimental results deriving from tests performed on SM walls.

First of all, each specimen is identified by the same code provided in the corresponding experimental campaign otherwise a more general code has been used. The code generally gives information about the performed test procedure and the applied materials.

For "in-situ" tests some authors (Corradi et al., 2002) derive the denomination from the building and the type of test: diagonal compression or shear compression test, followed by a progressive number and the type of reinforcement.

Other authors (Valluzzi et al., 2002) give information about the reinforcement materials and their application on one or both sides of the wall.

Finally the code can contain information about the applied vertical load, (Lourenço et al., 2005).

3.2.2 Reference codes for the USM wall database

The experimental database contains the geometrical and the mechanical characteristics of the wall specimens, according to the Italian and the European codes below:

- D.M. 14 gennaio 2008 - Norme tecniche per le costruzioni.
- Circolare n. 617 - 2 febbraio 2009 - Istruzioni per l'Applicazione Nuove Norme Tecniche Costruzioni di cui al Decreto Ministeriale 14 gennaio 2008.
- UNI ENV 1996-1-1 del 31.03.98, Eurocode 6, "Design of Masonry Structures" (1998).

Within the Italian Code framework (NTC, 2008), the database section contains the following information:

- the nature of the masonry units: natural stone or brick;
- the comparison between the characteristic values of the compressive strength $f_{b,k}$ of the resistant elements, as suggested by the code, and compressive strength f_b^{exp} resulted from the experimental tests;
- the type of mortar and the corresponding compressive strength class M_i.

Those values gave the possibility to determinate the characteristic value of the compressive strength f_{mk} of masonry. It depends on the characteristic value $f_{b,k}$ of the compressive strength of the masonry units and the class of mortar M_i, making a distinction between artificial masonry units and natural stone units.

Then it has been possible to determinate the characteristic value of the shear strength f_{vk0} under zero compressive stress, which depends on the characteristic value of the compressive strength $f_{b,k}$ of the masonry element. When the value of $f_{b,k}$ was not available, the shear strength f_{vk0} has been set on the minimum value prescribed by the Code (NTC, 2008).

Finally the characteristic shear strength f_{vk} of the masonry wall has been determined by means of the following equation (2.2):

$$f_{vk} = f_{vk,0} + \mu \cdot \sigma_0 \qquad (3.1)$$

The UNI ENV 1996-1-1 - Eurocode 6 (1998) code section of the database is now described.

As in the previous section, it is necessary to classify the typology of masonry, the mortar class M_i and the corresponding compressive strength f_m for the final determination of the shear strength.

The characteristic compressive strength of the masonry f_{mk} can be determined by means of the equation (3.2):

$$f_{mk} = k f_b^{0.65} f_g^{0.65} \qquad (3.2)$$

where:
k: is a constant which can be obtained depending on the class of the masonry unit;
f_b is the normalised compressive strength of the masonry units;
f_g is the mortar compressive strength

Then the determination of the shear strength of masonry without vertical loads has been determined, starting from the information about the group of masonry, the class of the mortar and the characteristic limit shear strength $f_{v,klim}$.

If the compressive strength of the mortar is not available from the experimental tests, the minimum value suggested by the code is assumed deriving the values of the shear strength of masonry f_{v0} and the characteristic limit shear strength $f_{vk,lim}$.

In case of mortar belonging to M9 class and natural elements, the Eurocode 6 (1998) does not give information on the shear resistance $f_{vk,}$ which has been finally assumed as:

$$0.065 f_b \tag{3.3}$$

and the shear strength is calculated by means of the equation:

$$f_{vk,0} = f_{vk} - 0.4\sigma_0 \tag{3.4}$$

When the above information were not available, the minimum suggested value of $f_{vk,0}$ has been considered.

The values of the shear strength in absence of vertical loads $f_{vk,0}$ determined by the Italian Code and the Eurocode 6 have been compared with the experimental values f_{v0}^{exp} in a previous work (Sguazzo, 2007).

3.2.3 Morphological and geometrical characteristics of specimens

The second section of the database contains the morphological and geometrical information of the specimens tested within the various experimental campaigns.

The walls included in the database are:

- single leaf walls;
- double leaf walls.

A single leaf wall does not present continuous vertical joint in its plain or cavity; a double leaf wall is constituted from two parallel leaves and a joint between them, filled with mortar. The leaves can be connected together with ties to achieve a solid wall cross section.

In the collected database both types of masonry made out of natural stone, clay and concrete bricks, have been tested in diagonal compression or shear-compression, for laboratory or "in situ" tests. Those information are included in the database classification.

A further classification of the specimens, presented in the database regards the presence or not of mortar within the resistant elements constituting a masonry wall; two types of masonry walls can be identified:

- dry-stack masonry walls, where the units are laid without mortar in the joints;
- masonry walls made out of high resistant elements (natural stones, bricks) and mortar, which has the principal function of connection.

Both typologies of masonry specimens are included in the database.

The geometrical dimensions of the tested walls cover a very huge range, especially for the specimens subjected to shear compression tests, while in case of diagonal compression tests the dimensions of the walls are generally standardised as prescribed by ASTM E 519 – 02 (2002):1.2 by 1.2 m (4 by 4 ft) by the thickness of the wall type being tested with the reduction of sizes within 6 mm (1⁄4 in.) of each other or have a dimension of 0.515 by 0.515 m.

3.2.4 Characteristics of the experimental tests

This section deals with the properties of experimental tests execution included in the database. The information is listed below:

- place where the tests have been performed: laboratory tests or "in situ" tests;
- type of performed test to determinate the shear strength f_{v0} of the wall: diagonal compression or shear compression test;
- peak load or ultimate load: in case of diagonal compression tests the reference is to the axial load while for the shear compression tests the value of the shear applied to the wall is reported;
- type of control during the test: load control or displacement control;
- load application: monotonic test, characterised by the load monotonically applied, or cyclic test, whose load is applied following a loading/unloading path made of predetermined consecutive steps; cyclic tests can provide an initial cycling phase (Filardi et al., 1996) followed by a monotonic increase of the load or loading/unloading cycles (Beolchini and Grillo, 1989).

The database sections previously described are common to both USM and SM databases; separated sets and data processing have been required for the SM section and reported in the following paragraph.

3.3 SM database: data processing

3.3.1 Introduction

The present section of the SM database has been necessary to determinate the theoretical contribution of FRP reinforcement to masonry. It collects all useful information derived from the experimental tests on walls reinforced by the various kinds of FRP composites and has been essential to determinate the theoretical shear contribution of FRP V_{Rf}^{th} to the global shear strength V_R^{th} and to compare it with the experimental evidence V_R^{exp}.

The extra section of the SM database is described in the following paragraph.

3.3.2 Reinforcement properties

The types of FRP strengthening materials present in the SM database are:

- CFRP: Carbon Fiber Reinforced Polymer.
- GFRP: Glass Fiber Reinforced Polymer.
- PVAFRP: PolyVinylAlcohol Fiber Reinforced Polymer.
- CFRCM: Carbon-Fiber Reinforced Cement Matrix.

Each reinforcement material is then characterised by:

- Young's modulus of elasticity of fiber itself: E_{fib}.
- Ultimate tensile strength of FRP reinforcement: $f_{f,u.}$
- Ultimate strain of the fiber: $\varepsilon_{fib,\,u.}$
- Thickness of the FRP composite reinforcement: $t_{f.}$
- Length of FRP reinforcement: l_f.
- Area of FRP reinforcement: $A_{f.}$
- Horizontal ratio of FRP reinforcement computed on the masonry wall section: ρ_f.

To calculate the horizontal ratio of FRP reinforcement $\rho_{f,}$ the database section also contains the following information:

- number of strips for each side of the wall;
- number of layers of strengthening;
- reinforced sides of the wall.

Further information about the reinforcement layout (horizontal, vertical, diagonal or grid layout), type of reinforcement (laminate or texture), direction of fibers (unidirectional or bidirectional) and angle on the horizontal direction are also included.

Finally the calculation of the FRP composite shear contribution V_{Rf}^{th}, according to the various prescriptions, has been individually done for the analytical models considered below.

3.4 Experimental vs. theoretical data comparisons

3.4.1 Introduction

The analytical models considered to calculate the theoretical shear strength V_R^{th} of the walls externally reinforced by FRP composites are the following:

- Tomazevic & Al (1993) model;
- Triantafillou (1998) model;
- EC6 (1998) model;
- AC125 (2001) model;
- CNR-DT 200/2004 guidelines (2009) model;
- ACI 440.7R-10 guide (2010) model.

The value of $V_{R,i}^{th}$ has been calculated for each specimen included in the SM database and has been finally compared with the corresponding experimental value $V_{R,i}^{exp}$, derived from the laboratory or "in situ" test campaigns.

The masonry contribution $V_{Rm,i}^{th}$ to the global shear strength of the wall $V_{R,i}^{th}$ has been firstly calculated, starting from the average experimental value $\bar{f}_{v0}^{exp}$ of the corresponding tests. The experimental value of the shear strength in absence of vertical loads $\bar{f}_{v0}^{exp}$ has been calculated considering the failure effectively shown by the unstrengthened walls for shear sliding failure:

$$f_{v0,i}^{exp} = f_{v,i}^{exp} - \mu\sigma_0^{exp} \tag{3.5}$$

or for diagonal tension failure:

$$P(f_{v0,i}^{exp}) = f_{v,i}^{th} - f_{v0,i}^{exp}\sqrt{1+\frac{\sigma_0^{exp}}{1.5\cdot f_{v0,i}^{exp}}} = 0 \Rightarrow f_{v0,i}^{exp} \tag{3.6}$$

Then the theoretical shear strength of masonry $V_{Rm,i}^{th}$ has been calculated, according to the prescriptions of each considered model and taking into account the shear strength $\bar{f}_{v0,i}^{exp}$ defined above, as:

$$V_{Rm,i}^{th} = f(\bar{f}_{v0,i}^{exp}) \tag{3.7}$$

Finally the contribution of FRP reinforcement to the shear strength $V_{Rf,i}^{th}$ has been calculated to obtain the global shear strength as:

$$V_{R,i}^{th} = V_{Rm,i}^{th} + V_{Rf,i}^{th} \tag{3.8}$$

3.4.2 Assessment

Any available capacity model is aimed at simulating the experimental evidence.

To assess the accuracy of a given analytical model, the experimental data can be compared with the theoretical data in a diagram where the line $y = x$ represents how much the model, whose value is reported on the y axis, fits the observed experimental evidence, whose value is reported on the x axis; in this case $V_{R,i}^{th}$ is the simulated datum and $V_{R,i}^{exp}$ is the observed datum.

This qualitative technique is not appropriate to evaluate a model by itself, so some parameters are necessary to get an objective evaluation.

The accuracy of the mentioned theoretical models for the ultimate shear capacity of masonry walls can be firstly measured by comparing the collected experimental results with the corresponding theoretical predictions. Then a parameter Δ measuring the average error of the theoretical predictions against the corresponding experimental evidence can be easily introduced for quantifying the accuracy of the various

models in reproducing the experimental results $V_{R,i}^{exp}$ collected in the database:

$$\Delta = \sqrt{\frac{\sum_{i=1}^{n}\left(V_{R,i}^{exp} - V_R^{th}(q_i)\right)^2}{n}} \tag{3.9}$$

where n is the total number of data and $V_R^{th}(q_i)$ is the theoretical prediction (derived by applying one of the models described above) obtained for the i-th experimental case, whose relevant geometric and mechanical parameters are collected within the vector q_i.

The parameter Δ, also known as Root Median Square Error (RMSE), cannot be considered for understanding whether a model is conservative or not and how the experimental-to-theoretical ratios is actually distributed. Consequently, further measures have to be introduced for assessing the accuracy of the various theoretical models and describing their possible errors and biases. The experimental-to-theoretical ratio δ_i in terms of shear strength V_R is one of those measures; it can be defined as follows:

$$\delta_i = \frac{V_{R,i}^{exp}}{V_R^{th}(q_i)} \tag{3.10}$$

The complete statistical characterization of such a distribution is beyond the scopes of the present work and will be addressed in the future; however, some key properties like its average value and standard deviation could be primarily estimated herein.

In the paragraphs which follow the experimental versus theoretical comparisons are presented, subdividing them into two parts: the first part regarding the data collected from diagonal compression tests and

the second part regarding the data collected from shear compression tests.

3.4.3 The model by Tomazevic et al. (1993)

The model by Tomazevic et al. (1993) is the first to be considered in the present study. Fig. 3.4 shows the results of the experimental comparison of diagonal compression tests on masonry walls reinforced by various kinds of FRP composites. All points reported in Fig. 3.4 are grouped in a bunch rather centred on the equivalence line. The walls made out of artificial bricks, i.e. the ones from Valluzzi et al. (2002), Erol et al. (2004), Silva et al. (2008), Mahmood et al (2008) experimental campaigns, present a more safe prediction of the shear strength. On average the model results in a rather accurate prediction of the experimental behaviour. An asymmetric cumulative distribution of the δ_i ratios (n_i in Fig. 3.5 is the number of cases with δ_i) can be observed. The assumption of normal distribution of $\hat{\delta}$ around the unit could not be accepted. Furthermore the model results not conservative for all natural specimens reinforced by GFRP (Prota et al., 2005; Aiello et al.,2007) while natural specimens reinforced by CFRP (Corradi et al., 2002; Micelli and Ombres, 2003; Faella et al.,2006) show different behaviour but are close to the equivalence line.

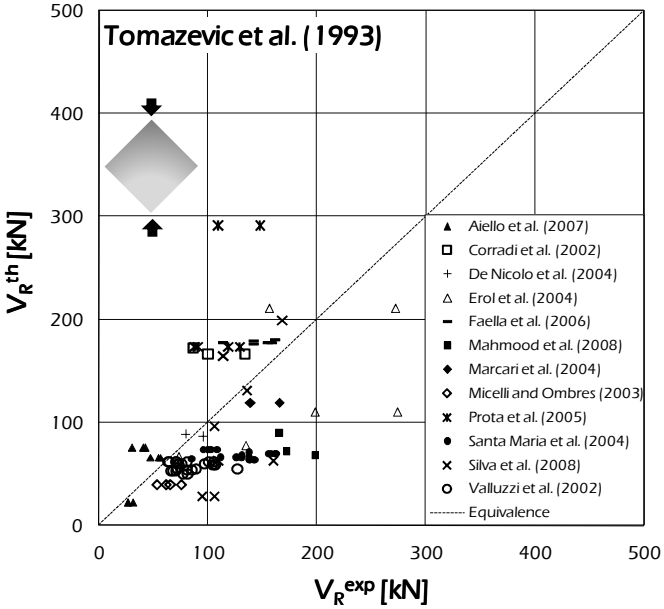

Fig. 3.4: Experimental-to-theoretical comparison in terms of shear strength V_R^{th} for specimens in diagonal compression: Tomazevic et al. (1993) model.

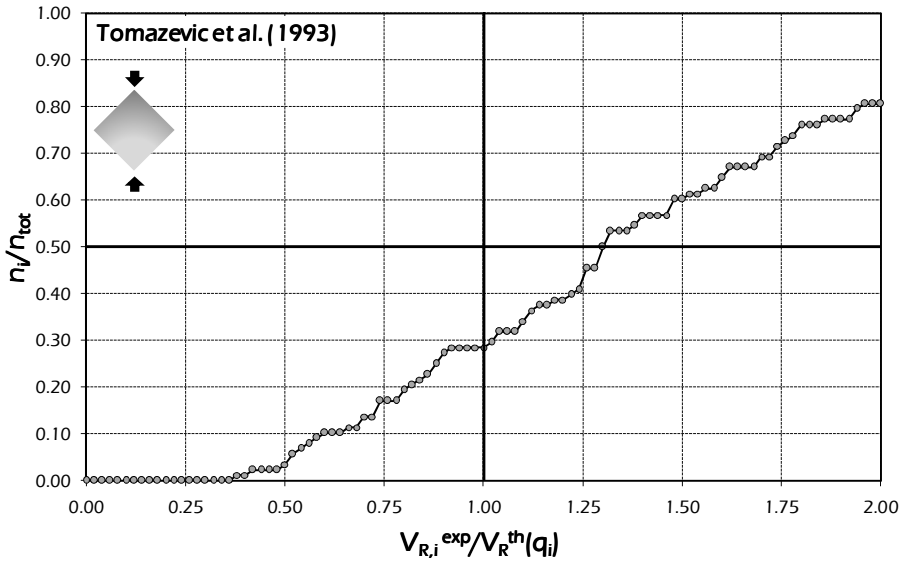

Fig. 3.5: Cumulative distribution of the experimental-to-theoretical ratios δ_i for specimens in diagonal compression: Tomazevic et al. (1993) model.

Fig. 3.6 compares the experimental results with the model predictions, referring to the shear-compression test results, collected within the experimental SM database.

The points reported in Fig. 3.6 are scattered and the model leads to a more visible dispersion for the stone masonry specimens (Marcari et al., 2004; Corradi et al., 2002), while performs quite well with artificial brick masonry, especially the walls made out of clay bricks (Olivito and Zuccarello, 2005).

Furthermore the comparisons result non-conservative for natural specimens and hollow bricks specimens reinforced by CFRP, while the model is in good prediction for the specimens , both artificial and natural, reinforced by GFRP (Marcari et al., 2004; Stratford et al., 2002).

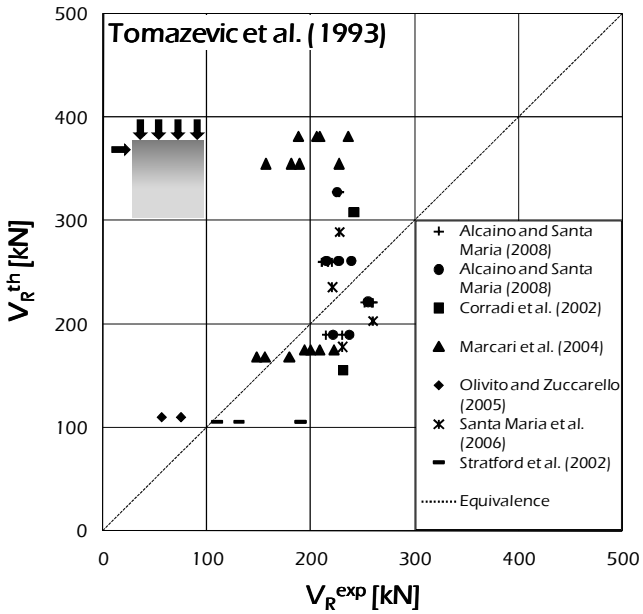

Fig. 3.6: Experimental-to-Theoretical Comparison in terms of shear strength V_R^{th} for specimens in shear compression: Tomazevic et al. (1993) model.

Consequently, the model results in rather accurate prediction of the experimental behaviour for artificial masonry. The distribution of the experimental-to-theoretical ratios represented in Fig. 3.7 shows that the

median value is close to the unity with an approximately symmetric shape of the cumulative distribution curve.

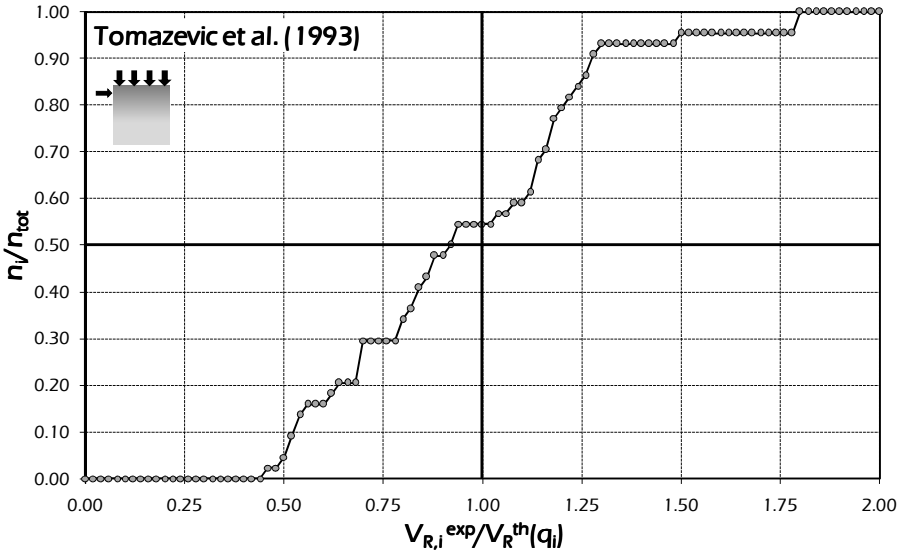

Fig. 3.7: Cumulative distribution of the experimental-to - theoretical ratios δ_i for specimens in shear compression: Tomazevic et al. (1993) model.

3.4.4 The Triantafillou (1998) model

The second comparison between experimental results and theoretical values deals with the model by Triantafillou (1998) outlined in the previous chapter.

The results of such a comparison in terms of experimental-to-theoretical values of shear strength, reported in Fig. 3.8 points out that the dispersion of the theoretical prediction is rather larger than the one obtained with the application of the model by Tomazevic et al. (1993) resulting in Fig. 3.4.

The comparisons regarding the experimental results of diagonal compression tests are firstly presented.

A more thorough analysis of Fig. 3.8 would emphasize that the model results in hugely non-conservative prediction especially in some cases of

walls made out of natural stones (i.e., those by Faella et al., 2006; Corradi et al., 2002; Prota et al. 2005). A conservative prediction results for wall specimens made out of natural stones with the inner filled with mortar and chips from stones (i.e. Marcari et al.,2004; Aiello et al.,2007). The points corresponding to artificial specimens, both full bricks (Silva et al., 2008) and hollow bricks walls (Santa Maria et al., 2004; Mahmood et al., 2008; Erol et al., 2004), are substantially grouped in a bunch rather centred on the equivalence line. Consequently, on average the model results in rather accurate prediction of the experimental behaviour of walls made out of artificial units, while is often unconservative for those made out of natural blocks.

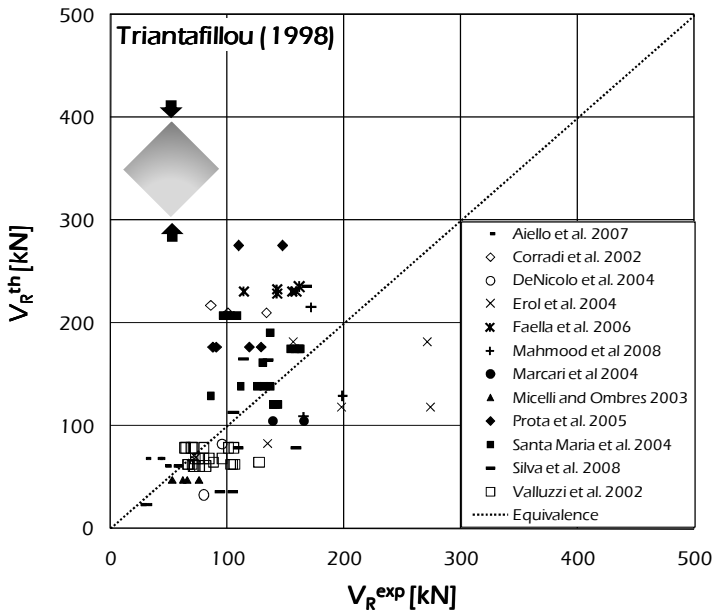

Fig. 3.8: Experimental-to-theoretical comparison in terms of shear strength V_R^{th} for specimens in diagonal compression: Triantafillou (1998) model.

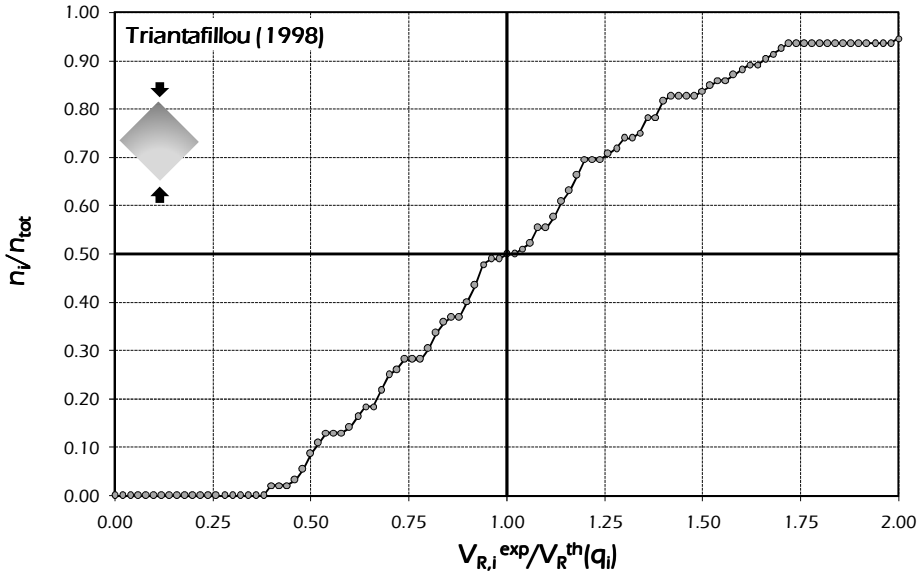

Fig. 3.9: Cumulative distribution of the experimental-to-theoretical ratios δ_i for specimens in diagonal compression: Triantafillou (1998) model.

Fig. 3.10 shows the results of such a comparison in terms of experimental-to-theoretical values of shear strength with respect to the experimental results obtained in shear-compression tests. The points reported in the mentioned figure are rather scattered and shear strength prediction is often unconservative for natural masonry (see the tests by Marcari et al., 2007), as already pointed out and commented in the previous section for the results of shear-compression tests (Alcaino and Santa Maria, 2008) while the representative points of masonry walls made out of hollow bricks are most centred. Consequently, in the present comparison, the model does not lead to an accurate prediction of the experimental behaviour. Furthermore, as Fig. 3.11 suggests, the distribution of the experimental-to-theoretical ratios is characterised by the median value not close to the unity and has not a symmetric shape.

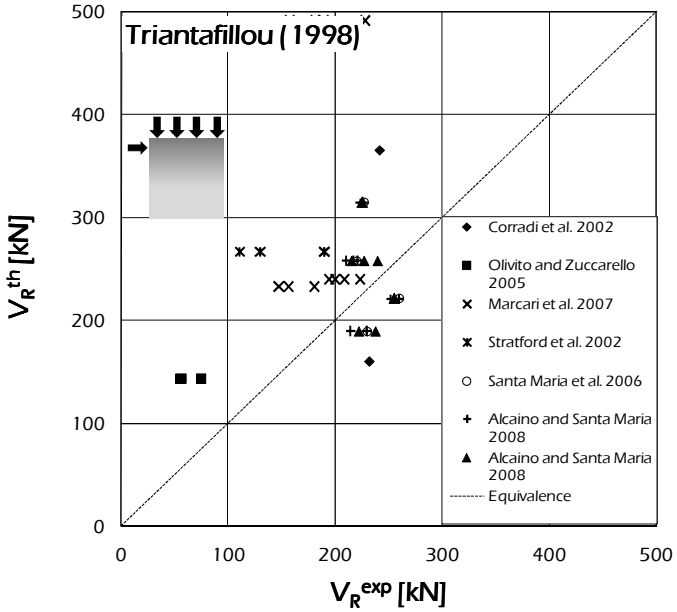

Fig. 3.10: Experimental-to-theoretical comparison in terms of shear strength V_R^{th} for specimens in shear compression: Triantafillou (1998) model.

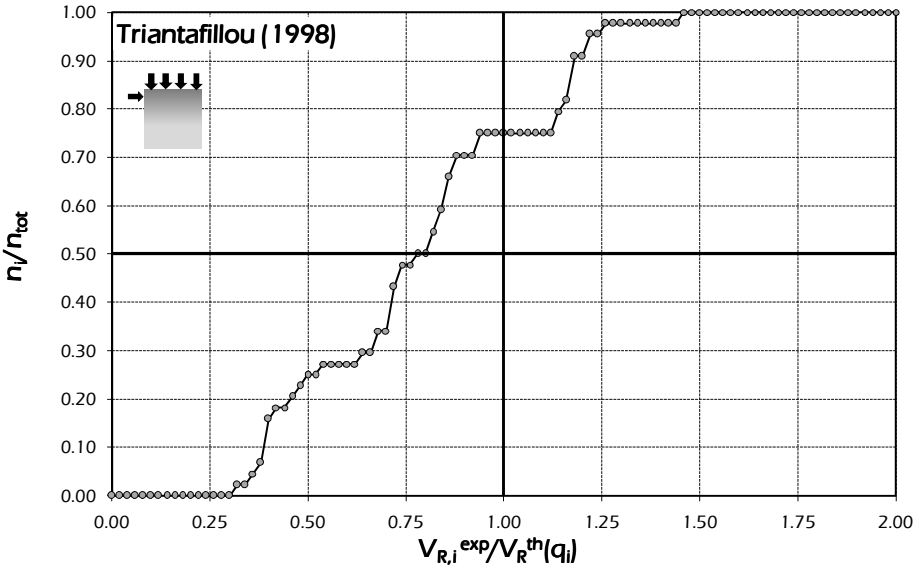

Fig. 3.11: Cumulative distribution of the experimental-to-theoretical ratios δ_i for specimens in diagonal compression: Triantafillou (1998) model.

3.4.5 EC6 (1998) model

The comparisons between the theoretical values deriving from the EC6 (1998) proposal and the corresponding experimental values, firstly resulted from diagonal-compression tests and then from shear-compression tests are discussed in this section.

Fig. 3.12 points out that the model is not adequately accurate for all the externally strengthened natural masonry walls. The equivalence line seems to draw a clear division between natural stone walls, whose shear strength prediction is unconservative, and artificial brick walls, which are in a conservative prediction, with the exception of only two specimens by Erol et al. (2004). The reason of an unsatisfactory predicting capacity for the cases of natural stones is probably due to the low adhesion of the support with the composite materials and points out a larger dispersion with respect to the previous models.

Furthermore the model seems to predict values of shear strength closer to the experimental ones for most of the specimens reinforced by CFRP (Valluzzi et al., 2002; Micelli and Ombres, 2003; Santa Maria et al., 2004).

The cumulative distribution of the δ_i ratios, is characterised by the median value close to the unit and has a quite symmetric shape (Fig. 3.13).

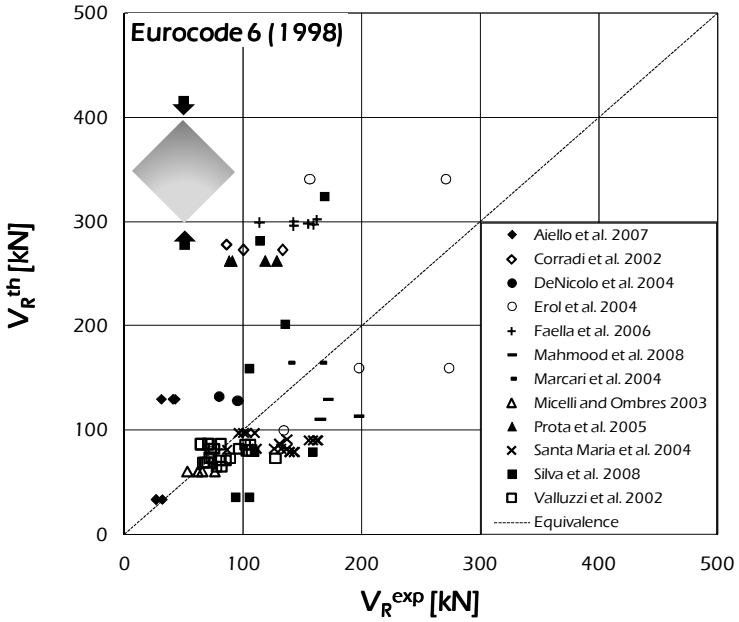

Fig. 3.12: Experimental-to-theoretical comparison in terms of shear strength V_R^{th} for specimens in diagonal compression: Eurocode 6 (1998) model.

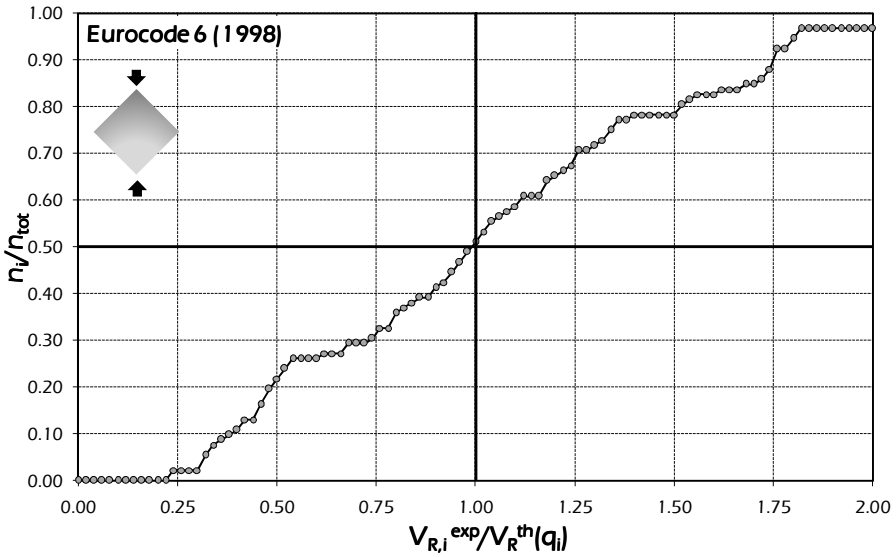

Fig. 3.13: Cumulative distribution of the experimental-to-theoretical ratios δ_i for specimens in diagonal compression: Eurocode 6 (1998) model.

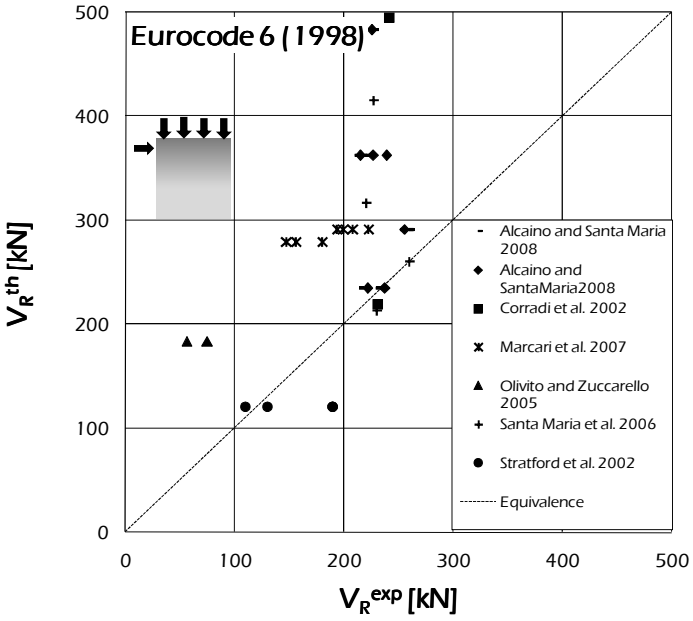

Fig. 3.14: Experimental-to-theoretical comparison in terms of shear strength V_R^{th} for specimens in shear compression: Eurocode 6 (1998) model.

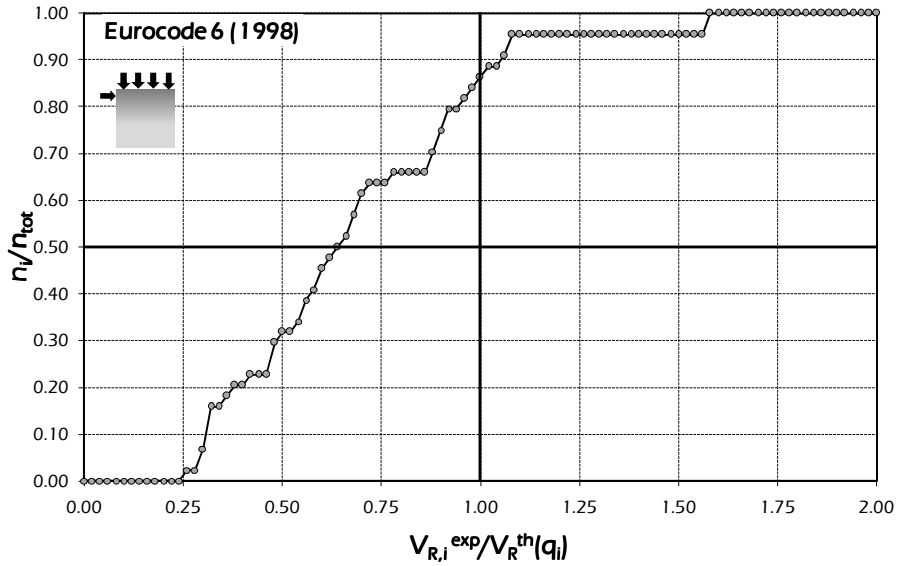

Fig. 3.15: Cumulative distribution of the experimental-to-theoretical ratios δ_i for specimens in shear compression: Eurocode 6 (1998) model.

The model proposed by EC6 for reinforced masonry is considered for the comparison in terms of experimental to theoretical values with respect to the experimental results obtained in shear-compression tests.

The results of such a comparison is reported in Fig. 3.14 whose points are affected by a huge dispersion with a general overestimation of shear strength in the cases of masonry walls made out of both natural stones and artificial units.

3.4.6 The AC125 (2001) model

The experimental-to-theoretical comparisons based on the proposal of IBC-AC125 (2001) model is represented in Fig. 3.16. The points are rather grouped across the equivalence line and the prediction is more frequently conservative especially for artificial masonry walls with respect to the previous models. The cumulative distribution of the δ_i ratios is rather asymmetric, as reported in Fig. 3.17.

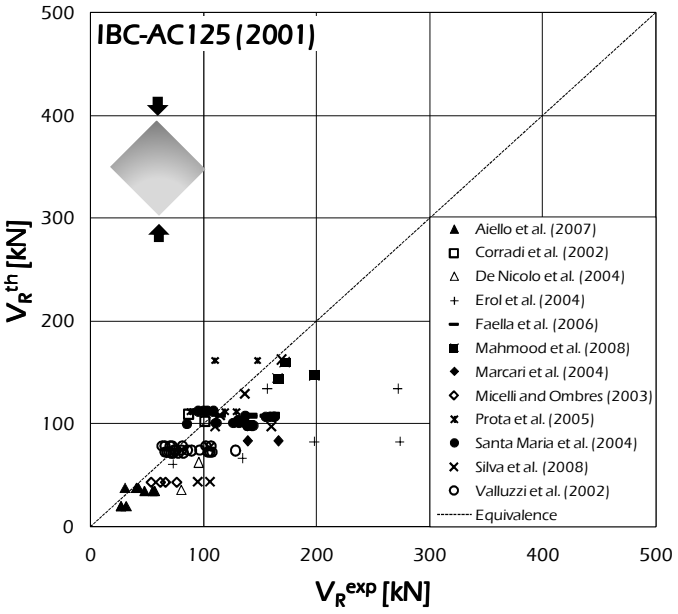

Fig. 3.16: Experimental-to-theoretical comparison in terms of shear strength V_R^{th} for specimens in diagonal compression: IBC–AC 125 (2001) model.

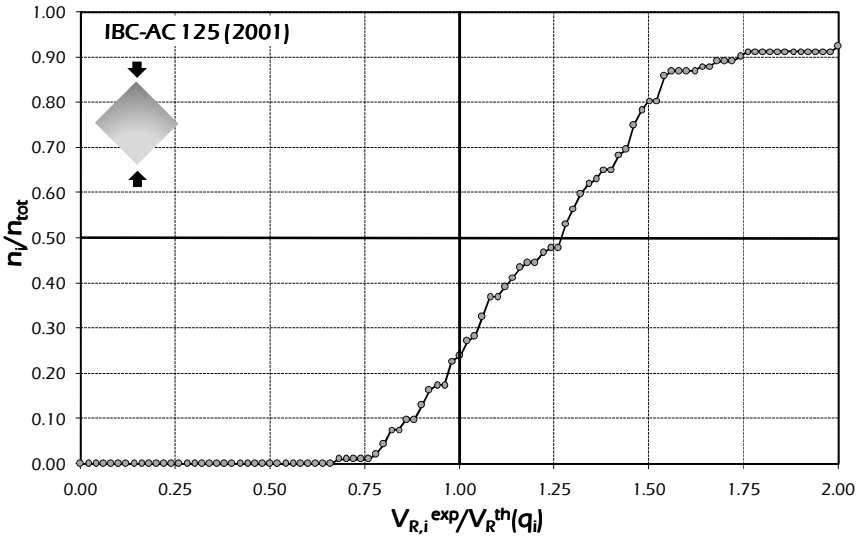

Fig. 3.17: Cumulative distribution of the experimental -to - theoretical ratios δ_i for specimens in diagonal compression: IBC–AC 125 (2001) model.

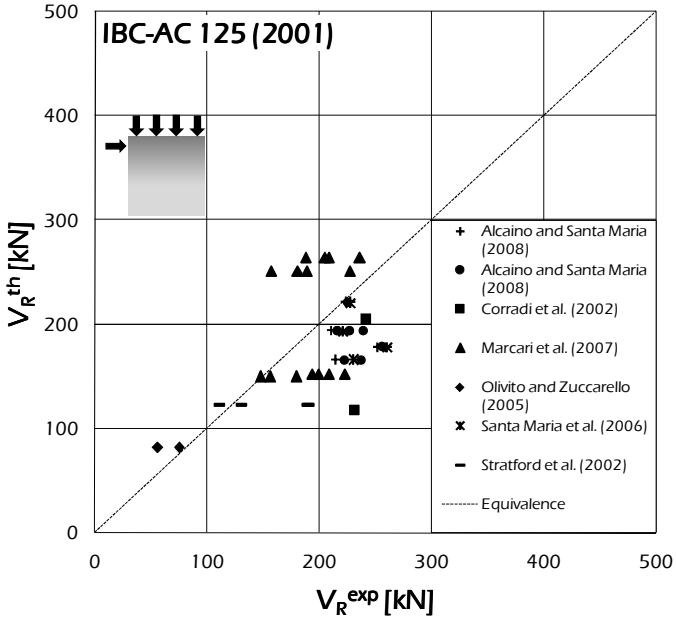

Fig. 3.18: Experimental-to-Theoretical Comparison in terms of shear strength V_R^{th} for specimens in shear compression: IBC–AC 125 (2001) model.

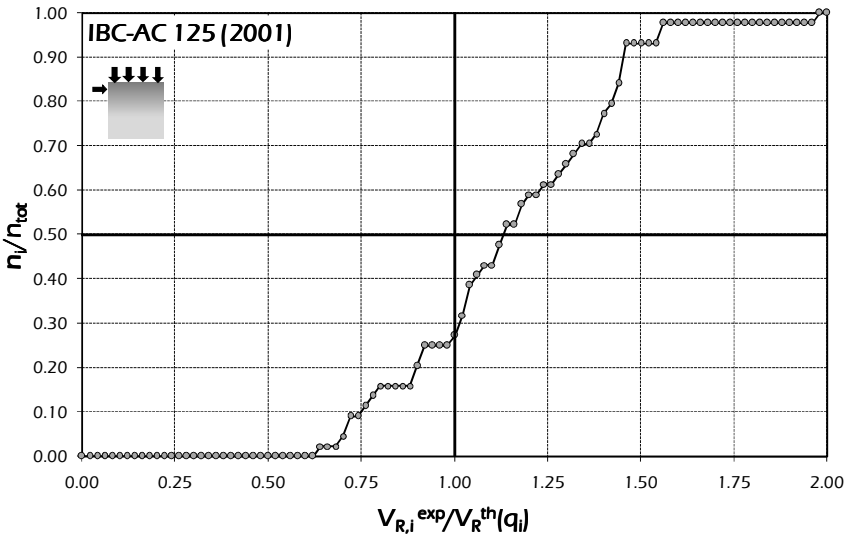

Fig. 3.19: Cumulative distribution of the experimental -to - theoretical ratios δ_i for specimens in shear compression: IBC – AC 125 (2001) model.

Fig. 3.18 shows the experimental-to-theoretical comparison of shear-compression tests which results from the application of the IBC-AC125 model: the points are more dispersed, if compared with the previous comparison of diagonal compression tests, and the prediction is non-conservative for natural specimens reinforced by CFRP (Marcari et al., 2007). Finally, the cumulative distribution of the δ_i ratios is rather asymmetric as reported in Fig. 3.19.

3.4.7 CNR-DT 200/2004 guidelines (2009) model

The comparison between the experimental results and the theoretical values obtained by the application of CNR-DT 200/2004 guidelines (2009) model is presented.

Fig. 3.20 shows the results of such a comparison in terms of experimental-to-theoretical values for diagonal compression tests.

A more thorough analysis of Fig. 3.20 would emphasize that the model results in a not conservative prediction in some cases of natural walls (i.e., those by Corradi et al., 2002; Mahmood et al., 2008; Aiello et

al., 2007; Micelli and Ombres, 2003) while the cumulative distribution of the δ_i ratios is asymmetric, as reported in Fig. 3.21.

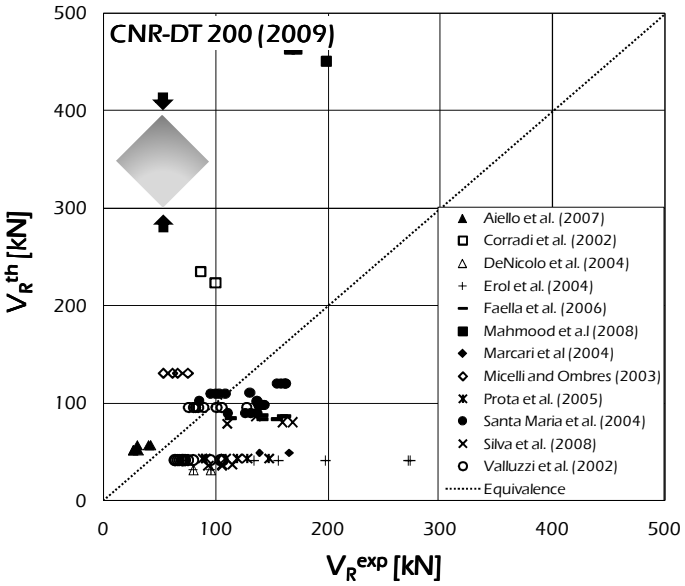

Fig. 3.20: Experimental-to-theoretical comparison in terms of shear strength V_R^{th} for specimens in diagonal compression: CNR-DT 200 (2009) model.

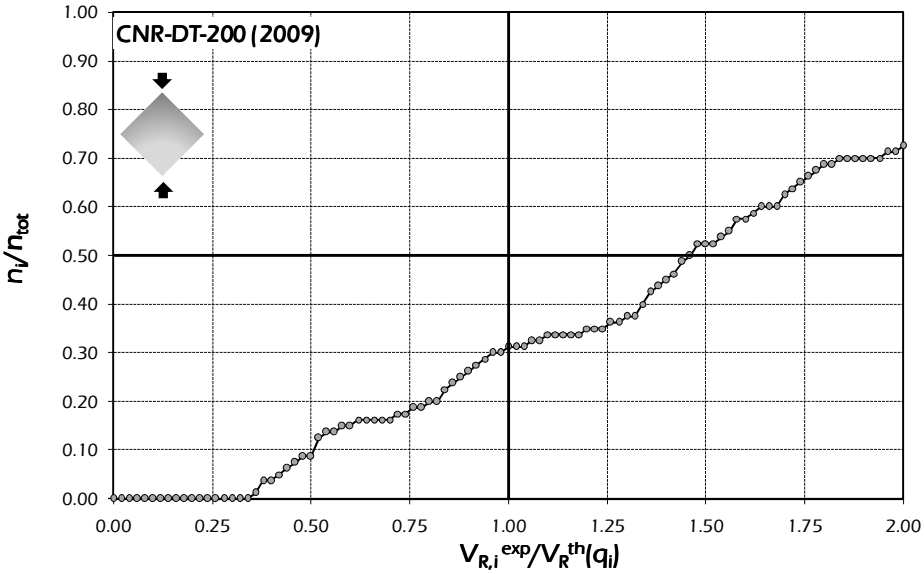

Fig. 3.21: Cumulative distribution of the experimental -to - theoretical ratios δ_i for specimens in diagonal compression: CNR-DT 200 (2009) model.

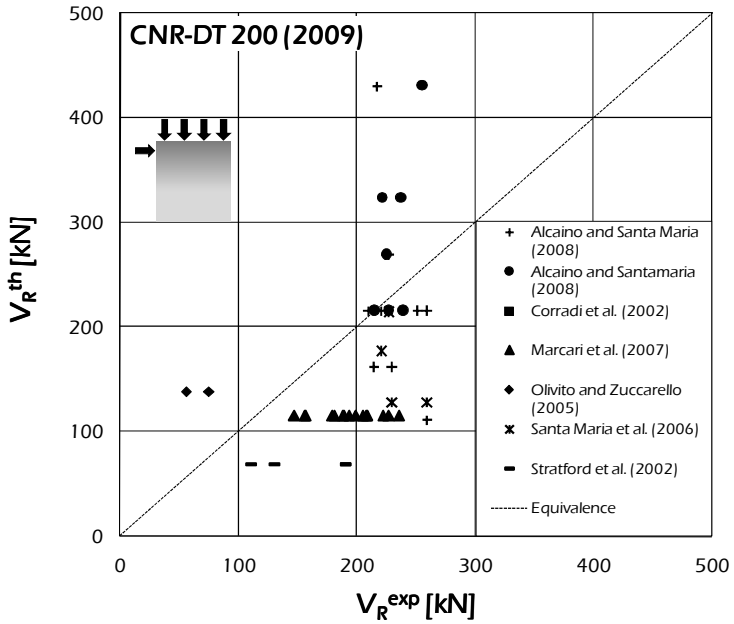

Fig. 3.22: Experimental-to-theoretical comparison in terms of shear strength V_R^{th} for specimens in shear compression: CNR-DT 200 (2009) model.

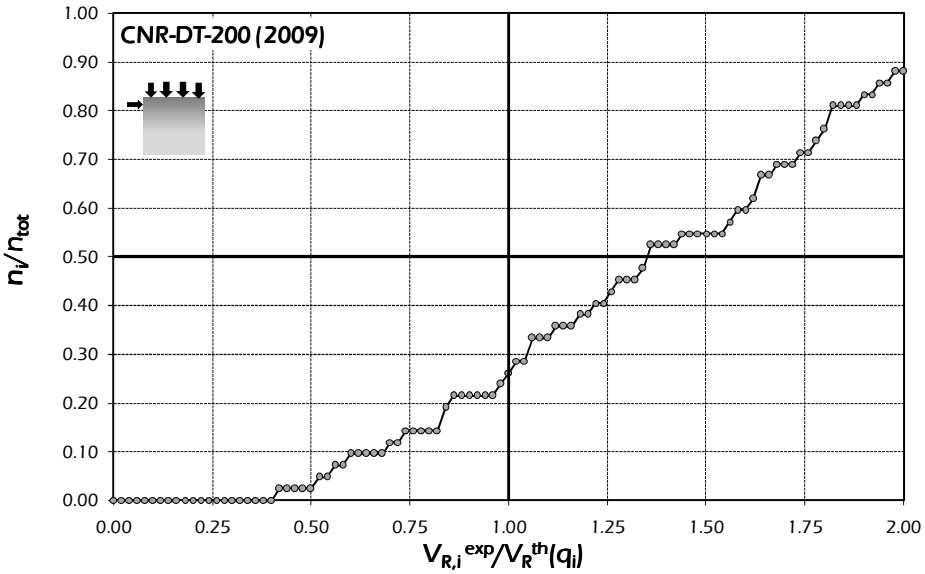

Fig. 3.23: Cumulative distribution of the experimental-to-theoretical ratios δ_i for specimens in shear compression: CNR-DT 200 (2009) model.

The experimental-to-theoretical comparison of shear-compression tests resulting from the application of CNR-DT 200/2004 guidelines (2011) model is finally presented in Fig. 3.22. The points are more dispersed, if compared with the previous comparison of diagonal compression tests, and the prediction is non-conservative for some artificial specimens reinforced by CFRP (Alcaino and Santa Maria, 2008; Olivito and Zuccarello, 2005). The cumulative distribution of the δ_i ratios is rather asymmetric, as reported in Fig. 3.23.

3.4.8 ACI 440.7R-10 guide (2010) model

The comparison between the experimental results and the theoretical values obtained by the application of ACI 440.7R-10 guide (2010) model is presented.

Fig. 3.24 reports the results of such a comparison in terms of experimental-to-theoretical values of shear strength.

A more thorough analysis of Fig. 3.24 would emphasize that in case of diagonal-compression tests, the model results in a conservative prediction in case of artificial walls (i.e., those by Valluzzi et al., 2002; Erol et al., 2004; Mahmood et al., 2008), whose points, for both full bricks and hollow bricks walls, are substantially grouped in a bunch rather centred on the equivalence line. The comparison results non-conservative in some cases of natural specimens (Micelli and Ombres, 2003; Prota et al., 2005; Marcari et al., 2004). Fig. 3.25 shows that the cumulative distribution of the δ_i ratios is rather asymmetric.

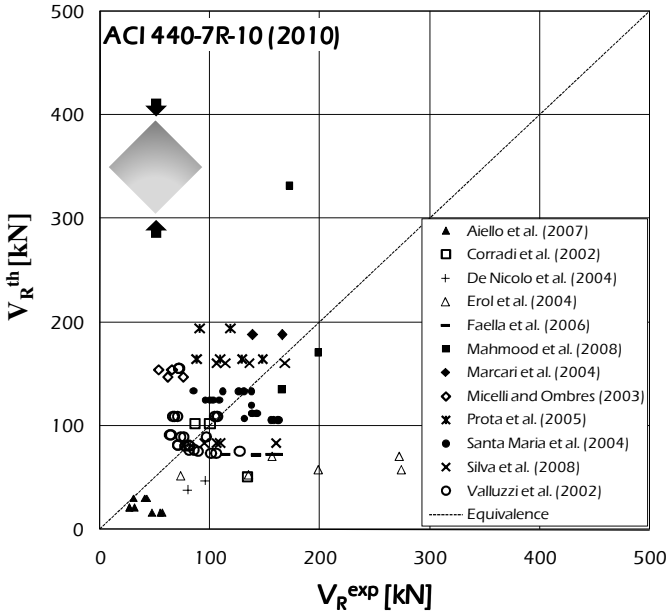

Fig. 3.24: Experimental-to-theoretical comparison in terms of shear strength V_R^{th} for specimens in diagonal compression: ACI 440-7R-10 (2010) model.

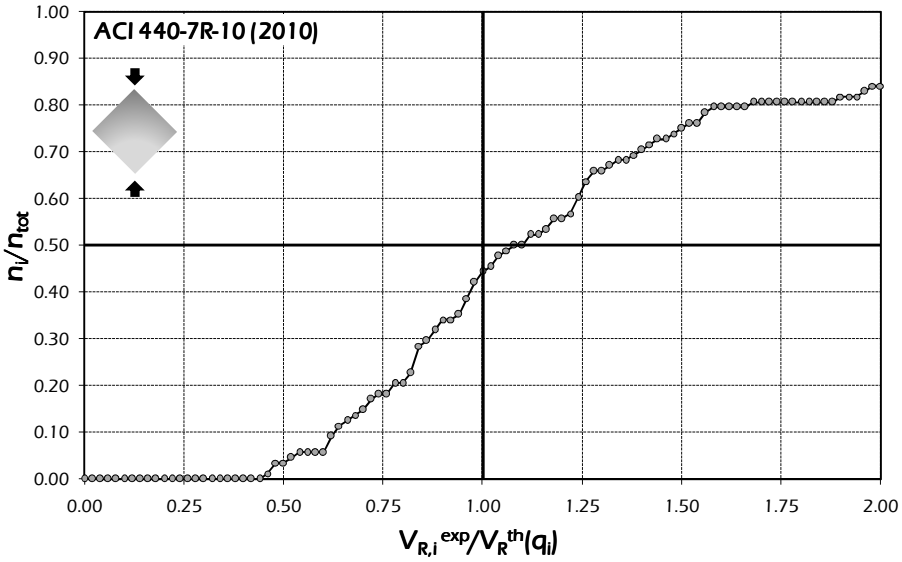

Fig. 3.25: Cumulative distribution of the experimental-to-theoretical ratios δ_i for specimens in diagonal compression: ACI 440-7R-10 (2010) model.

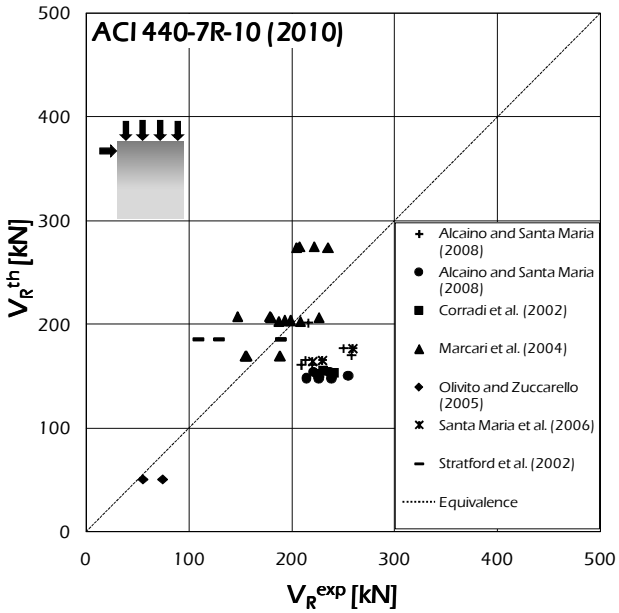

Fig. 3.26: Experimental-to-Theoretical Comparison in terms of shear strength V_R^{th} for specimens in shear compression: ACI 440-7R-10 (2010) model.

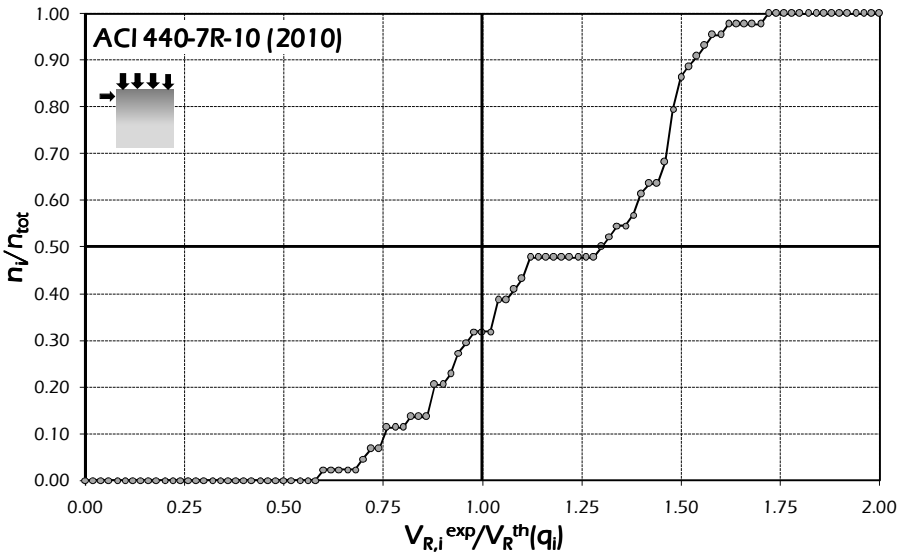

Fig. 3.27: Cumulative distribution of the experimental-to-theoretical ratios δ_i for specimens in shear compression: ACI 440-7R-10 (2010) model.

The model by ACI 440.7R-10 guide (2010) is also analysed with respect to the experimental results obtained by shear-compression tests.

Fig. 3.26 shows the results of such a comparison in terms of experimental-to-theoretical values of shear strength; the points reported in the mentioned figure are rather scattered and shear strength prediction results unconservative for natural masonry reinforced by CFRP (see the tests by Marcari et al., 2007).

Furthermore, as Fig. 3.27 suggests, the cumulative distribution of the experimental-to-theoretical ratios δ_i is characterised by the median value close to the unit and has not a symmetric shape.

3.5 Conclusions

This section reports the results of the comparative assessment of the theoretical models. It points out the accuracy of the various models in terms of Root Median Square Error Δ and distribution of the experimental-to-theoretical ratios.

Table 3.1 reports the Root Median Square Error Δ, calculated by Eqn. (3.9), and the median values $\hat{\delta}$ of the distribution of the experimental-to-theoretical values, defined by Eqn. (3.10), for each model and for both the testing procedures. The models generally lead to good predictions for diagonal compression tests. Larger dispersion affects the theoretical values in the case of shear compression tests.

Table 3.1: Values of Δ parameter corresponding to each model.

Models Presented	Diagonal Compression Tests		Shear Compression Tests	
	Δ [kN]	$\hat{\delta}$	Δ [kN]	$\hat{\delta}$
Tomazevic Et Al. (1993)	58.3	1.30	88.7	0.92
Triantafillou (1998)	57.1	1.01	145.2	0.79
IBC-AC 125 (2001)	45.5	1.27	52.9	1.13
Eurocode 6 (1998)	94.2	0.99	218.8	0.63
CNR-DT 200 (2009)	83.7	1.47	85.7	1.35
ACI 440.7R-10 Guide (2010)	58.9	1.08	61.9	1.30

Table 3.1 also shows that the formulae suggested by Tomazevic et al. (1993), IBC-AC125 (2001) and ACI 440.7R-10 (2010) present a small Root Median Square Error Δ and are also characterised by mean values of the ratio $\hat{\delta}$ close to the unity. For diagonal-compression tests the formula proposed by IBC-AC125 (2001) results significantly conservative. The formula proposed by CNR-DT 200 (2009) generally results in hugely conservative predictions.

The formula proposed by Triantafillou presents a small error in case of diagonal compression tests but its performance results unconservative in case of shear compression tests, presenting a high value of the Root Median Square Error.

As expected, the formula provided by EC 6 (1998) for internally reinforced masonry cannot be directly extended to the case of external reinforcement, especially in the case of shear-compression tests. In fact, the values of Root Median Square Error Δ are the highest, for both the testing techniques, and in the case of specimens tested in shear compression the model leads to hugely unconservative predictions.

The experimental-to-theoretical comparisons presented in this chapter show some common aspects.

The predictions of the examined formulations, except ACI 440.7R-10 guide (2010) model and the CNR-DT 200/2004 guidelines (2009) model, result unsafe in case of wall specimens made out of natural bricks like tuff stones, calcareous stones or local stones in general.

Within the comparisons elaborated here and having the SM database as a reference, it is not possible to observe a common behaviour of the predictions, conservative or not, connected to the nature of the reinforcement: Carbon or Glass FRP. In fact, comparisons for diagonal compression tests result in a non conservative prediction, for natural specimens reinforced by GFRP, in case of Tomazevic et al. (1993) model, and conservative for artificial bricks reinforced by CFRP, when Eurocode 6 (1998) model is applied. For the other models, it is not possible to identify a particular behaviour which depends on the nature of the external composite reinforcement. Moreover, for shear compression tests the results of comparisons for natural and artificial wall specimens reinforced by CFRP, derived from the application of Tomazevic et al. (1993) model, have a clear non conservative trend, confirmed only by the behaviour of natural specimens reinforced by CFRP in the comparisons resulted by the application of AC125 (2001) model.

Further studies are needed for extending the assessment to other formulations already available in the literature. Furthermore, a recalibration of some of those models can be carried out for minimizing the error between the experimental evidence and the theoretical prevision. Randomness deriving by the approximation of the model as well as uncertainty related to the mechanical properties of masonry will be considered in deriving a consistent design formula for shear strength of masonry walls externally strengthened by composite materials.

CHAPTER 4

4. Modelling Approaches of Masonry

4.1 Introduction

The nature of masonry as a composite material made out of units and mortar joints leads to two possible approaches of modelling (Lourenço, 1996):

- micro-modelling, which considers each distinct component of masonry: bricks in contact through the mortar joints;
- macro-modelling, which considers masonry as a continuum composite material.

Within the micro-modelling it is possible to have different levels of accuracy, so it can be recognized:

- a detailed micro-modelling, where units and mortar are modelled as continuum elements and discontinuous elements represent the unit-mortar interface;
- a simplified micro-modelling, where expanded units are modelled as continuum elements while discontinuous elements represent the unit-mortar interface and the mortar joints together.

4.2 Macro-modelling

The macro-modelling of masonry is intended at simulating the behaviour of a heterogeneous and discontinuous structure as it was a homogeneous continuum.

The more general strategy used in macro-modelling does not consider the mechanical properties of single components and takes into account constitutive laws derived from tests performed on masonry.

Looking to masonry as a homogeneous continuum various approaches can be distinguished in the macro-modelling (Trovalusci, 2009; Adams and Magenes, 2004; Lourenço, 1996; Magenes et al., 2000):

- macro-element models based on storey mechanism approach:
  - mono-dimensional models:
    - equivalent frame models;
    - equivalent truss models;
  - bi-dimensional models:
    - D'Asdia and Viskovic (1993) PEFV model;
    - Braga et al. (1990) Multi-FAN model;
    - Gambarotta et al. (1996) model;
- no-tension models;
- finite element models;
- homogeneous continuum models:
  - homogeneous anisotropic models based on Cauchy;
  - homogeneous equivalent continuum models based on Cosserat.

4.2.1 Macro-element models based on storey mechanism approach

4.2.1.1 Mono-dimensional models

4.2.1.1.1 Equivalent frame models

The POR method proposed by Tomazevic in 1978 (Magenes et al., 2000; Tomazevic, 1978) represents the first approach of modelling through the equivalent frame models.

In its initial version the following assumptions have been proposed:

- deformations and failures can only occur in the vertical resistant elements (piers) and not in the horizontal elements (spandrels);
- sliding failures and out-of plane failures are not considered as possible mechanisms in piers.

Later proposals to enhance the methods have been done by Dolce (1989) and Tomazevic and Weiss (1990), who introduced the failures not considered in the first version of the model.

The method is based on the nonlinear analysis of each separated storey and this represents a "limit" of the method because approximated calculations are necessary to consider the actions in the spandrels, as shown in the works of Braga and Dolce (1982) and Fusier and Vignoli (1993).

In 1996 Magenes and Calvi proposed the SAM (Simplified Analysis of Masonry structures) method for the analysis of simple URM walls. The method was after improved by Magenes and Della Fontana in 1998 for the application to more complex structures. In the proposed method a regular multi-storey masonry wall can be idealized by an equivalent continuous frame made up of vertical elements: piers, horizontal elements: spandrels, respectively modelled as columns and beams while the connections are modelled as rigid offsets, as shown in Fig. 4.1.

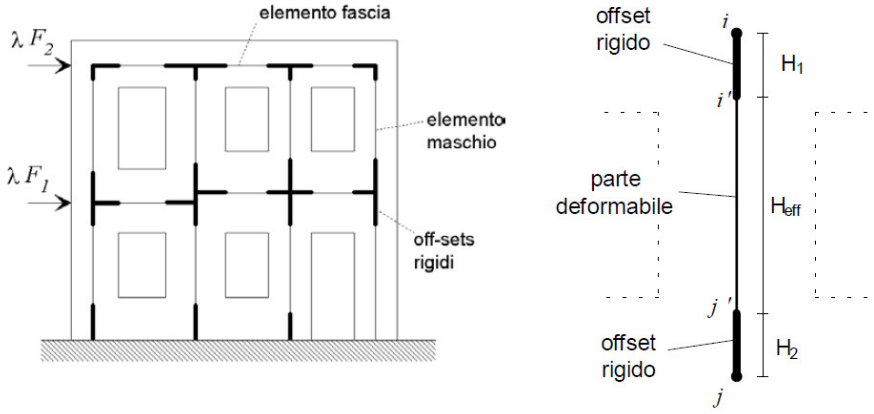

Fig. 4.1: Equivalent Frame Model (Magenes et al., 2000).

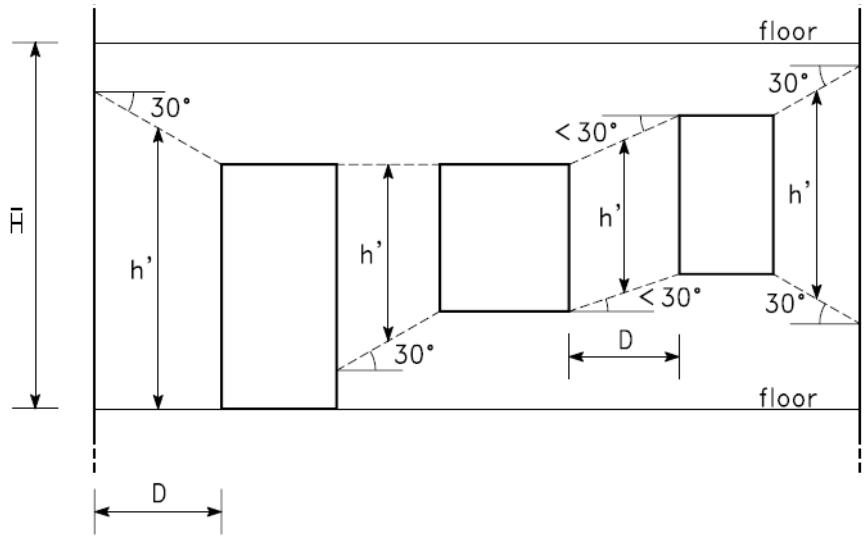

$$H_{eff} = h' + \frac{1}{3} D(\overline{H} - h')/h' \qquad \overline{H} = \text{altezza interpiano}$$

Fig. 4.2: Equivalent Frame Model: definition of effective height (Magenes et al., 2000).

Each pier is modelled as a deformed part with infinite rigid ends: the height of the deformable part is named effective height and is defined like in Dolce (1989) and shown in Fig. 4.2. It is supposed that the vertical element has a linear behaviour until the crisis is reached. Consequently the stiffness matrix of elasticity is determined once the Young modulus E, the shear modulus G and the geometry are fixed.

The possible failure modes considered by this method are shear failure and flexural failure while the constitutive relation of (Ricamato, 2007) structural members is idealised as elastic-perfectly plastic and the shear strength of members can be calculated by means of simple equations.

In 2005 Roca et al. (2005) also proposed a method for simulating the nonlinear material response of masonry wall systems, subject to gravity and horizontal loads, based on a treatment of the 2D wall panels as an equivalent system of one-dimensional members.

The formulation (Roca et al., 2005) of the method is based on the three following items:

- a basic formulation for one-dimensional elements curved in space: lintels or spandrels may be curved and have a variable cross section;
- a technique for the description of load-bearing wall panels as an equivalent system of linear members: the technique describes realistically the compatibility between the wall panels and the transverse members connecting them;
- a constitutive model for masonry elements subjected to biaxial states of stress: the interaction between axial and shear forces is considered through use of Mohr-Coulomb criterion as a biaxial stress envelope.

The technique can analyse historical or traditional wall façades or entire masonry buildings, including a widespread range of structural elements, such as spandrel, straight or curved beams, arches, buttresses, or curved lintels.

In 2007 Belmouden and Lestuzzi (2007) presented a model for structural walls with openings. The structural model can represent solid walls, frame structural elements (beams and columns), coupled walls and perforated walls (or framed walls). It consists of an assemblage of vertical plane walls with openings making up a single perforated wall. Each wall is modelled by means of piers, with or without rigid offsets, and a portion of spandrels such that there are two kinds of individual walls: exterior walls and interior walls (Fig. 4.3).

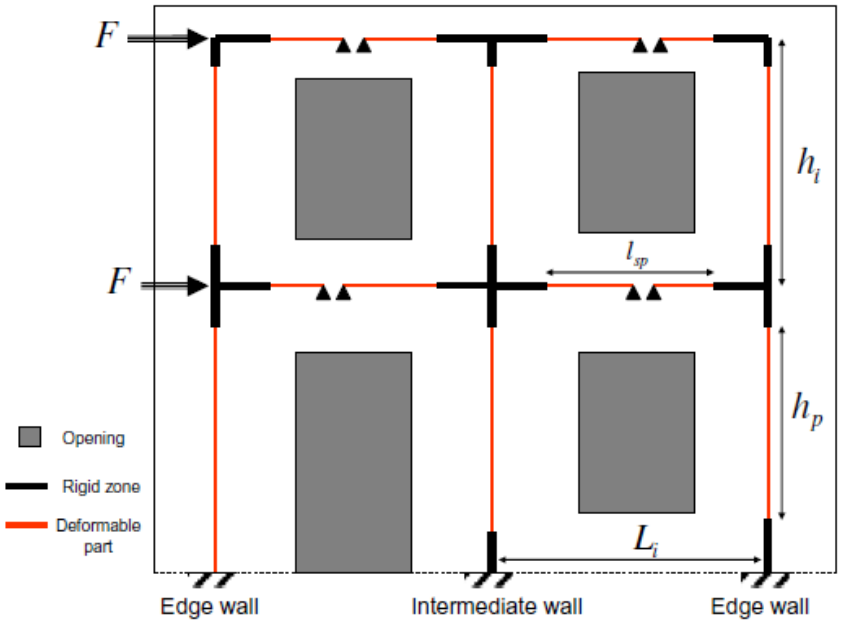

Fig. 4.3: A schematic representation of equivalent frame model for planar walls with openings (Belmouden and Lestuzzi, 2007).

The piers and spandrels are discretised into finite homogenized slices (Belmouden and Lestuzzi, 2007). Variable sections can be specified over both elements. Translational shear springs are added at each pier and spandrel at mid-points. These springs are expressed in terms of shear force–displacement laws.

Interactions between both axial force-bending moment and axial force-shear force are considered. Inelastic flexural as well as inelastic shear deformations are allowed for piers and spandrels.

The model allows the coupling effect in elevation due to the nonlinearity distribution in both piers and spandrels. The nonlinearity is treated using a smeared plasticity approach (Belmouden and Lestuzzi, 2007). The model can take into account both flexural and shear behaviour in the inelastic range. The nonlinear constitutive model for both flexural and shear behaviour is considered as a bilinear envelop curve with a very small post-yield stiffness to avoid numerical problems.

The flexural behaviour is modelled as a moment-curvature law that is based on an equilibrium statement in a cross-section.

4.2.1.1.2 Equivalent truss models

Within the mono-dimensional models (Magenes et al., 2000) a few authors (Calderoni et al., 1987; Calderoni et al., 1989) have proposed the idealisation through truss elements. The reactive portion of the masonry wall is modelled as a truss element whose inclination and stiffness reproduce the medium behaviour of the wall (Fig. 4.4). Since the geometrical properties of the truss (inclination, sizes of the section) vary with the increment of partialization, those kinds of methods are classified as variable geometry methods. The failure of each masonry element is reached when a limit equilibrium configuration is reached or with the crushing of the truss by compression.

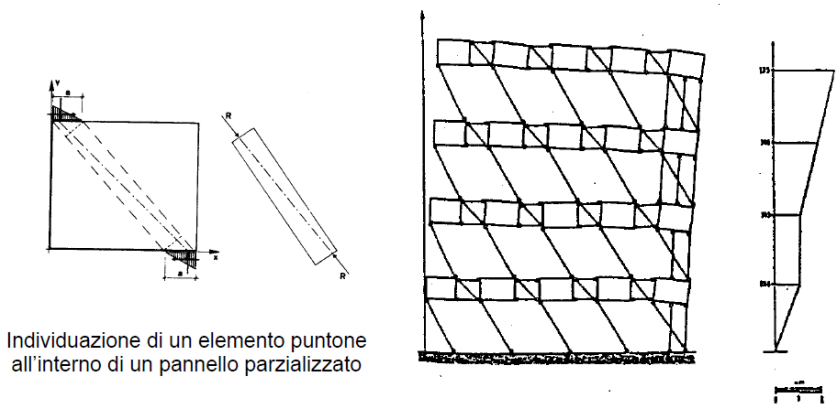

Fig. 4.4: Equivalent truss model (Magenes et al., 2000; Calderoni et al. 1987 and 1989).

4.2.1.2 Bi-dimensional models

4.2.1.2.1 D'Asdia and Viskovic (1993) PEFV model

The procedure developed by D'Asdia and Viskovic in 1993 named PEFV (in Italian: Parete ad Elementi Finiti a geometria Variabile) is based on a mathematical model simulating masonry by macro-finite elements (D'Asdia et al., 2005).

The key feature of the procedure is the way of dealing with the nonlinear behaviour of masonry. The method does not simulate the non linearity by modifying the properties and the mechanical characteristics of the material. The problem is based on geometric considerations: at each load step the shape of the model is updated to reproduce the variations of the resistant portions of the walls while the portions of the wall under tensile stresses or the cracked portions are excluded. Consequently the procedure is only load step dependent.

The method employs a reduced number of elements for each masonry wall as shown in Fig. 4.5.

The last developments of the model have been done in 2005 by D'Asdia, Viskovic and Brusaporci (2006) and is capable to consider different walls interconnected on the whole height of their junction with L or T horizontal configurations.

The aim of the method is to perform a nonlinear analysis of multi-storeyed masonry single walls under in plane actions and spatial masonry boxed structures more generally loaded.

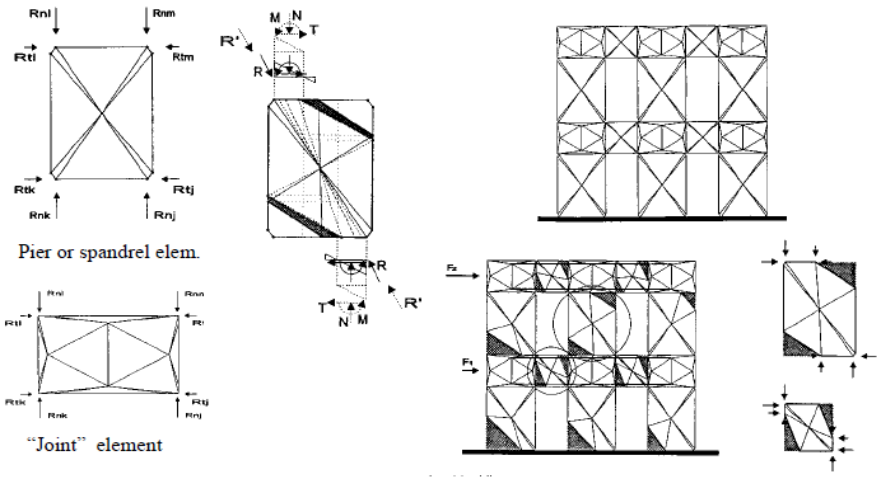

Fig. 4.5: Linear elastic finite elements with variable (adaptive) geometry (Abrams and Magenes, 2004b).

4.2.1.2.2 Braga et al (1990) Multi-FAN model

The present model was developed in 1990 by Braga and Liberatore (Braga et al., 1998).

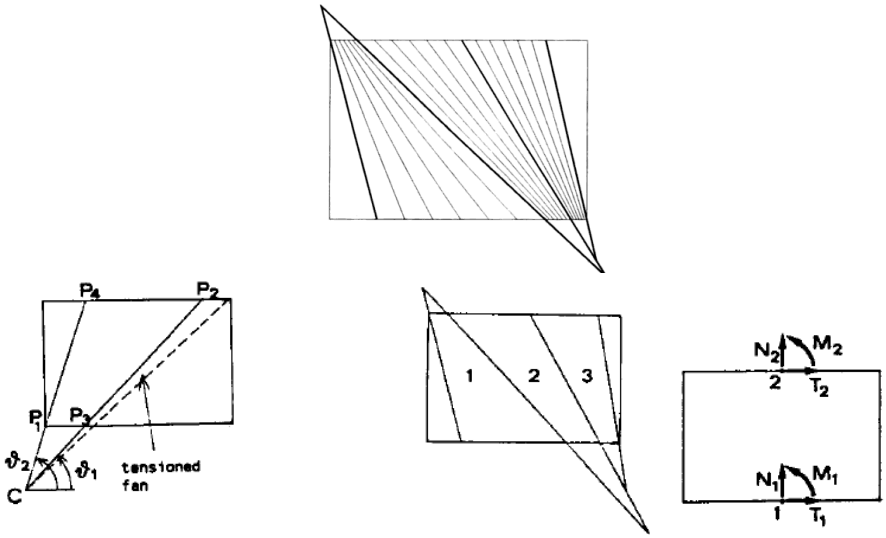

Fig. 4.6: Multi-FAN Model (Abrams and Magenes, 2004b).

It is based on a formulation of the panel element which assumes that the stress field of the panel follows a multi-fan pattern (Fig. 4.6). The material is a no-tension material characterised by a linear elastic behaviour in compression. The crushing happens when the maximum compressive stress is reached in the panel. Further assumptions of the model are the following:

- the upper and the lower edges of the panel are rigid;
- any interaction is allowed in the circumferential directions between the infinitesimal fans.

As a consequence of these hypotheses the circumferential and shear stresses are equal to zero and the stress state in each point is defined by the orientation of the radial stress. The vertices coordinates of the elementary fans completely define the stress field for prescribed displacements of the upper and lower faces of each panel element.

The stress based formulation of the element, characterizing the model, has an analytical formulation in closed form and has been then implemented into a displacement-based nonlinear FE program: MAS3D.

4.2.1.2.3 Gambarotta et al. (1996) nonlinear macro-element model

The present model was proposed by Gambarotta and Lagomarsino in 1996 (Gambarotta and Lagomarsino, 1996; Magenes, 2000) and further developed by Brencich and Lagomarsino in 1997 and 1998 (Brencich and Lagomarsino, 1997; Brencich and Lagomarsino 1998; Brencich et al., 1998).

The model can (Magenes et al., 2000) be used for the nonlinear static analysis of masonry walls and reproduces the cyclic behaviour of masonry walls. The kinematic and static variables to formulate the model are nodal displacements and rotations and shear, bending and normal resultant forces M,T and N.

It is characterised (Penna et al., 2004) by limited degrees of freedom and can represent masonry failure modes like bending-rocking and shear-sliding.

Each masonry wall can be subdivided into three main parts (Fig. 4.7):

- the bottom and the top layers, where bending and axial effects are concentrated but no shear deformation is allowed, characterised by three degrees of freedom: axial and horizontal displacements and rotation;
- the central part only allows shear-deformations and is characterised by two degrees of freedom: axial displacement and rotation.

Crack opening is (Brencich et al., 1998) represented and is forced to take place at the extremities of the element, while in the central area adequate constitutive equations are introduced to represent inelastic shear deformation and damage.

In addition to its geometrical characteristics, the macro-element is defined by six parameters: the shear module, the axial stiffness, the shear strength of the masonry, a non-dimensional coefficient which controls the inelastic deformation, the global friction coefficient and the factor that controls the softening phase.

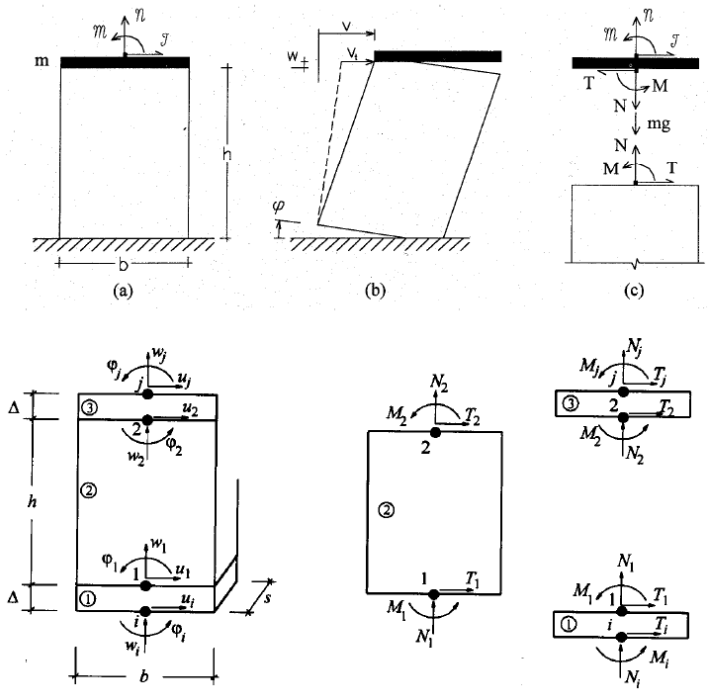

Fig. 4.7: Gambarotta, Lagomarsino and Brencich nonlinear macro-element model (Brencich et al., 1998).

4.2.2 No-tension models

Many constitutive models formulated during the last decades are based on the idealization of masonry as a no-tension material.

A first no-tension model, well known as Rigid No-Tension model (RNT) for masonry was proposed by Heyman in 1962 (Heyman, 1997). It is based on three essential assumptions:

- masonry has no tensile strength;
- stresses are so low that masonry has effectively an unlimited compressive strength;
- sliding failure does not occur.

As highlighted in the mentioned work (Heyman, 1997) each assumption is not strictly true and must be hedged with qualification: the first assumption is conservative; the second can be correct if average stresses are considered, because of the fact that stresses concentrations can arise locally and do not generally lead to overall failure of a structure; the last assumption can be accepted if thinking about a masonry structure which retains its shape. Those assumptions give the possibility to apply the basic theorems of plasticity within the method.

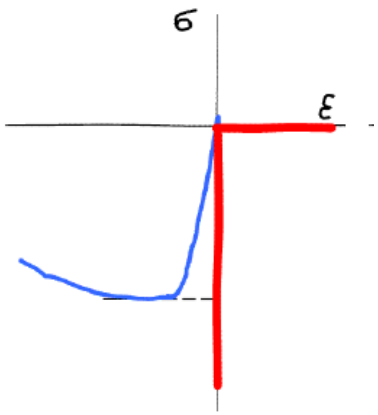

Fig. 4.8: Ideal uniaxial behaviour (Angelillo, 2011).

The definition of "no-tension material" has been proposed by Zienkiewicz et al. , 1968 (Ricamato, 2007) and has been used to study the behaviour of fractured rocks.

The method was characterised by an iterative solution process which achieved the no-tension state.

A further step in the development of these kinds of models is the one based on the so-called Elastic No-Tension (ENT) (Angelillo, 2011) material (Fig. 4.9). It has been developed since the late 70s by the Italian school of structural mechanics: many authors have proposed this model for the plane case, studying it from a mathematical point of view: Di Pasquale (1984), Como and Grimaldi (1985), Giaquinta and Giusti (1985). One of the main features of the model is that it is characterised by positive strains which constitute the fracture part of the deformation and negative strains which represent the elastic part of the deformation. A lucid and complete synthesis of the model for the threedimensional theory has been presented in Del Piero (1989).

The ENT material is globally elastic, in the sense that strain determines stress for any value of strain. The material is hyperelastic since there exists a stored elastic energy density ϕ such that σ is the derivative of ϕ with respect to ε. The elastic energy corresponding to this model is not strictly convex (major source of mathematical and numerical troubles, see Giaquinta & Giusti, 1985). This model requires only one material parameter: the elastic modulus E, since strength in compression is assumed to be infinite and strength and stiffness are completely neglected in tension.

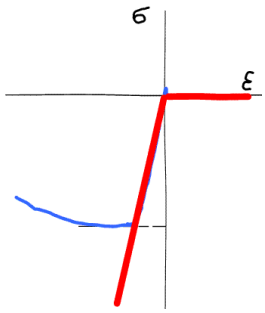

Fig. 4.9: ENT material model (Angelillo, 2011).

The no-tension material model received and still receives great attention by many (Ricamato, 2007) researchers to study the behaviour of old masonry structures.

Several studies have been developed regarding the no-tension material model from a mechanical and computational point of view.

A proposal of a no-tension model with limited compressive strength has been presented by Lucchesi (Ricamato, 2007): the model is characterised by a compression failure which is affected by progressive damage and inelastic irreversible strain.

Marfia and Sacco (Ricamato, 2007; Marfia and Sacco, 2005)developed a no-tension model which takes into account the inelastic behaviour in compression, considering a plasticity model which neglects the damage and softening effects. The model results appropriate for the description of the material crushing when limited values of the compressive strain arise.

The elasto-plastic model is characterised by a first linear elastic feature OD and a plateau with a constant stress DE, as illustrated in the following Fig. 4.10.

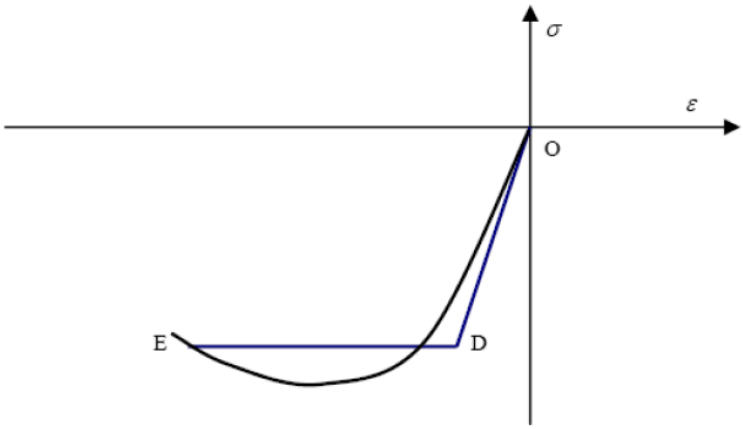

Fig. 4.10: Elato-plastic model (Ricamato, 2007).

The principal characteristics of this model (Ricamato, 2007; Olivito, 2003) are the possibility to determine the collapse load of masonry and the irreversible nature of strains in the plateau DE for cyclic loads.

4.2.3 Finite element models

The structural (Magenes and Abrams, 2004; Bosiljkov, 2004) behaviour of masonry can be modelled throughout the Finite Element Method (F.E.M.) when the complexity of the geometry and the necessity of more sophisticated simulations do not allow the equivalent frame idealization.

One of the first F.E. modelling (Tzamtzis and Asteris, 2003) approach to describe masonry behaviour has been the two-dimensional plane stress formulation in addition to an isotropic elastic behaviour. That approach, presented by Rosenhaupt (1965) and Saw (1974), did not include the influence of the mortar joints. A further proposal of material model with average properties also including local failures has been done by Ganju (1977) and Samarasinghe (1982).

More recently analytical procedures taking into account the nonlinear behaviour of masonry under static loads have been developed, while numerical models are still less commonly used for F.E. analysis of masonry subjected to cycling loads because of the complexities of modelling the material (Karapitta et al., 2010).

In the nonlinear F.E. modelling an important issue is represented by the constitutive laws of the material. Several categories of constitutive laws have been presented by researchers like standard plasticity based; damage coupled with plasticity; visco-elasticity and nonlinear fracture mechanics models associated to sophisticated F.E. analysis techniques.

4.2.4 Homogeneous continuum models

4.2.4.1 Homogeneous anisotropic continuum models based on Cauchy

The homogenous continuum anisotropic models reproduce the macroscopic behaviour of a medium (Trovalusci and Masiani, 2005) which does not consider the specific properties of all components or their texture.

The first types of those models have been described by the constitutive relations of the classical Cauchy continuum and did not include any length parameter of the microstructure. This aspect caused

their dependence on shape, orientation and arrangement of the units and led to numerical solutions strongly dependent on the adopted discretization.

In the past years considerable efforts have been made by researchers to estimate the average elastic properties and the failure criteria of equivalent continua within the context of the homogenisation theories (Rots et al., 1998; Kyoya et al., 1999; Banks-Sills et al., 1997).

The proposals to solve this aspect of the problem ranged over a wide variety of solutions: from the use of viscous models (Sluys and Wang, 1998) to the employment of grade two materials and non-local models (Peerlings et al., 1996; Svedberg and Runesson, 1998; Polizzotto et al., 1998).

They have been all related to the introduction of specific constitutive requirements involving spatial or temporal derivatives other than the first order in the equations of motion. These additional terms, related to an internal length parameter typical of the internal structure of the medium, gave the possibility to define a "non-simple" Cauchy continuum. Through those new kinds of models, the problem can be regularised and becomes well posed.

4.2.4.2 Homogeneous equivalent continuum models based on Cosserat

Masonry structures characterised by a texture made out of bricks or stones assembled together in various regular dispositions constitute a category of structure quite common. Their regularity in the geometry and the orientation and arrangement of the units influences their mechanical behaviour. Several authors are focused on developing models which can take into account that regularity. A possible approach is through the macro-modelling, especially for those kinds of systems with a large number of degrees of freedom.

As an alternative to Cauchy anisotropic continuum for those kinds of masonry with regular texture, some authors (Masiani et al., 1995; Masiani and Trovalusci, 1995) firstly proposed the Cosserat equivalent continuum as a possible model for the masonry, confirmed as effective

even when the size of the units is small (Trovalusci and Masiani, 2005). Their idea was reinforced by the possibility to apply Cosserat theory for the analysis of soil mechanic problems (Masiani et al., 1995; Trovalusci and Masiani, 2003), characterised by blocks even smaller than in masonry. Through numerical comparisons they have demonstrated that Cosserat solution is consistent if compared to a discrete solution both in quantitative and qualitative terms. Particularly the interlocking among the blocks presented in the discrete framework is well reproduced by Cosserat model.

Since the earlier works, the authors (Masiani and Trovalusci, 1995; Masiani and Trovalusci, 1996; Trovalusci and Augusti, 1998; Mariano and Trovalusci, 1999; Trovalusci and Masiani, 1999) have shown that information related to the actual heterogeneous and discontinuous nature of a material can be preserved using a macroscopic description in terms of continuous model with microstructure.

Then (Trovalusci and Masiani, 2003) the analyses on walls made of elements with various geometry and textures have shown that the Cosserat model allows discerning the behaviour of systems made of elements of different shape, size and arrangement. Moreover, since the strain and the stress tensors are not symmetric, this model can describe the asymmetries in the shear behaviour along different planes. This property proved useful for orthotropic materials like common masonry with regularly spaced bricks.

4.3 Micro-modelling

Micro-modelling represents the alternative approach of modelling masonry which considers the two distinct phases of masonry: units and mortar joints, constituting an heterogeneous system and is suitable when the insight of the local behaviour of masonry is required.

In the micro-modelling of masonry structures an essential role is the one of the interface elements, which have to reproduce the discontinuities between different materials represented by the mortar-brick joints interactions.

The basic assumption for interface elements is that they are elements where nonlinear effects are localized and displacement discontinuities can take place while from a geometrical point of view they represent thin layers that can be neglected in the mathematical model (Karapitta et al., 2010).

Consequently the nonlinear and inelastic effects (Giambanco and Mroz, 2001) such as contact friction and slip, asperity interaction, damage, dilatancy and asperity flattening, may affect significantly the interface response and overall performance of the structure.

Different proposals on the interface modelling are presented in the scientific literature characterizing the corresponding micro-model. Lofti and Shing (1994) proposed a constitutive model for interfaces which simulates the fracture propagation within the mortar joints, due to the normal and tangential stresses and including the dilatancy effects.

Gianbanco and Di Gati (1997) formulated an interface model suitable to predict the mechanical response of joints in block masonry structures. The interface laws have been formulated in the framework of softening materials elasto-plasticity and simulate the loss of cohesion process which occurs in the joint due to the shear or tension stresses. The cohesive-frictional joint transition has been treated incorporating some concepts derived from rock mechanics.

Gambarotta and Lagomarsino (1997) proposed a damage model for mortar joints which considers both the damage and the decohesion in the mortar-brick interface. In the interface model the extension and sliding of the mortar joints are linearly dependent on the mean stress and a damage variable, defined according to damage mechanics approach. The model has been applied to reproduce brick masonry walls subjected to horizontal cycling loads, where both brick units and mortar joints are defined by an inelastic behaviour.

Lourenço and Rots (1997) implemented a constitutive model of interface based on the plasticity theory able to describe cracking, slip and crushing of the material whose parameters derived from experiments in units, joints and masonry samples. The model has been later improved by Oliveira and Lourenço (2004) including the cyclic behaviour in the

cohesive zone. Such an interface model, object of study of the present thesis, will be more accurately described in the following chapter.

The model presented by Giambanco and Mroz (2001) is characterised by two interfaces separating the mortar joint from the adjacent material. The response of the interface depends on external (contact) stresses and strains interacting with the internal stresses or strains within the joint. The complex aspect of the model is that the displacement discontinuities may propagate on both sides of the layer and ultimate failure may occur under compression or shear.

Alfano and Sacco (2006) proposed an interface model where damage and friction are combined. The cohesive crack propagation is governed by nonlinear fracture mechanics. A non negligible inelastic zone, the so called process zone, develops ahead of the crack tip. In that zone, a partial decohesion occurs between the separating surfaces. At a micromechanical level the phenomenon of the partial decohesion is due to the nucleation of micro cracks, while the progressive interface damage corresponds to the micro crack growth and coalescence until the formation of macro cracks, representing the fracture.

At a meso-mechanical level, these phenomena have been modelled by assuming that a representative elementary area of the interface can be decomposed into an undamaged part and a completely damaged part, with the damage parameter D being the relative measure of the damaged part.

The main idea of the model consists in introducing an unilateral friction law only on the damaged part of the representative elementary area while a linear elastic behaviour is considered on the undamaged part. In the interface model the damage evolution law of the Crisfield's model has been assumed and a simple Coulomb friction law has been introduced on the damaged part.

CHAPTER 5

5. Definition of the Finite Element Model

The present chapter describes the finite element model employed in this research to simulate the behaviour of masonry walls under in-plane shear forces. The model simulates the behaviour of masonry walls externally strengthened by FRP composites arranged in diagonal configuration.

The adopted modelling approach for masonry can be regarded within the so-called macro-modelling according to the classification reported in section § 4.2. The interactions between the masonry and the FRP strengthening have been modelled through interface elements.

The chapter presents the mathematical and physical characterisation of the implemented model within the general framework finite element method: the kind of finite elements employed, the corresponding form of displacement functions, the material models adopted for masonry, FRP reinforcement and interface elements within the multiple yield surfaces plasticity are finally described.

5.1 Model for unstrengthened masonry walls

5.1.1 Idealisation and choice of the model geometry

The choice to reproduce a finite element model through linear, two-dimensional or fully three-dimensional elements constitutes the first step in the idealisation of the geometry.

Such a geometrical idealisation should be kept simple and adequate for the problem under consideration.

Within the Finite Element Method the fully three-dimensional models are very time consuming and are characterised by the risk of yielding meaningless results. The models incorporating shell elements can be reasonably difficult to analyse but in case of large thickness of structural elements their use could lead to a poor approximation of the actual state of stress (Lourenço, 2001).

The purpose in developing the present Finite Element Model of masonry walls reinforced by FRP has been to obtain a numerical model, capable of predicting the behaviour of masonry both in the elastic and inelastic range and to calibrate the response parameters of the masonry-FRP composite system, basing on laboratory tests.

For the reasons exposed above, the choice has been the F.E. modelling through a two-dimensional geometry essentially constituted by plane stress elements.

The final aim of the model is to reproduce the behaviour of a masonry wall strengthened by FRP strips under in-plane actions.

5.1.2 Type of elements and displacement functions.

The engineering approach to the discretization of continuous problems is to create an analogy between real discrete elements and finite portions of a continuum domain; the Finite Element Method constitutes such a *discretization procedure of continuum problems posed by mathematically defined statements* (Zienkiewicz and Taylor, 2000).

The Finite Element Method allows two possible formulations: the force formulation and the displacement formulation. The displacement formulation consists in dividing the continuum into a number of finite elements, which are interconnected at a discrete number of points; the displacements of points represent the unknown parameters of the problem; a set of functions defines the displacement within each element, so the state of strain is uniquely determined. The state of the stress throughout the element is defined by the strains and the

constitutive properties of the material. A system of forces concentrated at the nodes, equilibrating the boundary stresses and any distributed loads, is determined.

Within the displacement formulation, a two-dimensional problem can be modelled as a plane stress problem or a plane strain problem. In both problems the displacement field is uniquely defined by the displacements in the directions of the Cartesian orthogonal x and y axes; furthermore only the strains and the stresses, having the components in the xy plane have to be considered.

In case of plane stress problems all the other components of stress are equal to zero and give no contribution to internal work; while in the plane strain problems the stresses in the orthogonal direction to the xy plane are not zero.

The behaviour of masonry walls under in-plane horizontal force can be regarded as a "plane stress" problem. 2D Finite Elements are available for analysing this wide class of problems.

In the spirit of the well-known displacement formulation of F.E., the wall has been discretized into a certain number of quadrilateral and triangular plane elements (Fig. 5.1 and Fig. 5.2).

The implemented quadrilateral elements (Fig. 5.1) are eight-nodes isoparametric plane stress elements, whose displacement components are characterised by the following shape function:

$$u_i(\xi,\eta) = a_0 + a_1\xi + a_2\eta + a_3\xi\eta + a_4\xi^2 + a_5\eta^2 + a_6\xi^2\eta + a_7\xi\eta^2 \qquad (5.1)$$

The triangular elements (Fig. 5.2) are six-nodes isoparametric plane stress elements, whose displacements are characterised by the following shape function:

$$u_i(\xi,\eta) = a_0 + a_1\xi + a_2\eta + a_3\xi\eta + a_4\xi^2 + a_5\eta^2 \qquad (5.2)$$

These elements may only be applied if no bending out of plane occurs, so they perfectly meet requirements in a F.E. modelling of a wall subjected to in-plane actions.

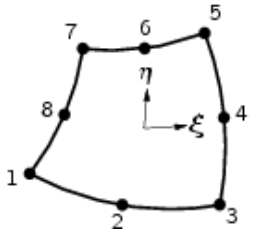

Fig. 5.1: Isoparametric quadrilateral plane stress CQ16M element (DIANA, 2010).

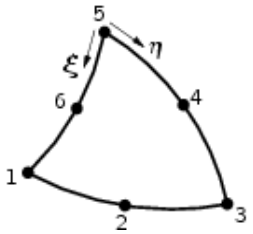

Fig. 5.2: Isoparametric triangular plane stress CT12M element (DIANA, 2010).

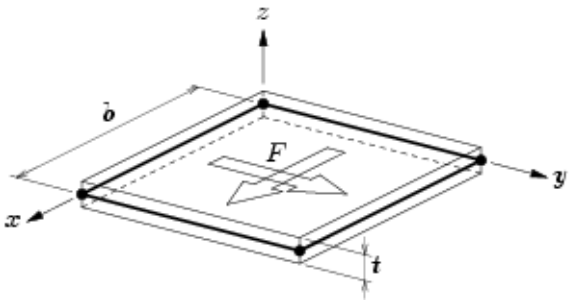

Fig. 5.3: Characteristics of plane stress elements (DIANA, 2010).

A stiffness matrix characterises each element; to define the stiffness matrix it is necessary to solve the element integrals whose solution can be analytical or numerical. Integrals of isoparametric elements are

suitable to be numerically solved. (Zienkiewicz and Taylor, 2000; DIANA, 2010; Ascione et al., 2010).

Several methods are possible to find numerically the integral of a function. The Gauss quadrature represents a helpful procedure, whose most general expression is:

$$\int_{-1}^{1} f(\xi)d\xi = \sum_{g=1}^{Ng} w_g f(\xi_g) \tag{5.3}$$

where:
N_g is the order of integration;
ξ_g represents the N_g Gauss points;
w_g describes the weight.

Gauss quadrature allows to obtain explicitly the solution of integrals in terms of Legendre polynomials and requires the least number of integration points. It has been applied to solve the isoparametric elements implemented in the developed model (Zienkiewicz and Taylor, 2000; DIANA, 2010; Ascione et al., 2010).

5.1.3 Material model for masonry

The constitutive behaviour of masonry is anisotropic due to the geometrical arrangement of units and mortar. To reproduce such a material as an anisotropic composite material, the material model proposed by Lourenço (1996) has been used within the adopted macro-modelling approach.

Such a model is based on the anisotropic plasticity and includes hardening/softening behaviour along each material axis.

Two possible approaches can be generally used to define an anisotropic plastic model:

- a first approach which describes the material behaviour with a single yield criterion;
- an alternative approach which considers different inelastic criteria for tension and compression.

The material model, implemented in the present thesis, follows the second approach and is an example of plasticity-based model with multiple yield surfaces (Lourenço, 1996; Jirasek and Bazant, 2001).

5.1.3.1 Elastoplastic constitutive models

Before introducing the material model for masonry, some basic notions of plasticity will be briefly exposed.

Within the plasticity theory (Jirasek and Bazant, 2001) the first condition which characterises a model is the yield surface, whose function is to define the stress states for which the material exhibits plastic flows and can be mathematically expressed as:

$$f(\sigma) = 0 \tag{5.4}$$

Other important elements, necessary to define a material model, are the flow rule, which describes the direction of the plastic flow, giving information on how the plastic strain rate evolves and on its component.

The usual decomposition of the strain rate vector $\dot{\varepsilon}$ can be expressed as a sum of the elastic reversible strain $\dot{\varepsilon}^e$ and the plastic irreversible strain $\dot{\varepsilon}^p$:

$$\dot{\varepsilon} = \dot{\varepsilon}^e + \dot{\varepsilon}^p \tag{5.5}$$

Since the yield surface is a graphical representation of the function $f(\sigma) = 0$, the direction normal to the yield surface can be easily defined in terms of gradient operator.

The flow rule can be represented by a normality rule, known as associated flow rule, whose expression is:

$$\dot{\varepsilon}^{p} = \dot{\lambda}\frac{\partial f}{\partial \sigma} \tag{5.6}$$

where λ is a scalar named plastic multiplier, which controls the magnitude of the plastic strain, and $\dot{\lambda}$ has the meaning of rate.

In case of associated perfect plasticity the mathematical description is complete through the relation (5.6), the elastic constitutive law and the following loading-unloading conditions, named Karush-Khun-Tucker conditions:

$$\dot{\lambda} \geq 0,\ f(\sigma) \leq 0,\ \lambda \dot{f(\sigma)} = 0 \tag{5.7}$$

For many pressure-sensitive materials the associated flow rule is often unrealistic, so a non associated flow rule is considered; whose mathematical equation is:

$$\dot{\varepsilon}^{p} = \dot{\lambda}\frac{\partial g}{\partial \sigma} \tag{5.8}$$

where $g(\sigma)$ is a new function called plastic potential.

5.1.3.2 Adopted material model

The material implemented in the Finite Element Model developed in the present thesis is the one proposed by Lourenço (1996).

The model is defined through different yield surfaces whose functions are:

$$f(\sigma, \bar{\sigma}(\kappa)) = 0 \tag{5.9}$$

where $\bar{\sigma}$ represents the yield stress value and is expressed as a function of the scalar κ, which measures the amount of inelastic strain; the function $\bar{\sigma}(\kappa)$ represents the hardening law.

Particularly the constitutive model is based on two yield criterions: the Rankine-type criterion, in tension, and the Hill-type criterion, in compression which will be briefly described in the following.

5.1.3.3 Rankine type criterion

The yield criterion characterizing the tensile mechanism is a Rankine type criterion (Lourenço,1996) which can be expressed as a function of the first principal stresses and the equivalent stress $\bar{\sigma}_t$:

$$f_1 = \frac{\sigma_x + \sigma_y}{2} + \sqrt{\left(\frac{\sigma_x - \sigma_y}{2}\right)^2 + \tau_{xy}^2} - \bar{\sigma}_t(\kappa_t) \tag{5.10}$$

In Eqn. (5.10) the equivalent stress $\bar{\sigma}_t$ describes the softening behaviour of the material and κ_t controls the amount of softening.

Considering different tensile strengths f_{tx} and f_{ty} along the x, y directions, the Rankine yield criterion is also proposed as:

$$f_1 = \frac{\left(\sigma_x - \bar{\sigma}_{t1}(\kappa_t)\right) + \left(\sigma_y - \bar{\sigma}_{t2}(\kappa_t)\right)}{2} + \sqrt{\left(\frac{\left(\sigma_x - \bar{\sigma}_{t1}(\kappa_t)\right) - \left(\sigma_y - \bar{\sigma}_{t2}(\kappa_t)\right)}{2}\right)^2 + \alpha\tau_{xy}^2} \tag{5.11}$$

The parameter α in Eqn. (5.11), controls the shear stress contribution to failure through the expression:

$$\alpha = \frac{f_{tx} f_{ty}}{\tau_u^2} \tag{5.12}$$

where f_{tx} and f_{ty} are the uniaxial tensile strengths in the x, y directions and τ_u is the pure shear strength.

The relations describing the tensile softening are expressed by means of different fracture energies for each yield value as:

$$\bar{\sigma}_{t1} = f_{tx} \exp\left(-\frac{h f_{tx}}{G_{fx}} \kappa_t \right) \tag{5.13}$$

and

$$\bar{\sigma}_{t2} = f_{ty} \exp\left(-\frac{h f_{ty}}{G_{fy}} \kappa_t \right) \tag{5.14}$$

where h is the equivalent length.

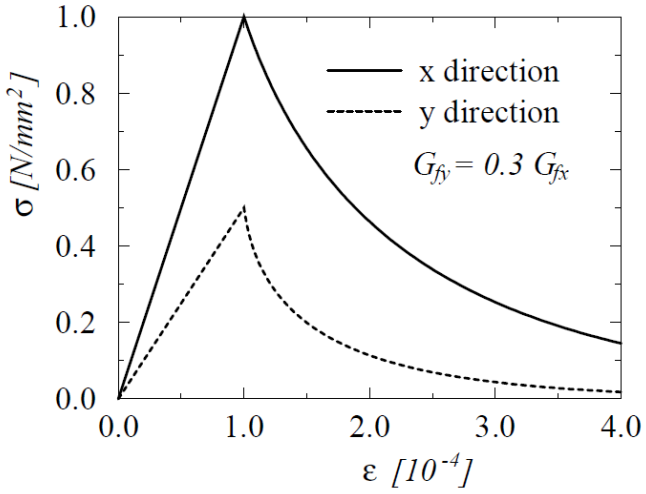

Fig. 5.4: Typical stress-strain response in uniaxial tension along the two material axes (Lourenço, 1996).

Fig. 5.4 shows an example of the response of the model in uniaxial tension.

In the work of Lourenço (1996), the equation (5.11), representing the Rankine type criterion, is rewritten in a matrix form:

$$f_t = (\frac{1}{2}\xi^T P_t \xi)^{1/2} + \frac{1}{2}\pi^T \xi \tag{5.15}$$

where:
P_t is the projection matrix:

$$P_t = \begin{bmatrix} 1/2 & -1/2 & 0 \\ -1/2 & 1/2 & 0 \\ 0 & 0 & 2\alpha \end{bmatrix} \tag{5.16}$$

π is the projection vector:

$$\pi = \{1 \quad 1 \quad 0\}^T \tag{5.17}$$

ξ is the reduced stress vector:

$$\xi = \sigma - \eta \tag{5.18}$$

σ and η are respectively the stress vector and the back stress vector:

$$\sigma = \{\sigma_x \quad \sigma_y \quad \tau_{xy}\}^T \tag{5.19}$$

$$\eta = \{\bar{\sigma}_{tx}(\kappa_t) \quad \bar{\sigma}_{ty}(\kappa_t) \quad 0\}^T \tag{5.20}$$

The flow rule for the Rankine yield surface is a non-associated plastic potential g_1, expressed in a matrix form as:

$$g_1 = (\tfrac{1}{2}\xi^T P_g \xi)^{1/2} + \tfrac{1}{2}\pi^T \xi \tag{5.21}$$

where:
P_g is the projection matrix:

$$P_g = \begin{bmatrix} 1/2 & -1/2 & 0 \\ -1/2 & 1/2 & 0 \\ 0 & 0 & 2 \end{bmatrix} \tag{5.22}$$

The last hypothesis which characterises the inelastic behaviour of Rankine-type yield criterion is a softening hypothesis involving the maximum principal plastic strain $\dot{\varepsilon}_1^p$, which in a matrix form has the following relation:

$$\dot{\kappa}_t = \dot{\varepsilon}_1^p = \left(1/2\left(\dot{\varepsilon}_1^p\right)^T Q\, \dot{\varepsilon}_1^p\right)^{1/2} + 1/2\pi^T \dot{\varepsilon}_1^p \tag{5.23}$$

where the matrix Q is:

$$Q = \begin{bmatrix} 1/2 & -1/2 & 0 \\ -1/2 & 1/2 & 0 \\ 0 & 0 & 1/2 \end{bmatrix} \tag{5.24}$$

So the inelastic behaviour adopted in the model can be finally expressed by the equation:

$$\dot{\kappa}_t = \dot{\lambda}_t \tag{5.25}$$

5.1.3.4 Hill-type criterion

The behaviour under compression is described (Lourenço,1996) by the mathematical equation of the Hill-type yield criterion, presented as:

$$f_2 = A\sigma_x^2 + B\sigma_x\sigma_y + C\sigma_y^2 + D\tau_{xy}^2 - 1 = 0 \tag{5.26}$$

with the coefficients A, B, C and D respectively defined as:

$$A = 1/(\bar{\sigma}_{cx}(\kappa_c))^2 \tag{5.27}$$

$$B = \beta/(\bar{\sigma}_{cx}(\kappa_c)\bar{\sigma}_{cy}(\kappa_c)) \tag{5.28}$$

$$C = 1/(\bar{\sigma}_{cy}(\kappa_c))^2 \tag{5.29}$$

$$D = \gamma/(\bar{\sigma}_{cx}(\kappa_c)\bar{\sigma}_{cy}(\kappa_c)) \tag{5.30}$$

In the above relations $\bar{\sigma}_{cx}$ and $\bar{\sigma}_{cy}$ represent the yield values along the material axes x and y; β and γ are additional parameters which determinate the shape of the yield surface and are functions of compressive strengths:

$$\beta = \left[\frac{1}{f_{45^o}^2} - \frac{1}{f_{cx}^2} - \frac{1}{f_{cy}^2} \right] f_{cx} f_{cy} \tag{5.31}$$

$$\gamma = \frac{f_{cx} f_{cy}}{\tau_{u,c}^2} \tag{5.32}$$

In a matrix form the yield function, characterizing the Hill-type criterion, is:

$$f_2 = (1/2 \, \sigma^T P_c \sigma)^{1/2} - \bar{\sigma}_c(k_c) \tag{5.33}$$

with the matrix P_c:

$$P_c = \begin{bmatrix} 2\frac{\bar{\sigma}_{cy}(\kappa_c)}{\bar{\sigma}_{cx}(\kappa_c)} & \beta & 0 \\ \beta & 2\frac{\bar{\sigma}_{cy}(\kappa_c)}{\bar{\sigma}_{cx}(\kappa_c)} & 0 \\ 0 & 0 & 2\gamma \end{bmatrix} \tag{5.34}$$

The yield criterion for compression is, finally, completed by an associated flow rule:

$$\dot{\kappa}_c = \frac{1}{\bar{\sigma}_c} \sigma^T \dot{\varepsilon}^p = \dot{\lambda}_c \tag{5.35}$$

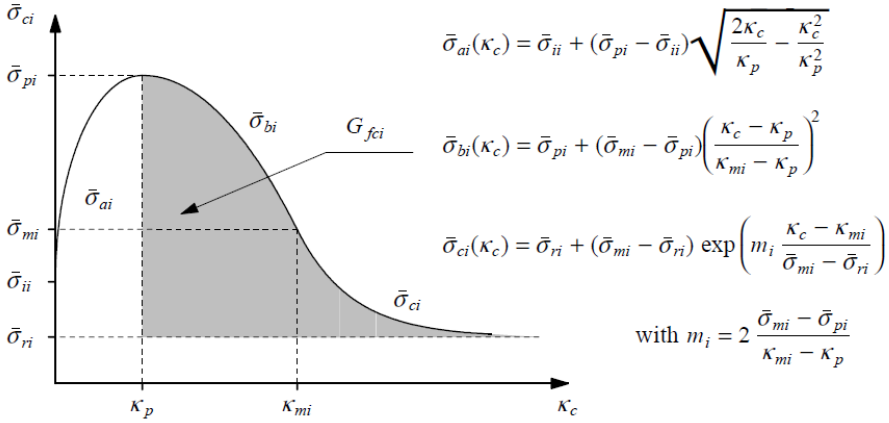

Fig. 5.5: Hardening/softening law for compression (Lourenço, 1996)

The work-like hardening/softening hypothesis, shown in Fig. 5.5, is characterised by a parabolic hardening followed by parabolic/exponential softening for both equivalent stress-equivalent strain diagrams, with different compressive fracture energies (G_{fcx} and G_{fcy}) along the material axes.

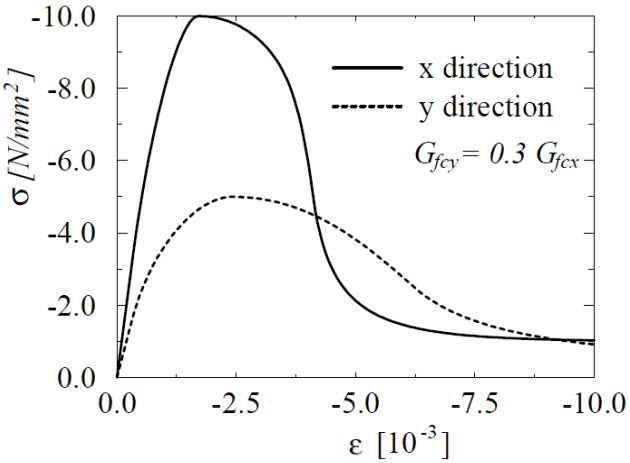

Fig. 5.6: Stress-strain response in uniaxial compression along the two material axes, (Lourenço, 1996).

An example of the response of the model in uniaxial compression is presented in Fig. 5.6.

5.1.3.5 Identification of the model

The above material model, (Lourenço,1996) expressed through two different yield criterions in tension and compression, has seven characterizing strength parameters: the tensile strengths along the material axes f_{tx} and f_{ty}, the compressive strengths along the material axis f_{cx} and f_{cy}, the parameters α, β and γ and five inelastic parameters G_{fx}, G_{fy}, G_{fcx}, G_{fcy} and κ_p.

To characterise the material model, the tensile and compressive strengths have to be determined, through some experimental tests suggested by the same author. Those tests have to be performed in displacement control conditions to obtain the inelastic parameters too: fracture energies and peak strain in compression.

Additionally to the above tests some non standard tests are also suggested to define the parameters α, β and γ. Those tests are fundamental because the intersection of the tension and compression yield surfaces of the Rankine-Hill criterion is not known in advance.

Fig. 5.7and Fig. 5.8 show both standard and non standard tests.

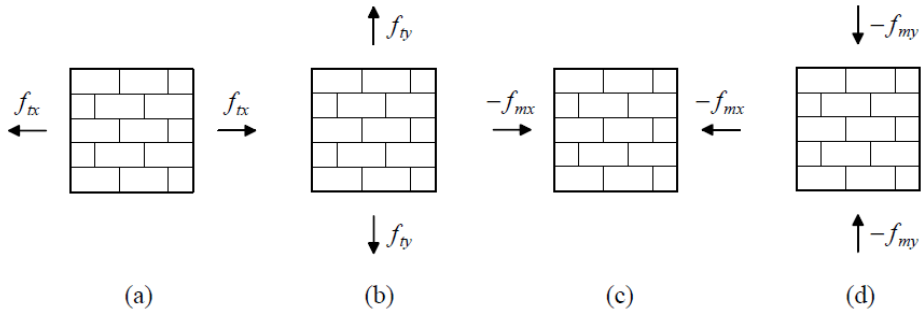

Fig. 5.7: Natural tests to calibrate the composite model: uniaxial tension (a) parallel to the bed joints and (b) normal to the bed joints; uniaxial compression (c) parallel to the bed joints and (d) normal to the bed joints; (Lourenço, 1996).

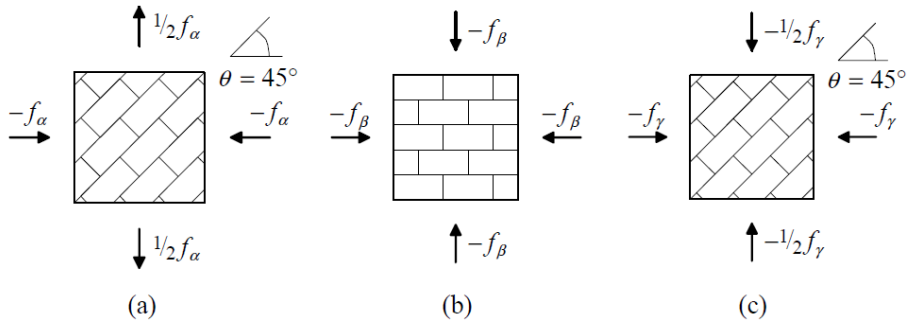

Fig. 5.8: Possible non-standard tests to calibrate the composite model and calculate (a) parameter α , (b) parameter β and (c) parameter γ; (Lourenço, 1996).

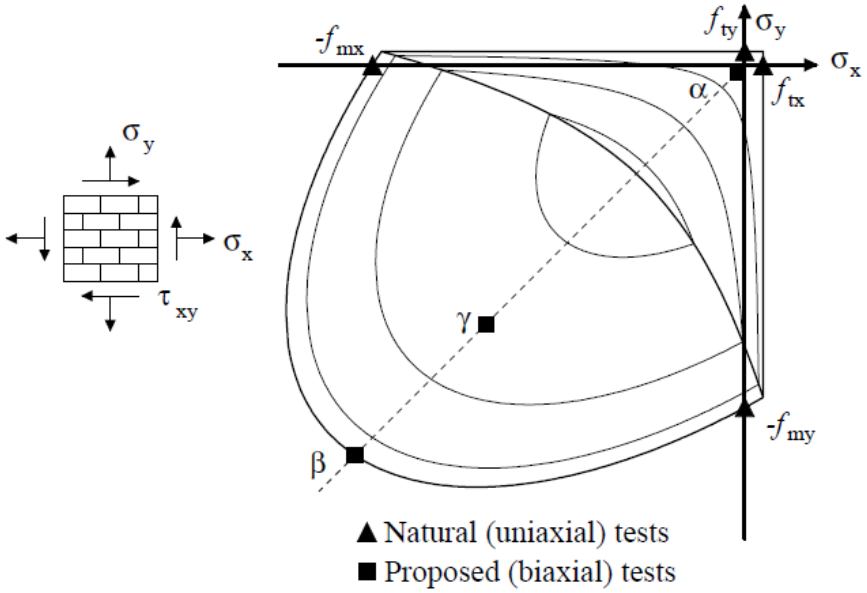

Fig. 5.9: Typical position of the natural tests and proposed non-standard tests with respect to the composite model (Lourenço,1996).

Fig. 5.9 shows the typical position of all tests described above with respect to the composite yield criterion.

5.2 Model for masonry walls strengthened by FRP composites

Within the scientific literature, various proposals are available to describe the behaviour of masonry walls reinforced by FRP composite following both the micro modelling approach (Cecchi et al., 2004; Milani et al., 2005; Milani, 2010) and the macro modelling approach (ElGawady et al., 2005; Grande et al., 2008).

The basic and innovative idea of the present model is to implement plane interface elements, generally available in the three-dimensional Finite Element modelling, into a two-dimensional plane stress problem.

Such a plane interface connects the FRP composite and the masonry, reproducing the nonlinear behaviour resulting from their interaction.

In the following a brief description of interface elements and constitutive model adopted to describe their behaviour is presented.

5.2.1 Interface elements

In the present developed model the connection between the masonry wall and the composite material has been modelled through interface elements.

The interface elements are special elements which can be used in addition to the conventional continuum elements, available in the finite element analysis, to discretize the space between two mechanically interacting bodies and to model the discontinuous behaviour between different materials (Hohberg, 1992; Potts et al., 2002).

Two families of interface models can be distinguished, depending on the approach used to their discretization: a phenomenological approach and a deductive approach (Lebon, 2011).

In the phenomenological approach the thickness of the interface is zero and the mechanical properties are obtained from physical considerations and experiments.

In the deductive approach a soft thin layer of interphase material is introduced near the interface. In the limit of vanishing layer-thickness, a link between the interfacial stress vector and the jump in displacement is obtained.

The zero-thickness interface elements are the types of interfaces implemented in the model object of the present research study.

Those elements relate the forces acting with the relative displacements of their two sides.

Two alternative formulations are possible for the zero-thickness element:

- a first formulation consists in considering the interface as a continuum element with a reduced aspect ratio, whose strains can be integrated analytically;
- a second formulation assumes unilateral constraints on the relative displacements between two substructures; the constrains are placed at discrete points. A numerical integration over the surface is performed and an isoparametric joint element results.

One of the first mathematical description (Potts et al., 2002) of a zero-thickness interface element was done by Beer (1985) and Carol and Alonso (1983). In their formulation the interface stress has a normal and a shear component, connected to the normal and tangential strains by the relation:

$$\begin{Bmatrix} \Delta\sigma \\ \Delta\tau \end{Bmatrix} = [D] \begin{Bmatrix} \Delta\varepsilon \\ \Delta\gamma \end{Bmatrix} \tag{5.36}$$

For isotropic linear elastic behaviour the stiffness matrix $[D]$ assumes the form:

$$[D] = \begin{bmatrix} k_n & 0 \\ 0 & k_s \end{bmatrix} \tag{5.37}$$

where k_n and k_s are the elastic normal and shear stiffness respectively.

In that formulation the interface element strain is defined through the relative displacement of the top and the bottom of the interface element (Fig. 5.10):

$$\varepsilon = \Delta v_i = v_i^{bot} - v_i^{top} \tag{5.38}$$

$$\gamma = \Delta u_i = u_i^{bot} - u_i^{top} \tag{5.39}$$

where:

$$\begin{cases} v_i = v\cos\alpha - u\sin\alpha \\ u_i = v\sin\alpha + u\cos\alpha \end{cases} \tag{5.40}$$

and u and v are the global displacements in the x_G and y_G directions respectively.

Substituting the expressions (5.38) and (5.39) in (5.40), results:

$$\begin{cases} \varepsilon = (v^{bot} - v^{top})\cos\alpha - (u^{bot} - u^{top})\sin\alpha \\ \gamma = (v^{bot} - v^{top})\sin\alpha + (u^{bot} - u^{top})\cos\alpha \end{cases} \tag{5.41}$$

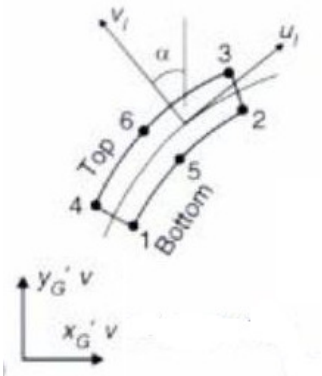

Fig. 5.10: Isoparametric interface element: six-noded element; (Potts et al., 2002).

The geometry of a three-dimensional interface with zero-thickness is fully described by the geometry of the element mid-plane, located half way between the joint faces (Fig. 5.11).

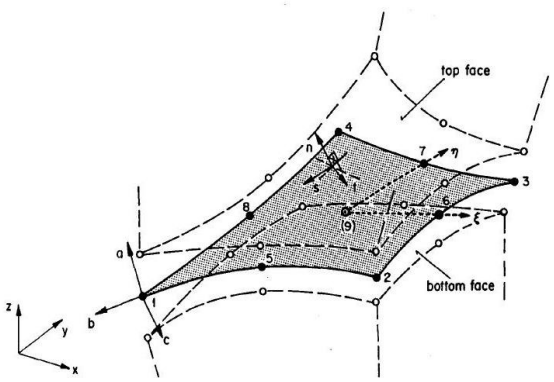

Fig. 5.11: Geometry of interface element with 4 to 9 double nodes (Hohberg, 1992).

Its formulation can be derived from a two-dimensional interface element formulation, considering three interface stresses: a normal stress σ and two mutually perpendicular shear stresses: τ_u and τ_b, three strains: ε, γ_u and γ_b and three displacements: u, v and w.

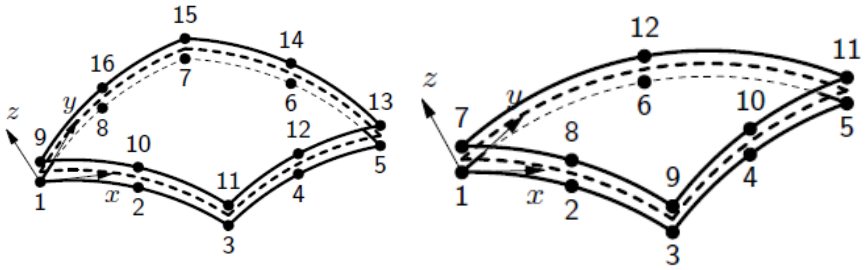

Fig. 5.12: Structural interface elements implemented in the developed model (DIANA, 2010).

Finally, Fig. 5.12 shows the two types of structural interfaces implemented in the model.

5.2.2 Material model for interface elements

The constitutive model of zero-thickness interface elements present an inelastic behaviour formulated using the plasticity theory; its numerical formulation has been developed by Lourenço and Rots (1997) for masonry joints.

The behaviour of an interface element can be described as a relation between the tractions t and the relative displacement u across the interface.

The elastic constitutive relation is expressed as:

$$\sigma = D\varepsilon \tag{5.42}$$

where:

$\sigma = \{\sigma, \tau\}^T$ represents the generalised stresses in a two-dimensional configuration;

$D = diag\{k_n, k_s\}^T$ is the elastic stiffness matrix;

$\varepsilon = \{\Delta u_n, \Delta u_s\}^T$ represents the generalised stresses.

The components of the elastic stiffness matrix k_n and k_t are respectively:

$$k_n = \frac{E_u E_m}{t_m (E_u - E_m)} \tag{5.43}$$

and

$$k_s = \frac{G_u G_m}{t_m (G_u - G_m)} \tag{5.44}$$

where E_u and E_m are the Young's modulus of the two materials connected by the interface element; G_u and G_m are the shear modulus of the two materials connected by the interface element; t_m is the thickness of joints.

The yield surface of the elastic domain is a composite yield surface defined by different yield functions whose general formulation in the plastic approach is the following:

$$f_i(\sigma, \kappa_i) = \Phi_i(\sigma) + \Psi_i(\kappa_i) \tag{5.45}$$

where Φ_i and Ψ_i are generic functions, characterizing the specific yield criterion considered, and the scalar κ_i expresses the amount of hardening or softening.

For yield criterions whose assumption is the one of non-associated plasticity, the scalar κ reads:

$$\dot{\kappa} = \sqrt{(\dot{\varepsilon}^p)^T \dot{\varepsilon}^p} \tag{5.46}$$

The constitutive model of the considered interface is composed by three different yield functions for tensile, shear and compressive criterions.

The yield function for the tensile criterion is the following:

$$f_I(\sigma, \kappa_I) = \sigma - \bar{\sigma}_I(\kappa_I) \tag{5.47}$$

where $\bar{\sigma}_I$ is the yield values expressed as:

$$\bar{\sigma}_I(\kappa_I) = f_t \exp\left(-\frac{f_t}{G_f^I}\kappa_I\right) \tag{5.48}$$

In Eqn (5.47) f_t represents the tensile strength of the joint and G_f^I is the mode I fracture energy.

The criterion is based on assuming an associated flow rule and a strain softening, only governed by the plastic relative displacement:

$$\dot{\kappa}_I = \dot{u}_n^p = \dot{\lambda}_I \tag{5.49}$$

The yield function for the shear mode is given by the following equation:

$$f_2(\sigma, \kappa_2) = |\tau| + \sigma \tan\phi(\kappa_2) - c(\kappa_2) \tag{5.50}$$

where c and ϕ are respectively the cohesion and the friction angle.

The non-associated plastic potential characterizing the shear yield function is expressed by:

$$g_2 = |\tau| + \sigma \tan\psi - c \tag{5.51}$$

The hypothesis for the softening is a strain hypothesis, governed by the only plastic relative displacement:

$$\dot{\kappa}_2 = \dot{u}_s^p = \dot{\lambda}_2 \tag{5.52}$$

Finally, the compression behaviour is described by a cap criterion with the following yield function:

$$f_3(\sigma, \kappa_3) = C_{nn}\sigma^2 + C_{ss}\tau^2 + C_n\sigma - (\bar{\sigma}_3(\kappa_3))^2 \tag{5.53}$$

where C_{nn}, C_{ss} and C_n are material parameters and $\bar{\sigma}$ is the yield value.

An associated flow rule is considered and expressed through a matrix notation as:

$$\dot{\kappa}_3 = \dot{\lambda}_3 \sqrt{(P\sigma + p)^T (P\sigma + p)} \tag{5.54}$$

where:
P is the projection matrix equal to $diag\{2C_{nn}, 2C_{ss}\}$ and p is the projection vector equal to $\{C_n, 0\}^T$.

The hardening/softening hypothesis considered in compression are the ones previously described for masonry in Fig. 5.5.

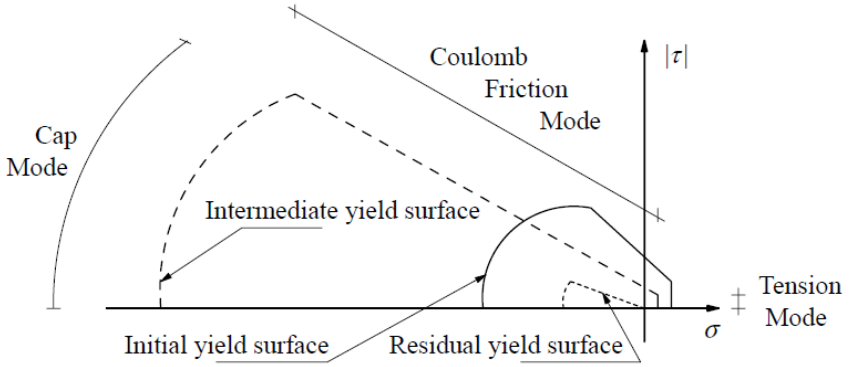

Fig. 5.13: Proposed model for interfaces; (Lourenço, 1996).

The total interface behaviour is given by the global yield surface shown in Fig. 5.13.

5.2.3 Material model for FRP composites

The behaviour of FRP composite has been considered linear elastic. The parameters necessary to describe the isotropic behaviour of the composite in the elastic range are the elastic Young modulus E_f and the Poisson's rate ν_f.

5.2.4 Geometrical modelling

Seven masonry walls made out of tuff stones, externally strengthened by FRP composite and tested under shear-compression tests, belonging to the wider experimental campaigns of Marcari et al. (2007) are object of the finite element model developed in the present thesis.

Fig. 5.14 shows the dimensions and the texture common to all the as-built walls (control specimens).

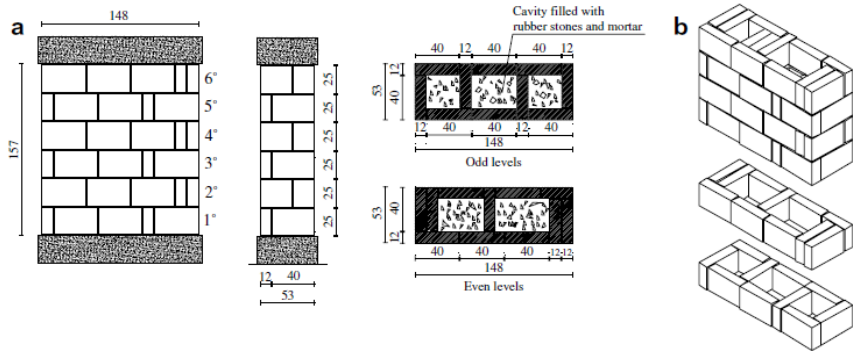

Fig. 5.14: Geometry of the masonry wall, (Marcari et al., 2007).

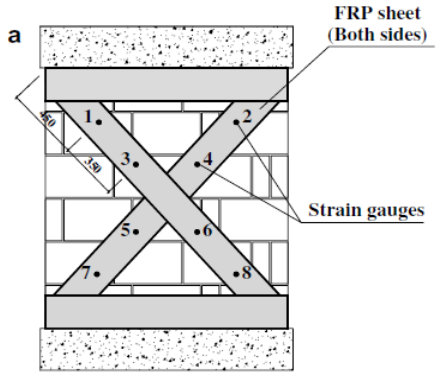

Fig. 5.15: Strengthening layout; (Marcari et al., 2007).

The seven walls externally strengthened and considered for developing the model had FRP strips in diagonal configuration placed on both sides, like shown in Fig. 5.15. The FRP reinforcement was applied with a low density, i.e. one ply of FRP for each strip, or with a high density, i.e. two plies of FRP for each strip (Marcari et al., 2007).

Among the walls with cross-layout configuration, four were reinforced by CFRP strips: two characterised by low density and two by high density and three were reinforced by GFRP: one characterised by low density and the remaining two by high density.

5.2.4.1 Finite Element mesh

This section describes the Finite Element Model implemented to simulate the masonry walls tested during to the experimental campaign (Marcari et al., 2007) described above.

The finite element model has been developed following the macro-modelling approach and consists in a bi-dimensional finite element mesh.

The built mesh is the same for both plain specimens and FRP strengthened specimens. It reproduces the shape and the real dimensions of the diagonal FRP strips. The two horizontal strips, placed at the top and bottom of the walls, have not been modelled, considering their mean function of fixing the diagonal reinforcement. The concrete beams placed at the top and the bottom of the walls have been also modelled.

As described in sections §5.1.2 and §5.2.1, the element types implemented in the model are: eight nodes plane stress elements CQ16M and six nodes plane stress elements CT12M for both masonry and FRP strips; eight plus eight nodes interface elements CQ48I and six plus six nodes interface elements CT36I have been implemented to model the interactions between masonry and FRP strips (§5.2.1).

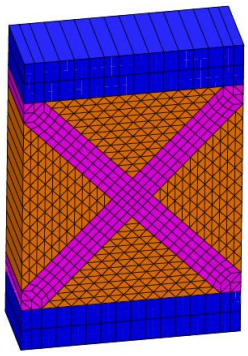

Fig. 5.16: Realistic representation of the finite element model.

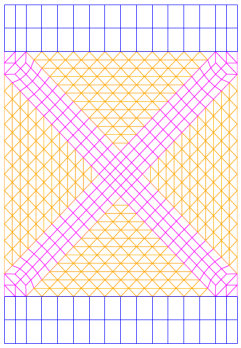

Fig. 5.17: Developed mesh of the two-dimensional finite element model.

Fig. 5.16 and Fig. 5.17 respectively show a realistic geometrical representation of the model and the corresponding mesh in the 2D model.

5.2.5 Boundary conditions

All the wall specimens were tested in shear compression tests. Each test was performed into two steps: the first step consisted in an axial load uniformly applied on the top of the wall and kept constant during the test; then the shear load was applied up the failure of the wall. Fig. 5.18 shows the test machine, whose complete description can be found in the original work (Marcari et al., 2007).

Boundary conditions in terms of constrains and applied load have been reproduced in the finite element model: the constraints of the bottom concrete beam suppress the translation in x and y directions; while the top of the wall presents constraints which do not allow relative displacement in y direction during the application of the vertical load.

Finally, to replicate the same conditions of the experimental test machine, the steel beam at the top has been also modelled, and constraints between steel beam and masonry wall were defined to assure that no relative rotations happen between the right and left extremities of the top concrete beam. The steel beam and the corresponding constraints reproduce the effect of the balancer actuator, shown in Fig. 5.18.

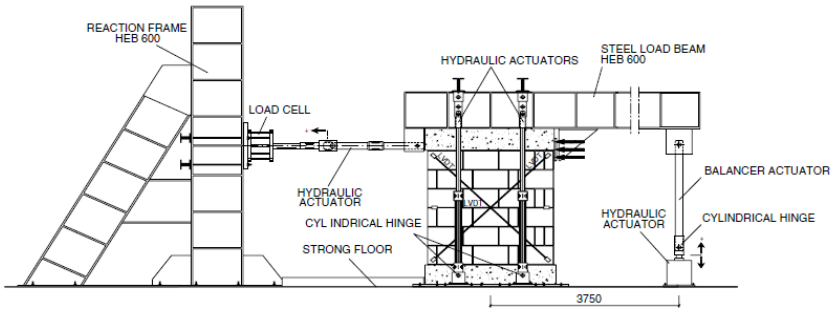

Fig. 5.18: Apparatus for testing walls; (Marcari et al., 2007).

The loads applied during the test have been modelled as a vertical distributed static load applied on the top of the concrete beam, while the horizontal action has been subdivided into two contributions: a horizontal pressure in correspondence to the steel plate and a distributed horizontal load along the top of the masonry wall, to avoid concentration of stresses and premature crises in correspondence to the corner.

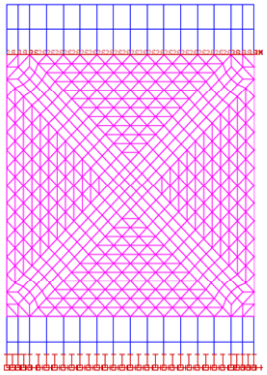

Fig. 5.19: Constraints of the developed F.E. model.

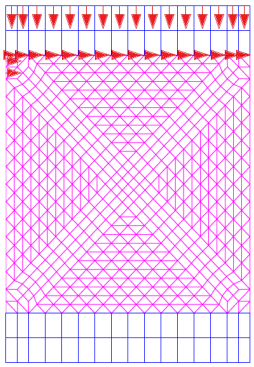

Fig. 5.20: Load conditions of the developed f.e. model.

Finally, Fig. 5.19 and Fig. 5.20 respectively show the boundary conditions in terms of constraints and load conditions of the model.

CHAPTER 6

6. Assessment of the Finite Element Model

The chapter presents the validation of the proposed numerical model in the elastic range. The implementation of plane interfaces in a two-dimensional F.E. model is firstly presented: few models with simple geometry have been developed to assess such interfaces and will be discussed in detail. The validation of the model for unreinforced masonry specimens is also presented through the comparison between the numerical model and the experimental evidence in the elastic range.

6.1 Implementation of the plane interface in a 2D model

This section proposes two numerical tests aimed at assessing the capability of the F.E. model under consideration to simulate the stress transfer process from masonry and externally glued FRP laminates.

A plane interface IS88 CQ48I is implemented with this aim in a two-dimensional structural model.

The tests consist of two simple models: in the first one masonry and FRP are not connected; in the second one the plane interface is introduced.

The wall and the FRP strengthening have been modelled in DIANA FEM code (DIANA, 2010) by means of QU8-CQ16M plane stress elements.

The geometry of the models consists of a masonry wall whose dimensions are 1 x 1 x 0.53 m^3 and an ideal Glass FRP layer covering one side of the whole masonry surface. The constraints at the bottom of the

model restraint displacements in x and y directions; the masonry wall also presents constraints on its left side which do not allow the horizontal translation. A horizontal action of 10 kN is applied to the GFRP layer on the top right point (see Fig. 6.1).

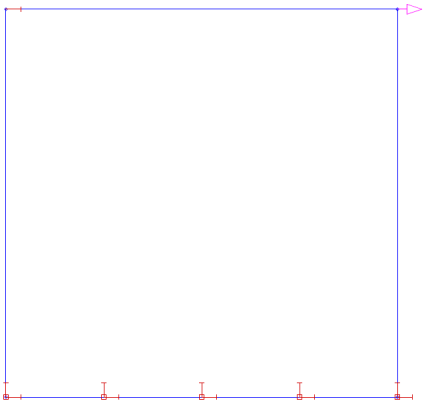

Fig. 6.1: Boundary conditions of the model.

The mesh of the model is coincident with the geometrical dimensions so that only one interface has been implemented between the two materials.

Table 6.1 reports the Poisson's ratio ν and the Young's modulus E for masonry and FRP layer; the normal k_n and tangential k_t stiffness, assigned to the interface to describe the behaviour in the elastic range, are also reported.

Table 6.1Mechanical properties of masonry, FRP and interface.

Mechanical properties	
Masonry	ν_m =0.2; E_m=1 GPa
FRP strengthening	ν_f =0.2; E_f=80 GPa
Interface	k_n=100 N/mm^3 k_t=50 N/mm^3

A linear static analysis has been performed in both cases.

Fig. 6.2 shows the deformed mesh and the maximum displacement of FRP set in the case of model without the structural interface. When the horizontal force F is applied, the FRP layer is in tension. The model without interface only presents displacements corresponding to the FRP set, where the horizontal force is applied. The nodes of masonry set do not present any displacement. The maximum values of displacements, for FRP set nodes, are reported in Table 6.2.

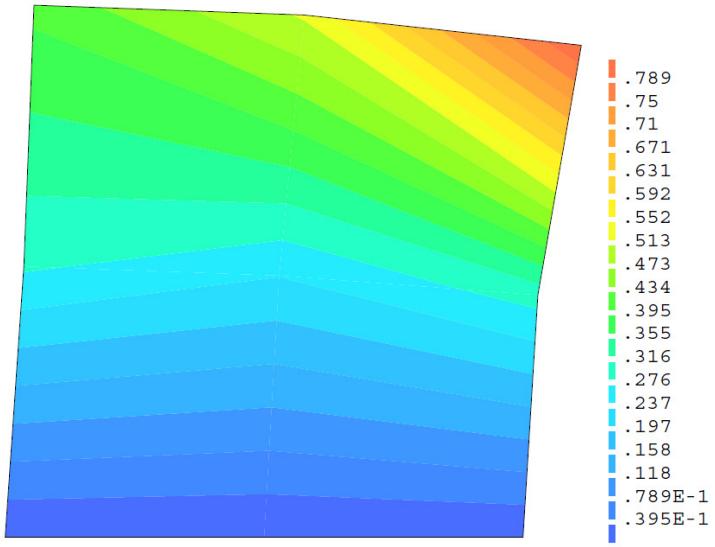

Fig. 6.2: Total displacements [mm] of the GFRP deformed mesh for the model without the structural interface.

Table 6.2: Maximum displacements of FRP and masonry for the model without the structural interface.

Test 1a	Masonry set node	$\delta_{m,max}$ [mm]	FRP set node	$\delta_{f,max}$ [mm]
Model without interface	top right	0.000	top right	0.829E+00

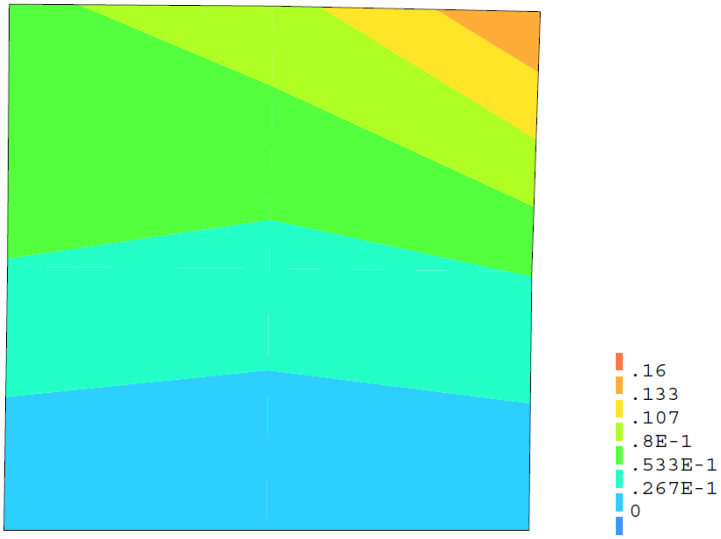

Fig. 6.3: Total displacements [mm] of the GFRP deformed mesh for the model with the structural interface.

Fig. 6.3 shows the deformed mesh and the maximum displacement of FRP set node in the case of model with the structural interface. When the horizontal force F is applied, the FRP layer is in tension and the interface transfers stresses to the masonry support. In this case the nodes of masonry set also present displacement components. The maximum values of displacements, for masonry and FRP set nodes, are reported in Table 6.3.

Table 6.3 Maximum displacements of FRP and masonry for the model with structural interface.

Test 1b	Masonry set node	$\delta_{m,max}$ [mm]	FRP set node	$\delta_{f,max}$ [mm]
Model with interface	top right	0.152E+00	top right	0.157E+00

A parametric comparison, based on the model introduced above, has been also considered for the assessment of the structural interface. Table 6.4 reports parameters object of investigation. The horizontal force F applied to the model is fixed on the value of 10 kN, while the nature of reinforcement, the type of interface and masonry constraints change. Test 1.b, regarding the model of masonry connected to the GFRP layer by means of plane structural interface, constitutes the term of comparison of the parametric investigation presented in the following.

Table 6.4: Model characteristics considered for parametric comparisons.

Test	Element type	Interf. type	Mas. Constr.	Int. Stiff. [N/mm^3]	E_m [GPa]	$\delta_{m,max}$ [mm]	E_f [GPa]	$\delta_{f,max}$ [mm]
1 a	CQ16M	-	x block	-	1	-	80 (GFRP)	0.829
1 b	CQ16M	CQ48I	x block	k_n 100 k_t 50	1	0.152	80 (GFRP)	0.157
2	CQ16M	CQ48I	x block	k_n 100 k_t 50	1	0.865E-01	**400 (CFRP)**	0.893 E-01
3	CQ16M	CQ48I	x block	**k_n 10^6** **k_t 10^6**	1	0.314E-07	80 (GFRP)	0.366 E-06
4	CQ16M	CQ48I	**free**	k_n 100 k_t 50	1	0.152	80 (GFRP)	0.157

In Test 2 the different nature of the FRP is considered: a layer of Carbon FRP is implemented by means of a different Young's modulus assigned to the plane element representing the strengthening.

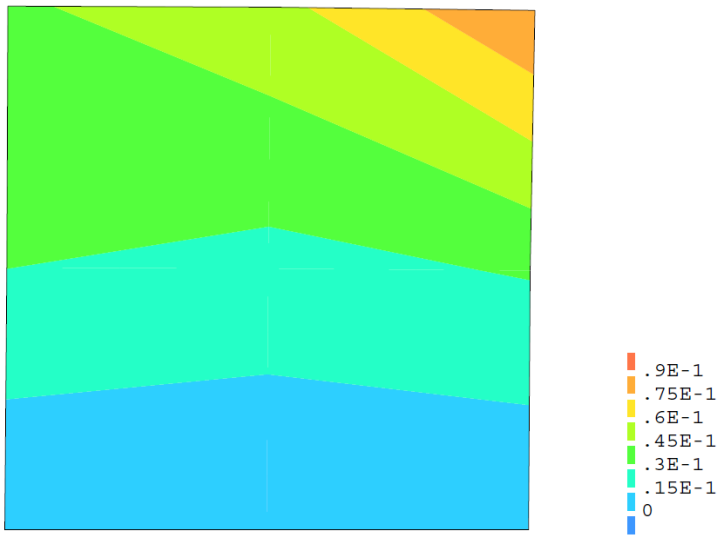

Fig. 6.4: Total displacements [mm] of the CFRP deformed mesh.

The results of the analysis in terms of displacements and deformed mesh are respectively reported in Table 6.4 and in Fig. 6.4. The CFRP layer appears stiffer then the GFRP layer; its displacement is about 43% of the GFRP displacement. Both in the case of GFRP strengthening and in the case of CFRP strengthening, the interface transfers the same amount of stresses to the masonry.

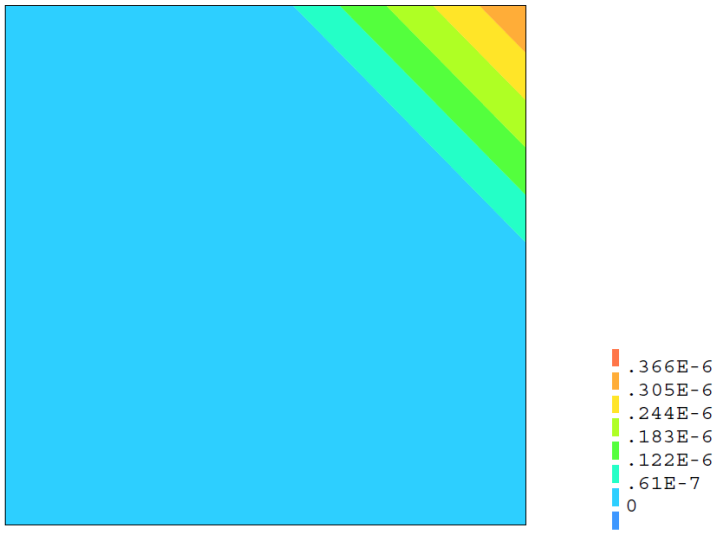

Fig. 6.5: Total displacements [mm] of the GFRP deformed mesh for the model with a rigid interface.

The case of a rigid interface characterised by high stiffness is presented in Test 3. If compared to the model with a low stiffness interface (Test 1.b), the present model reflects the expected behaviour.

The order of magnitude of FRP and masonry displacements for the present model is lower than ones of the model with a low stiffness interface as reported in Table 6.4. Fig. 6.5 shows the deformed mesh of the model.

The comparisons between two models with different constraints conditions is finally conducted. Particularly the model of Test 4 does not present constraints on the left top node of masonry blocking x direction.

If compared with the model of Test 1.b, the presence of constraints does not have any influence on the analysis results, which are the same for the two cases.

6.2 Graphical implementation of the plane interface

The graphical implementation of the interface, which takes into account the real geometrical configuration of the strengthening and can characterise a more robust finite element model, has been an important step in the development of the model.

An effective graphical procedure (DIANA, 2010) has been implemented for such purpose: it has been based on a transformation from a shell elements mesh to a plane stress elements mesh and it will be not reported in detail for sake of brevity.

To follow the initial purpose of a model with plane stress elements, which is not extremely time consuming, some comparisons between such a model, obtained by the mentioned transformation procedure, and the model with flat shell elements mesh have been performed. The geometrical and mechanical characteristics of the two considered models and the results of linear elastic analyses in terms of maximum displacements have been reported in Table 6.5.

Table 6.5: Comparisons between models with plane stress elements and flat shell elements.

Test	Element type	Int. Stiff. [N/mm^3]	$\delta_{f,max}$ [mm]	$\delta_{m,max}$ [mm]
3	CQ16M	$k_n=10^6$ $k_t=10^6$	0.314E-07	0.366E-06
3.b	CQ40F	$k_n=10^6$ $k_t=10^6$	0.314E-07	0.366E-06
4	CQ16M	$k_n=100$ $k_t=50$	0.152	0.157
4.b	CQ40F	$k_n=100$ $k_t=50$	0.152	0.157

The boundary conditions of the models (constraints and applied load) and the mechanical properties of materials are the ones reported in Table 6.4 for Test 3 and Test 4, respectively.

The models with plane stress elements mesh and flat shell elements mesh present the same results in terms of displacements and stresses; for this reason the graphical mapping of results has been omitted while the numerical results in terms of maximum displacements are reported in Table 6.5.

6.2.1 Model with one horizontal FRP strip

A Finite Element Model of the masonry wall with a horizontal GFRP strip on one side is finally considered. Two models, different in terms of mesh elements, have been considered. Fig. 6.6 shows the boundary conditions which characterise both models: the constraints at the bottom of the wall prevent the translations in the two orthogonal directions, while the top of the wall can only supports equal vertical displacements; a horizontal pressure p is applied on the left side of the wall for a length l, such as $F = p \cdot l = 10\text{kN}$. The mechanical properties of materials are reported in Table 6.6.

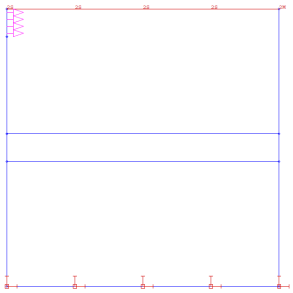

Fig. 6.6: Boundary conditions of the model with one horizontal GFRP strip.

Table 6.6: Mechanical properties of masonry, FRP strip and structural interfaces.

Mechanical properties	
Masonry	ν_m =0.2; E_m=1 GPa
FRP strengthening	ν_f =0.2; E_f=80 GPa
Interface	k_n=100 N/mm^3 k_t=50 N/mm^3

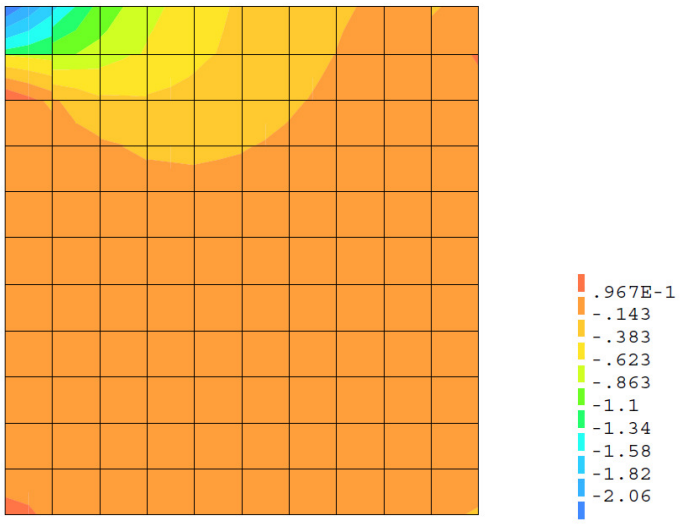

Fig. 6.7: Stress contour level [N/mm^2] on the undeformed plane stress elements mesh of the wall.

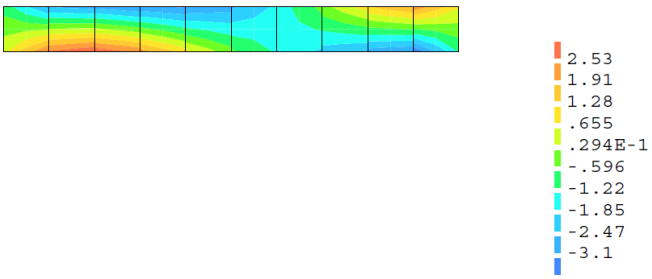

Fig. 6.8: Stress contour level [N/mm^2] on the undeformed plane stress elements mesh of GFRP strip.

Fig. 6.7 and Fig. 6.8 respectively show Cauchy stresses in horizontal direction of the wall and the GFRP strip modelled by means of a plane stress elements mesh.

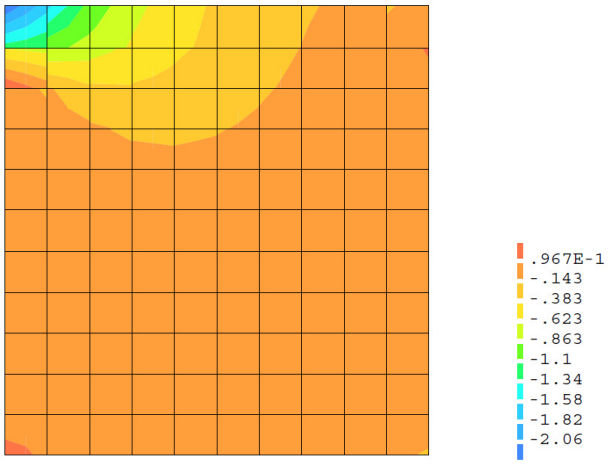

Fig. 6.9: Stress contour level [N/mm^2] on the undeformed flat shell elements mesh of the wall.

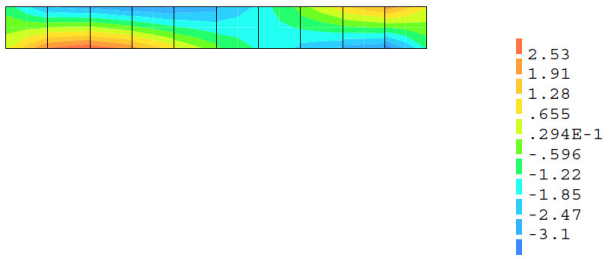

Fig. 6.10: Stress contour level [N/mm^2]on the undeformed flat shell elements mesh of GFRP strip.

Fig. 6.9 and Fig. 6.10 respectively show the Cauchy stresses in horizontal direction of the wall and the GFRP strip modelled by means of a flat shell elements mesh.
From the comparison between the model with plane stress elements mesh and the model with flat shell elements mesh no differences can be highlighted.

The examples which have been exposed above confirm the choice of developing a model with a plane stress elements mesh and open the possibility to a graphical implementation of structural interfaces. Further tests for the assessment of interfaces will be discussed in the following sections.

6.3 Model with two strips in cross configuration

The present model has been developed to verify the mesh continuity in correspondence to the FRP strips.

Fig. 6.11 shows the geometry of the model: the constraints block the displacements of the bottom in x and y directions and make the top of the wall move with the same rate of vertical displacements. Two FRP strips in cross configuration are implemented in the model; they are disconnected from the wall edges and present constraints, on one side, blocking the translations in the two orthogonal directions, while on the opposite side a tension of 100 N/mm is distributed along the width of each strip. The order of magnitude of the tension is the one of experimental pull out tests performed by Faella et al. (2012).

Structural interfaces connect the FRP strips to the wall and different interfaces are also present at the intersection of the two strips, making them independent one from each other.

A very low stiffness has been assigned to interfaces, as reported in Table 6.7: no significant stresses are expected to be transferred from each strip to the masonry wall.

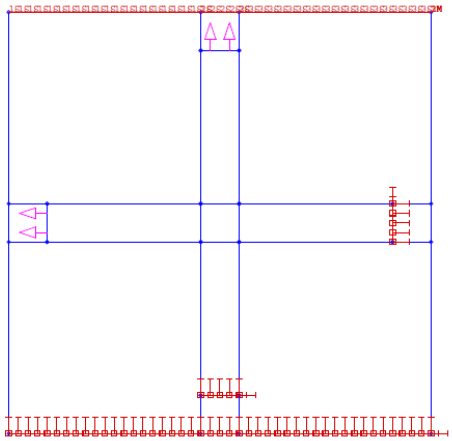

Fig. 6.11: Geometry of the model and boundary conditions.

Table 6.7: Mechanical properties of masonry, FRP strips and interfaces.

Mechanical properties	
Masonry	ν_m =0.2; E_m=1 GPa
FRP strips	ν_f =0.2; E_f=80 GPa
Interfaces	$k_n=10^{-3}$ N/mm^3 $k_t=10^{-3}$ N/mm^3

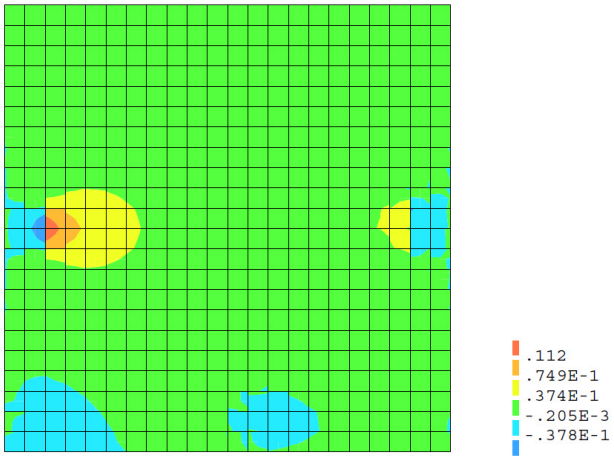

Fig. 6.12: Stress contour level [mm] on the undeformed mesh of the wall.

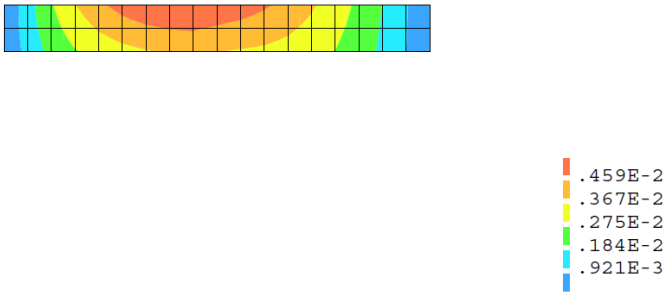

Fig. 6.13: Stress contour level [N/mm^2] on the undeformed mesh of the horizontal strip.

Fig. 6.12 and Fig. 6.13 respectively show the distribution of stresses in horizontal direction for the masonry and the horizontal FRP strip. When the tension is applied to the horizontal strip, the masonry wall does not show a significant variation in terms of stresses in correspondence to the strip, with the exception of a small concentration on the edges. Such stresses are essentially concentrated on the horizontal FRP strip, where the load is applied.

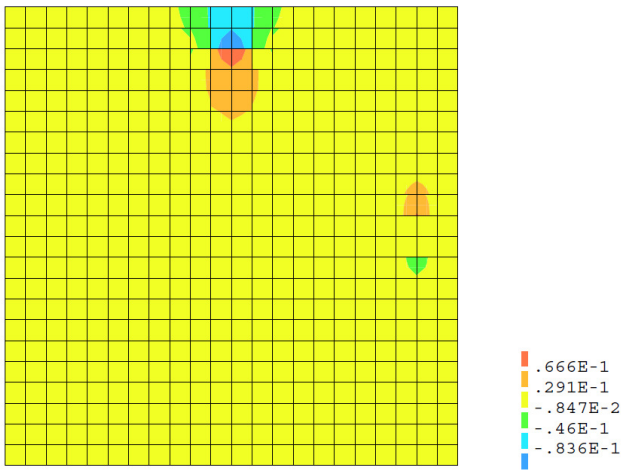

Fig. 6.14: Stress contour level [N/mm^2] on the undeformed mesh of the wall.

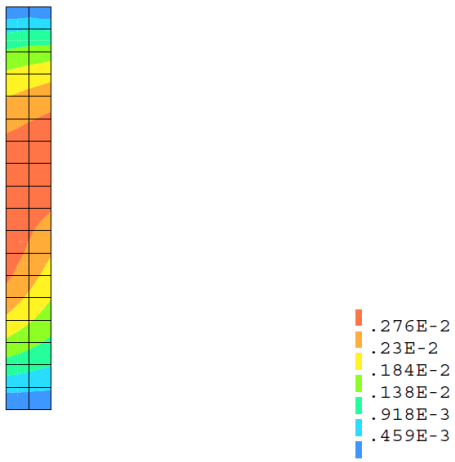

Fig. 6.15: Stress contour level [N/mm^2] on the undeformed mesh of the vertical strip.

Fig. 6.14 and Fig. 6.15 respectively show the case of tension applied along the vertical strip and distribution of stresses in y direction resulting

in the masonry wall and the FRP strip. As for the previous load case, masonry does not show a significant variation in terms of stresses.

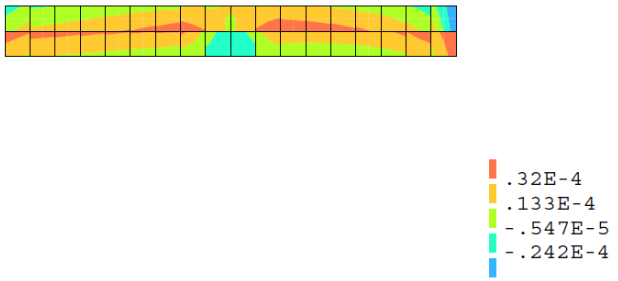

Fig. 6.16: Stress contour level [N/mm^2] on the undeformed mesh of the horizontal strip.

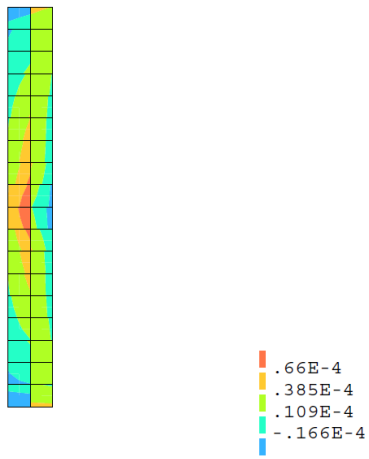

Fig. 6.17: Stress contour level [N/mm^2] on the undeformed mesh of the vertical strip.

Furthermore, Fig. 6.16 and Fig. 6.17 respectively show the distribution of stresses in horizontal direction for the vertical strip, when a tension is applied on the horizontal strip and vice versa. It can be noticed as each strip suffers a very small influence of load conditions of the opposite strip, confirming the effectiveness of low stiffness interfaces at their intersection.

6.4 Model with two overlapped strips

Various experimental campaigns testing masonry strengthened by FRP strips, generally consider specimens with both sides of the walls reinforced.

To simulate the presence of horizontal strips, one for each side of the wall, and to verify their possible independent behaviour in working conditions, the present model has been developed.

Fig. 6.18 shows the boundary conditions of the strengthened wall: the constraints of the masonry wall, are the ones considered for previous models. Both horizontal FRP strips present constraints blocking the horizontal translations on one side, while on the opposite side a tension of 100 N/mm is alternatively applied.

The two horizontal strips have been connected to the wall by means of interfaces with different stiffness: the strip which is connected by low stiffness interfaces will be indicated as LSTRIP; the other strip which is connected by high stiffness interfaces will be indicated as HSTRIP. In this way a different stress distribution is expected to be transferred to the masonry wall by each strip.

Two different load conditions have been considered for the model: in the first load condition the tension is only applied to the HSTRIP; in the second load condition the tension is only applied to the LSTRIP.

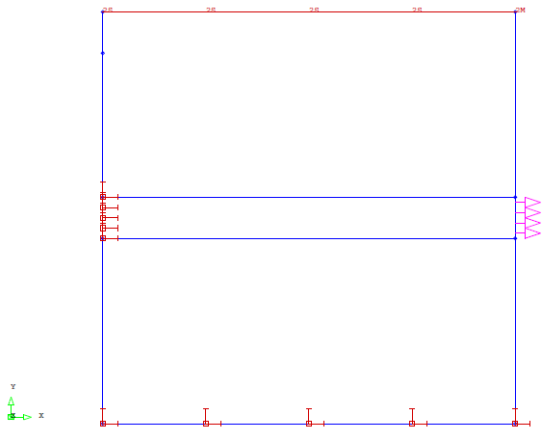

Fig. 6.18: Geometry of the model and boundary conditions.

Table 6.8: Mechanical properties of masonry, FRP strips and structural interfaces.

Mechanical properties	
Masonry	ν_m =0.2; E_m=1 GPa
FRP strengthening	ν_f =0.2; E_f=80 GPa
High stiffness interfaces	$k_n=10^2$ N/mm^3 k_t=1 N/mm^3
Low stiffness interfaces	$k_n=10^{-3}$ N/mm^3 $k_t=10^{-3}$ N/mm^3

Table 6.8 reports the mechanical properties of all materials assigned to different sets of model: masonry wall, FRP strips, high and low stiffness interfaces.

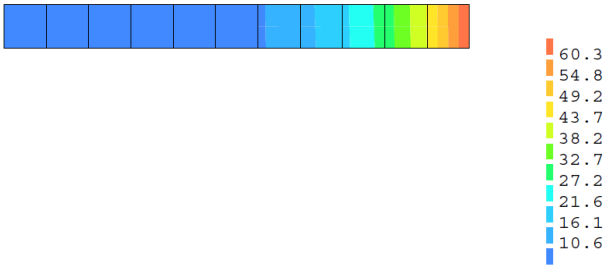

Fig. 6.19: Stress contour level [N/mm^2] on the undeformed mesh of the HSTRIP.

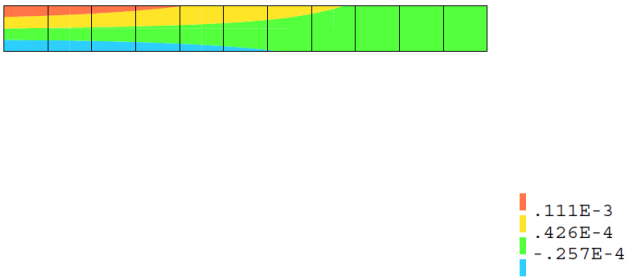

Fig. 6.20: Stress contour level [N/mm^2] on the undeformed mesh of the LSTRIP.

Fig. 6.19 shows the results in terms of horizontal stresses for the first load case: the strip, with high stiffness interfaces, subjected to tension.

When the horizontal action is applied to the HSTRIP, the stresses are not transferred to the LSTRIP on the opposite side.

Fig. 6.20 shows the distribution of horizontal stresses in the LSTRIP, which is not loaded: values of stresses are 10^5 times lower than the ones in the HSTRIP.

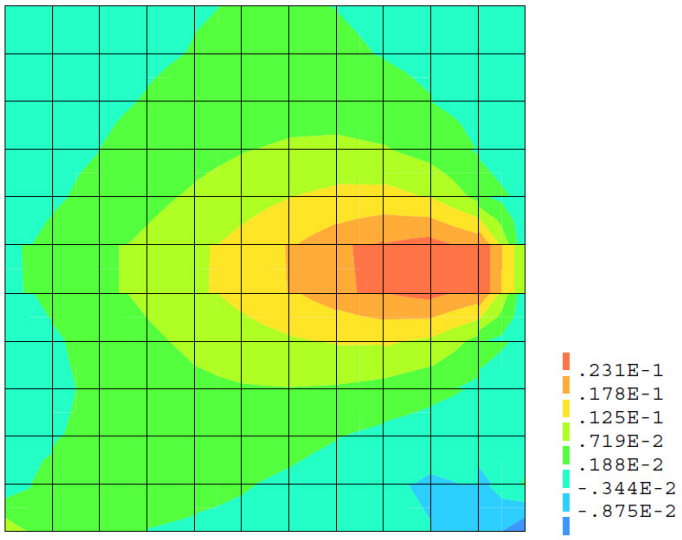

Fig. 6.21: Stress contour level [N/mm^2] on the undeformed mesh of the wall.

As expected, horizontal stresses deriving from the first load condition are only partially transferred to the wall, as shown in Fig. 6.21.

Therefore high stiffness interfaces placed between the loaded strip and the wall, only transfer a rate of stresses to the masonry while no significant stresses are transferred to the strip on the opposite side.

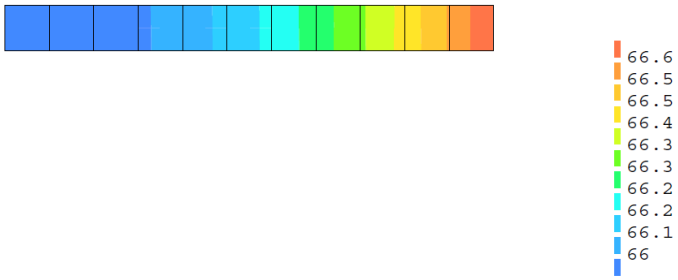

Fig. 6.22: Stress contour level [N/mm^2] on the undeformed mesh of the LSTRIP.

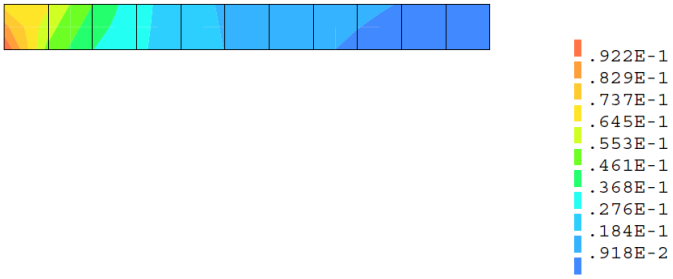

Fig. 6.23: Stress contour level [N/mm^2] on the undeformed mesh of the HSTRIP.

Fig. 6.22 shows the results of the second load case: a strip with low stiffness interfaces, LSTRIP, subjected to a tension of 100 N/mm. No significant migration of stresses to the HSTRIP on the other side of the wall can be noticed. Fig. 6.23 shows such a distribution where the values of stresses, in the not loaded HSTRIP, are 10^3 times lower than the stresses in the LSTRIP.

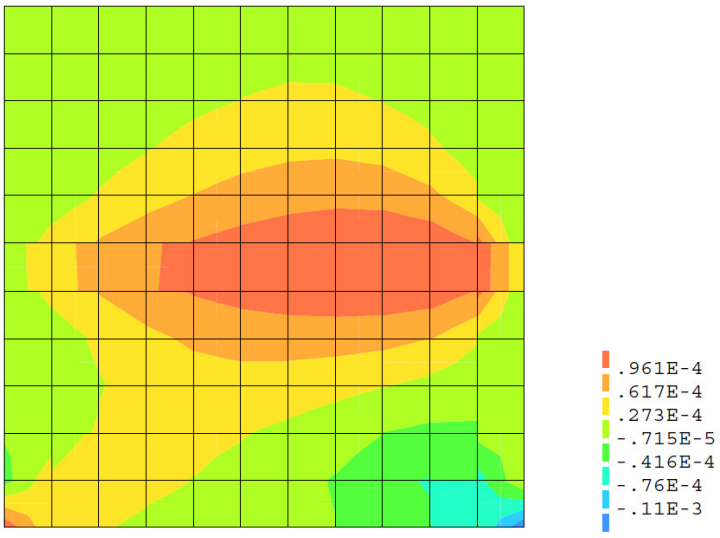

Fig. 6.24: Stress contour level [N/mm^2] on the undeformed mesh of the wall.

Furthermore, low stiffness interfaces do not transfer stresses to the masonry wall, as shown in Fig. 6.24 where the values of stresses are negligible as they are 10^{-6} times lower than ones of the loaded LSTRIP.

Also in this case low stiffness interfaces connecting the loaded strip and the wall, do not have any influence on the strip of the opposite side.

The two tests exposed above describe the independence in working conditions of two strengthening strips, one for each side of a masonry wall. The tests demonstrate how interfaces, connecting each strip to the wall, just transfer (or not) stresses to the wall depending on their stiffness. The distribution of stresses in the unloaded strip is not influenced by the working conditions of the other strip.

6.5 Final model geometry

6.5.1 Description of the model

A description of the final geometry of the model is presented. The model reproduce the geometrical dimensions characterising masonry walls of the experimental campaign object of study (Marcari, 2007).

Fig. 6.25 and Fig. 6.26 show the boundary conditions which characterise the model: the constraints at the bottom of the wall prevent the translations in the two orthogonal directions, while the top of the wall can only supports equal vertical displacements.

The loading history applied to the model consists in a distributed vertical load of 400 kN applied on the top beam. A distributed horizontal load, divided into two contributions (a horizontal pressure and a horizontal distributed load), has been applied on the left side of the wall; its order of magnitude has been set on 100 kN.

6.5.2 Model for unstrengthened masonry

The model simulates a masonry wall with FRP strengthening in cross configuration on both sides. Since it is necessary to firstly investigate the behaviour of the plain wall, some tests have been performed to verify if it was possible to consider the developed model both for the plain wall and the strengthened wall. Two possible ways of neglecting the presence of FRP strips have been investigated: the disconnection of FRP strips, considering very low stiffness interfaces, and the implementation of an ideal material, assigned to strips, which did not have a significant influence on the behaviour of the plain wall.

For the reasons exposed above, light tests described in Table 6.9 have been performed. Within the considered tests the interface shear stiffness, which plays the main role in transferring shear stresses from the masonry wall to the FRP strips, varies from low values until a value of reference for this kind of interaction (Lourenço and Rots, 1997). For each value of the considered shear stiffness, two different values of the strengthening Young's modulus have been considered: one corresponding to the Glass

FRP material and one corresponding to an ideal material characterised by a very low Young's modulus.

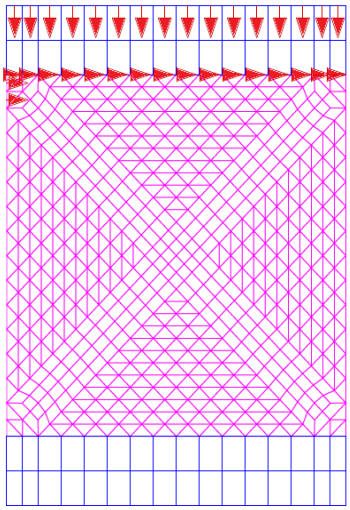

Fig. 6.25: Load conditions of the model for unstrengthened masonry walls.

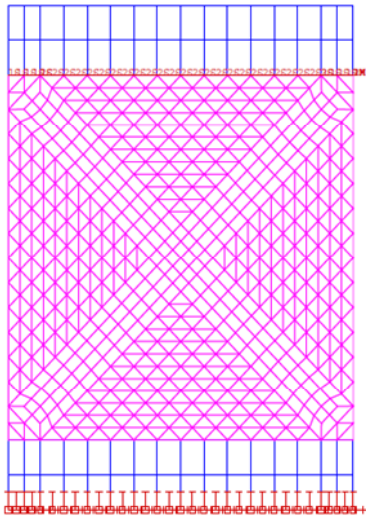

Fig. 6.26: Constraints of the model for unstrengthened masonry walls.

Table 6.9: Mechanical properties of strengthening material and interfaces.

Test	Interface shear stiffness [N/mm^3]	Strengthening Young's modulus [N/mm^2]
1.a	1E-6	80000
1.b	1E-6	1E-03
2.a	1E-03	80000
2.b	1E-03	1E-03
3.a	1	80000
3.b	1	1E-03
4.a	20	80000
4.b	20	1E-03

Among the considered tests only the Test 1.a, Test 1.b, Test 4.a and Test 4.b will be discussed, as they represent extreme cases among the ones considered. The results of the linear analyses in terms of maximum normal stresses in masonry and shear stresses in masonry and in the right strip are reported in Table 6.10.

Table 6.10: Stresses in masonry and FRP.

Test	$\sigma_{m,xx}$ [N/mm^2]	$\sigma_{m,yy}$ [N/mm^2]	$\tau_{m,xy}$ [N/mm^2]	$\tau_{f,xy}$ [N/mm^2]
1.a	max: 0.525 min: -1.49	max:0.276 min:-2.58	max: 0.334 min: -1.2	max: 0.116E-2 min: -0.116E-2
1.b	max: 0.525 min: -1.49	max:0.276 min:-2.58	max: 0.334 min: -1.2	max: 0.146E-3 min: -0. 146E-3
2.a	max: 0.526 min: -1.49	max:0.276 min:-2.58	max: 0.334 min: -1.2	max: 0.839E-1 min: -0.91E-1
2.b	max: 0.526 min: -1.49	max:0.276 min:-2.58	max: 0.334 min: -1.2	max:0.102E-5 min:-0.406E-6
3.a	max: 0.645 min: -1.27	max: 0.356 min: -2.65	max: 0.402 min: -1.2	max:3.2 min:-5.03
3.b	max: 0.525 min: -1.49	max: 0.276 min: -2.58	max: 0.334 min: -1.2	max: 0.32E-6 min: -0.642E-7
4.a	max: 0.708 min: -1.02	max: 0.523 min: -2.68	max: 0.404 min: -1.19	max: 12.3 min: -8.58
4.b	max: 0.525 min: -1.49	max: 0.276 min: -2.58	max: 0.334 min: -1.2	max: 0.32E-6 min: -0.642E-7

Test 1.b and Test 4.a represent extreme cases both in terms of shear stiffness of interfaces and in terms of Young's modulus of strengthening materials. Particularly, Test 4.a represents the case of a Glass FRP strip with a value of interface stiffness respecting the experimental evidence while Test 1.b represent the case of an ideal material with low values of stiffness and Young's modulus. Table 6.10 reports the results of linear analyses in terms of Cauchy normal stresses for the wall and Cauchy tangential stresses for the wall and FRP.

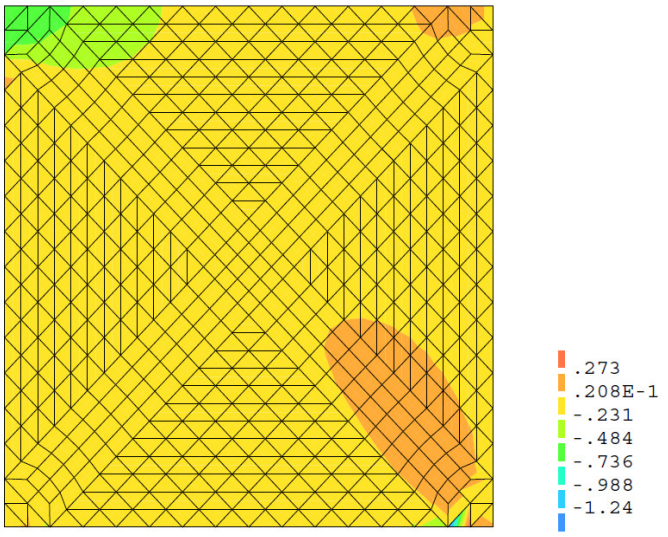

Fig. 6.27: Horizontal stress contour level [N/mm^2] on the undeformed mesh of the wall (Test 1.b).

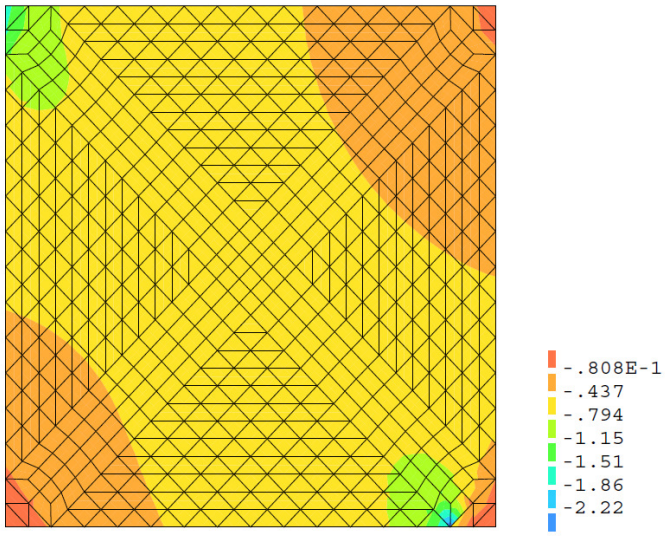

Fig. 6.28: Vertical stress contour level [N/mm^2] on the undeformed mesh of the wall (Test 1.b).

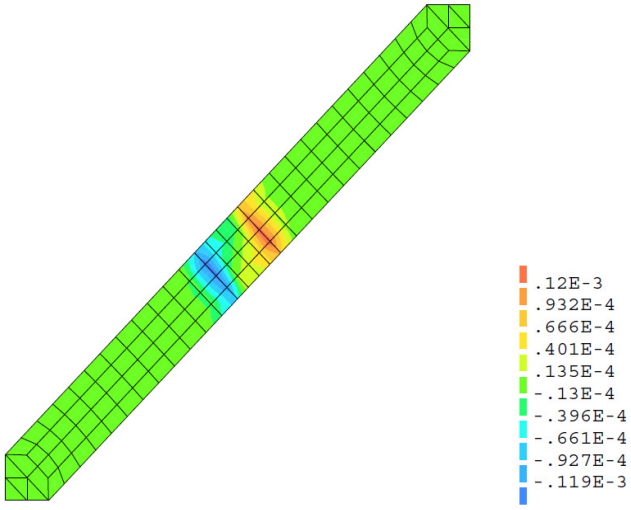

Fig. 6.29: Tangential stress contour level [N/mm^2] on the undeformed mesh of the FRP strip (Test 1.b).

It can be noticed as for the results of Test 4.a little increments in terms of maximum stresses are present in the masonry wall while a noticeable increment in terms of stresses is present in the GFRP strip. The results of analyses in terms of stress are also shown from Fig. 6.30 to Fig. 6.32. For the Test 1.b the distribution of shear stresses in the strip is quite negligible. The results of analyses in terms of stress are also shown from Fig. 6.27 to Fig. 6.29.

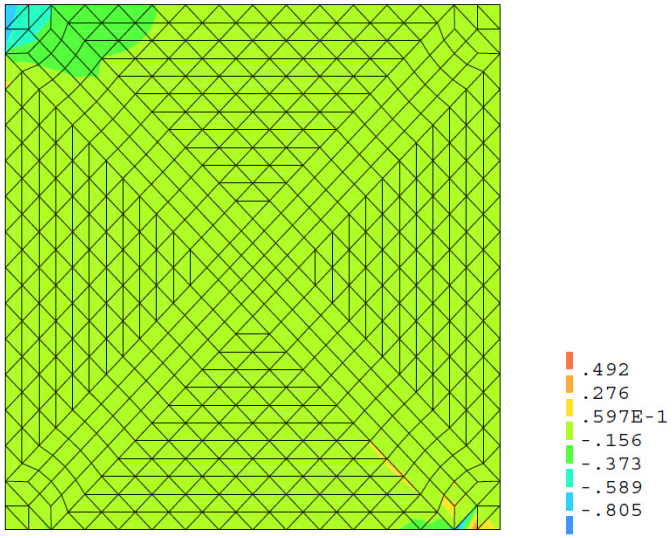

Fig. 6.30: Horizontal stress contour level [N/mm^2] on the undeformed mesh of the wall (Test 4.a).

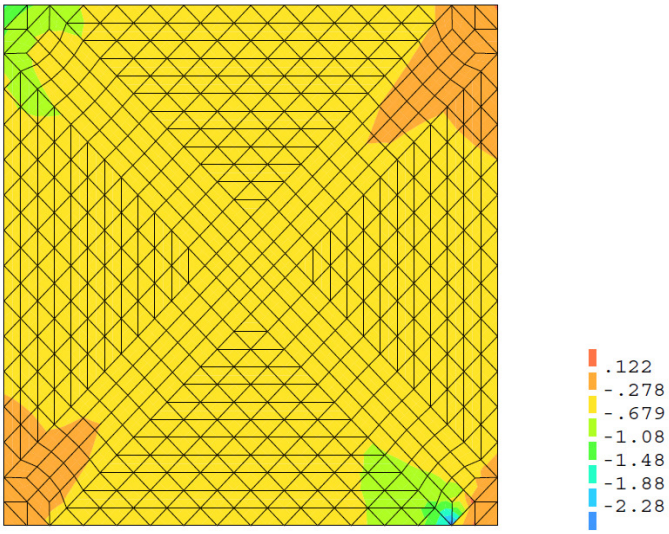

Fig. 6.31: Vertical stress contour level [N/mm^2] on the undeformed mesh of the wall (Test 4.a).

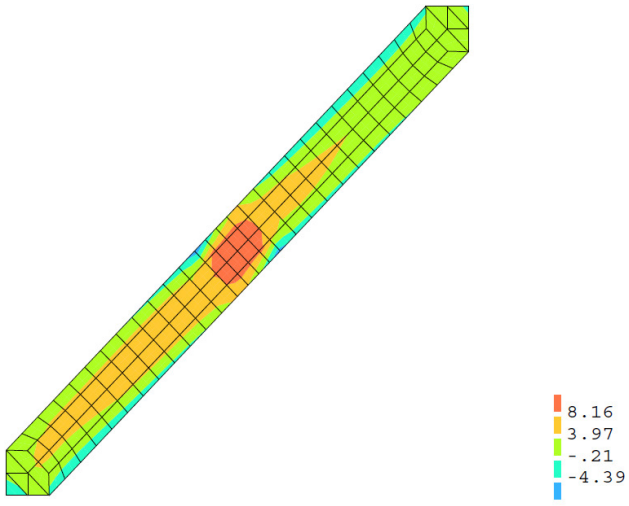

Fig. 6.32: Tangential stress contour level [N/mm^2] on the undeformed mesh of FRP strip (Test 4.a).

Test 1.a and Test 4.b can be also compared: the first represents a GFRP strengthening connected to the masonry by very low stiffness interfaces; the second represents an ideal material with a Young's modulus of 10^{-3} MPa connected to the masonry wall by interfaces with a high stiffness. The results of analyses in terms of stresses on the wall give the same results, but for Test 4.b the distribution of tangential stresses in the strip is even smaller than in case of Test 1.a, as reported in Table 6.10.

6.5.3 Vertical modulus

The present section addresses the numerical model validation related to the vertical Young's modulus of the plain masonry wall.

During the experimental campaign object of study (Marcari et al., 2007) the vertical elastic modulus has been derived from uniaxial compression tests on the plain masonry walls and calculated as a secant modulus in accordance with Eurocode 6 (1998) requirements.

To perform the numerical validation test, the plain model of Fig. 6.33 has been considered. As in the experimental tests, the geometrical and morphological characteristics of the model in vertical compression are the same of the model subjected to shear-compression tests. The load conditions, reproducing the experimental compression behaviour, consist in a vertical load of 400 kN distributed along the concrete beam placed on the top of the wall, in addition to the self weight.

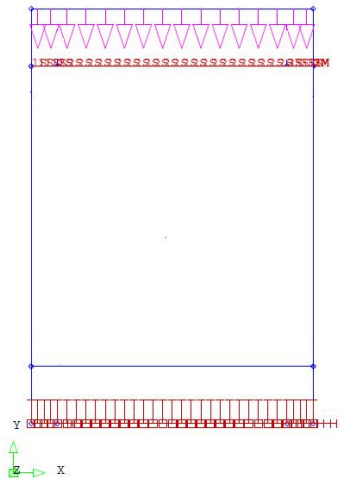

Fig. 6.33: Geometry of the model and boundary conditions.

Two main validation analyses have been performed: the first has been done in correspondence to the middle top node which represents the control node of the experimental tests.

Since the proposed analyses are aimed at validating the elastic response of the numerical model, the Young's modulus has been calculated starting from the vertical stress σ_{yy} and strain ε_{yy} by means of the following equation:

$$E_{m,num} = \frac{\sigma_{yy}}{\varepsilon_{yy}} \tag{6.1}$$

The second validation analysis has been performed by calculating first the average vertical stress σ_{yy} as:

$$\sigma_{yy} = \frac{Q}{t \cdot l} \tag{6.2}$$

where t and l are the dimension of the cross section of the wall.

Then the vertical average strain ε_{yy} as:

$$\varepsilon_{yy} = \frac{\delta_y}{h} \qquad (6.3)$$

where δ_y is the vertical displacement of the control node and h is the height of the wall; finally, the elastic modulus has been calculated by means of the equation (6.1).

Table 6.11: Young's modulus of the numerical model.

Control node	δ_y [mm]	h [mm]	ε_{yy} -	σ_{yy} [N/mm^2]	E_m [N/mm^2]
middle top node	-	-	8.07E-04	5.11E-01	633.6
middle top node	1.31	1570	8.35E-04	5.10E-01	610.7

Table 6.11 reports the values of the vertical modulus for the numerical model, calculated as exposed above; Table 6.12 reports the comparison between the experimental value and the numerical values of the Young's modulus.

Table 6.12: Comparison between the experimental value and the values of the F.E. model.

Type of value	E_m [N/mm^2]
average experimental	630.0
on point numerical	633.6
average numerical	610.7

6.5.4 Horizontal stiffness

The present section reports the calibration of the proposed model in terms of horizontal stiffness within the elastic range for the unstrengthened masonry walls subjected to shear-compression tests object of numerical investigation.

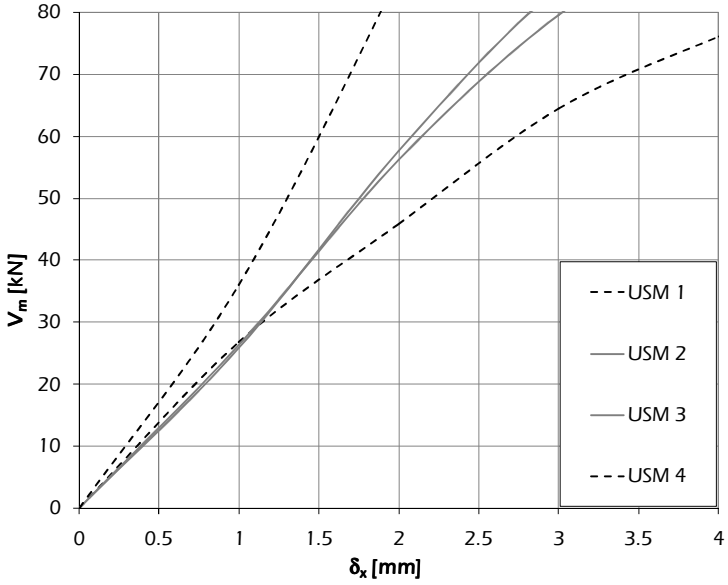

Fig. 6.34: Horizontal displacement vs. horizontal load relationships for unstrengthened masonry walls.

Fig. 6.34 shows the range of experimental values of the four shear-compression tests belonging to the experimental campaign under consideration (Marcari, 2007). The two tests having the extreme values, in terms of horizontal stiffness, have been highlighted in Fig. 6.34 by means of dashed lines and constitute the expected range for the horizontal stiffness of the developed model.

Before investigating the nonlinear behaviour of the numerical model for unstregthened walls, a first validation on its horizontal stiffness has been performed throughout the tests described in the following.

The first set of tests has been performed by considering a different distribution of the horizontal action applied during the experiments.

Since the validation analyses concern the elastic range delimited in Fig. 6.34, a total horizontal force F of 100 kN has been considered, while the vertical load has been set on the experimental value of 400 kN. The considered horizontal action has been divided into two contributions: a horizontal action distributed along the top of the wall and a horizontal pressure in correspondence to the position of the steel plate, where the experimental horizontal force F is applied.

Fig. 6.35 shows the load conditions of the model for the mentioned tests.

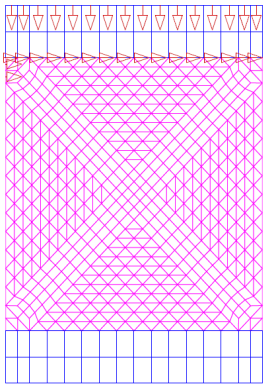

Fig. 6.35: Load conditions of the model.

Various hypotheses of percentage distribution have been considered for the horizontal load and are summarised in Table 6.13. It also reports the values of the horizontal displacement for the control node and the corresponding horizontal stiffness.

Table 6.13 Comparison between the experimental value and the values of the F.E. model.

Test	Horizontal force [kN]	p_3 %	p_4 %	Horizontal displacement [mm]	Horizontal stiffness [N/mm]
1	100	20	80	1.11	9.009E+04
2	100	50	50	1.31	7.616E+04
3	100	80	20	1.33	7.519E+04
4	100	100	-	1.36	7.353E+04

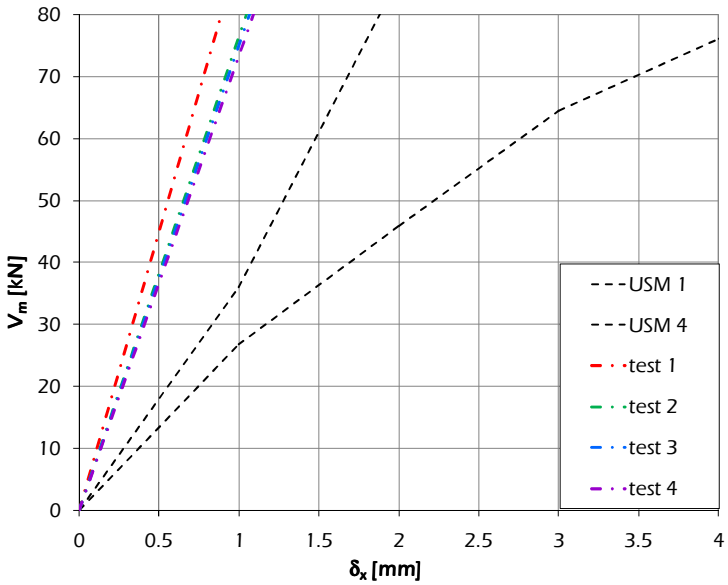

Fig. 6.36: Horizontal displacement vs. horizontal load relationships of the considered model at different load conditions with respect to unstrengthened masonry walls.

Fig. 6.36 shows how each considered test is placed within the experimental range of horizontal stiffness: the considered different distributions of the horizontal action F have a limited influence on the horizontal stiffness of the numerical model.

The division of the total horizontal load F, corresponding to Test 3, constitutes the load condition chosen for the next analyses. It consists into a distributed load along the top of the wall p_3 equal to 80% of the total horizontal action F and a pressure p_4 equal to 20% of the total action F. Such a distribution, in fact, respects the real application of the action itself and it is characterised by one of the lowest value of stiffness, but it is still far from the experimental values delimiting the range.

The masonry walls belonging to the experimental campaign under consideration are characterized by the inner filled with mortar and chips from yellow tuff blocks, to reproduce a typology of construction quite widespread in the South of Italy. The particular kind of texture may influence the horizontal behaviour of masonry in horizontal direction.

For this reason, a horizontal Young's modulus $E_{m,x}$, different from the vertical one, is expected to characterise the plain masonry walls. Since no specific information is available on such a mechanical characteristic from the experimental campaign, a further calibration has been considered for the numerical model.

Consequently the second set of tests have regarded the model characterised by orthotropic mechanical properties.

Table 6.14: Horizontal stiffness of the orthotropic model.

Test	Horizontal force [kN]	$E_{m,y}$ [MPa]	$E_{m,x}$ [MPa]	Horizontal displacement [mm]	Horizontal stiffness [N/mm]
1	100	630	630	1.31	7.669E+04
2	100	630	300	1.70	5.886E+04
3	100	630	150	2.14	4.677E+04
4	100	630	75	2.63	3.798E+04

Table 6.14 reports such mechanical characteristics for the performed tests: Test 1 corresponds to the isotropic model, while the next tests consider a value of the horizontal elastic modulus which halves; information on the displacement of the control node and the corresponding horizontal stiffness are also reported.

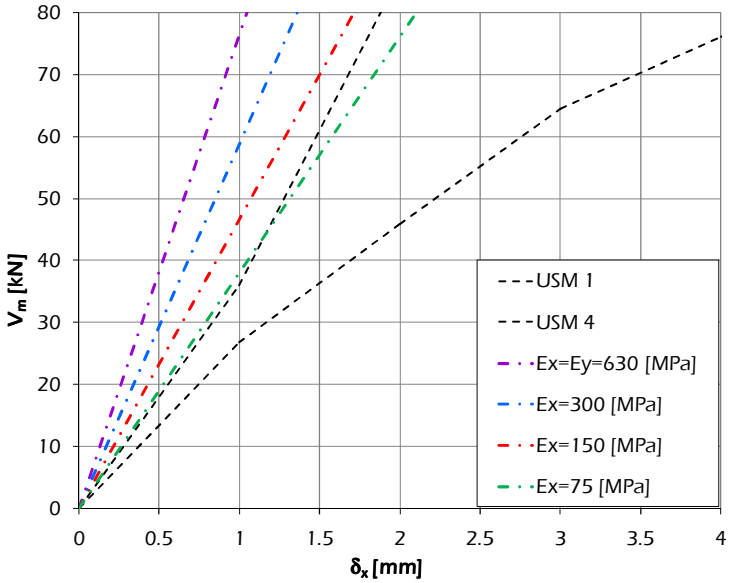

Fig. 6.37: Horizontal displacement vs. horizontal load relationships of the considered model with different values of Young's modulus with respect to unstrengthened masonry walls.

Fig. 6.37 shows the influence of the horizontal Young's modulus $E_{m,x}$ on the horizontal stiffness of the numerical model: the value of $E_{m,x,}$ which gives a stiffness kept down within the range delimited by the experimental tests, is rather low and it is not acceptable, also considering the particular nature of the inner.

The results of the previous set of tests led to the study of the shear behaviour of the model. It was not possible to have information on the shear modulus $G_{m,xy}$ from the experimental tests, so the third set of analyses regarded the investigation of such a mechanical parameter. The value of $E_{m,x}$ derived from the previous calibration was not acceptable, for this reason the model has again been considered isotropic for the present set of analyses.

Table 6.15: Tests on shear modulus of the F.E. model.

Test	Horizontal force [kN]	$E_{m,y}=E_{m,x}$ [MPa]	$G_{m,xy}$ [MPa]	Horizontal displacement [mm]	Horizontal stiffness [N/mm]
1	130	630	262.5	1.362	9.545E+04
2	130	630	150	1.368	9.503E+04
3	130	630	96	2.975	4.369E+04
4	130	630	63	4.266	3.047E+04

Table 6.15 reports the values of the shear modulus $G_{m,xy}$ considered for the calibration: Test 1 regards the value of $G_{m,xy}$ deriving from the theory of elasticity. Test 4 considers a value of the shear modulus of 10% of the Young's modulus and corresponds to a numerical behaviour which fits the experimental behaviour.

The value of the shear modulus $G_{m,xy}$ obtained in the calibration is rather low; however some proposals are present in the scientific literature and in the reference codes about possible reduction factors to apply to $G_{m,xy}$.

The Eurocode 6 suggests the calculation of the shear elastic modulus $G_{m,xy}$ as a percentage of 40% of $E_{m,y}$; considering the experimental value of E_y for the application of this recommendation, a value of $G_{m,xy}$ not far from the ones considered in Test 1, is obtained.

In the section regarding the existing masonry structures, the Italian Code (NTC, 2008) provides a value of $G_{m,xy}$ 230 N/mm^2 which corresponds to a masonry Young's modulus E_m of 690 N/mm^2; furthermore in case of masonry with wide inner core it suggests a reduction factor which homogenises the mechanical characteristics of the masonry through its thickness: such a reduction factor can be assumed as 0.7 for the modelled masonry walls. By applying these recommendations the shear modulus assumes a value near to the one considered in Test 2.

Within the scientific literature some authors (Augenti and Parisi, 2009) assume a modification factor of shear modulus for tuff masonry with poor and/or wide inner core equal to 0.85 of the mean properties estimated by code provisions. Such a reduction factor has been

calibrated on a wide experimental database. If applied to the present case it leads a shear modulus $G_{m,xy}$ in the range of Test1 and Test2.

Even though the shear modulus $G_{m,xy}$ obtained from the calibration of the numerical model is quite far from the values obtained by applying the reduction factors described above, numerical evaluations on the same walls (Marcari, 2010) have led to the same order of magnitude for the shear modulus $G_{m,xy}$, which has already been used in Marcari (2010) and thus assumed in the further analyses.

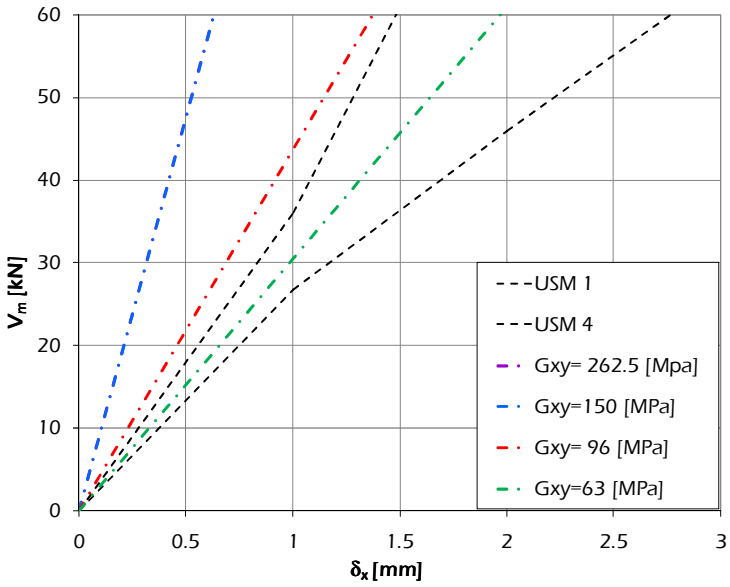

Fig. 6.38: Horizontal displacement vs. horizontal load relationships of the considered model with different values of shear modulus with respect to unstrengthened masonry walls.

Fig. 6.38 shows how the calibration of the shear modulus G_{xy} places the tests respect to the experimental range.

The last validation test of the numerical model regarded the possible influence of the steel beam on the top of the wall; the steel beam is part of the testing machine. It has been modelled considering the presence of constraints necessary to simulate the effect of the balancer actuator (Fig. 6.39), as shown in Fig. 6.40.

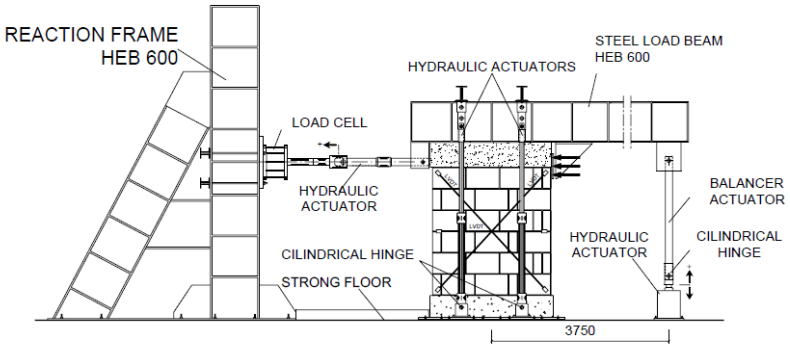

Fig. 6.39: Experimental set-up (Marcari, 2007).

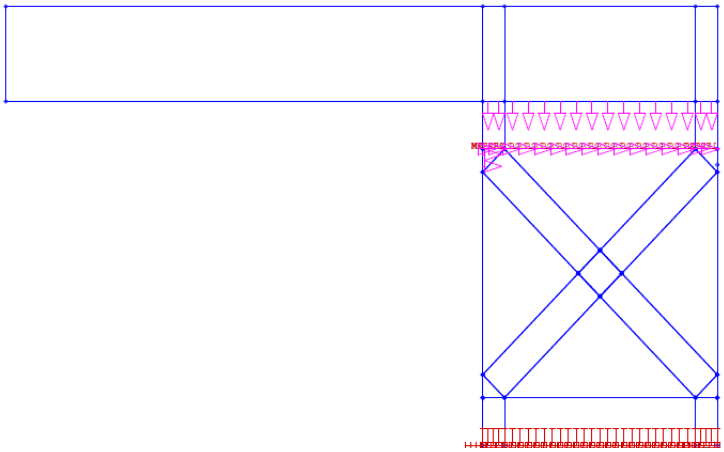

Fig. 6.40: Geometry of the model and boundary conditions.

Table 6.16 Horizontal stiffness of the model with and without the steel beam.

Test	Horizontal force [kN]	$E_{m,y}=E_{m,x}$ [MPa]	$G_{m,xy}$ [MPa]	Horizontal displacement [mm]	Horizontal stiffness [N/mm]
without steel beam	130	630.0	63.0	4.266	3.047E+04
with steel beam	130	630.0	63.0	4.266	3.047E+04

The results of the analysis in terms of horizontal displacement of the experimental control node and the comparison between the model without the steel beam and with the steel beam are reported in Table 6.16. As expected the presence of the steel beam does not influence the horizontal behaviour of the model.

CHAPTER 7

7. Parametric Assessment

7.1 Nonlinear analysis

The present chapter describes a parametric study performed through nonlinear analyses on both unstrengthened model and model strengthened with different types and amounts of FRP composites.

For the model reproducing unstrengthened masonry walls, the numerical investigation is aimed to better understand the influence of parameters which are generally difficult to determinate through experimental tests.

The study on the strengthened model is oriented to determinate the influence of geometrical and mechanical parameters of the strengthening in support of retrofitting design formulae, presented in chapter 2, and is open to a future study involving most various strengthening configurations, present in the collected database of chapter 3.

7.1.1 Loading history

The loading history applied to the model reproduces the set of the experimental tests under consideration. A distributed vertical load of 400 kN is applied on the top beam and kept constant while performing nonlinear analyses. A distributed horizontal load, divided into two contributions (a horizontal pressure and a horizontal distributed load), has been applied to the top corner of the wall. Its order of magnitude

has been set on the mean experimental value of each type of wall specimens reproduced.

7.1.2 Numerical algorithm for nonlinear analysis

The iteration method applied while performing the nonlinear analyses is the regular Newton-Raphson method, whose advantage is to reach convergence with lesser iterations, but each iteration is relatively time consuming (DIANA, 2010).

This iterative method consists in adapting the total displacement increment according to the following equation, until the equilibrium is reached with a prescribed tolerance:

$$\Delta u_{i+1} = \Delta u_i + \delta u_{i+1} \tag{7.1}$$

where:

Δu_i is the i-th displacement increment;

Δu_{i+1} is the incremental displacement at iteration i+1.

Each iterative increment is calculated by means of the following equation:

$$\delta u_i = K_i^{-1} g_i \tag{7.2}$$

where:

K_i^{-1} represents the inverse of the stiffness matrix at the considered i-th iteration;

g_i is the out of balance force vector at the start of iteration i.

The difference between several procedures is the way in which δu is determined.

In the regular Newton-Raphson method the stiffness matrix represents the tangential stiffness of the structure:

$$K_i = \frac{\partial g}{\partial \Delta u} \tag{7.3}$$

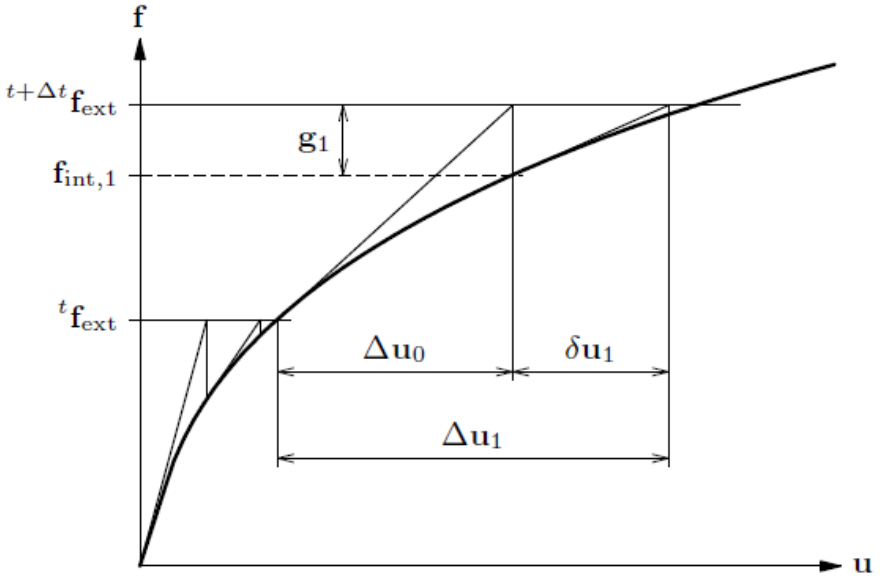

Fig. 7.1: Regular Newton-Raphson iteration (DIANA, 2010).

Fig. 7.1 represents the scheme of the regular Newton-Raphson method.

The Arc-length method has been used to determine the possible snap-through behaviour of the load-displacement relation in the structure. This method overcomes the problem of predicting a large displacement for a given force increment.

7.2 Unstrengthened masonry model calibration

7.2.1 Mechanical properties of masonry

Experimental data available from laboratory tests are essential to simulate the behaviour of the masonry both in the elastic range and in the nonlinear range.

The mechanical parameters characterizing the behaviour within the elastic range derive both from experimental data and the numerical calibrations described in Chapter 6. Particularly the Young's vertical modulus E_{my} of masonry walls has been set on the experimental value of

630 MPa. The horizontal modulus $E_{m,x}$ has been assumed equal to the vertical one and a value of the shear modulus $G_{m,xy}$ of 63 MPa, derived from the considerations previously exposed, has been assumed. The Poisson's coefficient ν_{xy} has been set on the value of 0.2.

The compressive strengths and the tensile strengths of the masonry are the ones presented in Marcari (2010), for the experimental campaign, and are reported in Table 7.1.

Table 7.1: Compressive and tensile strengths of the plain masonry in x and y directions.

$f_{m,y}$ [N/mm^2]	$f_{m,x}$ [N/mm^2]	$f_{mt,y}$ [N/mm^2]	$f_{mt,x}$ [N/mm^2]
1.1	0.5	0.06	0.17

Mechanical properties describing the performance of masonry in the inelastic range have been derived from sensitivity analyses, when experimental data from laboratory tests were not available and will be presented in the following.

Particular attention has been paid to the fracture energy characterizing the behaviour in compression and in tension, whose discussion is presented in the following sub-section.

7.2.1.1 Fracture energies in compression and in tensile regime

For the developed macro-modelling of masonry walls under shear-compression tests, few data regarding the compressive fracture energy and the fracture energy in tensile regime have been collected and organized in a database and will be described in the following.

Regarding the compressive fracture energy of masonry, it was not possible to collect enough data. On the contrary, major number of data have been collected from experimental tests determining the fracture energy of mode I in tensile regime.

In the scientific literature the values of 5 Nmm/mm^2 and 10 Nmm/mm^2 for the compressive fracture energies Γ_{cx} and Γ_{cy} have been respectively obtained from biaxial tests on masonry by Ganz and Thürlimann (1982). Such values have been also implemented by

Lourenço (1996) for numerical simulations of block masonry shear walls and concrete block masonry shear walls to validate the Rankine-Hill type model.

Values of 15 Nmm/mm^2 for Γ_{cx} and of 10 Nmm/mm^2 for Γ_{cy} have been obtained from numerical studies on plain tuff masonry walls under shear compression tests by Marcari (2010).

Extensive experimental campaigns determining the mode I fracture energy Γ_f^I have been conducted by Van der Pluijm (1997) which investigated the behaviour prior and beyond the maximum load of deformation controlled tensile and flexural tests; those tests have been performed on clay and calcium silicate bricks in a combination of different types of cement based mortars and will be briefly reported below.

For tensile tests on masonry prisms made out of clay bricks and mortar with a compositions of 1:2:9 (cement:lime:sand ratio by volume), a fracture tensile energy Γ_f^I varying between 0.0034 Nmm/mm^2 and 0.0135 Nmm/mm^2 associated to a tensile strength $f_{mt,y}$ whose values are included in a range of 0.04 and 0.37 N/mm^2 have been obtained.

Tensile tests on masonry prisms made out of clay bricks and mortar with compositions of 1:1:6 (cement:lime:sand ratio by volume) gave values of fracture tensile energy Γ_f^I between 0.0017 Nmm/mm^2 and 0.0148 Nmm/mm^2 associated to a tensile strength $f_{mt,y}$ ranging between 0.14 and 0.69 N/mm^2.

Calcium silicate masonry prisms with a thin layer of mortar subjected to tensile tests, were characterized by values of fracture tensile energy Γ_f^I between 0.0016 Nmm/mm^2 and 0.0056 Nmm/mm^2 associated to a tensile strength $f_{mt,y}$ whose range of values is between 0.18 and 0.51 N/mm^2.

Finally, tensile tests on high strength clay bricks with a thin layer of mortar have produced values of fracture tensile energy Γ_f^I between 0.0113 Nmm/mm^2 and 0.026 Nmm/mm^2 associated to a tensile strength $f_{mt,y}$ ranging between 0.5 and 3.06 N/mm^2.

A first set of flexural tests on masonry prisms made out of clay bricks and mortar whose compositions is of 1:1:6 (cement:lime:sand ratio by

volume) gave values of fracture tensile energy G_f^I between 0.0032 Nmm/mm^2 and 0.0289 Nmm/mm^2 associated to a flexural strength f_{mf} between 0.19 and 1 N/mm^2.

A second set of flexural tests on similarly assembled masonry prisms provided values of fracture tensile energy Γ_f^I between 0.0028 Nmm/mm^2 and 0.0118 Nmm/mm^2 associated to a flexural strength f_{mf} between 0.16 and 0.54 N/mm^2.

Further flexural tests on clay bricks masonry prisms with mortar compositions of 1:1:6 (cement:lime:sand ratio by volume) provided fracture tensile energy Γ_f^I between 0.0067 Nmm/mm^2 and 0.0477 Nmm/mm^2 associated to a flexural strength f_{mf} between 0.35 and 1.5 N/mm^2.

Finally, results from flexural tensile tests on brick masonry specimens of 500x150x100 mm^3 conducted by Carpinteri et al. (1998) provided fracture energy Γ_f^I values between 0.1207 Nmm/mm^2 and 0.4341 Nmm/mm^2.

7.2.2 Description of the sensitivity analyses

In order to evaluate the importance of the mechanical parameters which define the Rankine-Hill model and characterize the nonlinear behaviour of masonry, some sensitivity analyses have been carried out on the Finite Element Model intended at simulating unstrengthened masonry walls.

First of all, parameters which define the Rankine-Hill type criterion have been investigated and are listed below:

- the α parameter;
- the β parameter;
- the γ parameter.

Additionally to parameters described above, some inelastic mechanical properties have been also investigated and are listed below:

- fracture energy in compression in y direction: $\Gamma_{c,y;}$
- fracture energy in compression in x direction: $\Gamma_{c,x.}$

7.2.2.1 Rankine–type criterion α parameter

The present section regards a set of sensitivity analyses investigating within the variation of the parameter α, defined as the *parameter which weights the shear stress contribution to tensile failure* (Lourenço, 1996; §5.1.3)

In the scientific literature some values of reference for the parameter α derive from comparisons between the material model and experimental data (Lourenço, 1996) and provide the following values:

- α=1 for hollow concrete block masonry (Lurati et al., 1990);
- α=1.26 for solid clay brick masonry biaxially loaded (Page, 1981, 1983);
- α=1.73 for hollow clay units masonry biaxially loaded (Ganz and Thürliman,1982).

Table 7.2 reports the inelastic parameters considered while performing the nonlinear analyses of the unstrengthened model and the values attributed to the parameter α.

For the compressive fracture energies $\Gamma_{fc,x}$ and $\Gamma_{fc,y}$ the values of 1 Nmm/mm^2 and 2 Nmm/mm^2 respectively have been considered. The fracture energies for the tension regime $\Gamma_{ft,x}$ and $\Gamma_{ft,y}$ have been set to 0.01 Nmm/mm^2.

Table 7.2: Mechanical parameters considered for the sensitivity analysis on α.

Parameters	Test 1	Test 2
α	1	1.6
β	-1.5	-1.5
γ	3	3
$\Gamma_{c,x}$ [Nmm/mm^2]	1	1
$\Gamma_{c,y}$ [Nmm/mm^2]	2	2
$\Gamma_{t,x} = \Gamma_{t,y}$ [Nmm/mm^2]	0.01	0.01

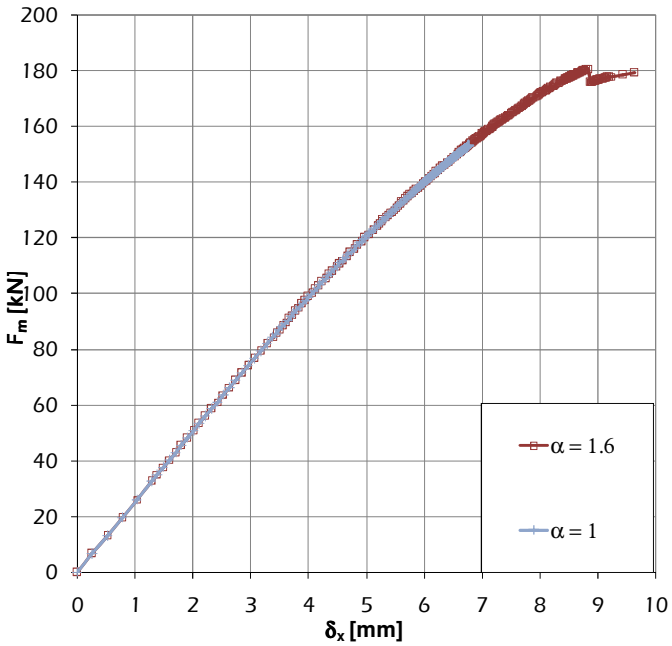

Fig. 7.2: Load-displacement curves for different values of α.

Fig. 7.2 shows the results in terms of horizontal force-displacement diagram: the nonlinear behaviour is mostly influenced by high values of the parameter α.

To better understand the influence of α on the nonlinear simulations, the Rankine-Hill yield surface has been transformed to a proper dimensionless expression dividing Eqn. (5.11) and (5.26) by the uniaxial compressive strength in x direction f_{cx} and in y direction f_{cy}.

The Rankine-type criterion, formulated in dimensionless form with respect to the uniaxial compressive strength f_{cx} in x direction and f_{cy} in y direction is reported:

$$f_l = \frac{1}{2}\left(x - \frac{f_{tx}}{f_{cx}}\right) + \frac{1}{2}\left(y - \left(\frac{f_{ty}}{f_{cy}}\right)\right)\cdot\frac{f_{cy}}{f_{cx}} + \sqrt{\frac{1}{4}\left(x - \frac{f_{tx}}{f_{cx}} - \left(y - \frac{f_{ty}}{f_{cy}}\right)\frac{f_{cy}}{f_{cx}}\right)^2 + \alpha\left(\frac{\tau_{xy}}{f_{cx}}\right)^2} \qquad (7.4)$$

The Hill-type criterion can also be written in a similar dimensionless form as follows:

$$f_2 = x^2 + \beta xy + y^2 + \gamma\left(\frac{\tau_{xy}}{f_{cx}}\right)^2 \cdot \frac{f_{mx}}{f_{my}} - 1 = 0 \tag{7.5}$$

where:

$$x = \frac{\sigma_x}{f_{cx}} \tag{7.6}$$

and

$$y = \frac{\sigma_y}{f_{cy}} \tag{7.7}$$

Starting from the non dimensional yield surfaces of Eqn. (7.4) and Eqn. (7.6), different values have been assigned to parameter α, while the remaining inelastic parameters have been fixed.

The values assigned to the compressive and the tensile strengths in x and y directions are the ones reported in Table 7.1.

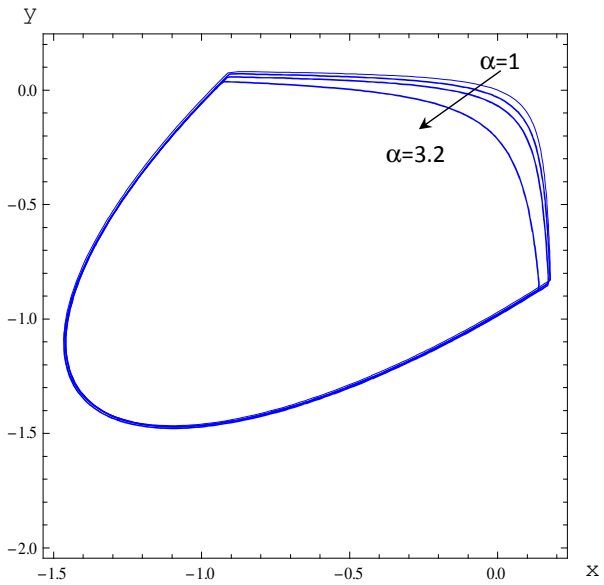

Fig. 7.3: Dimensionless yield surfaces for different values of α.

Fig. 7.3 shows the variation of the dimensionless surfaces with the parameter α, whose range of variation is between 1 and 3.2. The values of β and γ are the ones considered for sensitivity analyses and are reported in Table 7.2. A reference value of $\tau_{xy} = 0.1\,\text{MPa}$ has been considered.

From the analyses of Fig. 7.3, it can be noticed as higher values of α cause a reduction of the yield surface in tension.

The value of α=1 has been chosen for the following sensitivity analyses.

7.2.2.2 Hill-type criterion β parameter

The parameter β, defined as the *parameter which controls the coupling between normal stress value in the case of compressive failure* (Lourenço, 1996; §5.1.3), has been investigated by means of a sensitivity analyses whose results will be discussed in the present section.

In the scientific literature some comparisons between the material model and experimental data (Lourenço, 1996) have been performed providing the following reference values for the parameter β:

- β= -0.97 for hollow concrete block masonry (Lurati et al., 1990);
- β= -1.05 for hollow clay units masonry biaxially loaded (Ganz and Thürliman;1982);
- β= -1.17 for solid clay brick masonry biaxially loaded (Page, 1981, 1983).

Table 7.3 reports the inelastic parameters considered during the nonlinear analyses of the unstrengthened model and the values attributed to the parameter β.

For the compressive fracture energies $\Gamma_{c,x}$ and $\Gamma_{c,y}$ and the fracture energies in tension regime $\Gamma_{t,x}$ and $\Gamma_{t,y}$, the values of the previous analyses have been considered.

Table 7.3: Mechanical parameters considered for the sensitivity analysis on β.

Parameters	Test 1	Test 2	Test 3	Test 4
α	1	1	1	1
β	-0.97	-1	-1.2	-1.5
γ	6	6	6	6
$\Gamma_{c,x}$ [Nmm/mm^2]	2	2	2	2
$\Gamma_{c,y}$ [Nmm/mm^2]	4	4	4	4
$\Gamma_{t,x} = \Gamma_{t,y}$ [Nmm/mm^2]	0.01	0.01	0.01	0.01

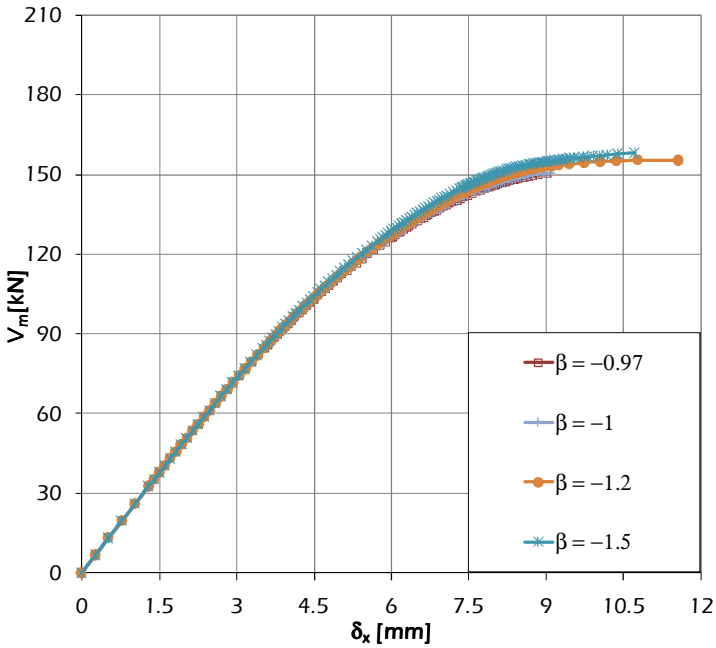

Fig. 7.4: Load-displacement curves for different values of β.

Fig. 7.4 shows the results in terms of horizontal force-displacement diagram: the nonlinear behaviour appears mostly influenced by higher values of the parameter β. Particularly the value of $\beta = -1.2$ is the one which gives the most marked nonlinear behaviour for the developed model.

The influence of parameter β on the nonlinear behaviour of the model, has been also investigated by means of the composite plasticity yield surfaces, in the same dimensionless form presented in the previous section.

The values assigned to the compressive and the tensile strengths in x and y directions are reported in Table 7.1.

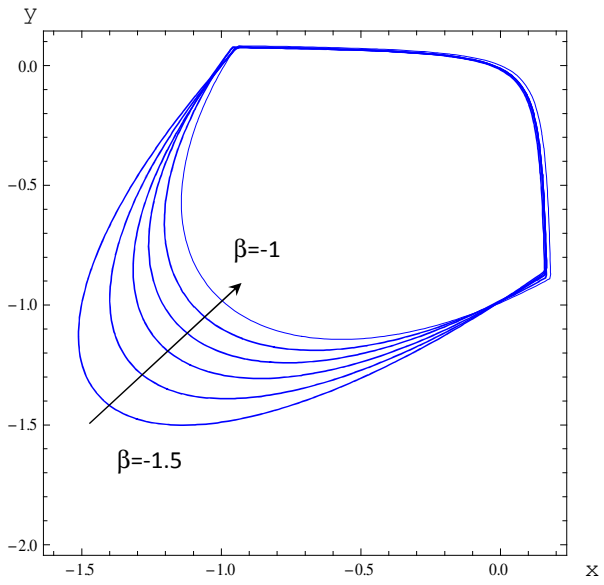

Fig. 7.5: Dimensionless yield surfaces for different values of β.

Fig. 7.5 shows the variation of the dimensionless surfaces with the parameter β, whose range of variation is between -1.5 and -1. The values of α and γ are reported in Table 7.3 while a reference value of $\tau_{xy} = 0.1\,\text{MPa}$ has been considered.

From the analysis of Fig. 7.5 it can be noticed as the yield surface in compression reduces significantly when values of β vary between -1.5 and -1.

The value of $\beta = -1.5$ has been chosen for the following sensitivity analyses.

7.2.2.3 Hill-type γ parameter

The present section describes the variation of the parameter γ, defined as the *parameter which weights the shear stress contribution to compressive failure* (Lourenço, 1996; §5.1.3), by means of sensitivity analyses.

Values of reference for the parameter γ derive from comparisons between the material model and experimental data (Lourenço, 1996) and are listed below:

- γ=1.20 for hollow clay units masonry biaxially loaded (Ganz and Thürliman;1982);
- γ= 3.36 for hollow concrete block masonry (Lurati et al., 1990);
- γ=9.59 in case of solid clay brick masonry biaxially loaded (Page, 1981, 1983).

Table 7.4 reports the inelastic parameters considered during the nonlinear analyses of the unstrengthened model and the values attributed to the parameter γ.

For the compressive fracture energies $\Gamma_{c,x}$ and $\Gamma_{c,y}$ and the fracture energies in tension regime $\Gamma_{t,x}$ and $\Gamma_{t,y}$, the same values of the previous analyses have been considered.

Table 7.4: Mechanical parameters considered for the sensitivity analysis on β.

Parameters	Test 1	Test 2	Test 3	Test 4
α	1	1	1	1
β	-1.5	-1.5	-1.5	-1.5
γ	3	6	7.5	9
$\Gamma_{c,x}$ [Nmm/mm^2]	2	2	2	2
$\Gamma_{c,y}$ [Nmm/mm^2]	4	4	4	4
$\Gamma_{t,x} = \Gamma_{t,y}$ [Nmm/mm^2]	0.01	0.01	0.01	0.01

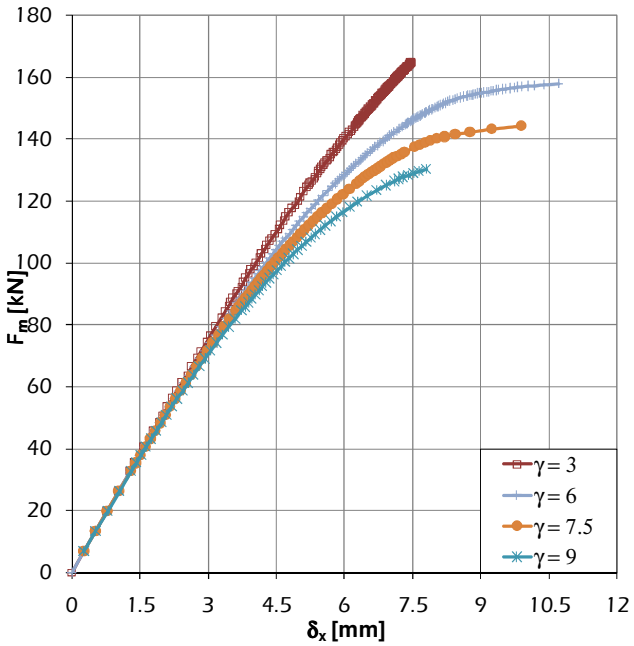

Fig. 7.6: Load-displacement curves for different values of γ.

Fig. 7.6 shows the results in terms of horizontal force-displacement diagram: for the developed model the nonlinear behaviour is mostly influenced by intermediate values of the parameter γ. Particularly the value of γ=6 is the one which gives a marked nonlinear behaviour.

To better understand the influence of such a parameter γ on the nonlinear behaviour of the numerical model, the previous composite plasticity yield surfaces, formulated in dimensionless form with respect to the uniaxial compressive strength f_{cx} in x direction and f_{cy} in y direction, have been also considered.

The values assigned to the compressive and the tensile strengths in x and y directions are reported in Table 7.1.

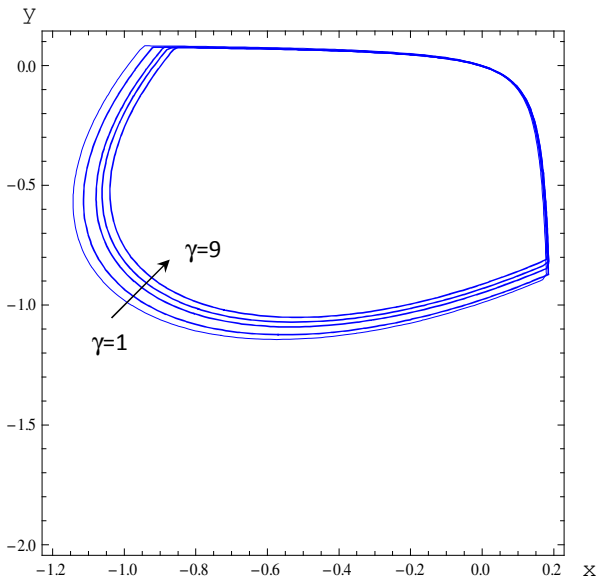

Fig. 7.7: Dimensionless yield surfaces for different values of γ.

Fig. 7.7 shows the variation of the dimensionless surfaces with the parameter γ, whose range vary from 1 to 9. The values of α and β are the ones of Table 7.4 while a reference value of $\tau_{xy} = 0.1\,\text{MPa}$ has been considered.

From the analyses of Fig. 7.7 it can be noticed as higher values of γ make the yield surface in compression reduce.

The value of γ=6 has been chosen for the following sensitivity analyses.

7.2.2.4 Sensitivity analyses on compression fracture energy

Sensitivity analyses on compressive fracture energies Γ_{cx} and Γ_{cy} along the x and y material axes, are the object of the present section.

Since a few experimental data are available, as previously commented, the analyses have been considered very important for the calibration of the finite element model.

The values of the fracture energy $\Gamma_{t,y}$ has been set on the same order of magnitude of the experimental tests collected and commented previously. In absence of experimental data in the horizontal direction, the fracture energy $\Gamma_{t,x}$ has been set on the same value of $\Gamma_{t,y.}$ Both mechanical characteristics have been reported below.

Table 7.5 reports the inelastic parameters considered in nonlinear analyses of the unstrengthened model and the values attributed to the compressive fracture energy $\Gamma_{c,x}$, keeping the value of the fracture energy in y direction $\Gamma_{c,y}$ unchanged.

Table 7.5: Mechanical parameters considered for the sensitivity analysis on $G_{fc,x}$.

Parameters	Test 1	Test 2	Test 3	Test 4	Test 5	Test 6
α_t	1	1	1	1	1	1
β	-1.5	-1.5	-1.5	-1.5	-1.5	-1.5
γ	6	6	6	6	6	6
$\Gamma_{c,x}$ [Nmm/mm^2]	2	4	6	8	10	12
$\Gamma_{c,y}$ [Nmm/mm^2]	4	4	4	4	4	4
$\Gamma_{t,x} = \Gamma_{t,y}$ [Nmm/mm^2]	0.01	0.01	0.01	0.01	0.01	0.01

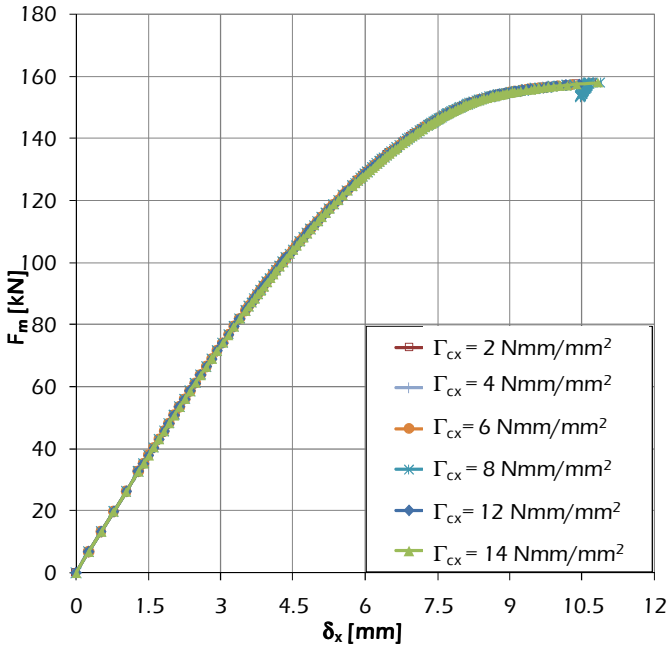

Fig. 7.8: Load-displacement curves for different values of Γ_{cx}.

Fig. 7.8 shows the results in terms of horizontal force-displacement diagram for the developed model: the value of $\Gamma_{c,x}$= 8Nmm/mm^2 gives clearer nonlinear behaviour.

Complementary sensitivity analyses on the compressive fracture energy $\Gamma_{c,y}$ have been finally conducted.

Table 7.6 reports the inelastic parameters considered during the nonlinear analyses of the plain masonry model and the values attributed to the compressive fracture energy $\Gamma_{c,y}$, keeping unchanged the value of the fracture energy in x direction $\Gamma_{c,x}$.

Table 7.6: Mechanical parameters considered for the sensitivity analysis on $\Gamma_{fc,y}$.

Parameters	Test 1	Test 2	Test 3	Test 4	Test 5	Test 6
$\alpha_t = \alpha_h$	1	1	1	1	1	1
β	-1.5	-1.5	-1.5	-1.5	-1.5	-1.5
γ	6	6	6	6	6	6
$\Gamma_{c,x}$ [Nmm/mm^2]	2	2	2	2	2	2
$\Gamma_{c,y}$ [Nmm/mm^2]	4	6	8	10	12	14
$\Gamma_{t,x} = \Gamma_{t,y}$ [Nmm/mm^2]	0.01	0.01	0.01	0.01	0.01	0.01

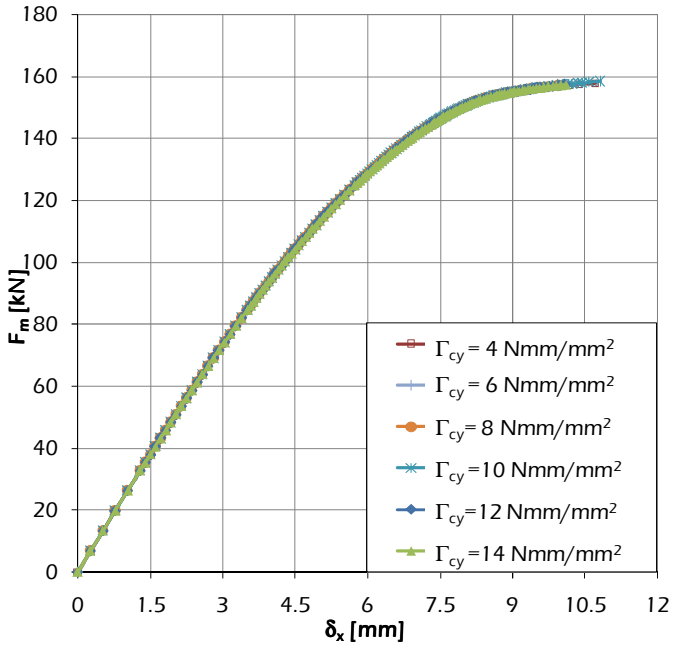

Fig. 7.9: Load-displacement curves for different values of Γ_{cy}.

Fig. 7.9 shows the results in terms of horizontal force-displacement diagram for the developed model: the value of $\Gamma_{c,y}$=10 Nmm/mm^2 gives a clearer nonlinear behaviour.

From the previous analyses came out that the variation of each single parameter of compressive fracture energy does not seem to have a really marked influence on the inelastic behaviour of the model.

Further sensitivity analyses have been performed by varying both values of compressive fracture energy. The result of such a calibration will be considered in the following analyses.

7.2.3 Calibration of the unstrengthened model

The present subsection describes the final calibration of the model of unreinforced masonry walls and the comparison with experimental results.

Table 7.7 reports the inelastic parameters assigned to the finite element model. Such parameters derive from the sensitivity analyses reported and commented in the previous sections.

Table 7.7: Mechanical parameters of the unstrengthened calibrated model.

Mechanical Parameters	
$f_{mt,x}$ [N/mm^2]	0.17
$f_{mt,y}$ [N/mm^2]	0.06
$f_{m,x}$ [N/mm^2]	0.5
$f_{m,y}$ [N/mm^2]	1.1
α	1
β	-1.2
γ	6
$\Gamma_{c,x}$ [Nmm/mm^2]	4
$\Gamma_{c,y}$ [Nmm/mm^2]	6
$\Gamma_{t,x}$ [Nmm/mm^2]	0.01
$\Gamma_{t,y}$ [Nmm/mm^2]	0.01

The comparison between numerical and experimental load-displacement diagrams is given in Fig. 7.10.

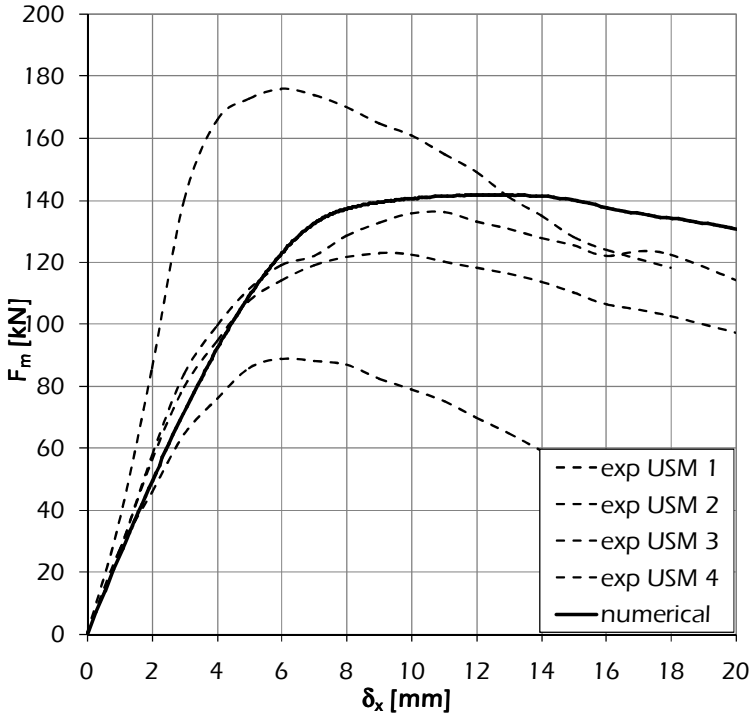

Fig. 7.10: Comparison between experimental and numerical load-displacement curves.

The numerical model accurately simulates the path of the experimentally tested walls in the elastic branch until 80 kN. The pre-peak nonlinear behaviour follows the two middle experimental curves up to a value of 110 kN. The peak predicted by the model is 143 kN and is of about 8% of the average experimental peak value of 132kN (Marcari et al., 2007). The difference between the peak value of the numerical model and the one of experimental walls is quite reasonable considering the scatter between the experimental values.

In the post-peak behaviour the discrepancies between the numerical model and the experimental results are more significant if compared to the extremities curves: the model shows a ductility which was not observed for the two experimental masonry walls, characterized by a noticeable softening. If compared to the middle curves, the model results

in a better prevision. However, the exact post-peak behaviour of the unstrengthened masonry wall is not the main issue of the present thesis.

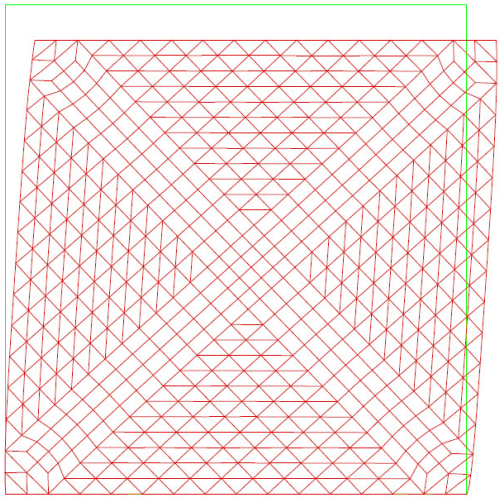

Fig. 7.11: Deformed mesh at a displacement of 2.5 mm.

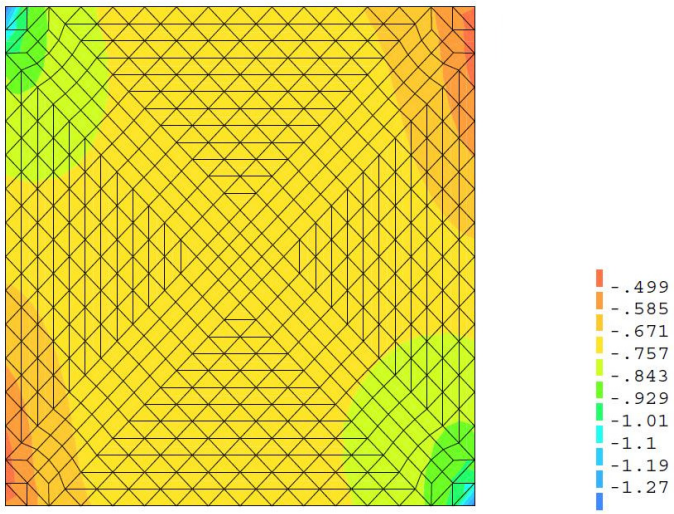

Fig. 7.12: Minimum principal stresses [N/mm^2] at a displacement of 2.5 mm.

Fig. 7.11 and Fig. 7.12 show the behaviour of the wall respectively in terms of deformed meshes and minimum principal stresses at a displacement of 2.5 mm.

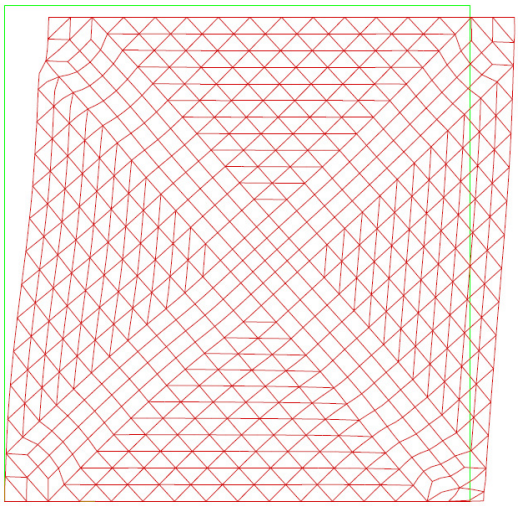

Fig. 7.13: Deformed mesh at a displacement of 21.6 mm.

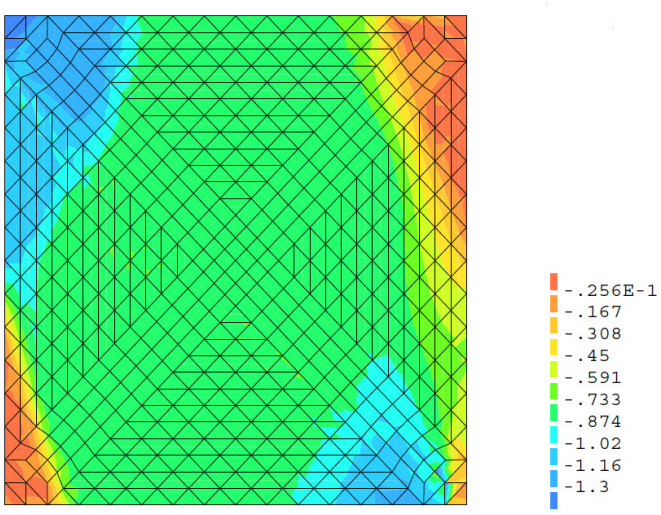

Fig. 7.14: Minimum principal stresses [N/mm^2] at a displacement of 21.6 mm.

Fig. 7.13 and Fig. 7.14 show the behaviour of the wall respectively in terms of deformed meshes and minimum principal stresses at a displacement of 21.6 mm.

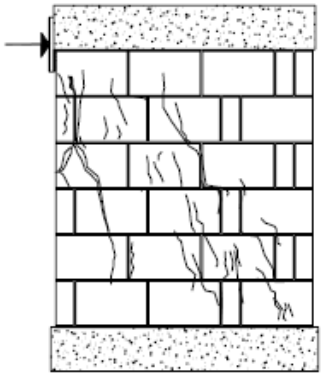

Fig. 7.15: Crack pattern at failure for the unstrengthened wall (Marcari, 2007).

Fig. 7.15 reports the crack pattern of the unstrengthened wall characterizing experimental tests.

Looking at the stress distribution characterising an initial step (Fig. 7.12) and at the final step (Fig. 7.14) of the horizontal load, it can be seen as cracks develop from the top left and the bottom right corners, reproducing the response of the experimental unreinforced walls (Fig. 7.15). Even though the tendency is of developing cracks along the diagonal band, the model does not catch clearly the compression strut shown in experimental tests and reported in Fig. 7.15.

7.3 FRP strengthened masonry model

7.3.1 Material properties of structural interfaces

Modelling the adhesion of FRP strips glued to masonry surface is a key aspect for obtaining accurate simulation of the nonlinear and fracture behaviour of masonry walls externally strengthened by FRP.

Pull-out tests can be usually carried out to quantify the mechanical characteristics of FRP-masonry bond behaviour.

In the scientific literature few experimental tests are available for different kinds of natural stones (Aiello and Sciolti, 2005) or clay bricks (Briccoli et al., 2007; Olivera et al. 2008). Particularly the interaction between tuff masonry and fibre-reinforced polymers (GFRP and CFRP) have been investigated in Faella et al. (2012). The key parameters of the masonry-to-composite interface and particularly the value of fracture energy have been evaluated and analysed by means of simplified analytical formulations.

In order to evaluate the influence of shear interfacial fracture energy Γ_f^{II} characterizing the model implemented for interfaces, some sensitivity analyses have been carried out considering a masonry wall reinforced by Glass FRP.

Table 7.8 reports the mechanical properties of structural interfaces. The normal k_n and tangential k_s stiffness have been calculated by means of Eqn. (5.43) and Eqn. (5.44), considering the mechanical and geometrical characteristics of the experimental wall reinforced by GFRP, belonging to the campaign under consideration.

The tensile strength of the interface f_{mt} and the compressive strength of masonry f_m for the characterisation of the bond behaviour between tuff masonry and FRP have been assumed according to the magnitude order of experimental values of experimental pull-out tests on yellow tuff masonry present in Faella et al. (2012).

The tensile Γ_f^{I} and compressive Γ_c fracture energies of the interface. have been assumed according to proposals presented in Lourenço (1996).

The shear fracture Energy Γ_f^{II} has been investigated through sensitivity analyses object of this paragraph: the magnitude order of

values have been assumed again according to experimental tests conducted by Faella et al. (2012).

The friction ϕ and and dilatancy ψ angles of the interface have been assumed again as proposed by Lourenço (1996).

The inelastic properties of masonry are the ones considered in Table 7.7.

For the cohesion of the interface c the value of the tensile strength has been assumed.

Table 7.8: Mechanical properties of structural interfaces considered in sensitivity analyses.

Mechanical properties	Test 1	Test 2
k_n [N/mm^3]	127	127
k_s [N/mm^3]	53	53
f_{tm} [N/mm^2]	0.5	0.5
Γ_f^I [Nmm/mm^2]	0.035	0.07
c	0.5	0.5
tanϕ	0.75	0.75
tanφ	0	0
Γ_f^{II} [Nmm/mm^2]	0.35	0.7
f_m [N/mm^2]	4.5	4.5
Γ_c [Nmm/mm^2]	5.0	5.0

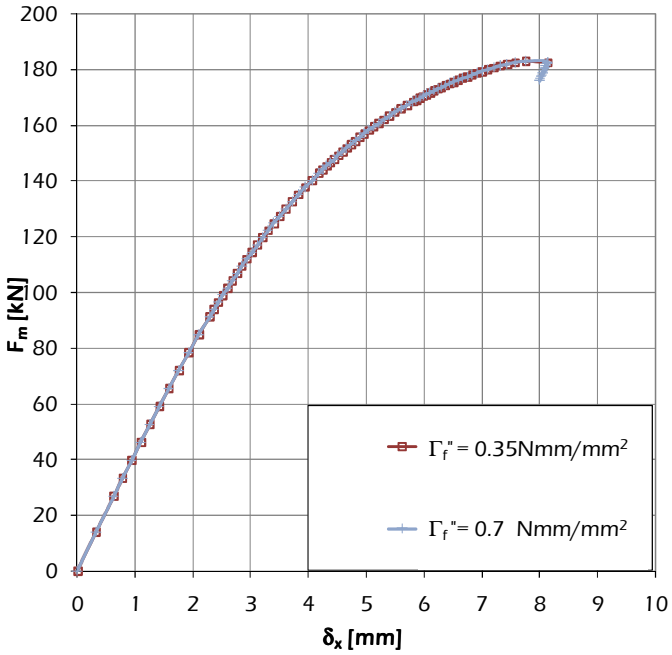

Fig. 7.16: Load-displacement curves for different values of Γ''_f.

Fig. 7.16 shows the results in terms of horizontal force-displacement diagram for the developed model: the value of Γ_f^{II}=0.7 Nmm/mm^2 is characterised by a nonlinear curve with a decreasing branch which is not present in the diagram obtained through nonlinear analysis characterised by a value of shear fracture energy of interface of 0.35 Nmm/mm^2.

7.3.1.1 Model calibration of masonry walls strengthened by Glass FRP

The calibration of the finite element model of a masonry wall strengthened by Glass FRP is presented here.

The cases of a single layer of GFRP and of two layers of GFRP for each strip will be discussed.

Table 7.9 and Table 7.10 report the mechanical properties of structural interfaces and the strengthened material implemented in the numerical simulation. The inelastic properties of masonry are the same of Table 7.7.

Table 7.9: Mechanical properties of structural interfaces.

Mechanical properties	
k_n [N/mm^3]	127
k_s [N/mm^3]	53
f_{mt} [N/mm^2]	0.5
Γ_f^I [Nmm/mm^2]	0.035
c	0.5
tanϕ	0.75
tanφ	0
Γ_f^{II} [Nmm/mm^2]	0.35
f_m [N/mm^2]	4.5
Γ_c [Nmm/mm^2]	5.0

Table 7.10: Mechanical properties of GFRP strengthening.

Mechanical properties	1 layer	2 layers
E_f [N/mm^2]	66000	66000
ν	0.2	0.2
t_f [mm]	1.5	3

7.3.1.1.1 Model of wall strengthened with low GFRP density

In the present subsection the results of the nonlinear analysis of the model reproducing the masonry wall strengthened by GFRP strips with a low density, corresponding to one layer of FRP for each strip, is discussed.

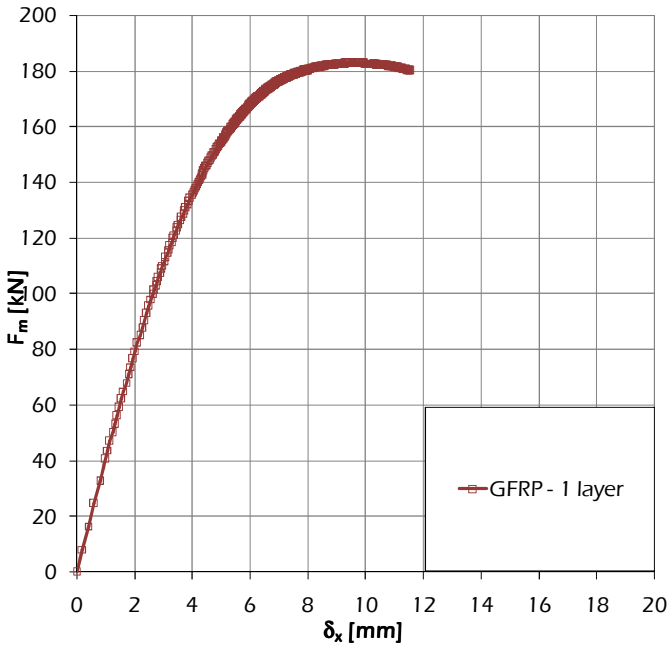

Fig. 7.17: Numerical load-displacement curve of the masonry strengthened by one layer of GFRP.

Fig. 7.17 shows the numerical load-displacement diagram of the nonlinear analysis of the model reproducing the masonry wall reinforced by one layer of GFRP for each strip in cross configuration.

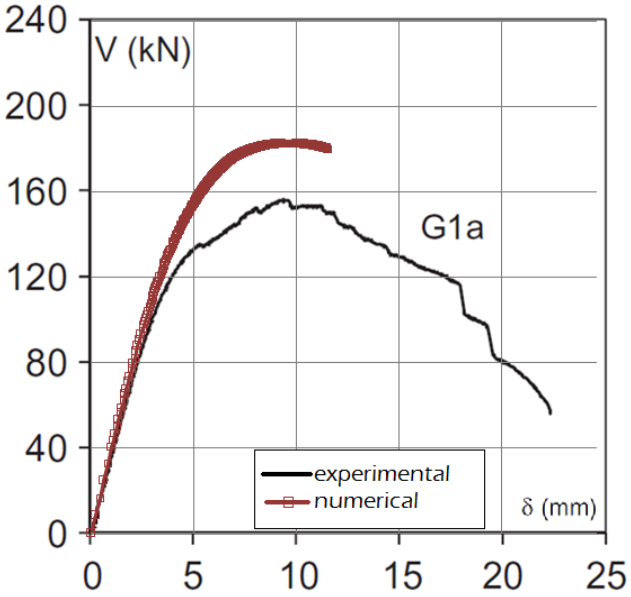

Fig. 7.18: Comparison between experimental and numerical load-displacement curves.

Fig. 7.18 shows the comparison between the numerical result of the analysis and the experimental diagram.

The finite element model is able to reproduce the path of the experimental wall in the elastic branch until 100 kN. The pre-peak nonlinear behaviour follows the shape of the experimental curve until a value of 130 kN. The peak predicted by the model is about 181 kN and is of about +16% of the average experimental peak value of 155.8 kN (Marcari et al., 2007) .

In the post-peak behaviour the discrepancies between the numerical model and the experimental results are more significant.

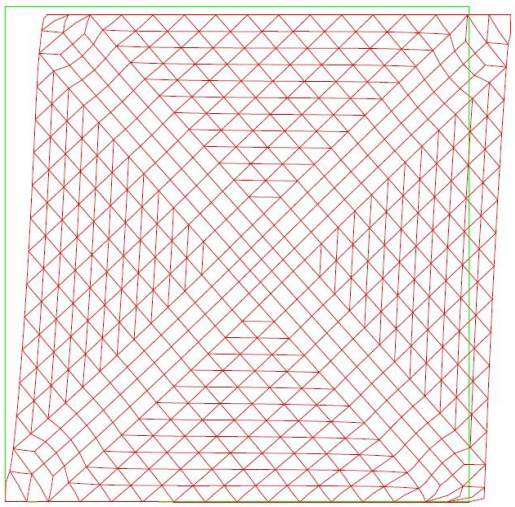

Fig. 7.19: Deformed mesh at a displacement of 12.4 mm.

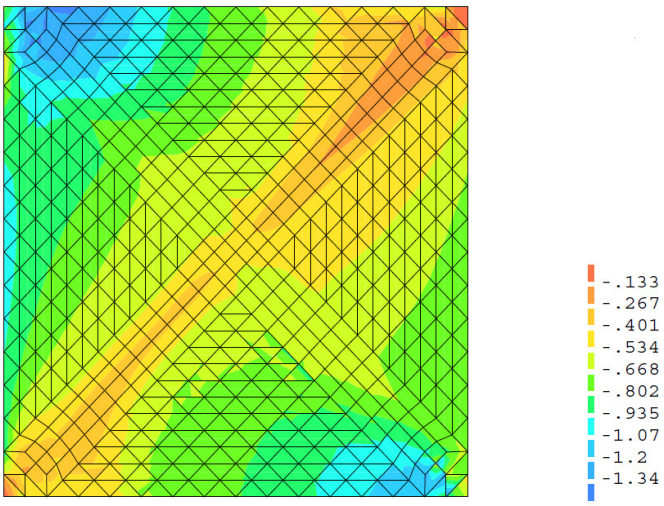

Fig. 7.20: Minimum principal stresses [N/mm^2] at a displacement of 12.4 mm.

Fig. 7.19 and Fig. 7.20 show the behaviour of the wall respectively in terms of deformed meshes and minimum principal stresses at a displacement of 11.5 mm.

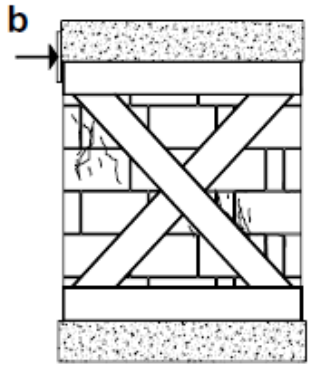

Fig. 7.21: Crack pattern at failure for a wall with low GFRP density (Marcari et al., 2007).

Fig. 7.21 reports the crack pattern of the experimental wall with GFRP strips in cross layout.

Looking at the stress distribution (Fig. 7.20), it can be noticed as the developing of cracks reproduces the response of experimental walls strengthened by one layer of GFRP.

The numerical output partially reproduces the experimental tendency in terms of minimum principal stresses: cracks extend throughout the masonry, starting from the top left corner and the bottom right corner, and develop along the shear band within the strengthened area; cracks also appear in the area close to the loaded edge.

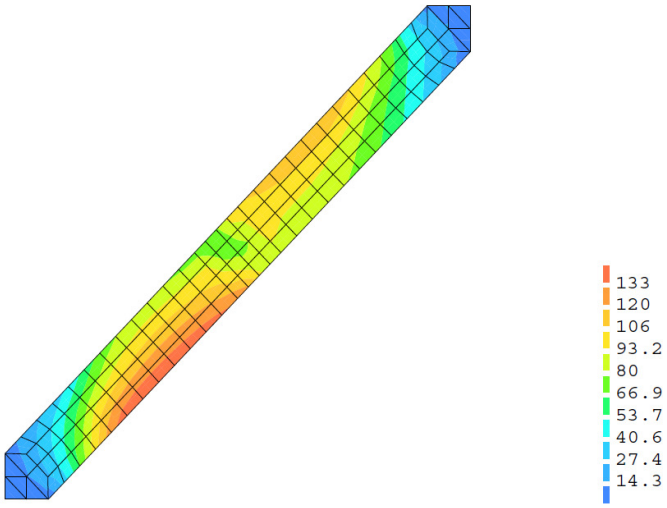

Fig. 7.22: Contour level of principal stresses [N/mm^2] for the GFRP strip in tension.

Fig. 7.22 shows the behaviour of the strip in tension on the two sides of the wall.

Looking at the maximum principal stress distribution along the strip, it can be noticed as the strip results in tension with higher values of principal stresses in correspondence to the central part of the strip while lower values characterise the ends of the strip.

Stresses are almost uniformly distributed along the strips on the two sides of the wall.

Although the numerical output cannot reproduce the experimental "out-of-plane" debonding of the plies in tension, the stress distribution along the strips in tension is consistent with such phenomena.

7.3.1.1.2 Model of wall strengthened with high GFRP density

In the present subsection the results of the nonlinear analysis of the model reproducing the masonry wall strengthened by GFRP strips with a high density, corresponding to two layers of FRP for each strip, is discussed.

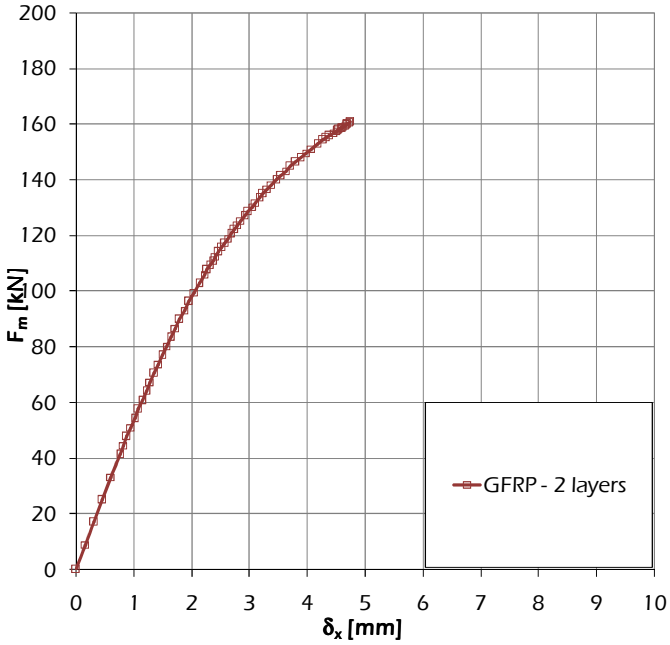

Fig. 7.23: Numerical load-displacement curve of the masonry strengthened by two layers of GFRP.

Fig. 7.23 shows the load-displacement diagram resulting from the nonlinear analysis performed on the model; it reproduces the masonry wall reinforced by two layers of GFRP for each strip in cross configuration.

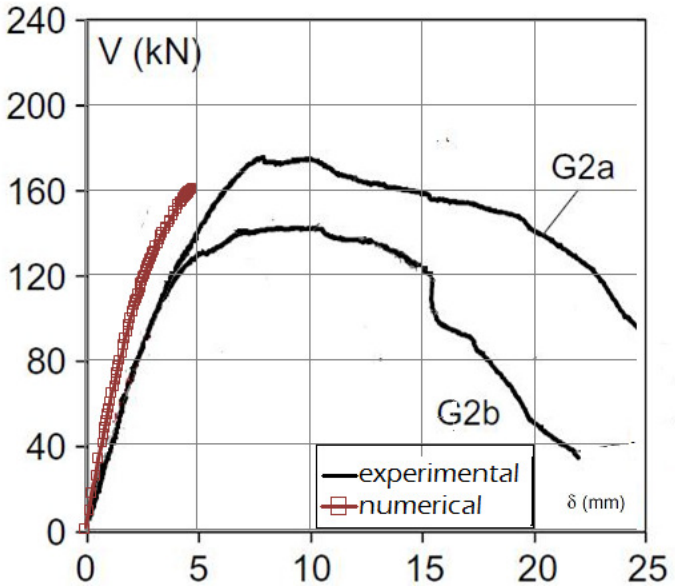

Fig. 7.24: Comparison between experimental and numerical load-displacement curves.

Fig. 7.24 shows the comparison between the numerical results of the nonlinear analysis and the diagrams corresponding to two experimental tests (Marcari et al., 2007) performed on GFRP strengthened masonry walls.

The finite element model is able to reproduce the path of the experimental walls in the elastic branch until 110 kN. The pre-peak nonlinear behaviour follows the shape of the experimental curve until a value of 161 kN, which represents also the peak value predicted by the model. It is very close to the average experimental peak value of 163.4 kN (Marcari et al., 2007). It is not possible to catch the post-peak behaviour with the numerical model.

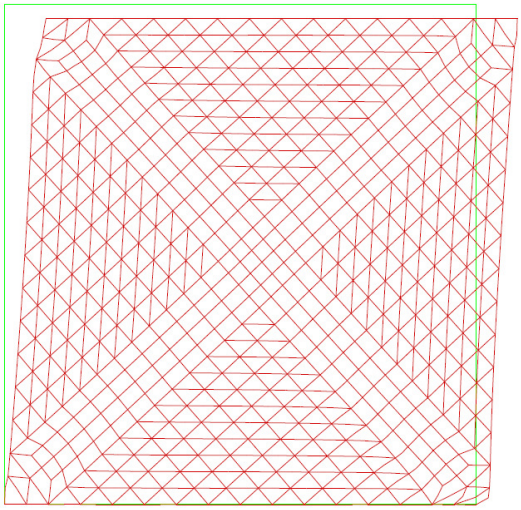

Fig. 7.25: Deformed mesh at a displacement of 5.2 mm.

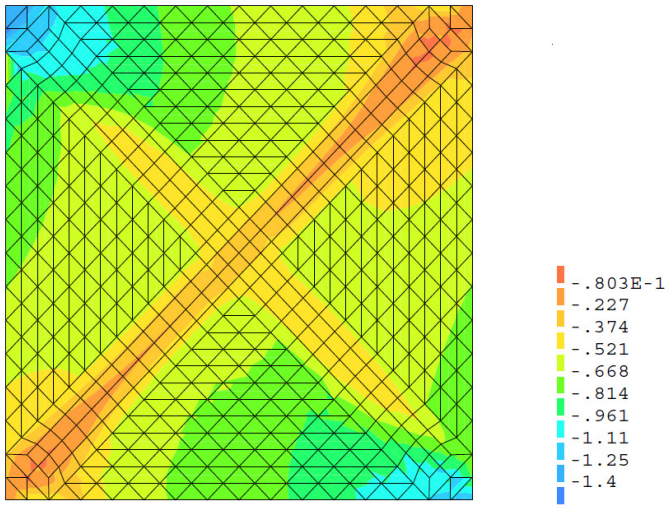

Fig. 7.26: Minimum principal stresses [N/mm^2] at a displacement of 5.2 mm.

Fig. 7.25 and Fig. 7.26 show the behaviour of the wall respectively in terms of deformed meshes and minimum principal stresses at the ultimate displacement.

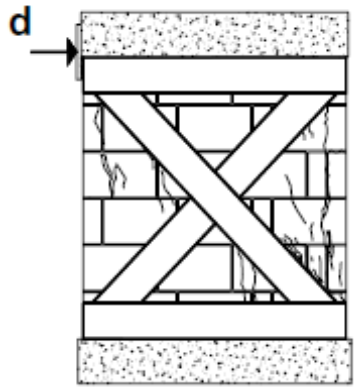

Fig. 7.27: Crack pattern at failure for walls with high GFRP density (Marcari et al., 2007).

Fig. 7.27 reports the crack pattern of the wall with GFRP strips in cross layout resulting from experimental tests.

Looking at the stress distribution (Fig. 7.26), it can be noticed as the developing of cracks partially reproduces the response of experimental walls strengthened by a high density GFRP (Fig. 7.27).

The experimental response was characterized by high compressive stresses at the base corner, which caused masonry crushing at the base of the compression strut. The damage implied also localised cracked zone near the loaded edge (Marcari et al., 2007).

The stress distribution of numerical model shows compressive stresses higher at the loaded edge and at base corners.

At the same time diagonal cracks spread along the shear band, characterizing the experimental response, have been caught by the numerical model as a tendency.

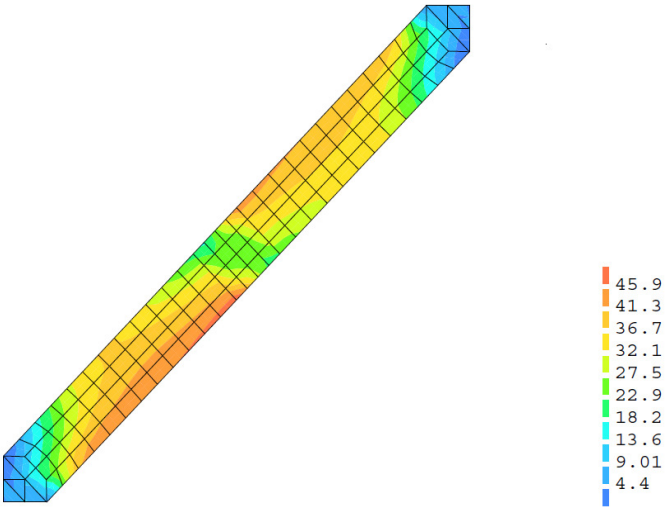

Fig. 7.28: Contour level of principal stresses [N/mm^2] for the GFRP strip in tension.

Fig. 7.28 shows the behaviour of the strip in tension on the two sides of the wall.

Stresses are uniformly distributed along the strips on the two sides of the wall, for this reason only one strip is represented.

The stress distribution along the strip, which results in tension, is characterised by tensile stresses higher in the central part of the strip, confirming the experimental result where debonding of the tensile plies started near mid-height, spreading gradually above and below the middle brick stones.

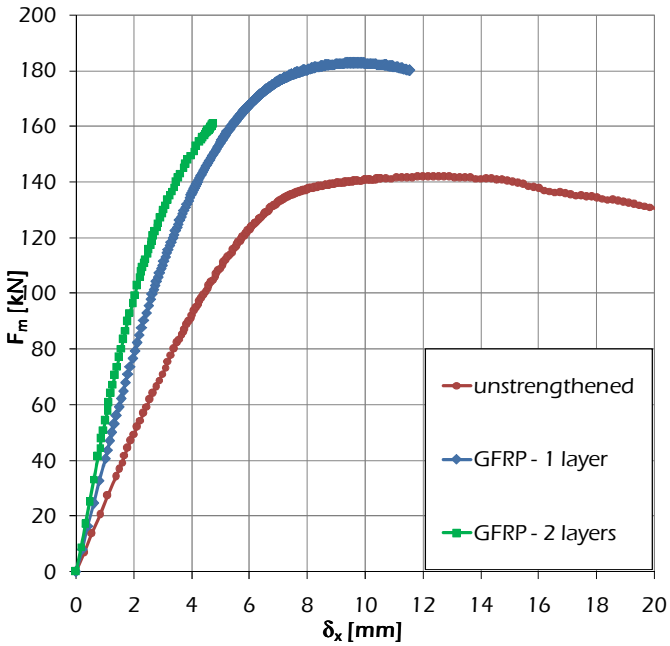

Fig. 7.29: Numerical load-displacement curves of the unstrengthened masonry and masonry strengthened by one and two layers of GFRP.

Fig. 7.29 shows the comparison between the nonlinear simulations corresponding to an unstrengthened wall and to a wall strengthened by cross layout characterised by low and high density GFRP strips.

The shear strength of the masonry wall model increases significantly with one layer of GFRP strengthening, varying from a peak load of 132 kN for the unreinforced wall model to 181 kN for the peak load of the wall model strengthened with one layer of GFRP.

The model which provides two layers of GFRP presents the highest stiffness, if compared to both unstrengthened model and model strengthened by one layer of GFRP, but it is not possible to catch the post-peak behaviour.

7.3.1.2 Model calibration of masonry walls strengthened by Carbon FRP

The calibration of the finite element model of a masonry wall strengthened by Carbon FRP is presented here.

The cases of a single layer of CFRP and of two layers of CFRP for each strip will be discussed.

Table 7.11 and Table 7.12 report the mechanical properties of structural interfaces and the strengthened material implemented in the numerical simulation.

The inelastic properties assigned to the masonry are the ones of Table 7.7.

Table 7.11: Mechanical properties of structural interfaces.

Mechanical parameters	
k_n [N/mm^3]	127
k_s [N/mm^3]	53
f_{mt} [N/mm^2]	0.5
Γ_f^I [Nmm/mm^2]	0.035
c	0.5
tanϕ	0.75
tanφ	0
Γ_f^{II} [Nmm/mm^2]	0.35
f_m [N/mm^2]	4.5
Γ_c [Nmm/mm^2]	5.0

Table 7.12: Mechanical properties of CFRP strengthening.

Mechanical parameters	1 layer	2 layers
E_f [N/mm^2]	230000	210000
ν	0.2	0.2
t_f [mm]	1.5	3

7.3.1.2.1 Model of wall strengthened with low CFRP density

In the present subsection the results of the nonlinear analysis of the model simulating the masonry wall strengthened by CFRP strips with a low density, corresponding to one layer of FRP for each strip, is discussed.

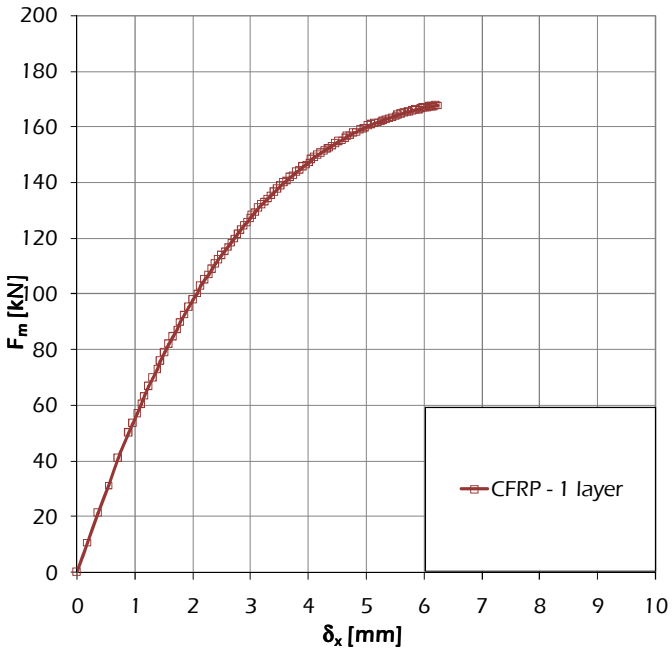

Fig. 7.30: Numerical load-displacement curve of the masonry strengthened by one layer of CFRP.

Fig. 7.30 shows the numerical load-displacement diagram of the nonlinear analysis of the model reproducing the masonry wall reinforced by one layer of CFRP for each strip in cross configuration.

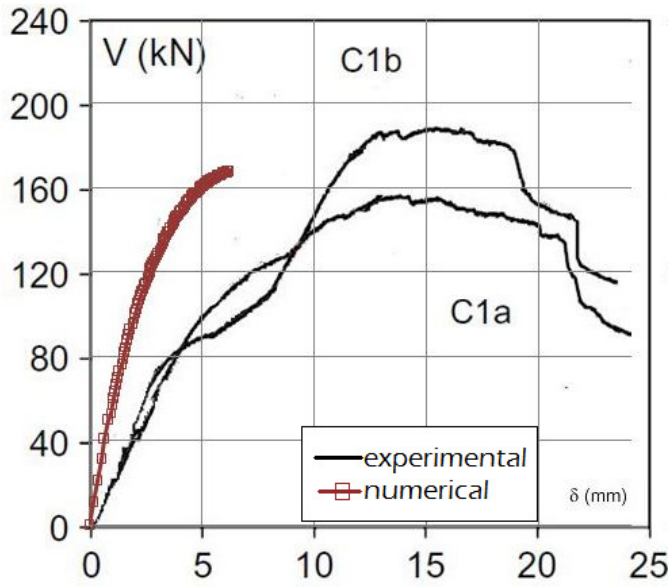

Fig. 7.31: Comparison between experimental and numerical load-displacement curves.

Fig. 7.31 shows the comparison between the numerical results of the analysis and the experimental diagram.

In the elastic branch, the Finite Element Model present a stiffness higher than the one of the two masonry walls strengthened by one layer of CFRP. The elastic branch of the numerical model is characterised by a maximum value of about 70 kN while the experimental curves are characterised by an elastic branch of about 50 kN. The peak predicted by the model is about 167 kN and is of about -3% of the average experimental peak value of 172.8 kN (Marcari et al., 2007).

In the nonlinear range, the discrepancies between the numerical model and the experimental results are significant, and it is probably due also to the scatter between the two numerical results.

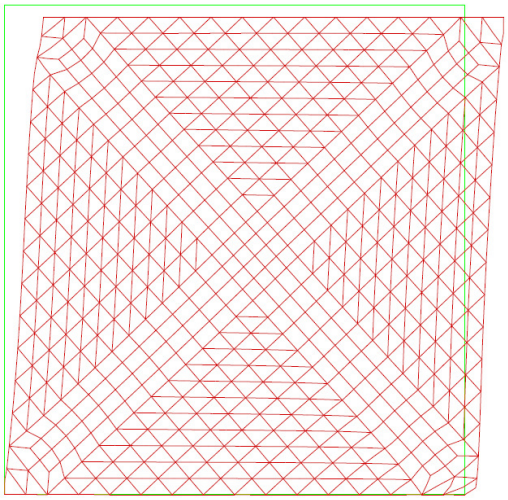

Fig. 7.32: Deformed mesh at a displacement of 6.78 mm.

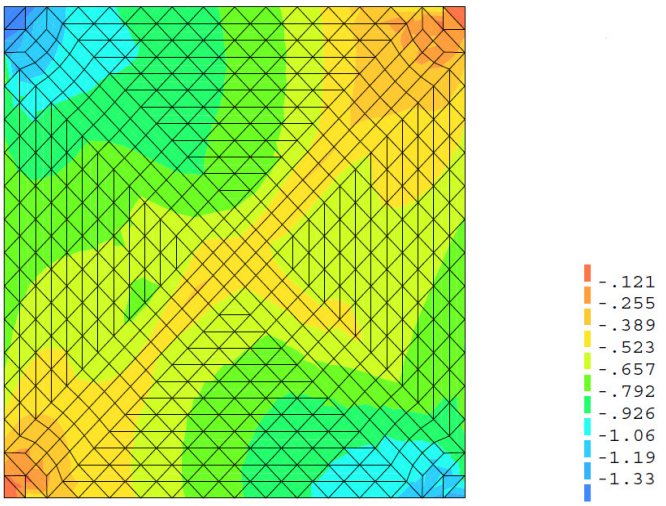

Fig. 7.33: Minimum principal stresses [N/mm^2] at a displacement of 6.78 mm.

Fig. 7.32 and Fig. 7.33 show the behaviour of the wall respectively in terms of deformed meshes and principal stresses at a displacement of 6.78 mm.

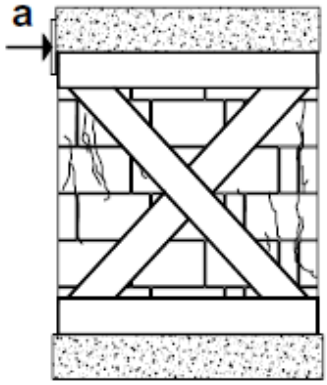

Fig. 7.34: Crack pattern at failure for walls with low CFRP density (Marcari et al., 2007).

Fig. 7.34 reports the crack pattern of the wall with CFRP strips in cross layout. Looking at the stress distribution, it can be noticed as it follows the developing of cracks during the experimental response of the two walls strengthened by one layer of CFRP.

The numerical output reproduces the experimental evidence: cracks extend throughout the masonry, starting from the top right corner and the bottom left corner, and develop along the shear band within the strengthened area; cracks also appear in the area close to the loaded edge.

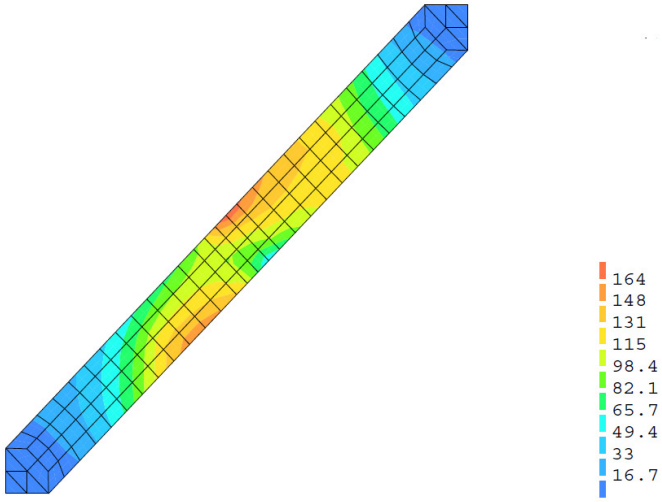

Fig. 7.35: Contour level of principal stresses [N/mm^2] for the CFRP strip in tension.

Fig. 7.35 shows the behaviour of the strip in tension on the two sides of the wall.

From the stress distribution along the strip, it can be noticed as it results in tension with higher values of the principal stresses in correspondence to the central part of the strip while lower values characterise the ends of the strips.

Stresses are uniformly distributed along the strips on the two sides of the wall.

Although the numerical output cannot reproduce the experimental "out-of-plane" debonding of the plies in tension, the stress distribution along the strips in tension is consistent with such phenomena.

7.3.1.2.2 Model of wall strengthened with high CFRP density

Results of the nonlinear analysis of the model reproducing the masonry wall strengthened by CFRP strips with a high density, corresponding to two layers of FRP for each strip, are discussed in the present subsection.

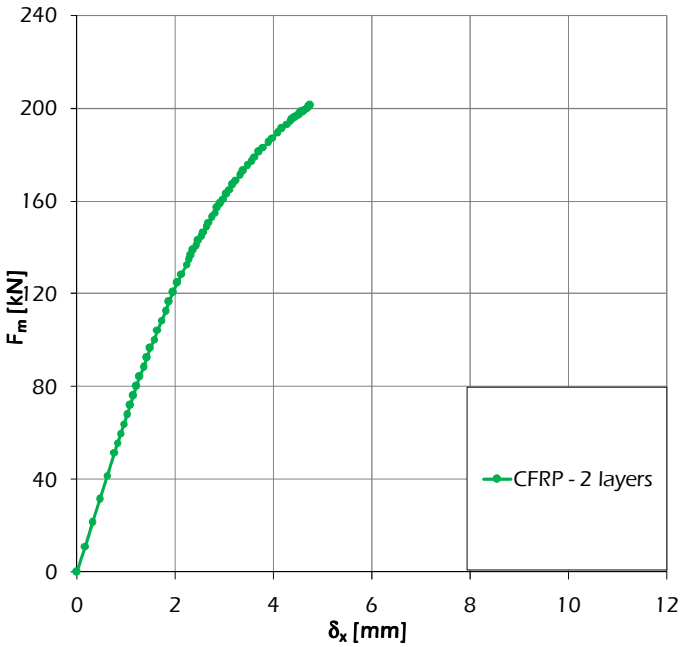

Fig. 7.36: Numerical load-displacement curve of the masonry strengthened by two layers of CFRP.

The load-displacement diagram which results from the nonlinear analysis performed on the model is shown in Fig. 7.36; it reproduces the masonry wall reinforced by two layers of CFRP for each strip in cross configuration.

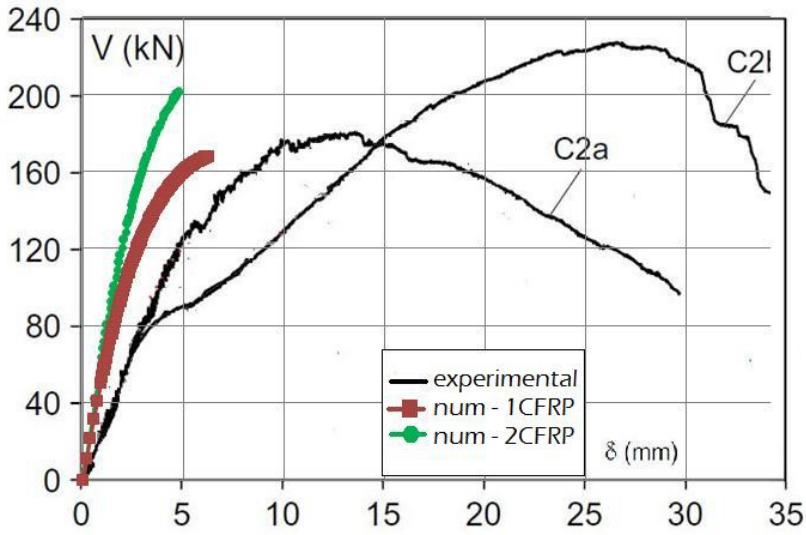

Fig. 7.37: Comparison between experimental and numerical load-displacement curves.

Fig. 7.37 shows the comparison between the numerical results of the nonlinear analysis for the model with one layer of CFRP, the model with two layers of CFRP and the diagrams corresponding to two experimental tests corresponding to masonry walls strengthened by two layers of CFRP.

In the elastic range the load-displacement diagram of the Finite Element Model, corresponding to a wall strengthened by two layers of CFRP, is characterized by a horizontal stiffness higher than the one corresponding to experimental results.

The ultimate load is of about 200 kN and is really near to the mean experimental peak value of 203.8 kN (Marcari et al., 2007). The model cannot reproduce the post-peak behaviour.

However if comparing the numerical results of the nonlinear analysis corresponding to the model with one layer of CFRP for each strip, the load-displacement curve partially fits one of the two experimental curves corresponding to the wall specimen strengthened by two layers of FRP.

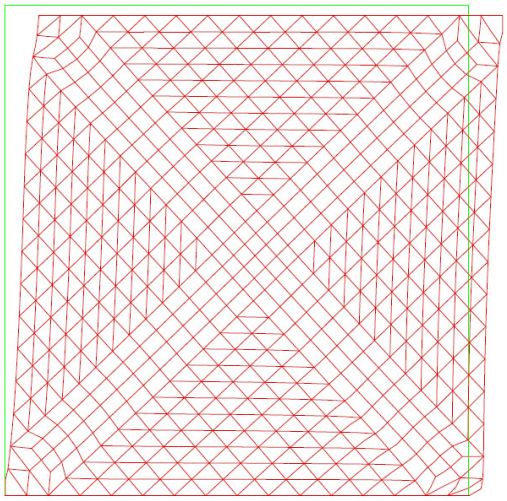

Fig. 7.38: Deformed mesh at a displacement of 6.02 mm.

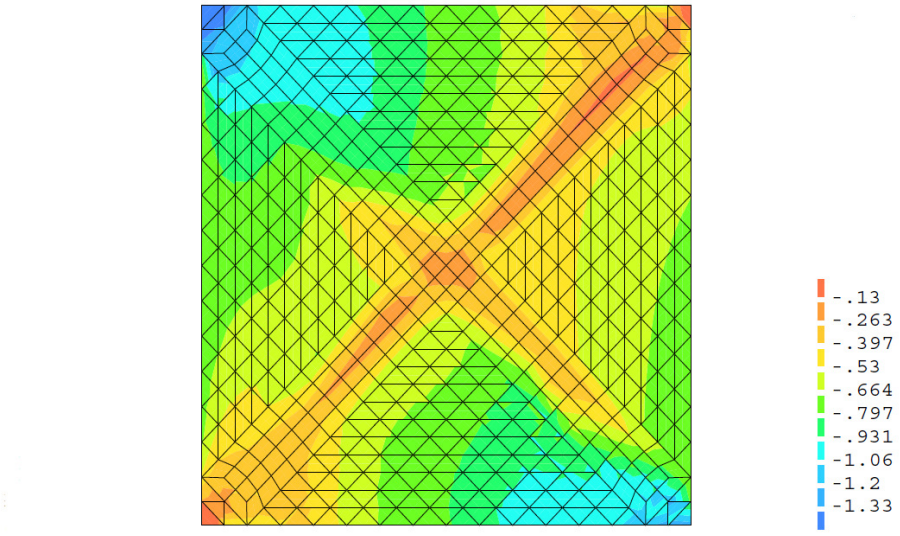

Fig. 7.39: Minimum principal stresses [N/mm^2] at a displacement of 6.02 mm.

Fig. 7.38 and Fig. 7.39 show the behaviour of the wall in terms of deformed mesh and principal stresses at the ultimate displacement.

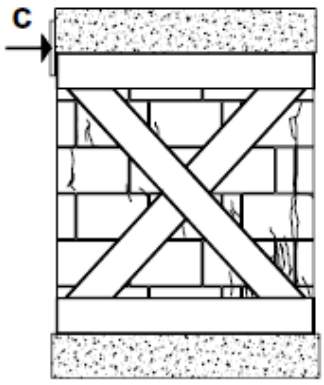

Fig. 7.40: Crack pattern at failure for walls with high CFRP density (Marcari et al., 2007).

Fig. 7.40 reports the crack pattern of the wall with two layers of CFRP for each strip in cross layout resulting from experimental tests.

Looking at the stress distribution, it can be noticed as cracks patterns are partially close to the expected ones of experimental walls strengthened by a high density of CFRP.

The experimental response was characterized by high compressive stresses at the base corner, which caused masonry crushing at the base of the compression strut. The damage implied also a localized cracked zone near the loaded edge (Marcari et al., 2007).

The stress distribution of the numerical model resulting from the analysis shows compressive stresses higher in the loaded edge and at base corners (Fig. 7.39). At the same time diagonal cracks spread along the shear band, characterizing the experimental response, have not been caught by the numerical model.

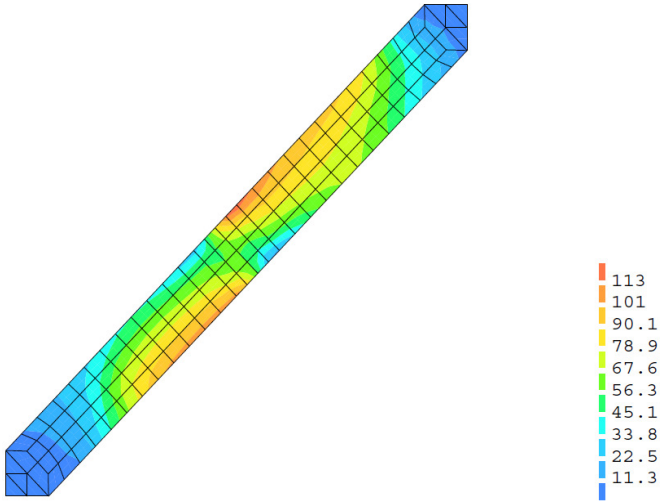

Fig. 7.41: Contour level of principal stresses [N/mm^2] for the CFRP strip in tension.

Fig. 7.41 shows the behaviour of the right strip on the two sides of the wall. From the stress distribution along the strip, it can be noticed as the strips results in tension with higher values of the principal stresses in correspondence to the central part of the strip while lower values characterise the ends of the strips.

Although the numerical output cannot reproduce the experimental "out-of-plane" debonding of the plies in tension, the stress distribution along the strips in tension is consistent with such phenomena.

Stresses are almost uniformly distributed along the strips on the two sides of the wall, so just one of them has been reported for each side of the wall.

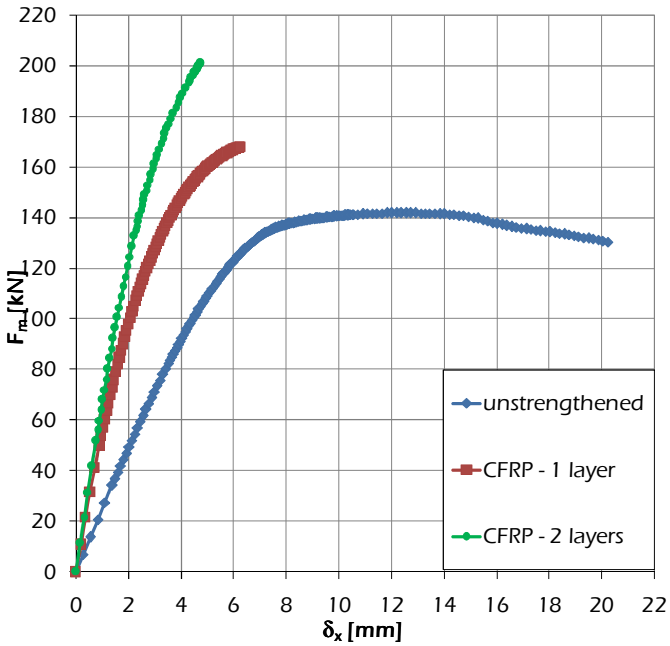

Fig. 7.42: Numerical load-displacement curves for unstrengthened masonry and masonry strengthened by one and two layers of CFRP.

Fig. 7.42 shows the comparison between the numerical results of the nonlinear analyses corresponding to the unstrengthened wall model and to the models corresponding to walls strengthened by cross layout with low and high density CFRP strips.

The shear strength of the masonry wall model increases significantly with one layer of CFRP strengthening, varying from a peak load of 132 kN for the unreinforced model to 167 kN for the peak load of the model strengthened with one layer of CFRP.

If compared to both unstrengthened model and model strengthened by one layer CFRP, the model with two layers of CFRP presents the highest stiffness but it is not possible to catch the post-peak behaviour.

7.4 Conclusions

Code provisions and analytical models are available in the scientific literature for quantifying shear strength in masonry walls, possibly externally strengthened by FRP composites. This thesis has firstly presented an in-depth review of such proposals.

A wide database collecting a set of experimental results of shear tests on unstrengthened masonry (USM) walls and strengthened masonry (SM) walls available in the scientific literature has been assembled for assessing the capacity models.

Several kinds of masonry, fibers quality, texture, composite materials and test arrangements characterise the geometric and mechanical properties of the collected tests.

The above mentioned models have been assessed by comparing their predictions with the experimental results collected in the experimental database.

The experimental to theoretical comparisons has shown some common aspects. The predictions of the examined formulations, except ACI 440.7R-10 Guide (2010) model and CNR-DT 200/2004 Guidelines (2009) model, result unsafe in case of wall specimens made out of natural bricks.

Based on the collected database, no general trends, either conservative or not, have been recognized for Carbon- and Glass-FRP reinforcement.

Further studies are needed for a recalibration of some of those models to minimize the error between the experimental evidence and the theoretical prevision.

Uncertainty deriving by the approximation of the model as well as randomness related to the mechanical properties of masonry will be considered in deriving a consistent design formula for shear strength of masonry walls externally strengthened by composite materials.

A finite element model has been developed to simulate the behaviour of masonry walls under in-plane shear forces. The model simulates the behaviour of masonry walls externally reinforced by FRP composites arranged in diagonal configuration.

The adopted modelling approach for masonry can be regarded within the so-called macro-modelling. The interactions between the masonry and the FRP strengthening have been modelled through structural plane interface elements.

A validation of the proposed numerical model for unreinforced masonry has firstly been presented in the elastic range by means of comparisons with the experimental evidence.

The implementation of plane interfaces in a two-dimensional F.E. model has been assessed by means of models with simple geometry.

Finally, a parametric study performed through nonlinear analyses on both unstrengthened model and model strengthened with different types and amounts of FRP composites has been presented.

A database collecting inelastic mechanical characteristics of masonry and of FRP-masonry bond behaviour, derived from experimental tests, has been collected to support nonlinear analyses.

The numerical investigation has been aimed to better understand the influence of parameters which are generally difficult to determinate through experimental tests.

The model reproducing unstrengthened masonry walls, accurately simulates the path of the experimental tested walls in the elastic branch. The pre-peak nonlinear behaviour follows the two middle experimental curves and the peak predicted by the model is very near to the average experimental peak value.

In the post-peak behaviour a good agreement between the numerical model and the average experimental results in terms of softening response has been obtained.

The overall response of masonry walls can be well predicted in terms of collapse load values by the model; aspects regarding failure mechanisms need further optimizations.

The model reproducing strengthened masonry walls, has been adopted for a parametric study regarding different nature of fibers (Glass and Carbon FRP) and densities (one and two layers of FRP).

The response of the developed model for GFRP strengthened walls results in better previsions than CFRP strengthened walls.

The study on the strengthened model is oriented to determinate the influence of geometrical and mechanical parameters of the strengthening in support of retrofitting design formulae, presented in this thesis, and is open to a future study involving most various strengthening configurations, present in the collected database.

References

AIELLO M.A., SCIOLTI M.S., RAINÒ A. and DE LORENZIS L., (2007); " Il rinforzo a taglio di pannelli murari in "pietra leccese" mediante tecniche innovative", XII Convegno Anidis L'ingegneria Sismica In Italia, Pisa, Italia, June 10-14, 2007.

ALCAINO, P. and SANTA-MARIA, H., (2008); "Experimental Response of Externally Retrofitted Masonry Walls Subjected to Shear Loading", Journal of Composites for Construction, ASCE, 12(5), p. 489-498.

ALCAINO, P. and SANTA-MARIA, H., (2008); "Shear response of masonry walls with external CFRP reinforcement", The 14th World Conference on Earthquake Engineering October 12-17, 2008, Beijing, China.

ALFANO G. AND SACCO E.,(2006); "Combining interface damage and friction in a cohesive-zone model", International Journal for Numerical Methods in Engineering, 68(5), 5p.42-582.

AMERICAN CONCRETE INSTITUTE 440.7R, "Guide for the Design and Construction of Externally Bonded Fiber-Reinforced Systems for Strengthening Unreinforced Masonry System," ACI, 2010.

ANGELILLO M., (2011); "Lecture 1: Masonry Mechanics and Masonry-Like materials", Course on Mechanics of Masonry Structures, CISM, Udine, 3-7 October 2011.

AS 3700, (2001); "Masonry Structures. Standards Australia International", Sydney, Australia, 2001.

ASCIONE L., FEO L. AND FRATERNALI F., (2010); "Appunti sul metodo degli elementi finiti", CUES, Salerno.

ASTM, (2002); Standard test method for Diagonal Tension (Shear) in Masonry Assemblages, ASTM E 519– 02, American Society for Testing Materials.

AUGENTI N. and PARISI F., (2009); "Experimental data analysis on mechanical parameters of tuff masonry", Workshop on Design for Rehabilitation of Masonry Structures - Wondermasonry 2009, Lacco Ameno, Italy, 8-10 October 2009.

BANKS-SILLS L., LEIDERMAN V. and FANG D., (1997); "On the effect of particle shape and orientation on elastic properties of metal matrix composites", Composites Part B: Engineering, 28 (4), p. 465–481.

BELMOUDEN, Y. and LESTUZZI, P., (2007), "An Equivalent Frame Model for Seismic Analysis of Masonry and Reinforced Concrete Buildings", Construction and Building Materials, 23 (1), p. 40-53.

BEOLCHINI G. C. and GRILLO F., (1989); "Prove statiche su pannelli murari di un edificio aquilano del '700"; Atti IV Convegno Nazionale: L' Ingegneria Sismica in Italia, Milano, 5-7 October 1989.

BEOLCHINI G. C., GRILLO F. and RICCIARDULLI G. L., (1997); "Prove cicliche a compressione diagonale su pannelli in muratura di pietrame rinforzati con diverse tecniche: confronto dei risultati", Atti 8° Convegno Nazionale ANIDIS: L'Ingegneria Sismica in Italia, Taormina, 21-24 September 1997.

BORRI A., CORRADI M. and VIGNOLI A. (2001); "Il Problema della Valutazione della Resistenza a Taglio della Muratura mediante Prove Sperimentali"; X Congresso Nazionale "L'ingegneria Sismica in Italia" a cura di ANIDIS, Potenza-Matera, 9-13 September 2001.

BORRI A., CORRADI M. and VIGNOLI A., (2000); "Il comportamento strutturale della muratura nelle zone terremotate dell'Umbria: alcune sperimentazioni", L'Edilizia, editrice De Lettera, n. 2, febbraio - marzo -aprile 2002, anno XVI, Milano, 50-58.

BOSILJKOV V., (2004); "Report on the State of the Art on Structural Modelling of Historical Masonry Structures", Technical report, ZAG, Available at: < http://www.onsiteformasonry.bam.de/Documents/CD_ONSITE/deliverables/D9_0_full.pdf> [Accessed Date 18 October 2011].

BRAGA, F. and DOLCE, M., (1982); "Un metodo per l'analisi di edifici multipiano in muratura antisismici", Proc. Of the 6th I.B.Ma.C., Roma, 1982, pp.1088-1099.

BRAGA, F., LIBERATORE, D. and SPERA, G., (1998); "A computer program for the seismic analysis of complex masonry buildings", Computer methods in structural masonry –4, Proc. of the Int. Symp., E&FN Spon, London, 1998, pp.309-316, G.N. Pande & J. Middleton (eds.).

BRAGA, F., LIBERATORE, D. AND SPERA, G., "A computer program for the seismic analysis of complex masonry buildings" in G.N. Pande & J. Middleton (eds.) Computer methods in structural masonry –4, Proc. of the Int. Symp., E&FN Spon, London, 1998, pp.309-316.

BRAGA, F. AND LIBERATORE, D., "A finite element for the analysis of the response of masonry buildings", Proc. of the 5th North American Masonry Conference, Urbana, 1990, pp. 201-212.

BRENCICH A. and LAGOMARSINO S., (1997); "Un modello a macroelementi per l'analisi ciclica di pareti murarie", Atti del VIII Convegno Nazionale "L'Ingegneria sismica in Italia", vol. 1, Taormina, pp. 319-326.

BRENCICH A. and LAGOMARSINO S., (1998); "A macroelements dynamic model for masonry shear walls", Proc. of the Fourth Int. Symposium on Computer Methods in Structural Masonry (STRUMAS), Firenze, 1997.

BRENCICH A., GAMBAROTTA L. and LAGOMARSINO S., (1998), "A macroelement approach to the three-dimensional seismic analysisof masonry buildings", Proceedings of 11th

European Conference on Earthquake Engineering, Paris, France, September 1998, Ed. Balkema, Rotterdam, NetherlandsBalkema, Rotterdam.

BRENCICH, A. AND LAGOMARSINO, S., "A macro-element dynamic model for masonry shear wals", in G.N. Pande & J. Middleton (eds.) Computer methods in structural masonry –4, Proc. of the Int. Symp., E&FN Spon, London, 1998, pp.67-75.

BRENCICH, A. AND LAGOMARSINO, S., "Un modello a macroelementi per l'analisi ciclica di pareti murarie", 8° Congresso ANIDIS, Taormina, Vol. 1, 1997, pp. 319-326.

CALDERONI B., (1996); "Valutazione sperimentale delle caratteristiche meccaniche di muratura di tufo per modelli in scala intermedia", Atti del Convegno Nazionale: La Meccanica delle Murature tra Teoria e Progetto, Messina, 18-20 September 1996.

CALDERONI, B., LENZA, P. and PAGANO, M., (1989); "Attuali prospettive per l'analisi sismica non lineare di edifici in muratura", Atti del 4° Congresso Nazionale ANIDIS, Milano, 1989.

CALDERONI, B., MARONE, P. and PAGANO, M., (1987); "Modelli per la verifica statica degli edifici in muratura in zona sismica", Ingegneria sismica, 3, pp.19-27.

Circolare n. 26/2010 del Ministero per i Beni e le Attività culturali - Linee Guida per la valutazione e riduzione del rischio sismico del patrimonio culturale allineate alle nuove Norme tecniche per le costruzioni (D.M. 14 gennaio 2008)

CNR DT200, (2009); "Linee guida per la Progettazione, l'Esecuzione ed il Collaudo di Interventi di Rinforzo di strutture di c.a., c.a.p. e murarie mediante FRP", Documento approvato il 24 luglio 2009 dall'Assemblea Geneale Consiglio Superiore LL PP.

COLOMBI M., BORZI B., CROWLEY H., ONIDA M., MERONI F. and Pinho R., (2008); "Deriving vulnerability curves using Italian earthquake damage data"; Bulletin of Earthquake Engineering, 6 (3), p. 485–504.

COMO M. and GRIMALDI A., (1985); "A unilateral model for the limit analysis of masonry walls", CISM Courses and Lectures 288, Springer.

CORRADI M., BORRI A. AND VIGNOLI A., (2002); "Strengthening techniques tested on masonry structures struck by the Umbria – Marche earthquake of 1997–1998", Construction and Building Materials, 16 (4), p. 229–239.

D'ASDIA P., VISKOVIC A. and BRUSAPORCI C., (2005); "Non linear step by step analysis for masonry strctures using changing shape finite elements – new developments and implementations", in Structural analysis of historical constructions – possibilities of numerical and experimental techniques, 1, Published by A.A. Balkema Publisher, Leiden, The Netherlands.

D'ASDIA, P., and VISKOVIC, A., (1994); "L'analisi sismica degli edifici in muratura", Ingegneria Sismica, Anno XI, n.1, 1994, pp. 32-42.

DANIELL, J.E., KHAZAI, B., WENZEL, F AND VERVAECK A., (2011); "The CATDAT Damaging earthquakes database", Natural Hazards and Earth System Sciences, 11 (2011), p. 2235–2251.

DE NICOLO, B., GROSSO, B. and VALDES, M., (2004); "Mechanical behavior of natural stone masonry strengthened with FRP. Part II: verification by using a finite element method", Proc. of the 1st Int.l Conf. on Innovative Materials and Technologies for Construction and Restoration, Lecce, Italy, 6-9 June 2004, Vol. II, p. 487-497.

DECANINI L., (2009a); "Approccio multidisciplinare alla valutazione dell'adeguatezza sismica degli edifici esistenti di muratura ", Lesson n. 1, Corso di Formazione Superiore Costruzioni di Muratura Modellazione, Sicurezza Sismica e Conservazione di Edifici Ordinari e Monumentali. Sapienza Università di Roma. Available at : <http://w3.disg.uniroma1.it/corsomuratura09/index.php?option=com_content&task=view&id=26&Itemid=49> [Accessed Date 24 July 2009].

DECANINI L., (2009b); "Approccio multidisciplinare alla valutazione dell'adeguatezza sismica degli edifici esistenti di muratura ", Lesson n. 3, Corso di Formazione Superiore Costruzioni di Muratura Modellazione, Sicurezza Sismica e Conservazione di Edifici Ordinari e Monumentali. Università di Roma. Available at <http://w3.disg.uniroma1.it/corsomuratura09/index.php?option=com_content&task=view&id=26&Itemid=49> [Accessed Date 24 July 2009].

DECANINI L., (2009c); "Esempi di danneggiamnti osservati. Conoscenze ed insegnamenti derivanti ", Lesson n. 10, Corso di Formazione Superiore Costruzioni di Muratura Modellazione, Sicurezza Sismica e Conservazione di Edifici Ordinari e Monumentali. Available at : <http://w3.disg.uniroma1.it/corsomuratura09/index.php?option=com_content&task=view&id=26&Itemid=49> [Accessed Date 24 July 2009].

DEL PIERO G., (1989); "Constitutive equations for linear elastic masonry-like materials", Meccanica, 24, 150-162.

DI PASQUALE S., (1984); "Problemi di equilibrio per materiali non reagenti a trazione", Atti Dip. Costr. Università di Firenze.

DIN 1053-100, (2007), "Masonry - Part 100: Design on the basis of semi-probabilistic safety concept", Deutsches Institut für Normung, Beuth Verlag, Berlin, 2007.

DOGANGÜN A., URAL A. and LIVAOGLU R., (2008); "Seismic Performance of Masonry Buildings during Recent Earthquakes in Turkey", The 14th World Conference on Earthquake Engineering October 12-17, 2008, Beijing, China.

DOLCE, M., (1989); "Schematizzazione e modellazione per azioni nel piano delle pareti", Corso sul consolidamento degli edifici in muratura in zona sismica, Ordine degli Ingegneri, Potenza, Italy.

ELGAWADY M., LESTUZZI P. and BADOUX M., (2004); "A Review of Conventional Seismic Retrofitting Techniques for URM", Proceedings of the 13th International Brick and Block Masonry Conference, Amsterdam, July 4-7, 2004.

ElGawady Mohamed A., Lestuzzi P. and Badoux M., (2006); "Analytical model for the in-plane shear behaviour of URM walls retrofitted with FRP", Composites Science and Technology, 66 (3-4), p. 459–474.

EROL G., YUKSEL E., SARUHAN H., SAGBAS G., TUGA P. T. and KARADOGAN H. F., (2004); "A complementary experimental work on brittle partitioning walls and strengthening by carbon fibers", 13th World Conference on Earthquake Engineering, Vancouver, B.C., Canada, 1-6 August, 2004.

EU-INDIA ECONOMIC CROSS CULTURAL PROGRAMME, (2006), "Identification of strengthening strategies", Project Contract No: ALA/95/23/2003/077-122. Project Beneficiary:Universidade do Minho, Portugal.

EUROCODE 6, (1998); "Design of masonry structures – Part 1-1: General rules for buildings – rules for reinforced and unreinforced masonry", UNI EN 1996-1-1.

FAELLA C., MARTINELLI E., NIGRO E. AND PACIELLO S., (2004); "Tuff masonry walls strengthened with a new kind of CFRP sheet: experimental tests and analysis", 13th World Conference on Earthquake Engineering, Vancouver, B.C., Canada 1-6 August 2004.

FAELLA C., MARTINELLI E., NIGRO E. and PACIELLO S., (2006); "Shear strength of tuff-masonry walls retrofitted with CFRCM; First European Conference on Earthquake Engineering and Seismology", Geneva, Switzerland, 3-8 September 2006.

FAELLA C., MARTINELLI E., SGUAZZO C. and NIGRO E., (2009); "Shear strength of masonry walls reinforced by composites: comparison among existing formulations", ANIDIS 2009, Bologna, Italy, 28 June – 2 July 2009.

FAELLA C., CAMORANI G., MARTINELLI E., PACIELLO S.O. AND PERRI F., (2012); "Bond behaviour of FRP strips glued on masonry: Experimental investigation and empirical formulation", Construction and Building Materials, 31, p.353-363.

FEDERAL EMERGENCY MANAGEMENT AGENCY, (2000); "FEMA 356 Pre-Standard and Commentary for the Seismic Rehabilitation of Buildings". Washington, D.C: FEMA.

FILARDI B., LIBERATORE D., MASI A. AND NIGRO D., (1996); "Valutazione della resistenza al taglio di una tipologia muraria tramite prove su pannelli, carote e triplette", Atti del Convegno Nazionale, La Meccanica delle Murature tra Teoria e Progetto, Messina, 18-20 settembre 1996.

FUSIER, F. and VIGNOLI, A., (1993); "Proposta di un metodo di calcolo per edifici in muratura sottoposti ad azioni orizzontali", Ingegneria Sismica, Anno X, N.1, 1993.

GAMBAROTTA L. and LAGOMARSINO S., (1997); "Damage Models For The Seismic Response Of Brick Masonry Shear Walls. Part I: The Mortar Joint Model And Its Applications", Earthquake Engineering and Structural Dynamics, 26 (4), p. 423-439.

GAMBAROTTA, L. AND LAGOMARSINO, S., "Damage models for the seismic response of brick masonry shear walls. Part II: the continuum models and its applications", Earthq. Engin. and Struct. Dyn., Vol. 26, 1997, pp.441-462.

GAMBAROTTA, L. AND LAGOMARSINO, S., "Sulla risposta dinamica di pareti in muratura", Atti del Convegno Nazionale "La Meccanica delle Murature tra Teoria e Progetto", Messina, 18-20 settembre 1996, , Pitagora Ed. Bologna, 1996.

GANJU T. N.,(1977); "Nonlinear Finite Element Analysis of Clay Brick Masonry", Proc. 6th Australasian Conf. on Mech. of Structures and Materials, 1977, pp. 59-65.

GANZ, H.R. AND THÜRLIMANN, B., (1982); "Tests on the biaxial strength of masonry (in German)", Report No. 7502-3, Institute of Structural Engineering, ETH Zurich, Zurich, Switzerland.

GIAMBANCO G. and Di Gati L., (2001); "A Cohesive Interface Model For The Structural Mechanics Of Block Masonry", Meccanica, 24 (5), p. 503-512.

GIAMBANCO G. and MROZ Z., (2001); "The Interphase Model for the Analysis of Joints in Rock Masses and Masonry Structures", Meccanica, 36, p. 111-130.

GIAQUINTA M. and GIUSTI E., (1985); "Researches on the equilibrium of masonry structures", Arch. Rat. Mech. Anal., 88, 359-392.

GRAUBNER C. A. and KRANZLER T., (2005); "Shear Design of unreinforced masonry panels - basic assumptions and comparison of different standards", Proceedings of 10th Canadian Masonry Symposium, Banff, Alberta, Canada, June 2005.

HEYMAN J., (1997), "The stone skeleton: structural engineering of masonry architecture", Cambridge, Cambridge University Press.

HOHBERG J.M., (1992); "Ajoint element for the non-linear dynamic analysis arch damns", Report n. 186, Institute of Structural Engineering, ETH Zurich, Zurich, Switzerland.

HONG N. K, KIM J. and MOSALAM K., (2004); "Seismic performance of unreinforced masonry building in low seismicity region", 13th World Conference on Earthquake Engineering, Vancouver, B.C., Canada, 1-6 August, 2004.

INTERNATIONAL CONFERENCE OF BUILDING OFFICIALS, AC125, (2001); "Acceptance criteria for concrete and reinforced or unreinforced masonry strengthened using fiber-reinforced polymers (FRP) composite systems", 1 February 2001, Whittier, California, ICBO Evaluation Service, Inc.

JÄGER W. and SCHÖPS P., (2008); "D9.1 Proposals for an advanced design model of masonry under lateral loads for the implementation in Eurocode 6-1-1", TU Dresden, Germany: Faculty of Architecture Chair of Structural Design. Available at :

<http://www.esecmase.org/doc/deliverables_public/D_9.1_Dresden.pdf> [Accessed Date 7 November 2011].

KAM W. Y , AKGUZEL U. and PAMPANIN S., (2011); "4 Weeks on: Preliminary Reconnaissance Report from the Christchurch 22 Feb 2011 6.3MW Earthquake", Christchurch (NZ): Dept of Civil and Natural Resources Eng, Uni. of Canterbury. Available at: <http://db.nzsee.org.nz:8080/it/web/chch_2011/geotechnical/-/blogs/56877/maximized?p_p_auth=tw00cSJg (2011-09-19)> [Accessed Date 20 September 2011].

KARAPITTA L., MOUZAKIS H. AND CARYDIS P., (2010); "Explicit finite-element analysis for the in-plane cyclic behavior of unreinforced masonry structures", Earthquake Engng Struct. Dyn.

KUWATA Y., TAKADA S. and BASTAMI M., (2005); "Building damage and human casualties during the Bam-Iran earthquake", Asian Journal Of Civil Engineering (Building and Housing), 6 (1, 2), p. 1-19.

KYOYA T., TERADA K. and KAWAMOTO T., (1999); "Multi-scale limit load analysis for discontinuous rock mass based on the homogenization method", Numerical and Analytical Methods in Geomechanics, 23 (10), 995–1019.

Lebon F., (2011); "On the modelling of interfaces in masonry Structures", Course on Mechanics of Masonry Structures, CISM, Udine, 3-7 October 2011.

LIEPING Y., XINZHENG L., ZHE Q. and PENG F., (2008); "Analysis on Building Seismic Damage in the Wenchuan Earthquake", The 14th World Conference on Earthquake Engineering, Beijing, China October 12-17, 2008.

LOURENÇO P. B., (2001); "Analysis of historical constructions: From thrust-lines to advanced simulations Historical Constructions", P.B. Lourenço, P. Roca (Eds.), Guimarães, 2001

LOURENÇO P. B., OLIVEIRA D.V., ROCA P. and ORDUÑA A., (2005); "Dry Joint Stone Masonry Walls Subjected to In-Plane Combined Loading", Journal of Structural Engineering, ASCE,131(11), p. 1665.

LOURENÇO, P. B. (1996), "Computational strategies for masonry structures." PhD dissertation; Delft, the Netherlands.

LOURENCO, P. B. AND ROTS J. G., (1997); "Multisurface interface model for analysis of masonry structures", Journal Of Engineering Mechanics-Asce, 123(7), p. 660-668.

LURATI, F. AND THÜRLIMANN, B., (1990) - Tests in concrete masonry walls (in German). Report No. 8401-3, Institute of Structural Engineering, ETH Zurich, Zurich, Switzerland.

LURATI, F., GRAF, H. AND THÜRLIMANN, B. (1990) - Experimental determination of the strength parameters of concrete masonry (in German). Report No. 8401-2, Institute of Structural Engineering, ETH Zurich, Zurich, Switzerland.

MAGENES G. AND ABRAMS D. P., (2004a); "Seismic Design and Assessment of Masonry Structures", Lesson no. 8 part1, ROSE School, Pavia, Italy.

MAGENES G. AND ABRAMS D. P., (2004b); "Seismic Design and Assessment of Masonry Structures", Lesson no. 9 part2, ROSE School, Pavia, Italy.

MAGENES G., BOLOGNINI D. and BRAGGIO C., (2000); "Metodi semplificati per l'analisi sismica non lineare di edifici in muratura"; casa ed.

MAGENES, G. and DELLA FONTANA, A., (1998); "Simplified Non-linear Seismic Analysis of Masonry Buildings", Proc. of the British Masonry Society, Vol. 8, October 1998, pp. 190-195.

MAHMOOD H., RUSSELL A. P. and INGHAM J. M., (2008); "Monotonic testing of unreinforced and FRP-retrofitted masonry walls prone to shear failure in an earthquake", The 14th World Conference on Earthquake Engineering, Beijing, China October 12-17, 2008.

MARCARI G., FABBROCINO G., PROTA A. and PECCE M., (2007); "In-plane shear performance of masonry panels strengthened with FRP"; Composites Part B: Engineering, 38 (7-8), p. 887-901.

MARCARI G., FABBROCINO G., PROTA A. AND PECCE M., (2010); "Experimental And Numerical Evaluation Of Tuff Masonry Panels Shear Seismic Capacity", Proceedings of the Tenth North American Masonry Conference (10thNAMC), June 3-5, 2007, Saint Louis, Missouri, USA, pp. 1063-1074.

MARCARI G., FABBROCINO G., PROTA A., MANFREDI G. and ALDEA C., (2004); "Diagonal tests on tuff masonry strengthened with CMF systems", CICE 2004 The Second International Conference on FRP Composites in Civil Engineering, Adelaide, Australia, 8-10 December 2004.

MARCARI G., MANFREDI G., PROTA A. AND PECCE M., (2007); "In-plane shear performance of masonry panels strengthened with FRP", Composites Part B: Engineering, 38 (7-8), p. 887-901.

MARFIA S. and SACCO E., (2001), "Modeling of reinforced masonry elements", International Journal of Solids and Structures, 38 (24-25), p. 4177-4198.

MARIANO P. M. and TROVALUSCI P., (1999); "Constitutive relations for elastic microcracked bodies: from a lattice model to a multifield continuum description", International Journal of Damage Mechanics, 8, pp. 153-173.

MASIANI R. and TROVALUSCI P., (1996); "Cosserat and Cauchy materials as continuum models of brick masonry", Meccanica, 31, pp. 421-432.

MASIANI R., RIZZI N. and TROVALUSCI P., (1995); "Masonry as Structured Continuum", Meccanica, 30, p. 673-683.

MERA W. and LA TEGOLA A., (2004); "Structural behaviour of fiber reinforced mortar with application to masonry walls", Proceedings of the First International Conference on

Innovative Materials and Technologies for Construction and Restoration, vol.1, Università degli studi di Lecce, 6-9 June 2004.

MICELLI F. and OMBRES L., (2003); "Natural masonry strengthened with CFRP: experiments and modelling on wall panels"; Composites in Construction, Bruno et al (eds)- Editoriale Bios.

MUMTAZ H., HABIB MUGHAL S. and STEPHENSON M., (2008); "The Challenges of Reconstruction after the October 2005 Kashmir Earthquake", 2008 NZSEE Conference Proceedings, Paper no 34. Wairakei, New Zealand April 11-13, 2008.

MYERS J.J., (2011); "Strengthening Unreinforced Masonry Structures using externally bonded fiber reinforced Polymer System: An Overview of the American Concrete Institute 440.7R Design Approach", 9th Australasian Masonry Conference, Queenstown, New Zealand,15 – 18 February 2011.

N.T.C., (2008); "Nuove norme tecniche per le costruzioni e Circolare esplicativa"– D.M. Infrastrutture 14/01/2008, CIRC. MIN. 617 2/2/2009.

NEW ZEALAND SOCIETY FOR EARTHQUAKE ENGINEERING, (2008); "Building Safety Evaluation During a Declared State of Emergency - Guidelines for Territorial Authorities", Wellington (NZ): New Zealand Society for Earthquake Engineering New Zealand. Available at: < http://www.dbh.govt.nz/UserFiles/File/Building/information%20for/Building-Safety-Evaluation-during-State-of-Emergency.pdf> [Accessed Date 21 September 2011].

O.P.C.M. 20 marzo 2003 n. 3274 – "Primi elementi in materia di criteri generali per la classificazione sismica del territorio nazionale e di normative tecniche per le costruzioni in zona sismica".

OLIVEIRA, D. V. AND LOURENCO P. B., (2004); "Implementation and validation of a constitutive model for the cyclic behaviour of interface elements." Computers & Structures, 82(17-19), p.1451-1461.

OLIVITO R. S. and ZUCCARELLO F. A., (2005); "Analisi sperimentale della durabilità di pareti murarie soggette ad azioni cicliche", XXXIV Convegno Nazionale, Politecnico di Milano, Milano, Italy, 14-17 September 2005.

OLIVITO R. S., (2003), "Statica e stabilità delle costruzioni murarie", Pitagora Editrice Bologna.

PAGE, A.W., (1981); "The biaxial compressive strength of brick masonry", Proc. Intsn.Civ. Engrs., Part 2, 71 , p. 893-906.

PAGE, A.W., (1983); "The strength of brick masonry under biaxial compression-tension", Int. J. Masonry Constr., 3(1) , p. 26-31.

PEERLINGS R.H., DE BORST R. AND BREKELMANS W.A.M., (1996); "Some observations on localisation in non-local and gradient damage models", European Journal of Mechanics, 6, p. 937–953.

PEIRIS N., ROSSETTO T., BURTON P. AND MAHMOOD S., (2008); "Kashmir Pakistan Earthquake of 8 October 2005 a field report by EEFIT", London, United Kingdom: Institution of Structural Engineers. Available at: <http://www.istructe.org/knowledge/EEFIT/Documents/Kashmir.pdf> [Accessed Date 16 September 2011].

PENNA A., CATTARI S., GALASCO A. and LAGOMARSINO S., (2004); "Seismic assessment of masonry structures by non-linear macro-element analysis", IV International Seminar Structural Analysis of Historical Construction-Possibilities of Numerical and Experimental Techniques, Padova, Italy, 10-12 November 2004.

PLUIJM R. VAN DER, (1997); "Non Linear Behaviour of Masonry under Tension", HERON, 4 (1) ISSN 0046-7316.

POLIZZOTTO C., BORINO G. and FUSCHI P., (1998); "A Thermodynamically Consistent formulation of nonlocal and gradient Plasticity", Mechanics Research Communications, 25, 75–82.

POTTS D., AXELSSON K., GRANDE L., SCHWEIGER H.F. AND LONG M. eds., (2002); "Guidelines for the use of advanced numerical analysis", London: Thomas Telford Ltd.

PROTA, A., MARCARI, G., FABBROCINO, G., MANFREDI, G. and ALDEA, C., (2005); "Experimental In Plane Behavior of Tuff Masonry Strengthened with Cementitious Matrix–Grid Composites", Journal Of Composites For Construction, ASCE,10 (3), p. 223-233.

RICAMATO M., (2007); "Numerical and experimental analysis of masonry arches strengthened with FRP materials", PhD thesis, University of Cassino.

ROCA P., MOLINS C., AND MARÍ A.R., (2005); "Strength Capacity of Masonry Wall Structures by the Equivalent Frame Method", J. Struct. Eng., 131 (10), p. 1601-1610.

ROSENHAUPT S. AND SOKAL Y., (1965); "Masonry Walls on Continuous Beams", J. Structural Division, ASCE, 91, No ST1, pp. 155-171.

ROTS J.G., LOURENCO P. and BLAAUWENDRAAD J., (1998); "Continuum model for masonry: parameter estimation and validation", Journal of Structural Engineering, 124 (6), p. 642–652.

SAMARASINGHE W. A. AND HENDRY W., (1980); "The Strength of Brickwork under Biaxial Tension-Compression", Proc. 7th Int. Symp. on Load Bearing Brickwork, London, 1980.

SANTA-MARIA, H., DUARTE, G. and GARIB, A., (2004); "Experimental Investigation Of Masonry Panels Externally Strengthened With CFRP Laminates And Fabric Subjected To In-Plane Shear Load", 13th World Conference on Earthquake Engineering, Vancouver, B.C., Canada, 1-6 August, 2004.

SAW C. B., (1974); "Linear Elastic Finite Element Analysis of Masonry Walls on Beams", Building Science, 9, 1974, pp. 299-307.

SGUAZZO C., (2007); "Rinforzo a taglio di pannelli murari con l'utilizzo di materiali compositi: confronto tra modelli analitici e calibrazione di una formula di progetto", Tesi di Laurea in Tecnica delle Costruzioni, Universita' degli Studi di Salerno.

SGUAZZO C., FAELLA C. and MARTINELLI E., (2010); "Shear Strength of Masonry Walls Reinforced by Composites", Proceedings of 14th European Conference on Earthquake Engineering, Ohrid, Republic of Macedonia, August 30 – September 3, 2010.

SIA 266; (2003) "Civil Engineering, Masonry", Zürich, Switzerland, 2003.

SILVA, P. F., YU, P. and NANNI, A., (2008); "Monte Carlo Simulation of Shear Capacity of URM Walls Retrofitted by Polyurea Reinforced GFRP Grids". Journal of Composites for Construction, ASCE, 12 (4), p. 405-415.

SLUYS L.J. and WANG W.M., (1998); "2D/3D viscoplastic modelling of shear banding", Journal de Phisique IV, 8, p. 375–382.

STRATFORD, T., PASCALE, G., MANFRONI, O. and BONFIGLIOLI, B., (2002); "Shear Strengthening Masonry Panels with Sheet Glass-Fiber Reinforced Polymer", Journal Of Composites For Construction, ASCE, 8(5), p. 434-443.

SVEDBERG T. and RUNESSON K., (1998); "An algorithm for gradient-regularised plasticity coupled to damage based on a dual mixedformulation", Computer methods in applied mechanics and engineering, 161, 49–65.

TNO BUILDING AND CONSTRUCTION RESEARCH, (2010); "Diana User's Manual Release 9.4" Delft, The Netherlands.

TOMAŽEVIC, M. and WEISS, P., (1990); "A rational, experimentally based method for the verification of earthquake resistance of masonry buildings", Proc. of the 4th U.S. National Conference on Earthquake Engineering, Palm Springs, 1990, Vol. 2, pp. 349-359.

TOMAŽEVIC, M., LUTMAN, M. and PETROVIC, L., (1993); "In plane behavior of reinforced masonry walls subjected to cyclic lateral loads", Report to the Ministry of Sciences and Technology of Republic of Slovenia, parts 1 and 2, Liubljana, Slovenia.

TRIANTAFILLOU T., (1998); "Strengthening of masonry structures using epoxy-bonded FRP laminates", Journal of Composite for Construction 2, ASCE, 2 (2), p. 96–104.

TROVALUSCI P. and AUGUSTI G., (1998); "A continuum model with microstructure for materials with flaws and inclusions", Journal de Physique IV, Pr8, pp. 383-390.

TROVALUSCI P. and MASIANI R., (1999); "Material symmetries of micropolar continua equivalent to lattices", International Journal of Solids and Structures, 36(14), pp. 2091-2108.

TROVALUSCI P. and MASIANI R., (2003); "Non-linear micropolar and classical continua for anisotropic discontinuous materials", Internationa Journal of Solids and Structures, 40 (5), p. 1281-1297.

TROVALUSCI P. and MASIANI R., (2005); "A multi-field model for blocky materials based on multiscale description", International Journal of Solids and Structures, 42, pp. 5778-5794.

TUMIALAN G., VATOVEC M. and KELLEY P.L., (2009); "FRP Composites for Masonry Retrofitting", STRUCTURE magazine, p. 12-14. Available at: <http://www.structuremag.org/article.aspx?articleID=907> [Accessed Date 30 September 2011].

TURNSEK, V. and CACOVIC, F., (1970); "Some Experimental Results on the Strength of Brick Masonry Walls", Proceedings of the Second International Brick Masonry Conference, Stoke-on-Trent, UK.

TZAMTZIS, A.D. AND ASTERIS, P.G., (2003); "Finite Element Analysis Masonry Structures: Part I-Review of Previous Works", Proceedings of the Ninth North American Masonry Conference (9thNAMC), June 1-4, 2003, Clemson, South Carolina, USA, pp. 101-111.

UNI ENV 1996-1-1, (1998), Eurocode 6, "Progettazione delle strutture di muratura".

VALLUZZI M.R., TINAZZI D. and MODENA C., (2002); "Shear behaviour of masonry panels strengthened by FRP laminates", Construction and Building Materials, 16 (7), p. 409–416.

XIONG Z.H., (2008); "Lessons Learned from Wenchuan Earthquake: to Improve the Seismic Design of School Buildings", The 14th World Conference on Earthquake Engineering, Beijing, China October 12-17, 2008.

ZIENKIEWICZ O.C., VALLAPIAN S. AND KING I.P., (1968); "Stress analysis of rock as a no-tension material", Geotechnique, 18, 1968.

ZIENKIEWICZ, O.C. AND TAYLOR, R.L., (1989); "The finite element method: Volume 1, Basic formulation and linear problems", Mc-Graw Hill, Berkshire, England, UK.

.

List of Figures

List of Tables